

**SYNTHESIS OF SILICONE MAGNETIC FLUIDS FOR USE
IN EYE SURGERY**

by

Metha Rutnakornpituk

Dissertation submitted to the faculty of the Virginia Polytechnic Institute and State University in
partial fulfillment of the requirements for the degree of

DOCTOR OF PHILOSOPHY

In

Chemistry

Approved by:

Judy S. Riffle, Chair

James E. McGrath

Allan R. Shultz

John G. Dillard

David G. I. Kingston

April 23, 2002

Blacksburg, Virginia

Keywords: Polysiloxanes, nanoparticles, superparamagnetic, retinal detachment, sol-gel process,
oxidation

Copyright 2002, Metha Rutnakornpituk

SYNTHESIS OF SILICONE MAGNETIC FLUIDS FOR USE IN EYE SURGERY

Metha Rutnakornpituk

Abstract

Stable suspensions of superparamagnetic cobalt nanoparticles have been prepared in poly(dimethylsiloxane) (PDMS) carrier fluids in the presence of poly[dimethylsiloxane-*b*-(3-cyanopropyl)methylsiloxane-*b*-dimethylsiloxane] (PDMS-PCPMS-PDMS) triblock copolymers as steric stabilizers. A series of the polysiloxane triblock copolymers with systematically varied molecular weights were prepared via anionic polymerization using LiOH as an initiator. These copolymers formed micelles in toluene or poly(dimethylsiloxane) (PDMS) carrier fluids and served as “nanoreactors” for thermal decomposition of the $\text{Co}_2(\text{CO})_8$ precursor. The nitrile groups on the PCPMS central blocks are thought to coordinate onto the particle surface, while the PDMS endblocks protrude into the reaction medium to provide steric stability. The particle size can be controlled by adjusting the cobalt to copolymer ratio. Ordered self-assemblies of these cobalt nanoparticles are observed when the dispersions are cast from toluene. Electron diffraction spectroscopy reveals that the cobalt nanoparticles have fcc crystal structures. TEM shows non-aggregated cobalt nanoparticles with narrow size distributions, which are evenly surrounded with copolymer sheaths. However, some degree of surface oxidation was observed over time, resulting in a decrease in magnetic susceptibility.

Novel poly[dimethylsiloxane-*b*-methyltriethoxysilylsiloxane-*b*-(3-cyanopropyl)methylsiloxane-*b*-methyltriethoxysilylsiloxane-*b*-dimethylsiloxane] (PDMS-PMTEOS-PCPMS-PMTEOS-PDMS) pentablock terpolymers were prepared. These terpolymers could fill the dual role both as steric stabilizers for preparing stable cobalt nanoparticle dispersions and

precursors for the particle coating process. Silica films coated on the particles surfaces were employed to prevent the surface oxidation of the nanoparticles. Specific saturation magnetic measurement indicates that coating the nanoparticles with silica thin films can effectively inhibit the oxidation process.

Acknowledgements

I would like to express my sincere appreciation to my advisor Dr. Judy Riffle for her guidance and encouragement throughout my education at Virginia Tech. I would also like to thank the members of my committee, Dr. James E. McGrath, Dr. Allan R. Shultz, Dr. John G. Dillard and Dr. David G.I. Kingston. I also appreciate Dr. J.P. Dailey for providing me the needed background concerning retinal detachment. My appreciation is also extended to Dr. Tim St. Pierre and Joan Connolly of the University of Western Australia for their helpful discussions and characterization regarding the magnetic properties of nanoparticles. I also appreciate Dr. Alan Esker and Cathy Farmer for their contribution and measuring surface tension of copolymers in solutions. I would like to thank Dr. Bill Reynolds for his valuable time for help in investigating crystal structures of cobalt particles via electron diffraction.

I would like to especially thank all the scientists who have helped throughout my graduate career including Tom Glass for tremendous help with the Varian 400 MHz NMR, Dr. Kim for GPC, Steve McCartney for TEM, and Frank Cromer for XPS. Much thank is also extended to my colleagues who assisted me in the material characterizations including Jody Streeter for DLS, Jeff Leach for VSM, and Sheng Lin-Gibson for SANS and SAXS.

My warmest appreciation is extended to my colleagues in Dr. Riffle's research group. Special thanks go to Angie Flynn who has helped with all the paper works, Paige Stevenson who was my first mentor in my graduate life, and Michael Shane Thompson and Vince Baranauskas who were my assistants in this dissertation. I am grateful to Linda Harris, Kristen Wilson, Christy Tyberg, Sheng Lin-Gibson, Brian Starr, Jen Hoyt and Maggie Bump for their valuable discussions.

I would like to express my deepest gratitude to my mother, father, sisters, and brother and my aunt for their love and inspiration. Finally, my warmest appreciation goes to my love and best friend, A, who makes me believe that this life is so beautiful.

This dissertation is dedicated to my family for their heartfelt support and in memory of my grandmother, Aung Sheng Huay (1904-1995) for her truly unselfish love.

Abbreviations

PDMS	Poly(dimethylsiloxane)
PCPMS	Poly(3-cyanopropyl)methylsiloxane
PMTMOS	Poly(methyltrimethoxysilylsiloxane)
PMTEOS	Poly(methyltriethoxysilylsiloxane)
PMVS	Poly(methylvinylsiloxane)
D ₄ CN	1,3,5,7-Tetramethyl-1,3,5,7-tetra(3-cyanopropyl)cyclotetrasiloxane
D ₄ H	2,4,6,8-Tetramethylcyclotetrasiloxane
D ₃	1,1,3,3,5,5-Hexamethylcyclotrisiloxane
D ₄	1,1,3,3,5,5,7,7-Octamethylcyclotetrasiloxane
D ₃ -vinyl	1,3,5-Trimethyl-1,3,5-trivinylcyclotrisiloxane
DBTA	Dibutyltin diacetate
TMS	Tetramethylsilane
THF	Tetrahydrofuran
TEGDME	Triethylene glycol dimethylether
NMR	Nuclear magnetic resonance
FTIR	Fourier transform infrared spectroscopy
GPC	Gel permeation chromatography
DSC	Differential scanning calorimetry
DLS	Dynamic light scattering
CMC	Critical micelle concentrations
D _T	Translational Diffusion Coefficients
R _h	Hydrodynamic radii
HPLC	High performance liquid chromatography
TEM	Transmission electron microscopy
FFT	Fast fourier transform
EDS	Electron diffraction spectroscopy
XPS	X-Ray photoelectron spectroscopy
VSM	Vibrating sample magnetometer
ICP	Inductively couple plasma

M_n	Number average molecular weight
T_g	Glass transition temperature
FW	Formal weight
b.p.	Boiling point
d.	Density
T_m	Melting point
MWCO	Molecular weight cutoff

Table of Contents

CHAPTER 1	Introduction.....	1
CHAPTER 2	Literature review.....	5
2.1	Overview.....	5
2.2	Introduction to the synthesis of polysiloxanes.....	5
2.2.1	Introduction to polysiloxanes.....	5
2.2.2	Preparation of cyclosiloxanes.....	15
2.2.3	Equilibrium ring-opening polymerization of cyclosiloxanes : Thermodynamic control.....	18
2.2.3.1	Acid-catalyzed ring-opening equilibration.....	25
2.2.3.2	Base-catalyzed ring-opening equilibration.....	28
2.2.4	Living anionic polymerization and it's application to block copolymers: kinetically controlled polymerization.....	33
2.2.4.1	Introduction to living anionic polymerization	33
2.2.4.2	Living anionic polymerization of D ₃	35
2.2.4.3	Siloxane-containing block copolymers.....	42
2.2.4.4	Micelle formation.....	46
2.3	Sol-gel chemistry.....	51
2.3.1	Introduction.....	51
2.3.2	Mechanisms of acid- and base-catalyzed sol-gel reactions.....	55
2.3.2.1	Hydrolysis reactions.....	55
2.3.2.2	Condensation reactions.....	59
2.3.3	Meachanism of tin-catalyzed sol-gel reaction.....	62
2.3.4	Current interests and applications in sol-gel reactions.....	65
2.4	Magnetisms and magnetic materials.....	68
2.4.1	Introduction to magnetic materials.....	68
2.4.2	Ferrofluids.....	72
2.4.3	Stabilization in magnetic fluids.....	79
2.4.3.1	Attractive forces.....	79
2.4.3.2	Repulsive forces.....	80

2.5	Preparation of cobalt magnetic fluids.....	82
2.5.1	Thermal decomposition of $\text{Co}_2(\text{CO})_8$	83
2.5.2	Reduction of CoCl_2	92
2.6	Retinal detachment.....	94
2.6.1	Anatomy of the eye.....	94
2.6.2	Retinal detachment.....	96
2.6.3	Current treatment of retinal detachment.....	98
CHAPTER 3 Synthesis and characterization of poly(siloxane) triblock copolymers.....		102
3.1	Synopsis.....	102
3.2	Experimental.....	104
3.2.1	Purification of solvents and reagents.....	104
3.2.2	Synthesis of 1,3,5,7-tetramethyl-1,3,5,7-tetra(3-cyanopropyl)cyclotetra- siloxane (D_4CN).....	106
3.2.3	Synthesis of poly(dimethylsiloxane-b-(3-cyanopropyl)methylsiloxane-b- dimethylsiloxane) triblock copolymers (PDMS-b-PCPMS-b-PDMS) with controlled block lengths.....	107
3.3	Characterization.....	109
3.3.1	Molecular weight determination.....	109
3.3.1.1	Potentiometric titration.....	109
3.3.1.2	^1H NMR.....	110
3.3.2	^{29}Si NMR.....	110
3.3.3	^{13}C NMR.....	110
3.3.4	Fourier transform infrared spectroscopy (FTIR).....	111
3.3.5	Gel permeation chromatography (GPC).....	111
3.3.6	Differential scanning calorimetry (DSC).....	111
3.4	Results and discussion.....	112
3.4.1	Preparation of D_4CN	112
3.4.2	Synthesis of poly(dimethylsiloxane-b-(3-cyanopropyl)methylsiloxane-b- dimethylsiloxane) triblock copolymers (PDMS-b-PCPMS-b-PDMS) with controlled block lengths.....	116

3.5	Conclusions.....	131
CHAPTER 4 Synthesis, characterization and properties of stable cobalt nanoparticles...132		
4.1	Synopsis.....	132
4.2	Experimental.....	132
4.2.1	Purification of solvents and reagents.....	132
4.2.2	Synthesis of a 2000 g/mol M_n poly(dimethylsiloxane) carrier fluid (PDMS).....	134
4.2.3	Synthesis of a superparamagnetic cobalt fluid stabilized with a (5000 g/mole PDMS)-(5000 g/mole PCPMS)-(5000 g/mole PDMS) block copolymer in toluene.....	134
4.2.4	Preparation of stable cobalt nanoparticle dispersions in 2000 g/mol M_n PDMS carrier fluids.....	135
4.3	Characterization.....	135
4.3.1	Surface tension.....	135
4.3.2	Dynamic light scattering (DLS).....	136
4.3.3	Fourier transform infrared spectroscopy (FTIR).....	136
4.3.4	Differential scanning calorimetry (DSC).....	136
4.3.5	High Performance Liquid Chromatography (HPLC).....	137
4.3.6	Transmission electron microscopy (TEM).....	137
4.3.7	Electron diffraction spectroscopy (EDS).....	138
4.3.8	X-Ray photoelectron spectroscopy (XPS).....	138
4.3.9	SQUID magnetometry.....	138
4.4	Results and discussion.....	139
4.4.1	Analysis of PDMS-PCPMS-PDMS micellar solutions in toluene.....	139
4.4.2	Synthesis of stable cobalt nanoparticles by thermolysis of dicobalt octacarbonyl in the micellar copolymer solutions	147
4.4.3	The cobalt dispersion in the presence of an external magnetic field.....	155
4.4.4	Effects of the $Co_2(CO)_8$ /copolymer ratio on cobalt nanoparticle size.....	156
4.4.5	Formation and characterization of poly(dimethylsiloxane) dispersions.....	159
4.4.6	Two-dimensional ordering of superparamagnetic cobalt nanoparticles....	161

4.4.7	Model cobalt nanoparticles coated with PDMS-PCPMS-PDMS copolymers.....	164
4.4.8	Magnetic properties of cobalt dispersions.....	167
4.4.9	XPS surface analysis of the cobalt dispersions.....	172
4.4.10	Purification of cobalt dispersions via dialysis.....	174
4.4.11	Thermal properties of the cobalt dispersions in 2000g/mol PDMS.....	176
4.4.12	Determination of crystal structures of cobalt nanoparticles.....	179
4.5	Conclusions.....	184
CHAPTER 5 Preparations of novel pentablock steric stabilizers and silica-coated cobalt nanoparticles via sol-gel process.....		185
5.1	Synopsis.....	185
5.2	Experimental.....	186
5.2.1	Purification of solvents and reagents.....	186
5.2.2	Synthesis of poly[dimethylsiloxane-b-methylvinylsiloxane-b-(3-cyanopropyl)methylsiloxane-b-methylvinylsiloxane-b-dimethylsiloxane] (PDMS- <u>PMVS</u> -PCPMS- <u>PMVS</u> -PDMS) pentablock terpolymers with controlled block lengths.....	188
5.2.3	Synthesis of poly[dimethylsiloxane-b-methyltriethoxysilylsiloxane-b-(3-cyanopropyl) methylsiloxane-b-methyltriethoxysilylsiloxane-b-dimethylsiloxane] (PDMS- <u>PMTEOS</u> -PCPMS- <u>PMTEOS</u> -PDMS) pentablock terpolymers.....	191
5.2.4	Preparation of silica-coated cobalt nanoparticles stabilized with a PDMS- <u>PMTEOS</u> -PCPMS- <u>PMTEOS</u> -PDMS pentablock terpolymer in 2000g/mol PDMS carrier fluids.....	195
5.3	Characterization.....	196
5.3.1	Magnetic properties.....	196
5.3.2	Determination of percent cobalt in dispersions.....	198
5.4	Results and Discussion.....	198
5.4.1	Synthesis of PDMS- <u>PMVS</u> -PCPMS- <u>PMVS</u> -PDMS pentablock terpolymers.....	199

5.4.2	Synthesis of alkoxy silane-containing pentablock terpolymers.....	206
5.4.3	Synthesis of cobalt nanoparticles by thermolysis of dicobalt octacarbonyl in the micellar terpolymer solutions of alkoxy silane-containing pentablock terpolymers.....	209
5.4.4	Monitoring the sol-gel reaction conversion using reaction models.....	212
5.4.4.1	Sol-gel reaction models using ethoxy silane-containing pentablock terpolymers.....	216
5.4.4.2	Sol-gel reaction models using methoxy silane-containing pentablock terpolymers.....	223
5.4.5	Preparation of silica-coated cobalt nanoparticles in 2000 g/mol PDMS carrier fluids.....	229
5.4.5.1	Preparation of silica-coated cobalt nanoparticles using ethoxy silane- containing pentablock terpolymers.....	229
5.4.5.2	Preparation of silica-coated cobalt nanoparticles using methoxy silane- containing pentablock terpolymers.....	232
5.4.6	Magnetic properties of the cobalt nanoparticle dispersions.....	234
5.5	Conclusions.....	244
CHAPTER 6 Conclusions.....		245
CHAPTER 7 Recommendations for future work.....		247
Bibliography		249
Vita		258

List of Figures

Figure 1.1 An internal tamponade using silicone magnetic fluids.....	2
Figure 1.2 Chemical structure of PDMS- <i>b</i> -PCPMS- <i>b</i> -PDMS steric stabilizers.....	3
Figure 1.3 Steric stabilization of cobalt nanoparticles using PDMS- <i>b</i> -PCPMS- <i>b</i> -PDMS Stabilizers, A) showing nitrile-functional blocks bound to the particle surface, and B) showing PDMS blocks providing steric stabilization.	3
Figure 2.1 PDMS chains showing bond angles in the siloxane skeleton	11
Figure 2.2 Hydrolysis of dichlorodimethylsilane to produce polydimethylsiloxanes (PDMS) and dimethylsiloxane cyclics.....	15
Figure 2.3 Preparation of hexamethylcyclotrisiloxane.....	17
Figure 2.4 Equilibration reactions of siloxanes.....	20
Figure 2.5 Variations of functional endgroups and backbone compositions.....	24
Figure 2.6 Proposed mechanism of acid-initiated ring-opening polymerization of D ₄ ...	26
Figure 2.7 The acid-catalyzed ring-opening polymerization mechanism catalyzed by triflic acid	27
Figure 2.8 Proposed mechanism of base-catalyzed ring-opening polymerization in D ₄ ..	30
Figure 2.9 Living anionic polymerization of D ₃	37
Figure 2.10 R _p /[M] vs. [C] for the anionic polymerization of D ₃ with Li ⁺ and [221] cryptand counterions in benzene at 20. °C.....	38
Figure 2.11 The conversion of D ₃ monomer and the formation of linear polymers, D ₄ , D ₅ and D ₆ as a function of time.....	39
Figure 2.12 Structures of dilithium dianionic silanolate initiators for D ₃	41
Figure 2.13 Synthesis of polydiphenylsiloxane- <i>b</i> -polydimethylsiloxane- <i>b</i> -polydiphenyl siloxane (PDPS- <i>b</i> -PDMS- <i>b</i> -PDPS).....	44
Figure 2.14 Preparation of polystyrene- <i>b</i> -polysiloxane liquid crystalline side-chain block copolymers	45

Figure 2.15 Schematic illustration of abrupt changes in physical properties at the critical micelle concentration (cmc).....	47
Figure 2.16 Various structures of self-assembled block copolymers in a selective solvent	48
Figure 2.17 Temperature-concentration diagram of PS- <i>b</i> -PDMS in <i>n</i> -octane methylcyclohexane mixture.....	50
Figure 2.18 Generalized reactions for the preparation of silicate networks.....	53
Figure 2.19 Processing scheme for the TEOS-ethanol-water system.....	54
Figure 2.20 Sequence of structural changes during a sol-gel process.....	54
Figure 2.21 The proposed mechanism of base-catalyzed hydrolysis in sol-gel reactions.....	56
Figure 2.22 The proposed mechanism of acid-catalyzed hydrolysis in a sol-gel reaction.....	58
Figure 2.23 The proposed mechanism of base-catalyzed condensation in a sol-gel reaction.....	60
Figure 2.24 The proposed mechanism of acid-catalyzed condensation in a sol-gel reaction.....	61
Figure 2.25 The proposed mechanism of a tin-catalyzed sol-gel reaction.....	64
Figure 2.26 Schematic diagram of the alignment of magnetic moments.....	72
Figure 2.27 A schematic diagram of the properties of superparamagnetic fluids.....	74
Figure 2.28 A hysteresis loop characteristic of typical magnetic materials	75
Figure 2.29 Steric and electrostatic stabilizations of colloidal suspensions.....	81
Figure 2.30 A schematic diagram of the electric double layer, and the plot of repulsive potential vs distance between two particles.....	81
Figure 2.31 Molecular structures of $\text{Co}_2(\text{CO})_8$ and $\text{Co}_4(\text{CO})_{12}$ showing the bridging and terminal carbonyls.....	86
Figure 2.32 IR spectra of $\text{Co}_2(\text{CO})_8$ and $\text{Co}_4(\text{CO})_{12}$ in toluene.....	87

Figure 2.33 Anatomy of the eye.....	95
Figure 2.34 Stages of retinal detachment.....	97
Figure 2.35 Demonstration of the treatment of retinal detachment using scleral buckles.....	100
Figure 2.36 Demonstration of the treatment of retinal detachment using internal tamponades.....	101
Figure 3.1 Synthetic scheme for preparing PDMS- <i>b</i> -PCPMS- <i>b</i> -PDMS triblock copolymers.....	103
Figure 3.2 ¹ H NMR monitoring the progress of D ₄ CN preparation.....	114
Figure 3.3 Markownikoff and anti-Markownikoff products.....	114
Figure 3.4 FTIR spectra showing the progress of D ₄ CN preparation.....	115
Figure 3.5 Mechanism of D ₄ CN anionic ring-opening polymerization to obtain difunctional PCPMS oligomers.....	117
Figure 3.6 Gel permeation chromatograms of D ₄ CN and PCPMS in CHCl ₃	118
Figure 3.7 Monitoring the living anionic synthesis of the PDMS endblocks on PDMS-PCPMS-PDMS via ¹ H NMR	119
Figure 3.8 A potentiometric titration plot used to determine the molecular weight of the PCPMS central block.	121
Figure 3.9 ¹ H NMR of the PDMS-PCPMS-PDMS triblock copolymers.....	125
Figure 3.10 ²⁹ Si NMR spectra of polysiloxane triblock copolymers.....	127
Figure 3.11 ¹³ C NMR analysis of a polysiloxane triblock copolymer.....	128
Figure 3.12 DSC thermograms showing microphase separated morphologies of block copolymers.....	130
Figure 4.1 Schematic of surface tension measurements.....	141
Figure 4.2 Surface tensions of solutions of the PDMS-PCPMS-PDMS triblock copolymers in toluene at 26 °C Showing a cmc of ≈0.01 g/L.....	143
Figure 4.3 Copolymer solutions a) below cmc, b) at the saturation concentration, and c) above cmc.....	143

- Figure 4.4** Surface tensions of solutions of (15000 g/mole PDMS)-(2000 g/mole PCPMS)-(15000 g/mole PDMS) copolymers in toluene at various temperatures145
- Figure 4.5** Preparation of a cobalt nanoparticle dispersion in toluene.....147
- Figure 4.6** Reaction conditions and concentrations used for preparing cobalt nanoparticles.....149
- Figure 4.7** FTIR spectra of a cobalt dispersion reaction using 1 g $\text{Co}_2(\text{CO})_8$ and 1 g of a (15000 g/mole PDMS)-(2000 g/mole PCPMS)-(15000 g/mole PDMS) copolymer in 20 mL toluene at different stages.....150
- Figure 4.8** TEM micrographs of cobalt dispersions using 0.2 g $\text{Co}_2(\text{CO})_8$ and 1 g of a (15000 g/mole PDMS)-(2000 g/mole PCPMS)-(15000 g/mole PDMS) copolymer in 20 mL toluene at different stages.....151
- Figure 4.9** TEM micrographs of cobalt dispersions using 1.0 g $\text{Co}_2(\text{CO})_8$ and 1 g of a (15000 g/mole PDMS)-(2000 g/mole PCPMS)-(15000 g/mole PDMS) copolymer in 20 mL toluene at different stages.....152
- Figure 4.10** TEM micrographs of cobalt dispersions using 3.2 g $\text{Co}_2(\text{CO})_8$ and 1 g of a (15000 g/mole PDMS)-(2000 g/mole PCPMS)-(15000 g/mole PDMS) copolymer in 20 mL toluene at different stages.....153
- Figure 4.11** TEM micrographs of cobalt dispersions using 1 g $\text{Co}_2(\text{CO})_8$ and 1 g of a (15000 g/mole PDMS)-(2000 g/mole PCPMS)-(15000 g/mole PDMS) copolymer in 20 mL toluene prepared in the presence of an external magnetic field.....156
- Figure 4.12** TEM micrographs showing the effects of the $\text{Co}_2(\text{CO})_8$ /copolymer ratio on cobalt nanoparticle size.....159
- Figure 4.13** TEM micrographs of cobalt dispersions in 2000 g/mol M_n PDMS carrier fluids.....160
- Figure 4.14** Magnetic separation of cobalt dispersions using an externally applied magnetic field gradient.....161
- Figure 4.15** Self-assembled two-dimensional ordering of magnetic field separated cobalt nanoparticles on a carbon film from a reaction using 1 g $\text{Co}_2(\text{CO})_8$ and 1 g of a (15000 g/mole PDMS)-(2000 g/mole PCPMS)-(15000 g/mole PDMS) copolymer in 20 mL toluene with different magnifications.....163
- Figure 4.16** TEM micrographs from a reaction using 1 g $\text{Co}_2(\text{CO})_8$ and 1 g of a (15000 g/mole PDMS)-(2000 g/mole PCPMS)-(15000 g/mole PDMS) copolymer in 20 mL toluene showing that the field gradient separation greatly increased the

order: (A) in the field with particle sizes of 10 nm, (B) in the decanted liquid with a particle size of 6 nm.....	163
Figure 4.17 Radially averaged FFT data of the central TEM image in Figure 4.14.....	164
Figure 4.18 Model cobalt nanoparticles coated with PDMS-PCPMS-PDMS copolymers: (A) model, and (B) TEM image of a 10 nm diameter cobalt particle with a 4 nm thick copolymer coating.....	165
Figure 4.19 Model for estimating the number of surface sites per particle.....	166
Figure 4.20 Hysteresis loops for an air-exposed cobalt nanoparticle dispersion (sample 3) at 5K after cooling the sample in zero field from room temperature.....	168
Figure 4.21 Hysteresis loops for a cobalt nanoparticle dispersion sealed under an argon atmosphere (sample 8) at 5K after cooling the sample in zero field from room temperature.....	169
Figure 4.22 Loss of cobalt specific saturation magnetization (or cobalt specific magnetization at 70 kOe) per day as a percentage of the original cobalt specific saturation magnetization (or cobalt specific magnetization at 70 kOe).....	170
Figure 4.23 Hysteresis loops for sample 5 at 5K after cooling the sample from 220 K in zero field and in a 70 kOe field	172
Figure 4.24 XPS spectrum of the cobalt dispersions analyzed at a 90° takeoff angle.....	173
Figure 4.25 (A) Apparatus for dialysis of the cobalt dispersions against hexamethyldisiloxane, and (B) schematic of the ideal diffusion equilibrium between the dimer and toluene through the membrane.....	175
Figure 4.26 Ratio of the toluene/diphenyl peak areas with dialysis time (days) showing a significant decrease of toluene at equilibrium.....	176
Figure 4.27 Differential scanning calorimetry thermograms of PDMS homopolymer/ copolymer blends and cobalt dispersions containing different cobalt concentrations.....	178
Figure 4.28 Two possible crystal structures of cobalt, fcc, where lattice parameter $a = b = c$, $\alpha = \beta = \gamma = 90^\circ$, and hcp, where lattice parameter $a = b \neq c$, $\alpha = \beta = 90^\circ$, $\gamma = 120^\circ$	179
Figure 4.29 The electron diffraction pattern of cobalt nanoparticles.....	182
Figure 5.1 Chemical structure of PDMS- <u>PMTEOS</u> -PCPMS- <u>PMTEOS</u> -PDMS pentablock terpolymers.....	186

Figure 5.2 Synthesis of PDMS- <u>PMVS</u> -PCPMS- <u>PMVS</u> -PDMS pentablock terpolymers.....	189
Figure 5.3 Vibrating sample magnetometer (VSM) used for measuring magnetic properties of cobalt dispersions.....	197
Figure 5.4 ¹ H NMR used to monitor the progress of PMVS and PDMS syntheses.....	201
Figure 5.5 Silicon NMR showing the resonance of PDMS, PCPMS and PMVS blocks.....	203
Figure 5.6 Differential scanning calorimetry (DSC) thermograms of PDMS homopolymers, PMVS homopolymers, and PDMS- <u>PMVS</u> -PCPMS- <u>PMVS</u> -PDMS pentablock terpolymers.....	205
Figure 5.7 ¹ H NMR showing the disappearance of vinyl and Si-H groups during hydrosilylation.....	207
Figure 5.8 ²⁹ Si NMR showing the formation of poly(triethoxysilylsiloxane) repeating units.....	208
Figure 5.9 Methodologies for preparing silica coated cobalt nanoparticles.....	210
Figure 5.10 TEM image of the dispersion prepared in the presence of pentablock steric stabilizers with triethoxysilyl-containing silica precursor blocks prepared in PDMS.....	212
Figure 5.11 The sol-gel reaction mechanism.....	214
Figure 5.12 Typical ¹ H NMR spectra showing the progress of the sol-gel reaction in 2000 g/mol PDMS as a reaction solvent.....	218
Figure 5.13 Monitoring %≡Si-OEt remaining (100%-% conversion) during sol-gel reaction using 1 g of a 15000 g/mol PDMS -2000 g/mole PMTEOS-2000 g/mol PCPMS-2000 g/mol PMTEOS-15000 g/mol PDMS terpolymer in 20 mL of 2000 g/mol PDMS.....	219
Figure 5.14 Typical ¹ H NMR spectra performed in toluene solvent showing the reaction progress of sol-gel reactions. The reaction was performed in the presence of 15k- <u>2k</u> - <u>2k</u> - <u>2k</u> -15k PDMS- <u>PMTEOS</u> -PCPMS- <u>PMTEOS</u> -PDMS pentablock terpolymers with 0.1 wt% DBTA and 1:2 molar ratio of H ₂ O:≡Si-OEt in (A) 160 mL toluene, and (B) 80 mL toluene.....	221
Figure 5.15 Monitoring %≡Si-OEt remaining (100%-%conversion) of the sol-gel	

reaction using 1 g of 15k-2k-2k-2k-15k PDMS-PMTEOS-PCPMS-PMTEOS-PDMS terpolymers in 80 and 160 mL of toluene, 0.1 wt% DBTA and 1:2 molar ratio of $\text{H}_2\text{O}:\equiv\text{Si-OEt}$222

Figure 5.16 Typical ^1H NMR spectra performed in 2000 g/mol PDMS showing the reaction progress of a sol-gel reaction. The reaction was performed in the presence of 15k-2k-2k-2k-15k PDMS-PMTMOS-PCPMS-PMTMOS-PDMS pentablock terpolymers, (A) without H_2O and catalyst, (B) with 1:2 molar ratio of $\text{H}_2\text{O}:\equiv\text{Si-OMe}$ and without catalyst, (C) with 1:2 molar ratio of $\text{H}_2\text{O}:\equiv\text{Si-OMe}$ and 1:1 molar ratio of $\text{NH}_4\text{OH}:\text{H}_2\text{O}$, and (D) with 1:2 molar ratio of $\text{H}_2\text{O}:\equiv\text{Si-OMe}$ and 0.1wt%DBTA catalyst.....225

Figure 5.17 Monitoring % $\equiv\text{Si-OMe}$ remaining (100%-%Conversion) of the sol-gel reaction using 1 g of 15k-2k-2k-2k-15k PDMS-PMTMOS-PCPMS-PMTMOS-PDMS terpolymers in 20 mL of 2000 g/mol PDMS.....226

Figure 5.18 Typical ^1H NMR spectra performed in toluene solvent showing the reaction progress of sol-gel reactions. The reaction was performed in the presence of 15k-2k-2k-2k-15k PDMS-PMTMOS-PCPMS-PMTMOS-PDMS pentablock terpolymers with 0.1 wt% DBTA and 1:2 molar ratio of $\text{H}_2\text{O}:\equiv\text{Si-OMe}$ in (A) 160 mL toluene, and (B) 80 mL toluene.....227

Figure 5.19 Monitoring % $\equiv\text{Si-OMe}$ remaining (100%-%Conversion) of the sol-gel reaction using 1 g of 15k-2k-2k-2k-15k PDMS-PMTMOS-PCPMS-PMTMOS-PDMS terpolymers in 80 and 160 mL of toluene, 0.1 wt% DBTA and 1:2 molar ratio of $\text{H}_2\text{O}:\equiv\text{Si-OMe}$228

Figure 5.20 Transmission electron microscopy (TEM) of cobalt dispersions prepared by using ethoxy-containing terpolymers in 2000 g/mol PDMS: A) before, and B) after silica coatings231

Figure 5.21 A cobalt dispersion prepared by using ethoxy-containing terpolymers in, (A) toluene, and (B) 2000 g/mol PDMS. The image (A) was taken after adding 2000 g/mol PDMS and removing toluene232

Figure 5.22 Macroscopic aggregation observed when the silica-coated cobalt dispersion reaction was performed in the presence of methoxy-containing pentablock terpolymers.....233

Figure 5.23 The magnetization curves of the dispersion during sol-gel reaction: the dispersion was performed using 1 g of 15k-1k-2k-1k-15k PDMS-PMTEOS-PCPMS-PMTEOS-PDMS terpolymers in 2000 g/mol PDMS carrier fluids.....236

Figure 5.24 The magnetization curves of the dispersion during sol-gel reaction:

the dispersion was performed using 1 g of 15k-2k-2k-2k-15k PDMS-PMTEOS-PCPMS-PMTEOS-PDMS terpolymers in 2000 g/mol PDMS carrier fluids.....237

Figure 5.25 The magnetization curves of the dispersion during sol-gel reaction: the dispersion was performed using 1 g of 15k-4k-2k-4k-15k PDMS-PMTEOS-PCPMS-PMTEOS-PDMS terpolymers in 2000 g/mol PDMS carrier fluids.....238

Figure 5.26 The specific saturation magnetization of a dispersion measured at various time intervals. The sample was prepared using 1 g $\text{Co}_2(\text{CO})_8$, and 1 g of 15k-1k-2k-1k-15k PDMS-PMTEOS-PCPMS-PMTEOS-PDMS terpolymers in 20 mL PDMS (approximately 1.6% Co).....240

Figure 5.27 The specific saturation magnetization of a dispersion measured at various time intervals. The sample was prepared using 1 g $\text{Co}_2(\text{CO})_8$, and 1 g of 15k-2k-2k-2k-15k PDMS-PMTEOS-PCPMS-PMTEOS-PDMS terpolymers in 20 mL PDMS (approximately 1.6% Co).....241

Figure 5.28 The specific saturation magnetization of a dispersion measured at various time intervals. The sample was prepared using 1 g $\text{Co}_2(\text{CO})_8$, and 1 g of 15k-4k-2k-4k-15k PDMS-PMTEOS-PCPMS-PMTEOS-PDMS terpolymers in 20 mL PDMS (approximately 1.6% Co).....242

Figure 5.29 Comparison of average percent loss per day within a four-month experimental period between coated and uncoated-nanoparticles in an air-containing atmosphere.....243

List of Tables

Table 2.1 Structural units of the polysiloxanes.....	7
Table 2.2 Natural abundance of silicon isotopes.....	8
Table 2.3 Silicon and carbon bond rotational energy barriers.....	10
Table 2.4 Comparison of silicon, carbon and oxygen radii.....	11
Table 2.5 Approximate bond dissociation energies.....	13
Table 2.6 Polysiloxane products and application areas.....	14
Table 2.7 Typical cyclosiloxane monomers used in the ring-opening polymerization...	19
Table 2.8 Influence of the reaction conditions on the position of the equilibrium.....	21
Table 2.9 Influence of the substituents on cyclosiloxane tetramers on the yield of linear polymers.....	22
Table 2.10 Classification of materials based on magnetic properties.....	71
Table 2.11 Properties of magnetic fluids.....	76
Table 2.12 Advantages and disadvantages of typical carrier fluids in magnetic fluids.....	78
Table 2.13 Classes of suitable cobalt precursors for preparing cobalt dispersions via thermal decomposition	84
Table 2.14 Physical properties of metal carbonyls.....	85
Table 2.15 Effect of polymer composition on particle size upon decomposition of $\text{Co}_2(\text{CO})_8$ in toluene.....	88
Table 2.16 Influence of commercial surfactants on colloidal stability and particle size upon decomposing $\text{Co}_2(\text{CO})_8$ in toluene.....	89
Table 2.17 Classes of solvents used in preparing cobalt dispersions.....	90
Table 2.18 Distinguished features of retinal detachment.....	99

Table 3.1 The formulations used for preparing triblock copolymers with different block lengths.....	108
Table 3.2 Number average molecular weight calculations of the PCPMS central block.....	122
Table 3.3 Summary of the calculated M_n of the PCPMS central block determined via potentiometric titration.....	123
Table 3.4 Summary of the calculated M_n of the PDMS-PCPMS-PDMS triblock copolymers determined via combinations of titration and ^1H NMR.....	126
Table 4.1 Sample codes and cobalt concentrations of dispersions used for magnetic measurements.....	139
Table 4.2 Hydrodynamic radii measured by dynamic light scattering demonstrate large increases in radii at the cmc, consistent with formation of micellar structures.....	146
Table 4.3 Particle size control studies: (A) effects of the ratio of $\text{Co}_2(\text{CO})_8$ to copolymer; (B) effects of the concentration of toluene in the reaction mixtures	158
Table 4.4 The theoretical d-spacing values of fcc and hcp crystal structures of cobalt.....	181
Table 4.6 The ratio of d-spacing values of hcp and fcc cobalt crystal structures compared to the inversed ratio of the corresponding R values.....	183
Table 5.1 Reactant concentrations for preparing pentablock terpolymers with various PMVS block molecular weights.....	191
Table 5.2 Reactants used for preparing pentablock terpolymers with various PMTEOS or PMTMOS block molecular weights.....	193
Table 5.3 An example calculation of the amounts of water needed for preparing silica-coated cobalt nanoparticle dispersions.....	195
Table 5.4 Summary of silica-coated cobalt nanoparticles prepared via sol-gel process.....	234
Table 5.5 Quantitative %cobalt in dispersions prepared in 2000 g/mol PDMS using various pentablock terpolymers.....	235

CHAPTER 1

Introduction

Retinal detachment is one of the most common diseases in the posterior segment of the eye. It is a major cause of vision loss in the adult population. Detachment occurs when vitreous fluid gradually passes through a break in the retina, resulting in the separation of the retina and choroid.

Current treatments for retinal detachment utilize scleral buckles and internal tamponades. Scleral buckling involves the use of encircling silicone bands sewn onto the sclera to compress the wall of the eye inward to close the holes in the retina.¹ This technique is invasive and produces an uneven and discontinuous surface on the sclera of the eye leading to excessive and unwanted pressure applied to a non-target area of the sclera. Injection of gases or liquids as internal tamponades into the vitreous cavity to seal the retinal breaks is an alternative to scleral buckling.² However, this technique provides only partial support to the retina. In addition, the internal tamponades fill up the vitreous cavity, which can decrease vision, and they also contact anterior segments (lens and cornea), which might cause cataracts.

The goal of this dissertation research has been to develop a magnetic internal tamponade from modified biocompatible silicone fluids containing stable cobalt nanoparticles for treating retinal detachment. These magnetic fluids would be held in place with an external magnetized scleral buckle to form a ring of magnetic silicone fluid in the vitreous fluid in apposition to the retinal periphery (Figure 1.1). Precedents have been reported in using an elastic silicone band as the scleral buckle.³ This method will provide 360° internal tamponades. In addition, the vitreous

¹ F. W. Newell, In *Ophthalmology: Principles and Concepts*, 6th Ed., The C.V. Mosby Company, St. Louis (1986)

² J. P. Dailey, J. P. Phillips, C. Li and J. S. Riffle, *J. Magn. Magn. Mat.*, **194**, 140-148 (1999)

³ Jap. Pat. JP 03011714 to Kanegafuchi Chemical Industry Co., Ltd., 1991.

cavity would be free of the magnetic fluid, and there would be no contact with anterior segments of the eye.

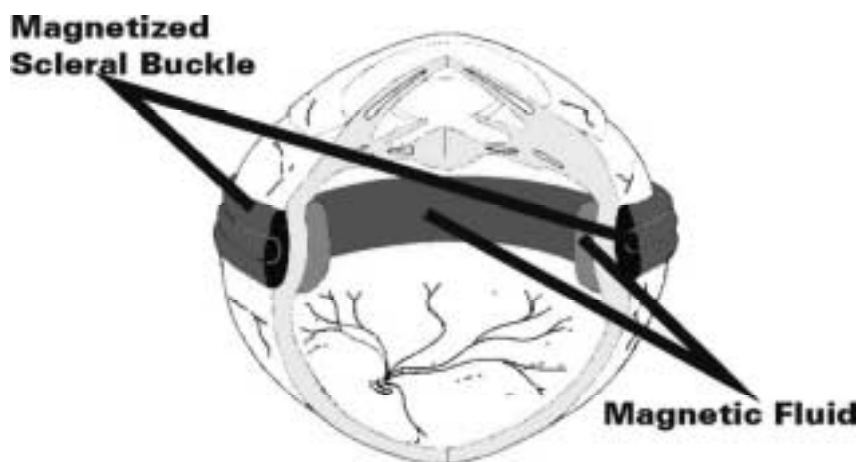


Figure 1.1 An internal tamponade using silicone magnetic fluids.²

Cobalt nanoparticles have been prepared via thermolysis of dicobalt octacarbonyl ($\text{Co}_2(\text{CO})_8$) in either toluene or PDMS carrier fluids in the presence of poly(dimethylsiloxane-*b*-(3-cyanopropyl)methylsiloxane-*b*-dimethylsiloxane) triblock copolymer (PDMS-*b*-PCPMS-*b*-PDMS) steric stabilizers (Figure 1.2) to produce ≈ 10 nm diameter cobalt particles. The central nitrile-functional blocks coordinate with the cobalt surface as an anchor block and the PDMS tail blocks extend into the carrier fluids to maintain the dispersion via an entropic mechanism (Figure 1.3). Chapter 3 presents the synthesis and characterization of PDMS-*b*-PCPMS-*b*-PDMS triblock copolymers. The preparation of magnetic cobalt nanoparticles and their properties are described in Chapter 4.

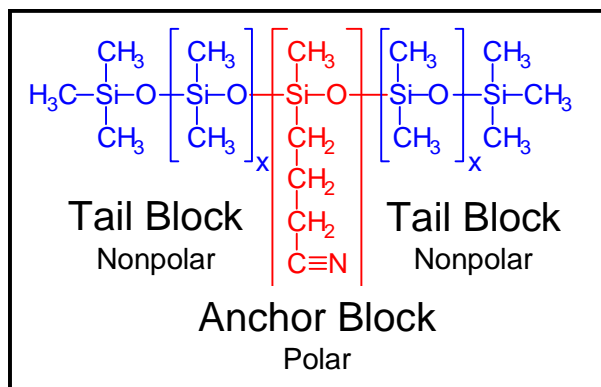


Figure 1.2 Chemical structure of PDMS-*b*-PCPMS-*b*-PDMS steric stabilizers.

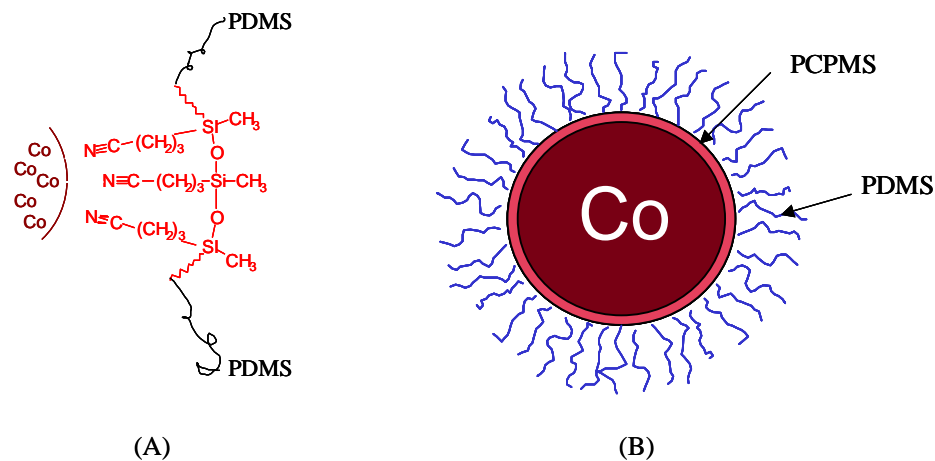


Figure 1.3 Steric stabilization of cobalt nanoparticles using PDMS-*b*-PCPMS-*b*-PDMS Stabilizers, A) showing nitrile-functional blocks bound to the particle surface, and B) showing PDMS blocks providing steric stabilization.

Environmental oxidation, which substantially suppresses their magnetic susceptibility over time, is a major drawback of magnetic cobalt nanoparticles. One method for inhibiting or eliminating oxidation is to coat the cobalt nanoparticles with oxygen-impermeable “pseudo-silica” thin films. Preparations of polysiloxane block terpolymer stabilizers containing alkoxy silane blocks as sol-gel process precursors, and of cobalt nanoparticles using these terpolymers as stabilizers, are discussed in Chapter 5. In addition, the magnetic properties of the nanoparticles over time will also be discussed.

CHAPTER 2. Literature Review

2.1. Overview

This chapter will focus primarily on the areas related to the research topic. It is divided into five sections. The first section will discuss polysiloxane chemistry including their physical properties, the preparation of cyclic siloxane monomers and the synthesis of polysiloxanes by both thermodynamic and kinetic control. Siloxane block copolymers prepared via an anionic living polymerization (kinetic control) will be discussed in detail. Formation of block copolymers having micelle structures in solution is also another important issue in this research. Because the sol-gel process was employed to stabilize cobalt particles against oxidation, sol-gel chemistry will be covered in the second section. In the third section, magnetic properties and nanoparticles will be introduced. Terminology related to magnetic properties which will be used throughout this dissertation will be defined in this section.

Preparation of stable cobalt dispersions via thermal decomposition of $\text{Co}_2(\text{CO})_8$ and reduction of CoCl_2 will be discussed in the fourth section. Because the first process is directly related to this dissertation, the physical properties of $\text{Co}_2(\text{CO})_8$ and the reaction conditions used will be covered in detail. The final section introduces retinal detachment and current treatments for this modality.

2.2 Introduction to the synthesis of polysiloxanes

2.2.1. Introduction to polysiloxanes

Polysiloxanes or silicones have been the most extensively-studied class of semi-inorganic polymers over the last forty years. They are structurally comprised of silicon atoms bound to

each other through oxygen atoms. Because of the combination of inorganic and organic character in their backbones, polysiloxanes provide a wide range of properties that are not found in other organic polymers. The term 'silicones' was first created because their structural units (R_2SiO) appear to be analogous to those of 'ketones' (R_2CO). However, structural studies show that, unlike $C=O$ in ketones, the $Si=O$ is unstable.⁴ Thus, $Si-O-Si$ single bonds form which lead to polymeric compounds. The term 'polysiloxane' was then proposed to be used instead of 'silicones.' The 'polysiloxane' nomenclature is based on the structure of the repeating unit in the polymer backbone (sil+oxane). However, the conventional 'silicone' terminology is still widely used, especially for technical, polymeric products, e.g., silicone rubber, silicone resins and silicone oils.

Therefore, silicones or polysiloxanes can be categorized according to their structure as follows:

1. They are polymeric compounds.
2. The backbone contains $Si-O$ bonds throughout the chains. They are thus basically analogous to the structural units of silicic acids and silicates.
3. Each silicon atom in polysiloxanes can be covalently bound to one, two or three organic hydrocarbon substituents, resulting in trifunctional (T), difunctional (D) or monofunctional (M) siloxanes, respectively (Table 2.1).⁴

⁴ W. Noll, In Chemistry and Technology of Silicones, Academic press Inc., New York (1968)

Table 2.1 Structural units of the polysiloxanes.⁴

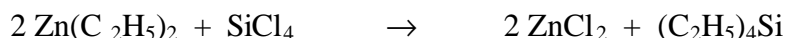
Structural formula	Composition	Functionality	Symbol
$\begin{array}{c} \text{R} \\ \\ \text{---Si---O---} \\ \\ \text{R} \end{array}$	$\text{R}_3\text{SiO}_{1/2}$	Monofunctional	M
$\begin{array}{c} \text{R} \\ \\ \text{---O---Si---O---} \\ \\ \text{R} \end{array}$	$\text{R}_2\text{SiO}_{2/2}$	Difunctional	D
$\begin{array}{c} \text{R} \\ \\ \text{---O---Si---O---} \\ \\ \text{O} \end{array}$	$\text{RSiO}_{3/2}$	Trifunctional	T
$\begin{array}{c} \text{O} \\ \\ \text{---O---Si---O---} \\ \\ \text{O} \end{array}$	$\text{SiO}_{4/2}$	Tetrafunctional	Q

The elementary abundance of silicon found in the earth's crust is approximately 27.6%, second only to oxygen, 46.4%.⁵ The natural abundance of the ²⁹Si isotope with spin 1/2 (NMR active) is only about 4.7% (Table 2.2).⁶

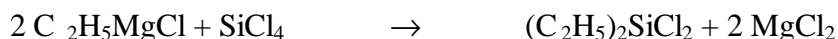
Table 2.2 Natural abundance of silicon isotopes.³

Isotope	Abundance	Spin quantum number, I
²⁸ Si	92.18	0
²⁹ Si	4.71	1/2
³⁰ Si	3.21	0

Historically, the synthesis of organosilicon compounds was first documented in 1863-1880 by Friedel and Craft, and later by Ladenburg.⁴ They found that the alkylation of silicon compounds could be achieved by heating dialkylzincs with silicon tetrachloride at about 160 °C.



Since then, numerous documents on organosilicon chemistry have been reported for over 100 years. One of the prominent chemists in this field was Frederick Stanley Kipping, who published over 57 papers from 1910 to 1940.^{4,7,8} His major contribution was to demonstrate the successful preparation of organosilicon compounds via the Grignard reaction.



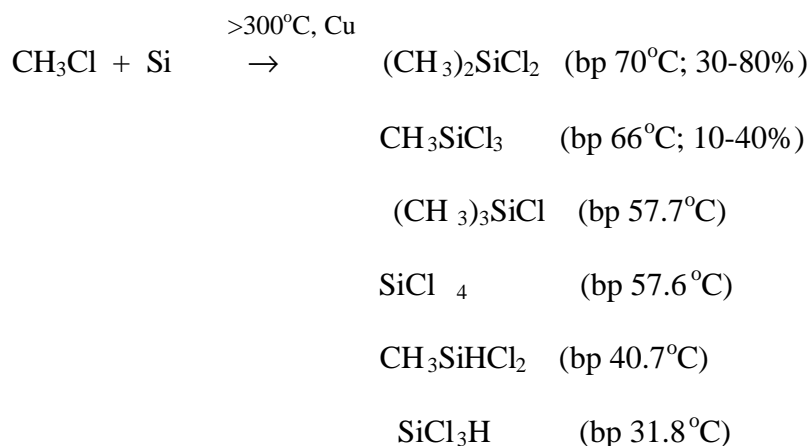
⁵ B. Mazumder, In Silicon and Its Compounds, Science Publishers, New Hampshire (2000)

⁶ R. B. Sosman, In The Properties of Silica, The Chemical Catalog Company, New York (1927)

⁷ E. G. Rochow, In Silicon and Silicones, Springer-Verlag, Germany (1987)

⁸ M. A. Brook, In Silicon in Organic, Organometallic and Polymer Chemistry, John Wiley&Sons, Inc., New York (2000)

In 1941-1942, a major change in organosilicon chemistry took place when Eugene Rochow and Richard Muller discovered the direct synthesis of methylchlorosilanes, the so-called “Rochow synthesis”.^{8, 9, 10}



Although the reaction produces a number of products, dichlorodimethylsilane ((CH₃)₂SiCl₂), the desired product, can be produced in yields up to 80%. Dichlorodimethylsilane is commonly used as a reactive precursor for preparing cyclosiloxane monomers.

Polysiloxanes are highly flexible molecules due to their exceptionally low bond rotational energy barrier around Si-O bonds compared to hydrocarbons (Table 2.3).^{11, 12, 13} This freedom of rotation imparts unique and intriguing properties to these materials, e.g., an extremely low glass transition temperature (≈-125 °C for polydimethylsiloxane, PDMS), a large molar volume (75.5 cm³/mole)¹⁴, low surface tension (≈20 mN/m for PDMS)^{15, 16} and low viscosity. This is

⁹ J. M. Zeigler and F. W. Gordon Fearon (Eds.), In *Silicon-Based Polymer Science: A Comprehensive Resource*, Advances in Chemistry Series 224, American Chemical Society, Washington DC (1990)

¹⁰ G. Koerner, M. Schulze and J. Weis, In *Silicones: Chemistry and Technology*, Vulkan-Verlag, Germany (1991)

¹¹ F. O. Stark, J. R. Falendar and A. P. Wright, In *Comprehensive Organometallic Chemistry*, v.2, Pergamon Press, New York (1982)

¹² F. Liebau, In *Structural Chemistry of Silicates: Structure, Bonding and Classification*, Springer-Verlag, New York (1985)

¹³ L. V. Myshlyaeva and V. V. Krasnoshchekov, In *Analytical Chemistry of Silicon*, Translated by J. Schmorak, John Wiley and Sons, New York (1974)

¹⁴ C. B. Hurd, *J. Am. Chem. Soc.*, **68**, 364 (1946)

¹⁵ X. Chen and J. A. Gardella JR., *Macromolecules*, **27**, 12 (1994)

¹⁶ R. J. Roe, *J. Phys. Chem.*, **72**, 2013 (1968)

generally due to the long Si-O bonds combined with the open structure of the polysiloxane backbone. The Si-O skeleton bond has a length of 1.64 Å which is significantly longer than C-C single bonds (1.53 Å) in organic compounds. This leads to a reduction of steric interferences or intramolecular congestion. In PDMS, the bond angles of 143° in Si-O-Si and 110° in O-Si-O are significantly more than the tetrahedron bond angle of 110° in hydrocarbon chains, resulting in a more open structure and the low rotational energy barrier in polysiloxanes (Figure 2.1). In addition, the oxygen atoms in the siloxane skeleton are relatively small (Table 2.4) and are not burdened with side groups, thus allowing the chains to have a high freedom of rotation.

Table 2.3 Silicon and carbon bond rotational energy barriers.^{11, 12, 13}

Bond	Energy (kJ/mole)
Si-O	< 0.8
C-O	11.3
Si-CH ₃	6.7
C-CH ₃	15.1

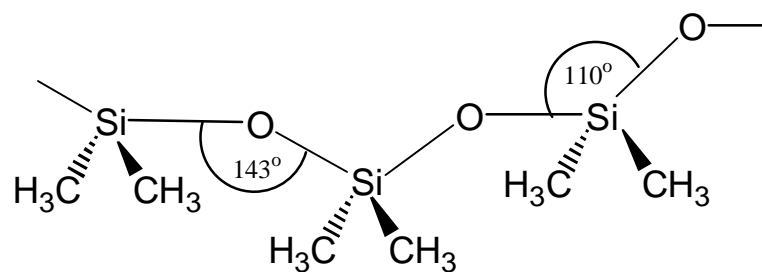


Figure 2.1 PDMS chains showing bond angles in the siloxane skeleton.⁹

Table 2.4 Comparison of silicon, carbon and oxygen radii.^{4, 8}

Element	Atomic Radii (angstrom)	Covalent Radii (angstrom)
Si	1.06	1.17
C	0.66	0.77
O	-	0.66

In the absence of acid or base, polysiloxanes are highly thermally stable. Degradation of PDMS starts at about 350 °C which is generally significantly higher than for other organic compounds. This is primarily because the bond dissociation energy of Si-O bonds is significantly higher than that of C-C bonds or C-O bonds (Table 2.5).⁸ In addition, the partial ionic character of the Si-O bond contributes to its thermal stability.

Polysiloxanes are widely used in electrical applications due to their excellent electrical resistance. The relative permittivity of PDMS fluids is about 2.75 which is significantly lower than 20.7 and 78.5 for acetone and water, respectively.⁸

Another very interesting property of polysiloxanes, especially PDMS, is their exceptional hydrophobicity. This is a consequence of the unusually high flexibility of the chains which allows the pendent methyl groups to orient toward the hydrophobic air interface resulting in a hydrophobic surface.

The wide range of polysiloxane applications is summarized in Table 2.6.¹⁷ These applications include silicone fluids, silicone resins, siloxane-containing room-temperature-vulcanized (RTV) rubbers and siloxane-containing heat-cured rubbers.^{18, 19, 20}

¹⁷ H. F. Mark, N. M. Bikales, C. G. Overberger, G. Menges and J. I. Kroschwitz (Eds.), In Encyclopedia of Polymer Science and Engineering, v. 15, Wiley-Interscience Publication, New York (1990), p.204-308.

¹⁸ S. Pawlenko, In Organosilicon Chemistry, Walter de Gruyter, Berlin (1986)

¹⁹ W. Lynch, In Handbook of Silicone Rubber Fabrication, Van Nostrand Reinhold Co., New York (1978)

²⁰ P. F. Bruins, In Silicone Technology, Interscience Publisher, New York (1970)

Table 2.5 Approximate bond dissociation energies.⁸

Bond	Compound	Bond Energy (kJ/mole)
Si-O	Me ₃ Si-OH	536
	Me ₃ Si-OMe	477
	Me ₃ Si-OEt	484
	Me ₃ Si-OSiMe ₃	549
C-C	H ₃ C-CH ₃	334
C-O	Me ₃ C-OH	340

Table 2.6 Polysiloxane products and application areas.¹⁷

Silicone Fluids	Silicone Resins
Plastic additives Hydraulic fluids Vibration damping Release agents Antifoamers Dielectric media Water repellence Surfactants Greases Coagulants Particle and fiber treatments Cosmetic and health product additives Heat-transfer media Polishes Lubricants	Varnishes Paints Molding compounds Protective coatings Encapsulants Junction coatings Electric insulation Pressure-sensitive adhesives Laminates Release coatings Adhesives
RTV Rubbers	Heat-Cured Rubbers
Sealants Adhesives Conformal coatings Gaskets Foams Molding parts Encapsulants Electric insulation Glazing Medical implants Surgical aids Mold making	Tubing and hoses Belting Wire-cable insulation Surgical aids Fuel-resistant rubber parts Penetration seals Molded parts Embossing-calendering rollers Extruding Medical implants Laminates Electrically conducting rubber Fabric coating Foams

2.2.2. Preparation of cyclosiloxanes

Cyclosiloxanes can be prepared via various procedures. Since dichlorodimethylsilanes are commercially available, hydrolysis of these reactive precursors is the most common method for preparing cyclosiloxanes. Dichlorodimethylsilane can be easily hydrolyzed to give an unstable diol which spontaneously undergoes condensation to produce mixtures of polydimethylsiloxanes (PDMS) and dimethylsiloxane cyclics (Figure 2.2).²¹ The cyclics, predominantly x=4-6, can be recovered by fractional distillation.

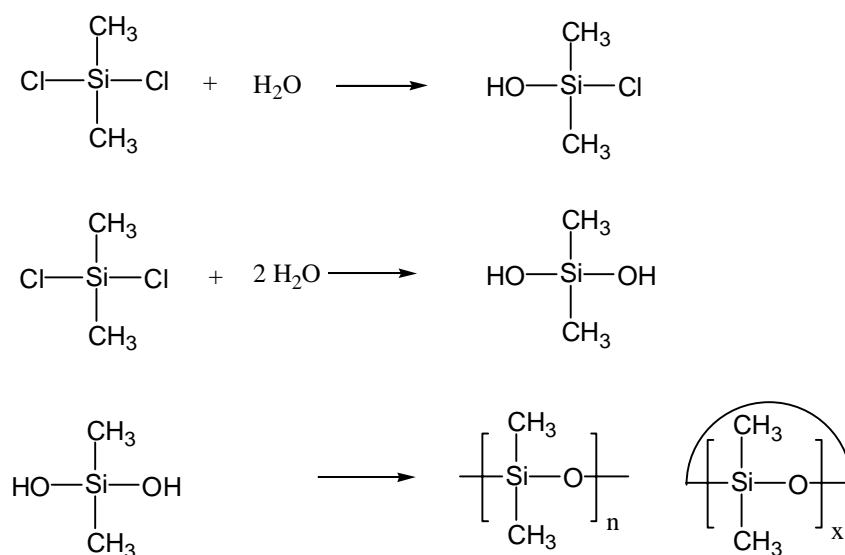


Figure 2.2 Hydrolysis of dichlorodimethylsilane to produce polydimethylsiloxanes (PDMS) and dimethylsiloxane cyclics.²¹

²¹ K. C. Frisch, In *Cyclic Monomers*, Wiley&Sons, New York (1972)

The proportions of the linear and cyclic siloxanes generated strongly depends on the reaction conditions. To obtain high yields of cyclosiloxanes, it is necessary to increase intramolecular condensation and simultaneously control the extent of intermolecular condensation in such a way that the degree of the condensation is about 4. Intramolecular condensation is facilitated over intermolecular condensation by low concentrations of the reactants. Thus, the slow addition of dimethyldichlorosilane to an excess of water favors the production of cyclics.²² If a solvent is used in the reaction, a water-miscible solvent, e.g., methanol, also favors the production of the cyclics. The polarity of the solvent also has a significant effect on formation of cyclic compounds. For example, hydrolysis of dichlorodiethylsilane in ether yields 41% trimer (Et₂SiO)₃, and 31% tetramer (Et₂SiO)₄, whereas the hydrolysis in aqueous methanol yields 70% tetramer without trimer produced.²³ In addition, it has been reported that reaction under strongly acidic conditions can promote the formation of cyclics and low molecular weight polymers. On the other hand, reaction in a basic medium predominantly yields high molecular weight linear polysiloxanes.²⁴

The thermodynamically stable cyclotetrasiloxane, D₄, is typically manufactured by the process discussed above. It is commonly used as a monomer for the equilibrium reaction to prepare PDMS because of its cost-effectiveness. The strained cyclotrisiloxane, D₃, is typically used as a monomer for living anionic polymerization. Hexamethylcyclotrisiloxane is commercially prepared using 1,3-dihydroxy-1,1,3,3-tetramethyldisiloxane and dichlorodimethylsilane in the presence of pyridine as a proton scavenger (Figure 2.3).^{25, 26} Condensation of dichlorodimethylsilane in the presence of 10 mol% excess of zinc oxide also

²² N. N. Sokolov and S. M. Akimova, *J. Gen. Chem. (USSR)*, **26**, 2276 (1956); 2545 CB trans.

²³ D. G. Dobay, U. S. Patent 2,769,829 (1956)

²⁴ W. I. Patnode and D. F. Wilcock, *J. Am. Chem. Soc.*, **68**, 362 (1946)

²⁵ P. I. Prescott and T. G. Selin, U. S. Paten 3,317,578 assigned to General Electric Company (1967)

²⁶ N. Grassie, K. F. Francey and I. G. MacFarlane, *Polym. Degrad. and Stab.*, **2**, 67 (1993)

yields hexamethylcyclotrisiloxane.^{27, 28} Cyclotrisiloxanes with different substituents can be prepared by the same process using corresponding precursors.

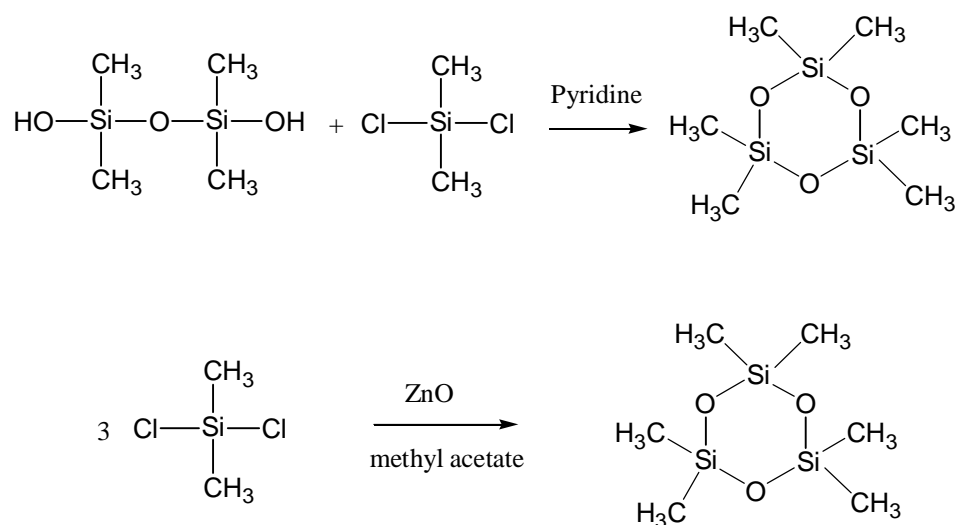


Figure 2.3 Preparation of hexamethylcyclotrisiloxane.^{25, 26}

²⁷ T. Takiguchi, M. Sakurai and T. Kishi, *J. Org. Chem.*, **25**, 310 (1960)

²⁸ B. Momper, T. Wagner, U. Maschke, M. Ballauff and E. W. Fisher, *Polym. Commun.*, **31**, 186 (1990)

2.2.3 Equilibrium ring-opening polymerization of cyclosiloxanes: thermodynamic control

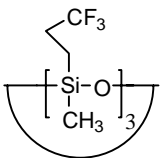
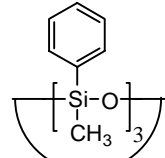
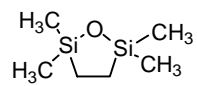
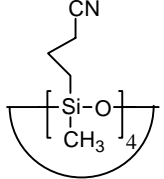
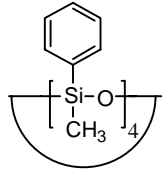
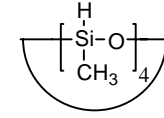
Two general routes commercially used for preparing polysiloxanes are acid and base-catalyzed equilibration polymerizations. Unstrained cyclics, e.g., D₄, are typically used as monomers for preparing polysiloxanes via this process. Utilization of a strained cyclic, e.g., tricyclosiloxane or D₃ (12-15 kJ/mole) has also been reported.²⁹ Other monomers which have been used in this process, including both strained and unstrained rings, are shown in Table 2.7. It is well known that siloxane bonds are exceptionally thermally stable. In the presence of strong acid or base, however, rearrangement or the so-called ‘redistribution’ or ‘equilibration’ of the siloxane bond takes place (Figure 2.4).³⁰ The siloxane bonds in both cyclic and linear species are continuously broken and reformed until the reaction reaches the thermodynamic equilibrium state. At equilibrium, a distribution of cyclics and linear polymers are obtained. The molecular weights of these linear polymers have a relatively broad, Gaussian distribution compared to the distributions produced via living anionic polymerization.³¹

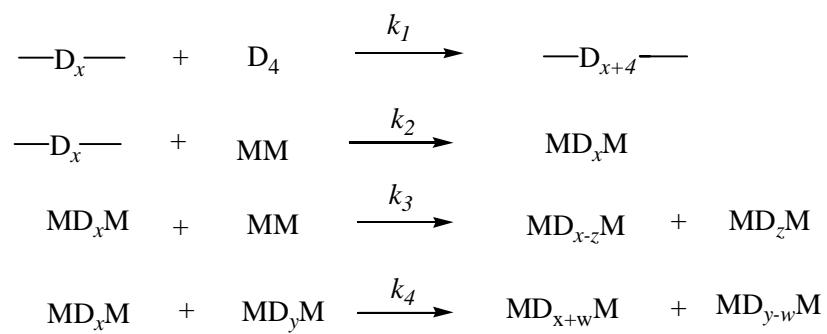
²⁹ J. Chajnowski, In *Siloxane Polymers*, S. J. Clarson and J. A. Semlyen (Eds.), PTR Prentice Hall, Englewood Cliffs, New Jersey (1993)

³⁰ S. W. Kantor, W. T. Grubb and R. C. Osthoff, *J. Am. Chem. Soc.*, **76**, 5190-5197 (1954)

³¹ D. J. Brunelle (Ed.), In *Ring-Opening Polymerization; Mechanisms, Catalysis, Structure, Utility*, Hanser Publishers, Germany (1993)

Table 2.7 Typical cyclosiloxane monomers used in the ring-opening polymerization.⁹

Strained Rings	Unstrained Rings
<p style="text-align: center;">D₃</p>   	<p style="text-align: center;">D₄, D₅, D₆, D₇</p>   



where $k_1 \gg k_2, k_3$

$k_4 > k_2, k_3$

$k_2 = k_3$

Figure 2.4 Equilibration reactions of siloxanes.³⁰

The percentages of cyclics and linear polymers at equilibrium are influenced by substituents on the silicon atoms as well as the reaction conditions (Table 2.8^{32, 33, 34} and 2.9²⁹). The cyclic and linear polymer concentrations at equilibrium depend on the Gibbs free energy change (ΔG). ΔG is made up of two important parameters, polymerization enthalpy change (ΔH) and polymerization entropy change (ΔS), along with the temperature with respect to the fundamental thermodynamic equation^{35, 36}:

$$\Delta G = \Delta H - T\Delta S.$$

Table 2.8 Influence of the reaction conditions on the position of the equilibrium.^{9, 32, 33, 34}

Conditions	Linear Polymers	D ₄	D ₅ -D ₉
135°C, toluene, KOH ³²	29	33	31
20°C, benzene, Li cryptate ³³	70	2.7	11.5
20°C, CH ₂ Cl ₂ , CF ₃ SO ₃ H ³⁴	28	32	27
20°C, CH ₂ Cl ₂ , CF ₃ SO ₃ H-(CF ₃ SO ₂) ₂ O ³⁴	0	38	22

³² J. B. Carmichael, D. J. Gordon F. J. Isackson, *J. Phys. Chem.*, **71**, 2011 (1967)

³³ S. Boileau, In Ring Opening Polymerization, J. E. McGrath (Ed.), ACS Monograph 286, American Chemical Society, Washington, DC, p.23 (1985)

³⁴ G. Sauvet, J. J. Lebrun and P. Sigwalt, In Cationic Polymerization and Related Processes, E. J. Goethals, Ed., Academic, New York, p.237 (1984)

³⁵ M. Spinu and J. E. McGrath, *J. Polym. Sc., Part A, Polym. Chem.*, **29**, 657-670 (1991)

³⁶ P. C. Painter and M. M. Coleman, In Fundamental of Polymer Science; An Introduction Text, 2nd ed., Technomic Publishing, Pennsylvania (1997)

Table 2.9 Influence of the substituents on cyclosiloxane tetramers on the yield of linear polymers²⁹: R and R' are substituents in the same silicon atom.

R	R'	Approximate Yield (%)
Me	Me	82
Me	Et	74
Me	CF ₃ CH ₂ CH ₂	17
Ph	Me	70
Ph	Ph	0

If polymerization occurs, ΔG must yield a negative value for the transformation of cyclic siloxanes to linear structures. Because there is no net change of chemical bonding in the polymerization of the unstrained D₄, ΔH is nearly zero. Therefore, ring-opening polymerization of D₄ is driven only by ΔS (6.7 J/mole-K)^{37, 38}, including entropy due to mixing of cyclics and polymers (+), configurational entropy change (+) and translational entropy change (-).³⁹ This positive value of ΔS is very infrequent for polymerization reactions.

Another important variation in this system is to use siloxane dimers or end-blocking reagents to control molecular weights of the polymers. These 'end-blockers' usually contain not only Si-O-Si bonds, but also Si-C bonds which cannot undergo the interchange in the equilibration. As a result, the polymers are blocked at the chain terminals providing a strategy to

³⁷ C. L. Lee and O. K. Johanson, *J. Polym. Sci.*, **A-1**(4), 3013 (1966)

³⁸ C. L. Lee and O. K. Johanson, *J. Polym. Sci. Polym. Chem. Ed.*, **14**, 729 (1976)

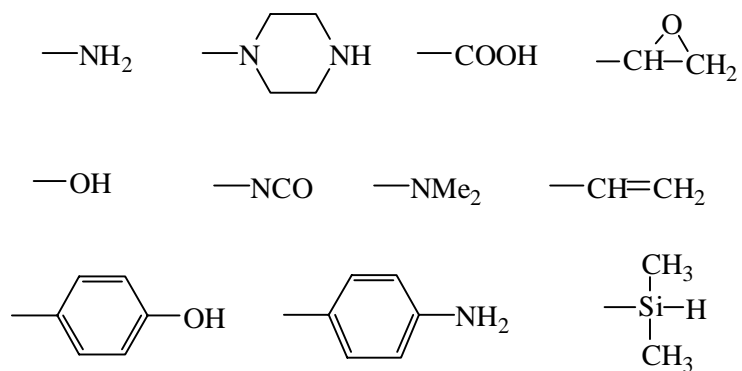
³⁹ C. Li, In Preparation of Nitrile Containing Siloxane Triblock Copolymers and Their Applications As Stabilizers for Siloxane Magnetic Fluids, Master Thesis, Virginia Tech (1996)

efficiently target the molecular weight of the polymers. A wide variety of functional groups can be employed at the chain termini, which can also be further reacted with other functional groups to form siloxane-containing block copolymers or networks.⁴⁰ Variations of backbone composition is another alternative method of introducing functional groups into the polymer chains. Variations of functional endgroups and backbone compositions which have been employed are depicted in Figure 2.5.⁴¹

⁴⁰ J. E. McGrath, In Ring-Opening Polymerization, J. E. McGrath (Ed.), ACS Monograph 286, American Chemical Society, Washington, DC, p.1 (1985)

⁴¹ I. Yilgor, J. S. Riffle and J. E. McGrath, In Reactive Oligomers, v.282, Reactive Difunctional Siloxane Oligomers, F. W. Harris and H. J. Spinelli (Eds), p.161, American Chemical Society, Washington DC, (1985)

Functional End Groups



Backbone Composition

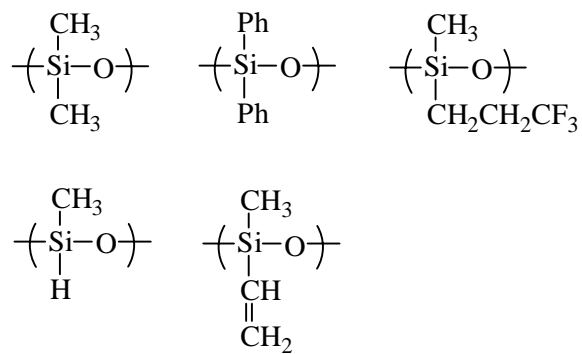


Figure 2.5 Variations of functional endgroups and backbone compositions.⁴¹

The average molecular weights of linear polymers prepared by this method can be estimated using the following simple equation:²⁹

$$M_n = \frac{2 \cdot [-R_2SiO-]_{eq} \cdot M_o}{[endgroup]}$$

where $[-R_2SiO-]_{eq}$ is the concentration of the siloxane unit in the linear chains at equilibrium, M_o is the molecular weight of the siloxane repeat unit and $[endgroup]$ is the concentration of the endgroup. If siloxane dimers are utilized as endblocking reagents, the factor 2 is omitted.

2.2.3.1 Acid-catalyzed ring-opening equilibration

A wide variety of catalysts, both in homogeneous and heterogeneous processes, have been used in this reaction, such as ion-exchange resins^{42, 43}, UV radiation⁴⁴, Lewis acids, electron-deficient organosilicon reagents^{45, 46, 47} and organic acids. Trifluoromethanesulfonic acid (triflic acid)^{48, 49, 50} has been used most extensively. Other catalysts, e.g., dodecylbenzenesulfonic acid⁵¹, metals (Pt, Co and Rh)⁵² and tris(4-methylphenyl)sulfonium hexafluoroantimonate⁵³ have also been recently reported. Many mechanisms have been proposed but the acid-catalyzed equilibration mechanism is still not fully understood.¹⁷ It has

⁴² M. Cazacu, M. Marcu, A. Vlad, D. Caraiman and C. Racles, *Eur. Polym. J.*, **35**(9), 1629-1635 (1999)

⁴³ M. T. Btyk, N. N. Baglei and O. D. Kurilenko, *Vysokomol. Soedin., Ser.A*, **17**(5), 1034-9 (1975)

⁴⁴ K. D. Belfield and G. Zhang, *Polym. Bull. (Berlin)*, **38**(2), 165-168 (1997)

⁴⁵ Q. Wang, G. K. Surya Prakash, G. A. Olah, P. Donal and B. Ketherine, *Recnet Res. Dev. Polym. Sci.*, **2**(pt.2), 555-567 (1998)

⁴⁶ Q. Wang, H. Zhang, G. K. Surya Prakash, T. E. Hogen-Esch and G. A. Olah, *Macromolecules*, **29**, 6691-6694 (1996)

⁴⁷ G. A. Olah, Q. Wang, G. Golam, G. K. Surya Prakash, H. Zhang, T. E. Hogen-Esch, *Polym. Prepr. (Am. Chem. Soc., Div. Polym. Chem.)*, **37**(1), 805-806 (1996)

⁴⁸ G. Toskas, G. Besztercey, M. Moreau, M. Masure and P. Sigwalt, *Macromol. Chem. Phys.*, **196**(9), 2715-35 (1995)

⁴⁹ P. Sigwalt, M. Masure, M. Moreau and R. Bischoff, *Makromol. Chem., Macromol. Symp.*, **73**, 146-166 (1993)

⁵⁰ M. Rodriguez-Baeza and M. Zapata, *Polym. Bull. (Berlin)*, **36**(2), 173-180 (1996)

⁵¹ S. Maisonnier, J. C. Favier, M. Masure and P. Hemery, *Polym. Int.*, **48**(3), 159-164 (1999)

⁵² J. V. Crivello and M. Fan, *Macromol. Symp.*, **77**, 413-421 (1994)

⁵³ K. D. Belfield and G. Zhang, *Polym. Prepr. (Am. Chem. Soc., Div. Polym. Chem.)*, **36**(2), 267-8 (1995)

been proposed that, in the presence of a protonic acid, e.g., sulfuric acid, the oxygens in siloxanes are first protonated to form $\equiv\text{Si}^+\text{OH-Si}\equiv$ species. These protonated species are then attacked by nucleophiles at the partially positive silicon atoms and eventually the Si-O bonds cleave (Figure 2.6).³⁰ Wilczek, Chojnowski, and Sigwalt have proposed a mechanism for ring-opening polymerization using triflic acid as a catalyst (Figure 2.7).^{9, 34, 54, 55, 56} Analogous mechanisms may be operative for H_2SO_4 -catalyzed systems.

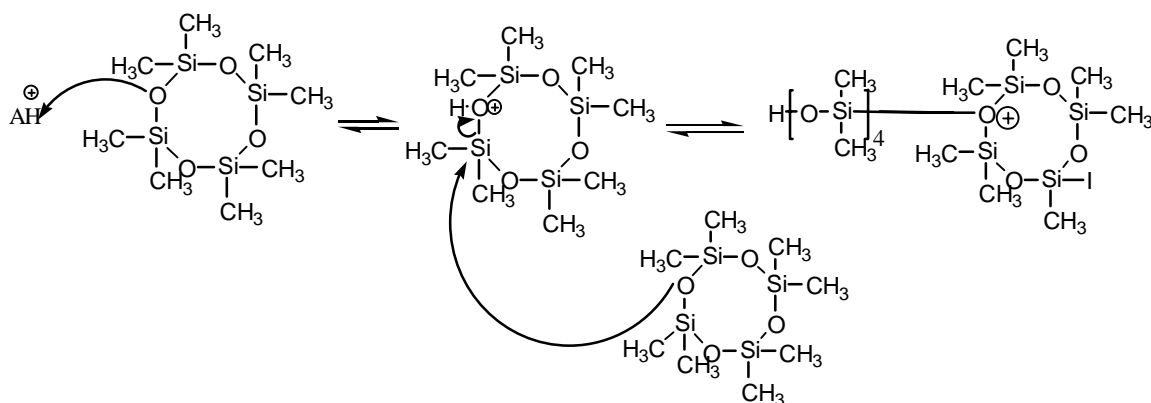


Figure 2.6 Proposed mechanism of acid-initiated ring-opening polymerization of D₄.³⁰

⁵⁴ J. Chojnowski and L. Wilczek, *Makromol. Chem.*, **180**, 117-130 (1979)

⁵⁵ P. Sigwalt, *Polym. J.*, **19**, 567 (1987)

⁵⁶ L. Wilczek, S. Rubinsztain and J. Chojnowski, *Macromolecule*, **20**, 2345-2355 (1987)

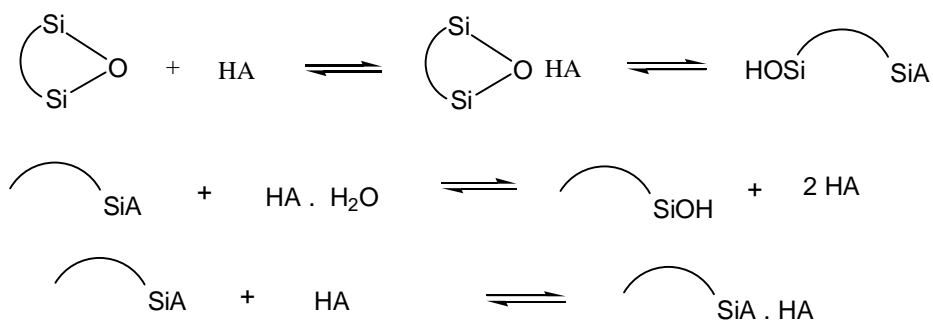
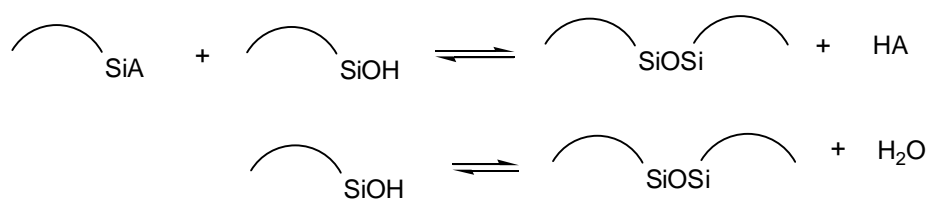
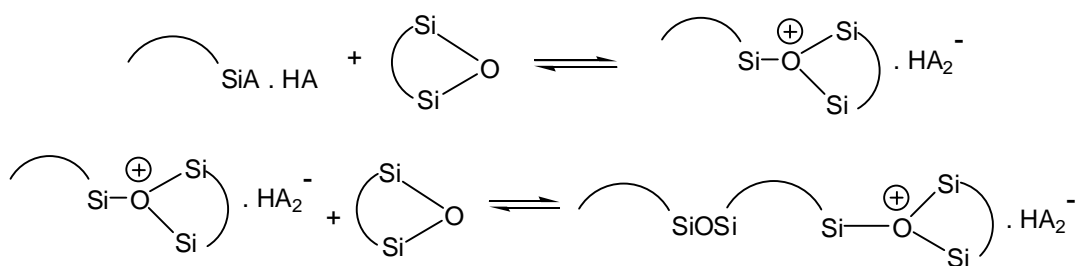
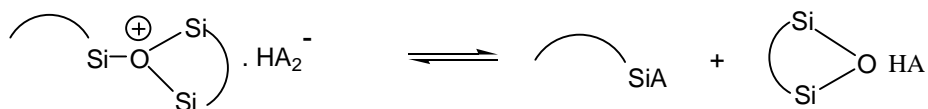
Initiation;**Step Growth;****Chain Growth;****Termination;**

Figure 2.7 The acid-catalyzed ring-opening polymerization mechanism catalyzed by triflic acid (HA represents $\text{CF}_3\text{SO}_3\text{H}$).

The kinetics of this system has been studied extensively by Wiczek et al. They found that the initial rate for the polymerization of D₄ with trifluoromethanesulfonic acid (TfOH) was as follows:⁵⁷

$$R_p = [\text{TfOH}]^{2.2} [\text{D}_4]^{0.7}$$

The reaction rate also depends strongly on solvents, monomers and catalysts used in the reaction.

Kantor et al. has reported the order of reactivity of the cyclics and linear polymers toward acid catalysts as follows:³⁰



D₃ is the most reactive species in the series due to its large degree of ring strain in combination with low activation energies for ring-opening, 16.5 ± 1.0 kcal/mole, compared with D₄, 19.5 ± 1.0 kcal/mole.⁵⁸ The disiloxane (MM) shows higher reactivity than the trisiloxane (MDM) and the tetrasiloxane (MD₂M) because there are fewer oxygens bonded to the silicon atoms.⁵⁹

2.2.3.2 Base-catalyzed ring-opening equilibration

The base-catalyzed ring-opening polymerization was first discovered by Hyde in 1949, and then Grubbs et al. proposed the mechanism a few years later. Unstrained cyclicsiloxanes, e.g., D₄, are typically used in this reaction. It is thought that the silicon atoms are attacked by bases, then Si-O bonds cleave to produce silanolate reactive species, which can then dimerize. As the reaction proceeds, the silanolate reactive species can react either with cyclosiloxanes to propagate the chain, backbite to reform the cyclic structures, or react with other linear polymers

⁵⁷ L. Wilczek, S. Rubinsztain and J. Chojnowski, *Makromol. Chem.*, **187**, 39-51 (1986)

⁵⁸ M. G. Voronkov, V. P. Mileshekevich and Y. A. Yuzhelevskii, In *The Siloxane Bond: Physical Properties and Chemical Transformations*, Consultants Bureau, New York (1978)

⁵⁹ L. A. Kiefer, In *Synthesis and Characterization of Novel Polyester/Polysiloxane and Polyester/Arylphosphine Oxide Copolymers*, Ph.D. Dissertation, Virginia Tech (1993)

(Figure 2.8). Siloxane dimers as shown in Table 2.5 can also be used as endblocking reagents in this reaction to control the molecular weights of the linear polymers.

The reactivity order of the low molecular weight siloxanes toward bases is as follow:³⁰



Excluding D_3 , this series is inverse to reactivities in an acid-initiated system. The high reactivity of D_3 is again due to the ring strain of the siloxane trimer. Considering the other species, the reactivity increases as more oxygens are attached to the silicon atoms, resulting in greater partial positive charge. This allows such silicon atoms to be more susceptible to attack by bases. In agreement with this series, McGrath has reported that the rate of reaction of aminopropyl-substituted disiloxanes (MM) using KOH as a catalyst was significantly slower than the rate of the reaction of D_4 .^{60, 61}

⁶⁰ C. S. Elsbernd, P. M. Sormani, S. Kilic and J. E. McGrath, *Polym. Prep. (Am. Chem. Soc., Div. Polym. Chem.)*, **27**(2), 152-3 (1986)

⁶¹ P. M. Sormani and J. E. McGrath, *Polym. Prep. (Am. Chem. Soc., Div. Polym. Chem.)*, **26**(1), 258-9 (1985)

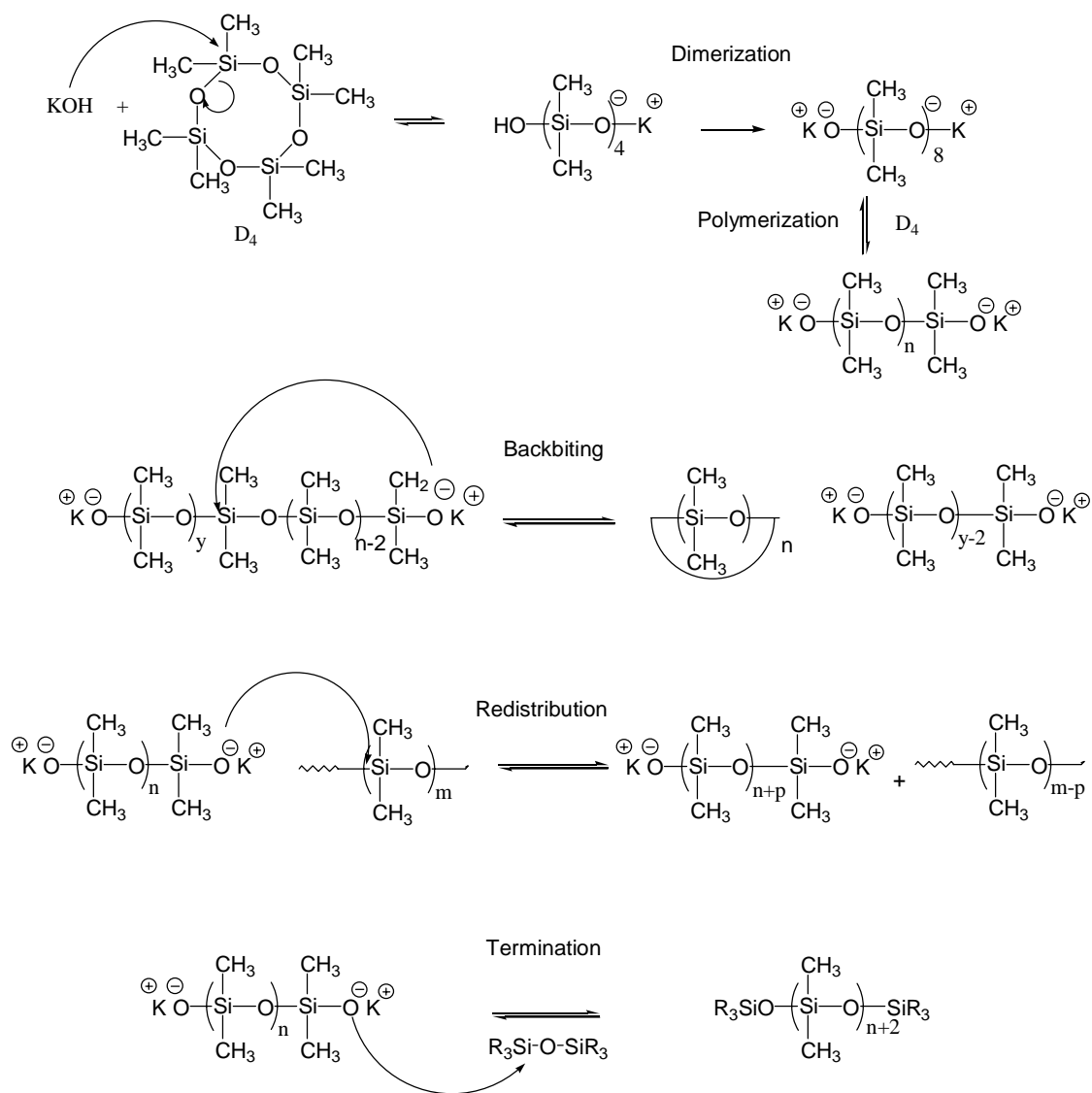
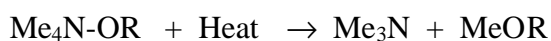


Figure 2.8 Proposed mechanism of base-catalyzed ring-opening polymerization in D_4 .^{39, 40}

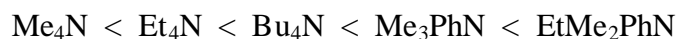
In this system, alkali metal hydroxides, quaternary ammonium hydroxides and phosphonium hydroxides are typically used to polymerize unstrained cyclosiloxanes. Other strong inorganic and organic bases have also been reported.⁶² The reactivity order of the alkali metal hydroxides is as follows:^{63, 64}



The reactivity decreases as the size of the cation decreases. This trend is in agreement with the degree of ionization of their corresponding metal-silanolates. Polymerizations using these alkali metal hydroxides or their corresponding silanolates can be carried out above 140 °C without degradation of the catalysts. It is necessary to remove these catalysts after equilibrium to prevent depolymerization in subsequent processes due to remaining catalysts. Quaternary ammonium hydroxides and phosphonium hydroxides, the so-called ‘transient catalysts’, are attractive as catalysts for these equilibrations because they can be thermally removed *in-situ*. Quaternary ammonium hydroxides rapidly decompose above 130 °C to produce by-products which volatilize. This yields stable polysiloxanes without the need for repeated washing or careful neutralization to remove the catalyst.²⁹



The activation energy of the catalyst decomposition reaction is 42 kcal/mole. Quaternary ammonium hydroxides with different substituents on nitrogen have been studied. The rate of thermal decomposition has been reported as follows:



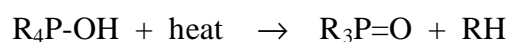
⁶² T. C. Kendrick, B. M. Parbhoo and J. W. White, In *Comprehensive Polymer Science*, G. Allen, J. C. Bevington, G. C. Eastmaond, A. Ledwith, S. Susso and P. Sigwalt (Eds.), v.4, p. 459, Pergamon, Oxford (1989)

⁶³ S. W. Kantor and A. R. Gilbert (to Central Electric Co.), U.S. Pat. 2,883,366 (1959)

⁶⁴ E. E. Bostick, In *Kinetics and Mechanisms of Polymerization*, v.2, Ring Opening Polymerization, K. C. Frisch and S. L. Reegan (Eds), p.327, Marcel Dekker, New York (1969)

Elsbernd et al.⁶⁵ and McGrath et al.⁶⁶ have studied the reactivities of tetramethylammonium silanolate, tetrabutylammonium silanolate and potassium silanolate toward the anionic ring-opening polymerization of D₄. It was observed that potassium silanolate was significantly less effective than the others. As a result, higher catalyst concentrations and/or reaction times and temperatures were required using potassium counterions to incorporate the endblocking reagents effectively at the chain termini.

The decomposition of phosphonium hydroxide also produces inert products:



The reactivity of the transient catalysts is close to that of cesium hydroxide.

The rate of the polymerization (R_p) exhibits a second-order dependence on the cyclosiloxane and a fractional order on the initiator:⁹

$$R_p = [\text{Initiator}]^{1/n} \cdot [D_x]^2$$

where n varies from 1 to 4, depending on the type of counterion. For example, $n = 1$ when cryptate-coordinated lithium silanolates or $R_4NOSi\equiv$ is used, whereas $LiOSi\equiv$ gives $n = 4$.

Cazacu et al. have recently reported the utilization of anionic ion-exchange resins as catalysts for the equilibration of D₄ or 1,3,5,7-tetravinyl-1,3,5,7-tetramethylcyclotetra siloxane (V₄).^{67, 68} The reactions containing the anionic OH⁻ form were carried out under mild temperature conditions (50-90 °C) and an inert atmosphere. The anion-catalyzed reaction was more successful when V₄ was used as a monomer. This comes from the fact that the electronegative substituents (vinyl functional groups) can induce partial positive charge on silicon atoms. Several advantages of this catalyst over the conventional process are reported,

⁶⁵ C. S. Elsbernd, M. Spinu, S. Kilic and J. E. McGrath, *Polym. Prep. (Am. Chem. Soc., Div. Polym. Chem.)*, **29**(1), 355-7 (1988)

⁶⁶ J. E. McGrath, P. M. Sormani, C. S. Elsbernd and S. Kilic, *Makromol. Chem., Macromol. Symp.*, **6**, 67-80 (1986)

⁶⁷ M. Cazacu, M. Marcu, S. Dragon and C. Matricala, *J. Appl. Polym. Sci.*, **60**, 731-734 (1996)

⁶⁸ M. Cazacu, M. Marcu, A. Vlad, D. Caraiman and C. Racles, *Eur. Polym. J.*, **35**, 1629-1635 (1999)

e.g., the simplicity of catalyst separation after the reaction by filtering, mild reaction conditions and high selectivity.

2.2.4 Living anionic polymerization and it's application to block copolymers: kinetically controlled polymerization

2.2.4.1 Introduction to living anionic polymerization

Living anionic polymerization is defined as a base-initiated polymerization in the absence of termination and chain transfer reactions.⁶⁹ Although it was named differently, Ziegler originally identified this particular type of reaction via addition reaction of alkyllithiums to olefins in 1929.^{70, 71} The concept of termination-free polymerization was explained by Mark and Dostal⁷² and then by Flory.⁷³ In 1956, Szwarc et al. was the first to define the term “living anionic polymerization” via electron transfer initiation.⁷⁴ Since then, living anionic polymerization has been employed for the precise control of molecular weight and molecular weight distributions. In addition, it has been effectively utilized for terminating polymers with specified functional groups, tailoring block copolymer architecture and for controlling of polydiene microstructure.

⁶⁹ M. Szwarc, In *Anionic Polymerization: Kinetics, Mechanisms and Synthesis*, J. E. McGrath (Ed.), ACS Symposium Series 166, American Chemical Society, Washington DC (1981)

⁷⁰ K. Ziegler and K. Bahr, *Chem. Ber.*, **61**, 253 (1928)

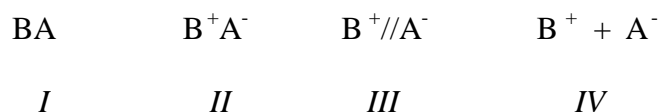
⁷¹ K. Ziegler, F. Dersch and H. Wolltham, *Ann. Chem.*, **511**, 13 (1934)

⁷² H. Dostal and H. Z. Mark, *Phys. Chem. B.*, **29**, 299 (1935)

⁷³ P. J. Flory, In *Principles of Polymer Chemistry*, Cornell Press (1953)

⁷⁴ M. Szwarc, M. Levy and R. Milkovich, *J. Am. Chem. Soc.*, **78**, 2656 (1956)

A variety of propagating species may co-exist in a polymerizing system. They range from the most stable and least reactive species (*covalent bonds*, species I) to the most reactive species (*free ions*, species IV),^{75,76}



where A represents polymer chains and B represents a counter-ion. The contributions of these species in a polymerization are affected by the nature of counter-ions and solvent. The reactivity of counter-ions is analogous to those previously discussed in the base-catalyzed ring-opening equilibration section. Briefly, the reactivity increases as the size of the cation increases.



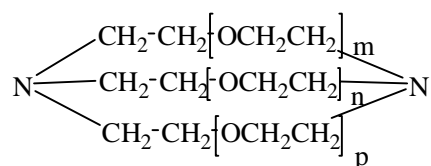
Solvents of high polarity are not suitable for these reactions due to several reasons. For example, polar protic solvents, e.g., H₂O, MeOH, can provide protons to terminate the living ends. Other solvents, e.g., acetone, ether, are capable of forming highly stable complexes with the initiators. Therefore, living anionic polymerizations are usually carried out in solvents of low to moderate polarity, e.g., hexane or nitrobenzene. In cases of non-polar hydrocarbon media like hexane, organolithium compounds are almost uniquely suitable as initiators since other organoalkali compounds are often insoluble in such media.⁷⁷ In solvents of low to moderate polarity, the intermediate species formed due to ionic aggregation is *the tight or contact ion pair* (species II). The reactivity rates of such species are relatively slow in polymerizations and they do not increase significantly with temperature. Adding trace amounts of electron releasing compounds can solvate the cation and increase the concentration of free-silanolate ions, resulting

⁷⁵ J. March, In *Advanced Organic Chemistry; Reaction, Mechanisms and Structure*, 4th ed., John-Wiley & Sons, New York (1992)

⁷⁶ G. Odian, In *Principles of Polymerization*, 3rd Ed., p.356, John Wiley & Sons, Inc., New York (1991)

⁷⁷ M. Morton, In *Anionic Polymerization: Kinetics, Mechanisms and Synthesis*, J. E. McGrath (Ed.), ACS Symposium Series 166, American Chemical Society, Washington DC (1981)

in *solvent-separated* or *loose ion pairs* (species III). This can significantly increase the rates of polymerization. These electron-releasing compounds are called co-catalysts or promoters. Monodentate reagents, e.g., tetrahydrofuran (THF),⁷⁸ ethyl ether, dimethyl sulfoxide (DMSO),⁷⁹ hexamethylphosphoramide (HMPA) and phosphine oxide, are typically used for this purpose. It has been reported that multidentate promoters, e.g., poly(ethylene glycol), crown ethers⁸⁰ and cryptands⁸¹ (macrobicyclic ligands), are much more effective than using monodentate promoters.



Cryptate [221] where $m = n = 2$, and $p = 1$

2.2.4.2 Living anionic polymerization of D_3

Cyclic monomers with high ring strain are important in living anionic polymerizations of polysiloxanes since this minimizes or eliminates side reactions, e.g., depolymerization and redistribution. This can be attributed to the higher reactivities of the Si-O bonds in strained monomers relative to those in the linear polysiloxanes.⁸² The cyclosiloxane trimer (D_3) is somewhat strained and polymerizes with a significant exothermic enthalpy. Thus, it is typically utilized as a starting material for these reactions. The polymerizations are commonly carried out

⁷⁸ U. Maschke and T. Wagner, *Makromol. Chem.*, **193**, 2453-2466 (1992)

⁷⁹ C. A. Veith and R. E. Cohen, *J. Polym. Sci. A: Polym. Chem.*, **27**, 1241-1258 (1989)

⁸⁰ R. C. Hedden and C. Cohen, *Polymers*, **41**, 6975 (2000)

⁸¹ J. M. Yu, D. Teyssie, R. B. Khalifa and S. Boileau, *Polymer Bulletin*, **32**, 35-40 (1994)

⁸² C. L. Frye, R. M. Salinger, F. W. G. Fearon, J. M. Klosowski and T. DeYoung, *The Journal of Org. Chem.*, **35**(5), 1308 (1970)

in non-polar solvents, e.g., hexane or xylene, with an organolithium compound as the initiator. Addition of 1-5% of a polar solvent is an important factor to initiate the polymerization.

n-Butyllithium⁸³ and secondary butyllithium⁸⁴ are commonly used as initiators in D₃ polymerizations (Figure 2.9). n-Butyllithium associates into hexamers in cyclohexane whereas *sec*-butyllithium associates into tetramers in the same solvent. Aggregation of three to four active silanolate groups on propagating chains has also been observed when lithium 2,4,4-trimethyl-1-pentanoate, (CH₃)₃CCH₂CH(CH₃)CH₂OLi, was used to initiate D₃ polymerization in THF⁸⁵. Trimethylsilylmethylithium (Me₃SiCH₂Li) is an effective initiator to give mono-modal distributions of polysiloxane molecular weights.⁸⁶ High yields of telechelic polysiloxanes have been achieved using acetylacetonone functioning as both initiator and endcapping reagent.⁸⁷ Living PDMS with silanolate active ends can be terminated with specified functional groups, e.g., trivinylchlorosilane or trimethoxychlorosilane, through the typical S_N2 substitution of chlorine. This produces polysiloxanes with functionalized endgroups which can further react with appropriate functional groups of other polymers to form siloxane-containing block copolymers or networks.

⁸³ T. Suzuki, *Polymer*, **30**, 333 (1989)

⁸⁴ W. H. Dickstein, *Macromolecules*, **22**, 3882-3885 (1989)

⁸⁵ L. Wilczek and J. P. Kennedy, *Polymer Journal*, **19**(5), 531-538 (1987)

⁸⁶ T. Zundel, J. M. Yu, L. Lestel, D. Teyssie and S. Boileau, *Macromol. Symp.*, **88**, 177-189 (1994)

⁸⁷ A. Kumar and B. E. Eichinger, *Macromolecules*, **23**, 5358 (1990)

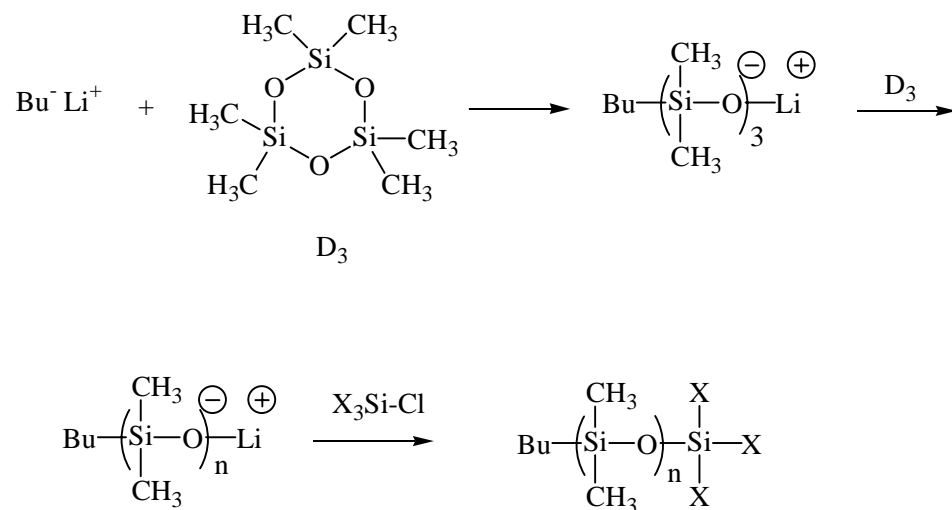


Figure 2.9 Living anionic polymerization of D_3 ; X = functional groups (modified from Reference 40).

Boileau has reported kinetic studies of living anionic polymerizations of D_3 in benzene using n-butyllithium as an initiator and [211]-cryptand as a promoter.⁸⁸ The disappearance of D_3 was first order at least up to 80% conversion. Plotting $R_p/[M]$ versus $[C]$ yields a straight line originating from the zero co-ordinates, indicating a first-order dependence on reactive centers (Figure 2.10). These polymerization conditions produced fairly narrow molecular weight distributions (~ 1.01) of predictable molecular weights.

⁸⁸ S. Boileau, In *Anionic Polymerization: Kinetics, Mechanisms and Synthesis*, J. E. McGrath (Ed.), ACS Symposium Series 166, American Chemical Society, Washington DC (1981)

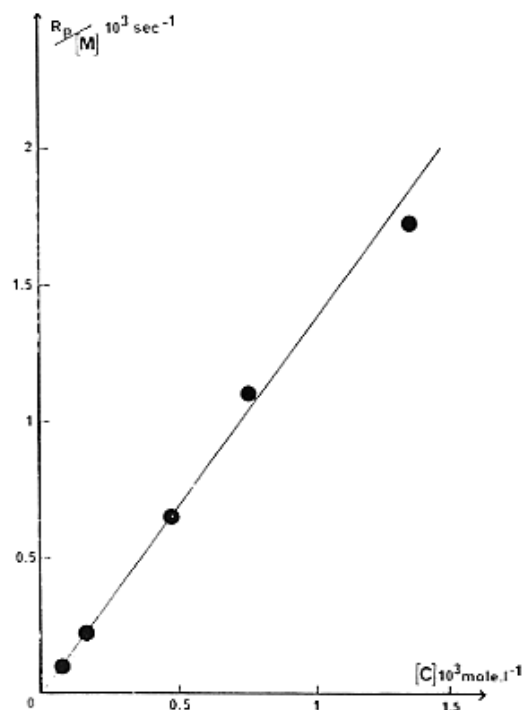


Figure 2.10 $R_p/[M]$ vs. $[C]$ for the anionic polymerization of D_3 with Li^+ and [221] cryptand counterions in benzene at 20 °C.⁸⁸

Although these reactions were conducted under conditions which yielded narrow molecular weight distributions (using the ring-strained D_3), small concentrations of cyclic oligomers (D_x) still formed as by-products during propagation. Rapid formation of linear polymers up to 90% conversion was observed within 20 min. whereas the proportion of cyclosiloxanes (D_4 , D_5 and D_6) was very low. Figure 2.11 shows the conversion of D_3 monomers and the formation of linear polymers, D_4 , D_5 and D_6 as a function of time.

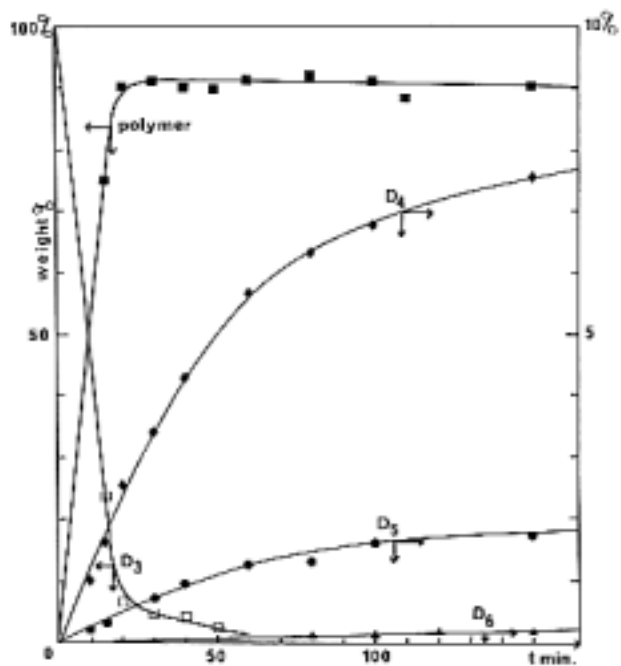


Figure 2.11 The conversion of D₃ monomer and the formation of linear polymers, D₄, D₅ and D₆ as a function of time: $[C] = 3.08 \times 10^{-4} \text{ mol.L}^{-1}$; $[M]_0 = 0.49 \text{ mol.L}^{-1}$.⁸⁸

Both monofunctional initiators and a wide variety of difunctional siloxane initiators have been utilized in living anionic polymerizations of polysiloxanes. Difunctional initiators are of particular interest for preparing monodisperse telechelic polymers and A-B-A block copolymers (Figure 2.12). These dianionic silanolates are typically prepared by deprotonating the corresponding silanediols using butyllithiums in THF at $-40\text{ }^{\circ}\text{C}$.⁸⁹ Aliphatic dianionic silanolates, e.g., structures A and B, have been reported to be effective difunctional initiators which produce PDMS with monomodal molecular weight distributions.^{90, 91} In contrast, aromatic dianionic silanolates, e.g., structures E, F and G, were slow initiators and yielded PDMS with broad molecular weight distributions.⁹² It was rationalized that the aromatic rings can somewhat stabilize the negative charge and suppress the reactivities of the active species. Imai has shown that dilithium salts of bis(p-hydroxydimethylsilyl)phenyl ether (structure C) yielded PDMS with a narrower molecular weight distribution than those of bis(p-hydroxydimethylsilyl) benzene (structure D) and diphenylsilane diol (structure E).⁹³

⁸⁹ M. Morton and E. E. Bostick, *J. Polym. Sci.*, **A3**, 971 (1965)

⁹⁰ Y. Gnanou and P. Rempp, *Makromol. Chem.*, **189**, 1997-2005 (1988)

⁹¹ J. Chojnowski, K. Rozga, W. Fortuniak and A. Kowalewska, *Makromol. Chem. Macromol. Symp.*, **73**, 183-201 (1993)

⁹² E. E. Bostick, In *Block Copolymer*, S. L. Aggarwal (Ed.), Plenum Press, New York (1970)

⁹³ H. Kazama, Y. Tezuka and K. Imai, *Polymer Bulletin*, **21**, 31-37 (1989)

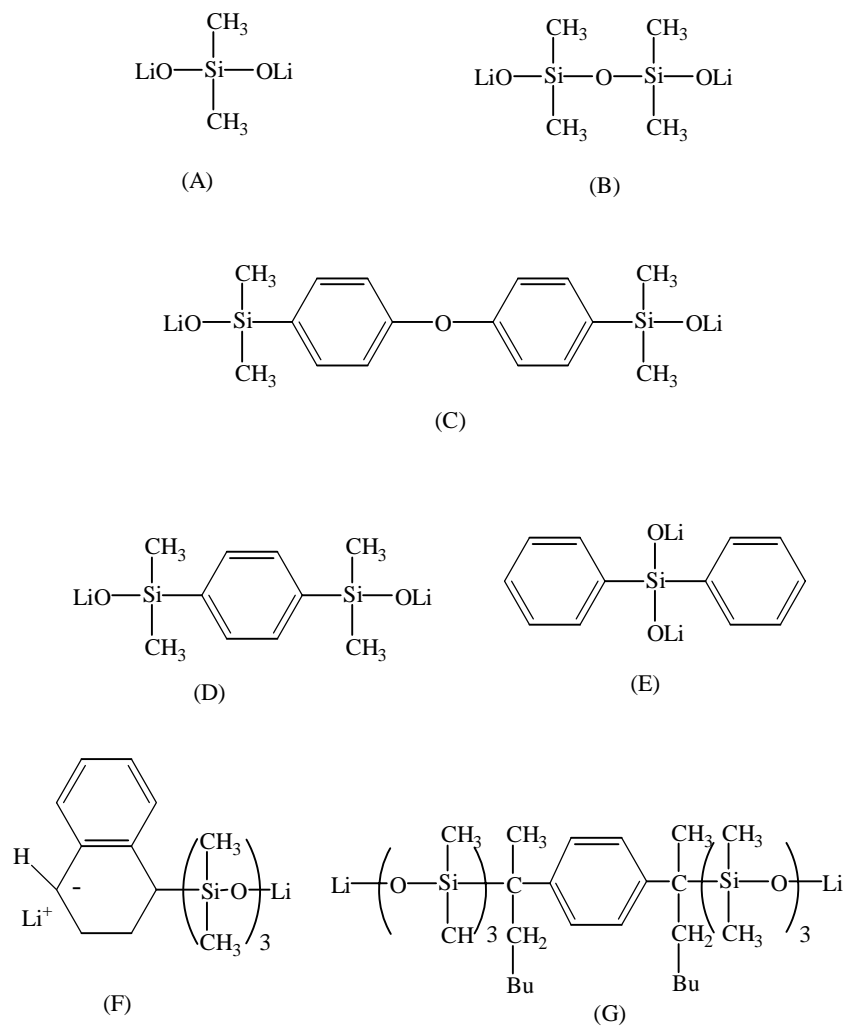


Figure 2.12 Structures of dilithium dianionic silanolate initiators for D₃.

2.2.4.3 Siloxane-containing block copolymers

In general, block copolymers are comprised of two or more polymeric segments with different chemical compositions covalently bound together. They have been of special interest since Milkovich discovered their intriguing properties that do not exist in random copolymers or polymer blends.^{94, 95} The glass transition temperatures (T_g s) and/or melting points (T_m s) of each component can be observed in phase-separated block copolymers. This provides the ability to tailor and precisely control their physical properties.⁹⁶ There are a variety of block copolymer architectures containing A and B blocks, e.g., diblock (AB), triblock (ABA), multiblock (-ABAB-), star and graft structures.^{97, 98} Kinetically controlled living anionic polymerization is typically utilized to prepare well-defined diblock and triblock copolymers by sequential addition of monomers. A well-known example of ABA triblock copolymers is polystyrene-polybutadiene-polystyrene (PS-PBd-PS) thermoplastic elastomers containing features of thermoplastic behavior combined with rubber-like behavior.

Syntheses of polysiloxane-containing block copolymers have been developed since the early 1950's.⁹⁹ A wide variety of copolymers have been prepared including polysiloxane-polysiloxane copolymers comprised of different types of siloxane blocks,¹⁰⁰ and copolymers of

⁹⁴ R. Milkovich, S. African Pat. No. 280,712 (1963). Assigned to Shell Oil Company.

⁹⁵ J. E. McGrath, In *Block Copolymers: Science and Technology*, D. J. Meier (Ed.), MMI Press Symposium Series, v.3, Harwood Academic Publishers, New York (1983)

⁹⁶ F. J. B. Calleja and Z. Roslaniec, In *Block Copolymers*, Marcel Dekker, New York (2000)

⁹⁷ B. Lindman and P. Alexandridis, In *Amphiphilic Block Copolymers; Self-Assemble and Applications*, P. Alexandridis and B. Lindman (Eds.), Elsevier, New York (2000)

⁹⁸ A. Noshay and J. E. McGrath, In *Block Copolymers: Overview and Critical Survey*, Academic Press, New York (1977)

⁹⁹ J. B. Plum and J. H. Atherton, In *Block Copolymers*, D. C. Allport and W. H. Janes (Eds.), Applied Science Publishers, London (1973)

¹⁰⁰ N. V. Gvodzdic, J. Ibemesi and D. J. Meier, *Proc. IUPAC, Macromol. Symp.*, **69**, 168 (1982)

polysiloxanes with polyimides,^{101, 102, 103, 104} polymethacrylate,^{105, 106, 107} polystyrene,¹⁰⁸ polyurethanes,^{109, 110, 111} and polyoxyalkylene.^{112, 113}

Bostick has reported the preparation of polydiphenylsiloxane-*b*-polydimethylsiloxane-*b*-polydiphenylsiloxane (PDPS-*b*-PDMS-*b*-PDPS) via living anionic polymerization by sequential addition of D₃ followed by hexaphenylcyclotrisiloxane using dilithium diphenylsilane as the initiator (Figure 2.13).¹¹⁴ Because PDPS homopolymers have a T_g of 49 °C, they behave like physical crosslinking sites in the block copolymers, similar to PS in PS-PBd-PS thermoplastic elastomers. In addition, incorporation of PDPS segments into PDMS homopolymers can decrease the low temperature crystallization and increase thermal and radiation stability.^{1, 115}

¹⁰¹ S. Andre, F. Guida-Pietrasanta, A. Rousseau and B. Boutevin, *J. Polym. Sci. A: Polym. Chem.*, **39**, 2414 (2001)

¹⁰² Y. Yamada and N. Furukawa, *Polymer J.*, **29**(11), 923 (1997)

¹⁰³ J. Zhao, S. R. Rojstaczer, J. Chen, M. Xu and J. A. Gardella Jr., *Macromolecules*, **32**, 455 (1999)

¹⁰⁴ W. Volksen, J. L. Hedrick, T. P. Russell and S. Swanson, *J. Appl. Polym. Sci.*, **66**, 199 (1997)

¹⁰⁵ K. Huan, L. Bes, D. M. Haddleton and E. Khoshdel, *J. Polym. Sci. A: Polym. Chem.*, **39**, 1833 (2001)

¹⁰⁶ J. P. Mason, T. Hattori and T. E. Hogen-Esch, *Polym. Prepr. (Am. Chem. Soc., Div. Polym. Chem.)*, **30**(1), 259 (1989)

¹⁰⁷ T. C. Chang, H. B. Chen, Y. C. Chen and S. Y. Ho, *J. Polym. Sci. A: Polym. Chem.*, **34**, 2613 (1996)

¹⁰⁸ T. C. Chang, H. B. Chen, Y. S. Chiu and S. Y. Ho, *Polym. Degrad. Stab.*, **57**, 7-14 (1997)

¹⁰⁹ Y. C. Chun, K. S. Kim and J. S. Shin, *Polym. Int.*, **27**, 177 (1992)

¹¹⁰ R. Benrashid, G. L. Nelson, J. H. Linn, K. H. Hanley and W. R. Wade, *J. Appl. Polym. Sci.*, **49**, 523 (1993)

¹¹¹ M. Pegoraro, F. Severini, R. Gallo and L. Zanderighi, *J. Appl. Polym. Sci.*, **57**, 421 (1995)

¹¹² D. Giurgiu, V. Hamciuc, E. Butuc, V. Cozan, A. Stoleriu, M. Marcu and C. Ionescu, *J. Appl. Polym. Sci.*, **59**, 1507 (1996)

¹¹³ Z. Kiraly and B. Vincent, *Polym. Int.*, **28**, 139 (1992)

¹¹⁴ E. E. Bostick, In *Block Copolymers*, S. L. Aggarwal (Ed.), Plenum, New York (1970)

¹¹⁵ C. Chou and M. H. Tang, *J. Thermal Anal.*, **40**, 657-667 (1993)

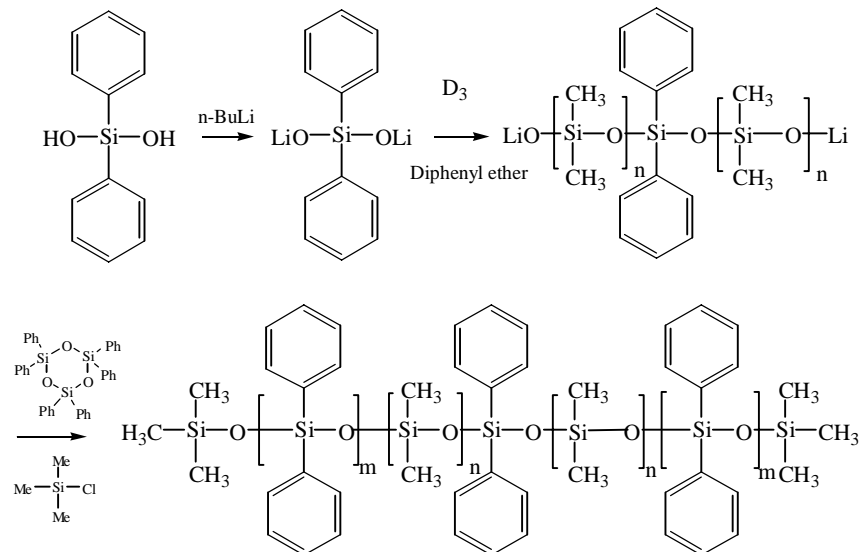


Figure 2.13 Synthesis of polydiphenylsiloxane-*b*-polydimethylsiloxane-*b*-polydiphenyl siloxane (PDPS-*b*-PDMS-*b*-PDPS).¹¹⁴

Liquid crystalline block copolymers containing a polystyrene block and a side-chain liquid crystalline siloxane block have been prepared by anionic polymerization of styrene, then a blend of D₃/trimethyltrivinylcyclotrisiloxane (to form a random block) followed by hydrosilylation with side chain mesogens containing Si-H groups (Figure 2.14).¹¹⁶ These copolymers were designed to possess a high-*T_g* amorphous block of PS coupled to a low-*T_g* liquid polysiloxane crystalline block. These copolymers exhibited a liquid crystalline (LC) phase transition below the *T_g* of PS allowing LC mobility of this material at room temperature. These copolymers are of particular interest due to their ability to orient mesogens with mechanical and electrical fields. Such properties, combined with mechanical properties of the

¹¹⁶ A. Moment, R. Miranda and P. T. Hammond, *Macromol. Rapid Commun.*, **19**, 573-579 (1998)

copolymers, may lead to applications, e.g., electro-optic free standing thin films and ‘mechano-optic’ materials.

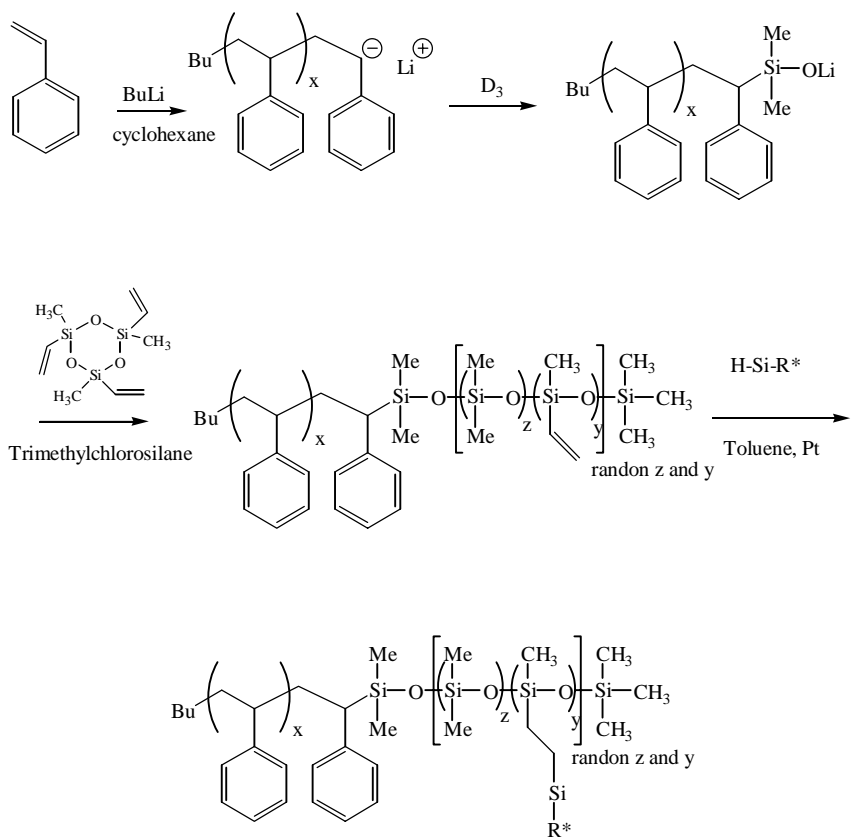


Figure 2.14 Preparation of polystyrene-*b*-polysiloxane liquid crystalline side-chain block copolymers: R* is side-chain mesogen.¹¹⁶

2.2.4.4 Micelle formation

Micellization, or micelle formation, occurs when diblock or triblock copolymers are introduced into a solvent which preferentially solvates one block in the copolymers. The selective solvent results in aggregation of the non-solvated block.¹¹⁷ The driving force for solution micellization of block copolymers is the solvent selectivity of different blocks. The concentration at which micellization begins is called “the critical micelle concentration”, abbreviated as “cmc”.¹¹⁸ Below the cmc, the insoluble blocks migrate to the surface of a solution in an attempt to ‘escape’ from the medium whereas the soluble blocks protrude into the solution. In addition to the aggregated molecules at the solution surface, free chains or unimers also exist in the solution and act as a normal solute. The concentration of these unimers depends upon several parameters, e.g., types of copolymer and solvent, temperature and pH. At the cmc, abrupt changes in many physical properties, including osmotic pressure, turbidity, electrical conductivity and surface tension, occur (Figure 2.15).^{119, 120} Because the self-assembly of block copolymers is a dynamic equilibrium process, these unimers are constantly diffusing in and out of micelles.¹²¹ Micelle structures are the most common and studied type of self-association of block copolymers. However, aggregate morphologies other than micelles can also form in solution, e.g., cylinders, lamellae, bicontinuous structures and vesicles (Figure 2.16).¹²² Sadron

¹¹⁷ J. Selb and Y. Gallot, In *Developments in Block Copolymers-2*, I. Goodman (Ed.), Elsevier Applied Science Publishers, London (1985)

¹¹⁸ P. C. Hiemenz, In *Principles of Colloid and Surface Chemistry*, Marcel Dekker, Inc., New York (1977)

¹¹⁹ D. J. Shaw, In *Introduction to Colloid and Surface Chemistry*, 3rd Ed., Butterworths, London (1980)

¹²⁰ P. C. Hiemenz and R. Rajagopalan, In *Principles of Colloid and Surface Chemistry*, 3rd Ed. Revised and Expanded, Marcel Dekker, New York (1997)

¹²¹ D. G. Hall, B. A. Pethica, *Nonionic Surfactants*, Marcel Decker Inc., New York (1967)

¹²² D. F. Evans and H. Wennerstrom, In *The Colloidal Domain; Where Physics, Chemistry, Biology and Technology Meet*, 2nd Ed., Wiley-VCH, New York (1999)

has reported that the various structures existing in solution are dependent on the solution concentration¹²³ as follows:

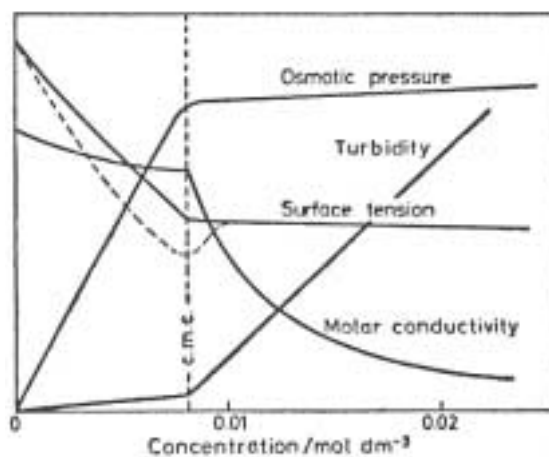
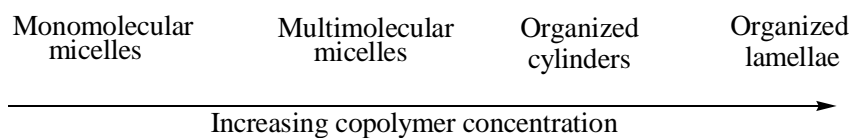


Figure 2.15 Schematic illustration of abrupt changes in physical properties at the critical micelle concentration (cmc).^{119, 120}

¹²³ C. Sandron, *Angew. Chem.*, **75**, 472 (1963)

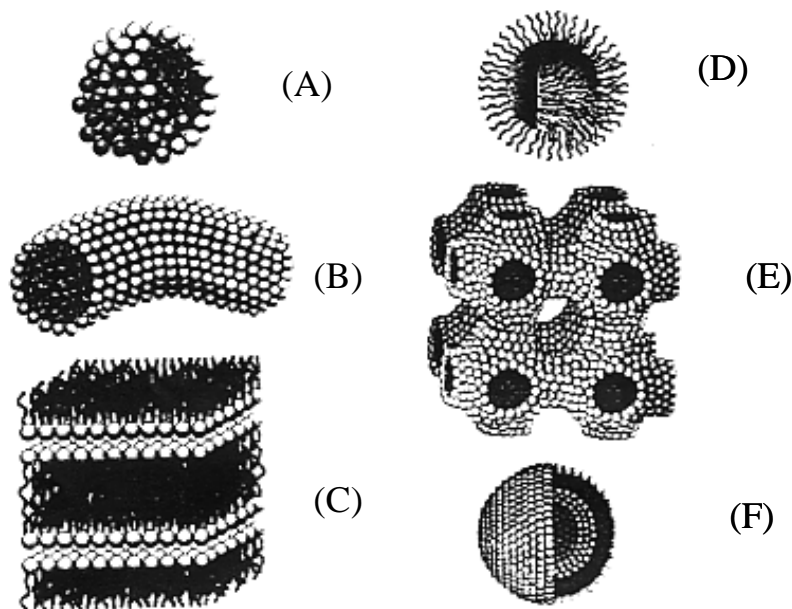


Figure 2.16 Various structures of self-assembled block copolymers in a selective solvent: (A) spherical micelles, (B) cylindrical micelles, (C) planar bilayers, (D) inverted micelles, (E) bicontinuous structure, and (F) vesicles.¹²⁰

Micelle structures have been extensively studied in aqueous solutions using block copolymers containing hydrophilic and hydrophobic segments, e.g., PEO-*b*-PPO-*b*-PEO,^{124, 125, 126, 127, 128} PS-*b*-PEO¹²⁹ or PEOX-*b*-PTMC (polyethyloxazoline-*b*-poly(trimethylene carbonate))¹³⁰. The hydrophobic blocks aggregate and form the micellar core whereas the hydrophilic blocks are solvated and form the micellar corona. In addition to aqueous solutions, non-aqueous solvents have also been utilized for self-assembled block copolymers and this has

¹²⁴ Y. Liu, S. H. Chen and J. S. Huang, *Macromolecules*, **31**, 2236 (1998)

¹²⁵ P. Alexandridis and L. Yang, *Macromolecules*, **33**, 5574 (2000)

¹²⁶ L. Yang and P. Alexandridis, *Langmuir*, **16**, 4819 (2000)

¹²⁷ P. Alexandridis and L. Yang, *Macromolecules*, **33**, 3382 (2000)

¹²⁸ L. Yang and P. Alexandridis, *Langmuir*, **16**, 8555 (2000)

¹²⁹ L. M. Bronstein, D. M. Chernyshov, G. I. Timofeeva, L. V. Dubrovina, P. M. Valetsky and A. R. Khokhov, *J. Colloid and Interface Science*, **230**, 140 (2000)

¹³⁰ C. Kim, S. C. Lee, J. H. Shin and J. S. Yoon, *Macromolecules*, **33**, 7448 (2000)

continuously drawn attention in the last few decades, although much less work has been reported.¹³¹ Leading to diversity in the association behavior, non-aqueous solvents can vary from organic solvents or supercritical fluids (e.g., supercritical CO₂) to low molecular weight homopolymers corresponding to one block of the copolymers.

Many investigators have conducted studies the micelle formation and behavior using copolymers containing PDMS blocks. Nose et al. have studied the association behavior of polystyrene-*b*-polydimethylsiloxane (PS-*b*-PDMS) in a selective solvent near a transitional region between free chains and micelles as a function of temperature and concentration using static and dynamic light scattering.¹³² A mixed solvent comprised of *n*-octane and methylcyclohexane was used as a selective solvent, and this system had a PS micelle core and a PDMS micelle corona. Three different temperature-concentration regions excluding free chains were found (Figure 2.17). In region *I*, known as the anomalous micellization region, large spherical particles are formed at high temperature. In region *II*, stable vesicles are observed at all temperatures and concentrations except close to the cmc and cmt (critical micelle temperature). The cylindrical micelle region is found at lower temperature and concentration in region *III*. It is thought that the micelle structures in this region are rigid hollow cylinders.

The adsorption behavior of polydimethylsiloxane-*b*-polyethyloxazoline (PDMS-*b*-PEOX) copolymers from an aqueous solution onto silica (SiO₂) and titania (TiO₂) have been investigated by Cohen Stuart et al.¹³³ The copolymers form micelles in the solution with PDMS cores and PEOX coronas. It was found that both blocks had an affinity for silica but only PDMS blocks had an affinity for the titania surfaces. Adsorption kinetic studies indicated that micelles

¹³¹ A. Kitahara and K. Kon-No, In Colloidal Dispersions and Micellar Behavior, K. L. Mittal (Ed.), ACS Symposium Series 9, American Chemical Society, Washington DC (1975)

¹³² K. Iyama and T. Nose, *Polymer*, **39**(3), 651 (1998)

¹³³ H. D. Bijsterbosch, M. A. Cohen Stuart and G. J. Flee, *Macromolecules*, **31**, 9281 (1998)

had broken up into free chains before they arrived at the surface. The adsorption rate increased linearly as a function of time and eventually reached a plateau. The concentration of copolymers absorbed onto the silica surface was significantly higher than on the titania surface. Because PDMS was more strongly adsorbed onto the silica surface relative to the titania surface, the density of the copolymers on the silica surface was higher.

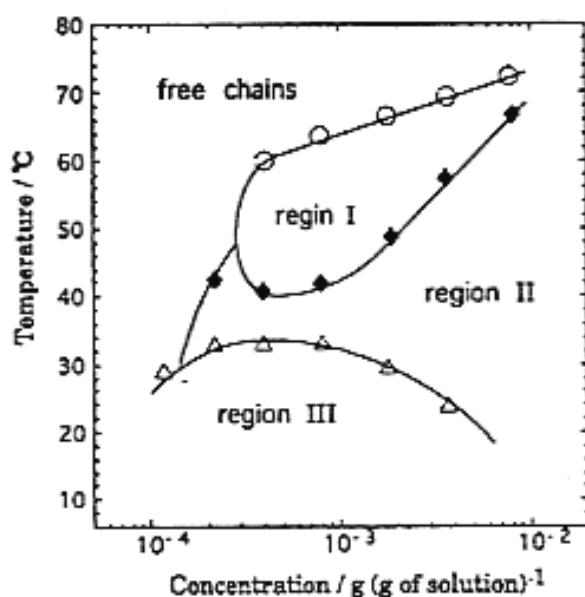


Figure 2.17 Temperature-concentration diagram of PS-*b*-PDMS in *n*-octane-methylcyclohexane mixture. Three distinct regions are depicted by plotting the temperature T_1 (O), T_2 (♦) and T_3 (Δ) against the polymer concentrations.¹³²

2.3 Sol-gel chemistry

2.3.1 Introduction

In general, sol-gel reactions involve a process where a soluble species in a solution (sol) becomes a colloidal sol and eventually forms an insoluble three dimensional network (gel).¹³⁴ This process is well-known in materials engineering as a low temperature (ambient) method for preparing inorganic glasses and ceramics based on the hydrolysis and condensation of metal or semi-metal alkoxides, halides, nitrates and other salts.¹³⁵ The sol-gel process primarily involves the hydrolysis and condensation of tetraalkylorthosilicates ($\text{Si}(\text{OR})_4$) abbreviated as TMOS (where R = methyl) or TEOS (where R = ethyl) as precursors.¹³⁶ Compared to other metallic elements, e.g., aluminum, titanium, boron and sodium, silicon has the slowest rate of reaction allowing one to control the reactions and study their kinetic and mechanistic details.

The earliest work on the sol-gel process was reported by Ebelmen in 1846.^{137, 138} He incidentally observed hard and clear monolithic products obtained from the hydrolysis and condensation of tetraethylorthosilicate (TEOS) after storage at room temperature for several months. The earliest patent on the sol-gel process was documented in 1943.¹³⁹ This patent covered the preparation of silica thin films from colloidal solutions of silicic acid. In 1968, Stoeber and Bohn developed 'the Stoeber process' for the controlled growth of monodisperse silica microspheres. A year later, Shroeder contributed many useful methods related to silica

¹³⁴ R. C. Mehrotra, In Structure and Bonding; Chemistry, Spectroscopy and Applications of Sol-Gel Glasses, v.77, M. J. Clarke, J. B. Goodenough, C. K. Jorgenson, J. B. Neilands, D. Reinen and W. Weiss (Eds.), p.1, Springer-Verlag, Berlin (1992)

¹³⁵ C. Li, Inorganic-Organic Sol-Gel Derived Hybrid Materials as Abrasion Resistant Coatings, Ph.D. Dissertation, Virginia Tech (1999)

¹³⁶ J. E. McGrath, J. P. Pullockaren, J. S. Riffle, S. Kilic and C. S. Elsbernd, In Ultrastructure Processing of Advanced Ceramics, J. D. Mackenzie and D. R. Ulrich (Eds.), p.55, A Wiley-Interscience, New York (1988)

¹³⁷ Ebelmen, *Ann ales de Chimie et de Physique*, **57**, 319 (1846)

¹³⁸ M. Spinu, Silicon-Based Organic and Inorganic Polymers, Ph.D. Dissertation, Virginia Tech (1990)

¹³⁹ R. W. Jones, In Fundamental Principles of Sol-Gel Technology, p.1, The Institute of Metal, Great Britain (1989)

coatings, including surface preparations and multi-layer coatings. Since then, sol-gel technology has been of great interest both in academic and industrial research.¹⁴⁰ A number of studies have thus been conducted to elucidate the reaction mechanisms and develop the products to serve particular needs.¹⁴¹

Sol-gel reactions are usually conducted in homogeneous solution using an inert solvent, e.g., ethanol, due to the immiscibility of TEOS and H₂O. The reaction media allow for many possible variations in reaction parameters.¹⁴² The concentrations of water, TEOS, catalyst, and solvent as well as types of catalyst and solvent play important roles in determining structure.¹⁴³ A number of studies have been carried out with the goals of optimizing the reaction conditions in such a way that the process is at least initiated and fully reacted. Generalized reactions for the preparation of silicate networks are depicted in Figure 2.18.

¹⁴⁰ S. Komarneni, S. Sakka, P. P. Phule and R. M. Laine (Eds.), In Sol-Gel Synthesis and Processing, The American Chemical Society (1998)

¹⁴¹ L. L. Hench and D. R. Ulrich (Eds.), In Science of Ceramic Chemical Processing, John Wiley&Sons, New York (1986)

¹⁴² K. D. Keefer, In Better Ceramics Through Chemistry, C. J. Brinker, D. E. Clark and D. R. Ulrich (Eds.), North-Holland, New York (1984)

¹⁴³ B. K. Coltrain and L. W. Kelts, In The Colloid Chemistry of Silica, H. E. Bergna (Ed.), American Chemical Society (1994)

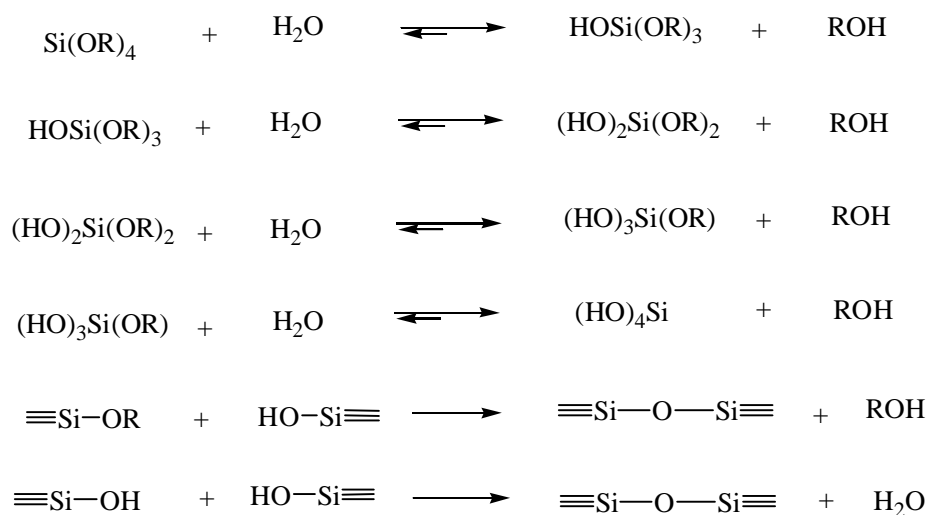


Figure 2.18 Generalized reactions for the preparation of silicate networks.^{138, 144}

The process occurs in two major stages, hydrolysis and condensation, under either acidic, basic or neutral conditions.^{145, 146} The first four reactions demonstrate the hydrolysis stage and the others show the condensation stage to produce the idealized gelled network. In the hydrolysis process, the reaction proceeds in a step-wise manner to produce trialkoxysilanols, dialkoxysilanedioles and alkoxy-silanetriols, respectively. The first hydrolysis step is relatively slow compared to the others. Typically, the gel structure is eventually densified by heating to higher temperature to obtain the dried gel and eventually the dense glass (Figure 2.19 and 2.20).

¹⁴⁴ D. R. Ulrich, *Chemtech*, 242 (1988)

¹⁴⁵ Y. Wei, W. Wang, J. M. Yeh, B. Wang, D. Yang, J. K. Murray, Jr. D. Jin and G. Wei, In *Hybrid Organic-Inorganic Composites*, J. E. Mark, C. Y-C, Lee and P. A. Bianconi (Eds.), ACS Symposium Series 585, American Chemical Society, Washington DC (1995)

¹⁴⁶ C. J. Brinker, In *The Colloid Chemistry of Silica*, H. E. Bergna (Ed.), American Chemical Society, Washinton DC (1994)

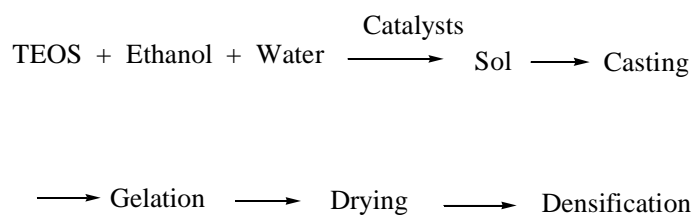


Figure 2.19 Processing scheme for the TEOS-ethanol-water system.¹³⁶

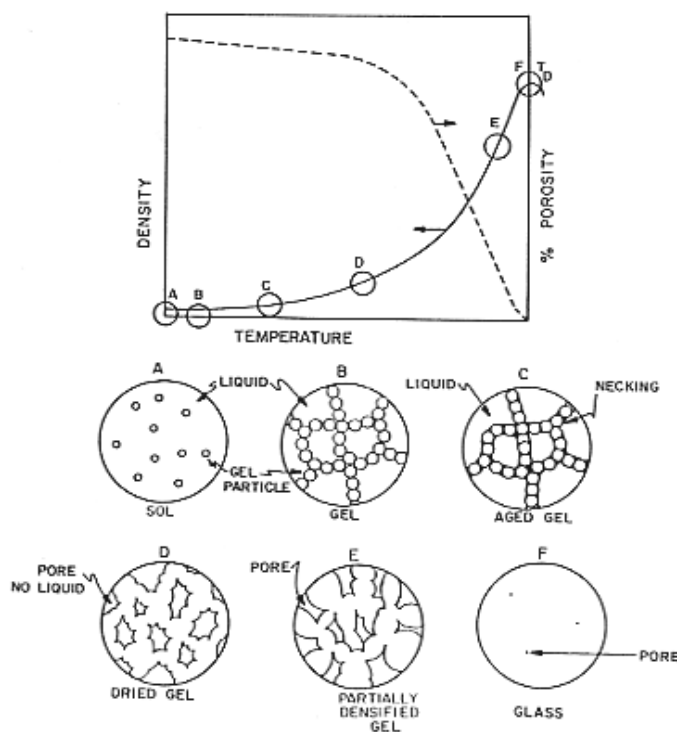


Figure 2.20 Sequence of structural changes during a sol-gel process.^{141, 147}

¹⁴⁷ R. K. Iler, In *The Chemistry of Silica: Solubility, Polymerization, Colloid and Surface Properties, and Biochemistry*, Wiley-Interscience, New York (1979)

2.3.2 Mechanisms of acid- and base-catalyzed sol-gel reactions

Sol-gel reactions can be catalyzed by acids, bases or metal salts. Acid and base-catalyzed systems are commonly used in sol-gel processes whereas metal salts, e.g., dibutyltin dilaurate or dibutyltin diacetate, are typically used when a room-temperature neutral reaction condition is required. The mechanisms of acid- and base-catalyzed sol-gel reactions are difficult to study owing to difficulties in separating hydrolysis from condensation. Some studies have reported that these two reactions occur simultaneously. However, in an effort to understand their mechanisms, the fundamental nucleophilic substitution mechanism has been utilized. Many reactions occur during sol-gel processes including hydrolysis, condensation, re-esterification and trans-esterification. Only the two principal steps, hydrolysis and condensation, will be discussed herein.

2.3.2.1 Hydrolysis reactions

Base-catalyzed hydrolysis is thought to proceed via a bimolecular nucleophilic substitution reaction (S_N2) (Figure 2.21).¹⁴⁸ Hydrolysis is initiated as the base (OH^-) attacks a silicon atom on an alkoxy silane through transition state 1 (TS1). A pentacoordinate intermediate is formed with the central silicon possessing a negative charge. The intermediate decomposes through transition state 2 (TS2) and eventually yields an alkoxy silanol and alkoxide anion. The alkoxide anion can abstract a proton from water to essentially form alcohol and regenerate the base (OH^-). This reaction can occur via either S_N2^{*-Si} or S_N2^*-Si mechanisms. The rate

¹⁴⁸ E. R. Pohl and F. D. Osterholtz, In *Molecular Characterization of Composite Interfaces*, Y. Ishida and G. Kumar (Eds.), Plenum Press, New York (1985)

determining step in the S_N2^{**} -Si mechanism is formation of the intermediate ($k_{-1} < k_2$), and the rate determining step in the S_N2^* -Si mechanism is breakdown of the intermediate ($k_{-1} > k_2$).

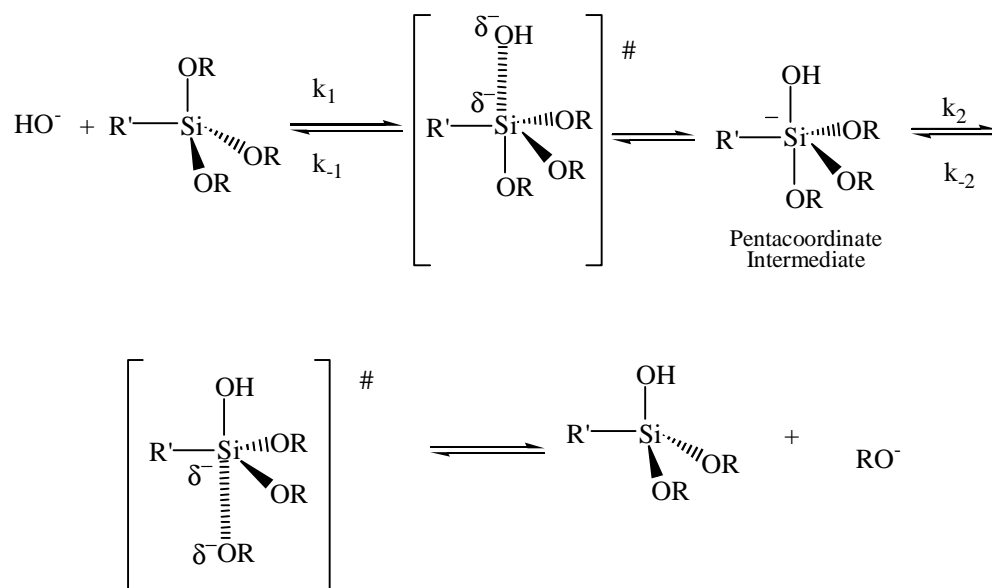


Figure 2.21 The proposed mechanism of base-catalyzed hydrolysis in sol-gel reactions.¹⁴⁸

According to the structure of the pentacoordinate intermediate in Figure 2.21, the silicon atom in both the transition states and intermediate possesses a negative charge. Thus, substituents which can stabilize the negative charge should increase the rate of the base-catalyzed hydrolysis. In addition, according to the S_N2 mechanism, as steric crowding on the silicon atom decreases, the rate of the hydrolysis should also increase. To prove the proposed S_N2 mechanism, Pohl et al. have studied kinetics of the base-catalyzed hydrolysis using alkoxy silanes with different alkyl

groups. The observed rate of base-catalyzed hydrolysis of γ -glycidoxypropyl trimethoxysilane is approximately ten times faster than that of n-propyl-tris(2-methoxyethoxy)silane. Because γ -glycidoxypropyl and n-propyl groups have somewhat similar steric and polar effects, the significant difference in hydrolysis rate must come from the alkoxy leaving groups. The methoxy groups are smaller than methoxyethoxy groups, and this promotes back-side attack from the hydroxyfunctional nucleophile to give inversion of the stereochemistry at silicon.

Acid-catalyzed hydrolysis of alkoxy silanes is also thought to occur via a S_N2 mechanism (Figure 2.22). In the first step of this reaction, H^+ protonates the oxygen atom of the alkoxy group to give an oxonium ion intermediate. The protonation changes the leaving group from RO^- to ROH which is a good leaving group (weak base). Water can then attack at the silicon atom and simultaneously eliminate ROH to yield a protonated silanol intermediate. A triangular bipyramid transition state occurs during the transformation. A proton from the protonated silanol is then removed resulting in an alkoxy silanol.

According to the S_N2 mechanism, bulky alkyl groups should suppress the acid-catalyzed hydrolysis rate due to blocking the nucleophile from approaching the silicon atom. Under acidic conditions, the rate of hydrolysis of γ -glycidoxypropyl trimethoxysilane is approximately a factor of ten faster than that of n-propyl-tris(2-methoxyethoxy)silane. This can be rationalized by the fact that the small methoxy group allows the nucleophile to approach the central silicon more easily relative to the bulky methoxyethoxy group.

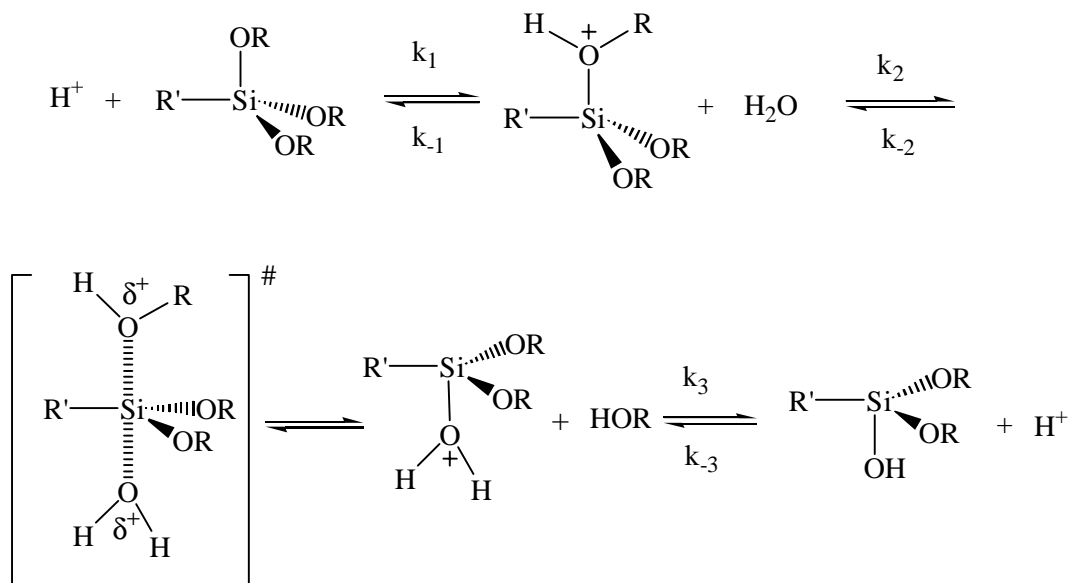


Figure 2.22 The proposed mechanism of acid-catalyzed hydrolysis in a sol-gel reaction.¹⁴⁸

According to Pohl's kinetic studies of dilute aqueous solutions, the rate of hydrolysis is first order with regard to both alkoxy silane concentration and catalyst concentration according to the steady state approximation as shown in the following equation:

$$-d[\text{silane}] / dt = k^{OH} [\text{OH}^-] [\text{silane}] + k^H [\text{H}^+] [\text{silane}] + k^B [\text{B}] [\text{silane}]$$

where [B] is the concentration of the conjugate base of the buffer calculated from pH, pK and the total buffer concentration.

2.3.2.2 Condensation reactions

Acid- and base-catalyzed condensations of alkoxy silanes are not fully understood, partially because of difficulties in studying such reactions. There are only a few thermally stable silanols available that can be utilized as starting materials for such studies, e.g., γ -aminopropylsilanetriol, and diphenylsilanediol. It has been reported that the rate of silica formation is at a minimum around pH 2.¹⁴⁸ Since this is the isoelectric point of silica, it is thought that H^+ is the primary catalyst species at pH below 2 and OH^- is the primary catalyst species at pH above 2. Pohl et al. have studied kinetics of acid- and base-catalyzed condensations using deuterium ions and deuterioxide anions as catalysts, respectively. The rates of condensation of γ -glycidoxypropylsilanetriol were first order in the catalyst concentration and second order in silanetriol concentration (as shown in the following equation):¹⁴⁸

$$-d[\text{silanetriol}] / dt = k_c^{DO} [DO^-] [\text{silanetriol}]^2 + k_c^D [D^+] [\text{silanetriol}]^2$$

Base-catalyzed condensation is proposed to proceed through an S_N2 mechanism. According to the mechanism in Figure 2.23, the deuterioxide anion first abstracts a deuterium from the trialkoxy silane starting reagent to yield a silanolate ion. The resulting silanolate nucleophile then reacts with a neutral silanol to form a pentacoordinate intermediate with a negative charge on the central silicon. This intermediate subsequently decomposes to yield a siloxane dimer and deuterioxide anion. The first step of the reaction proceeds rapidly compared to the second step. Further condensation of trialkoxy silane with the siloxane dimer was not observed at short reaction times. This was attributed to the increase in steric crowding around the silicon in dialkyltetrahydroxydisiloxane that can block the approach of a nucleophile toward a silicon atom resulting in significantly slower rates of condensation.

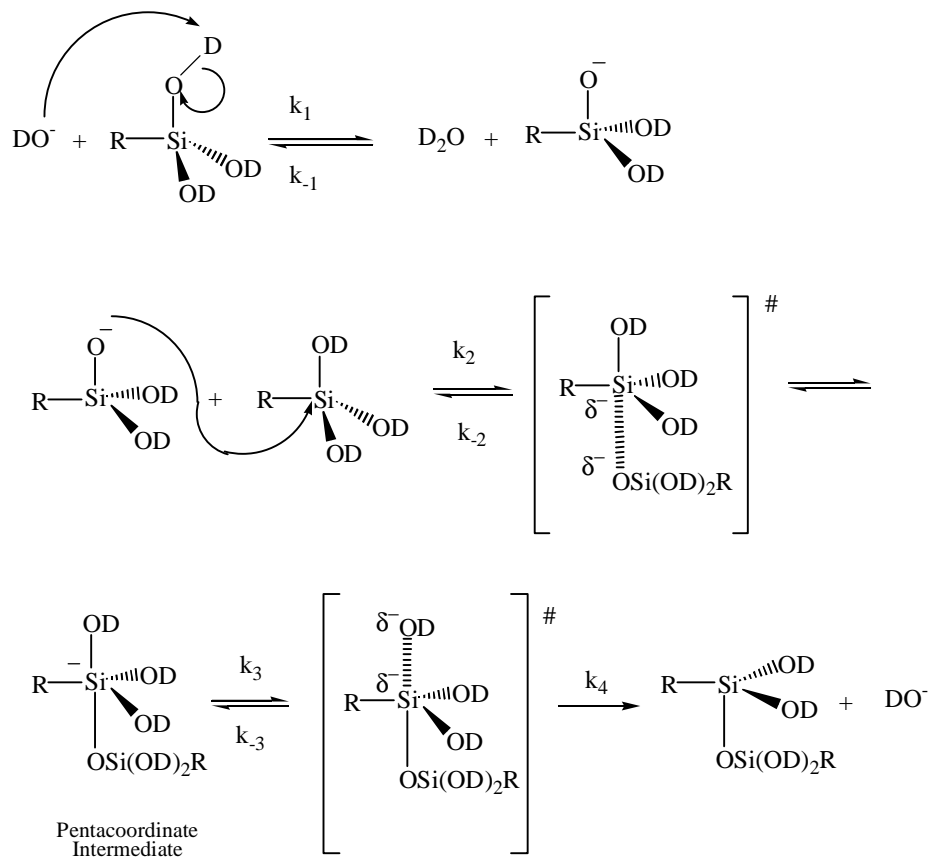


Figure 2.23 The proposed mechanism of base-catalyzed condensation in a sol-gel reaction. modified according to Pohl et al. and Swain et al.^{148, 149}

¹⁴⁹ C. G. Swain, R. M. Esteve and H. J. Jones, *J. Am. Chem. Soc.*, **11**, 965 (1949)

The S_N2 mechanism is usually used to explain acid-catalyzed condensations in sol-gel reactions (Figure 2.24). Based on the proposed mechanism of Pohl et al., an oxygen atom on trialkoxysilane first attacks deuterium ion to form a DOD leaving group.¹⁴⁸ An oxygen from a neutral alkoxide then attacks at the resultant deuterated silanol to form a triangular bipyramid transition state, then subsequently removes a D_2O molecule and forms a deuterated siloxane dimer. The deuterium ion is later transferred to D_2O or another alkoxy silane. According to the bimolecular rate law, steric factors are expected to play an important role on the rate of the reaction.

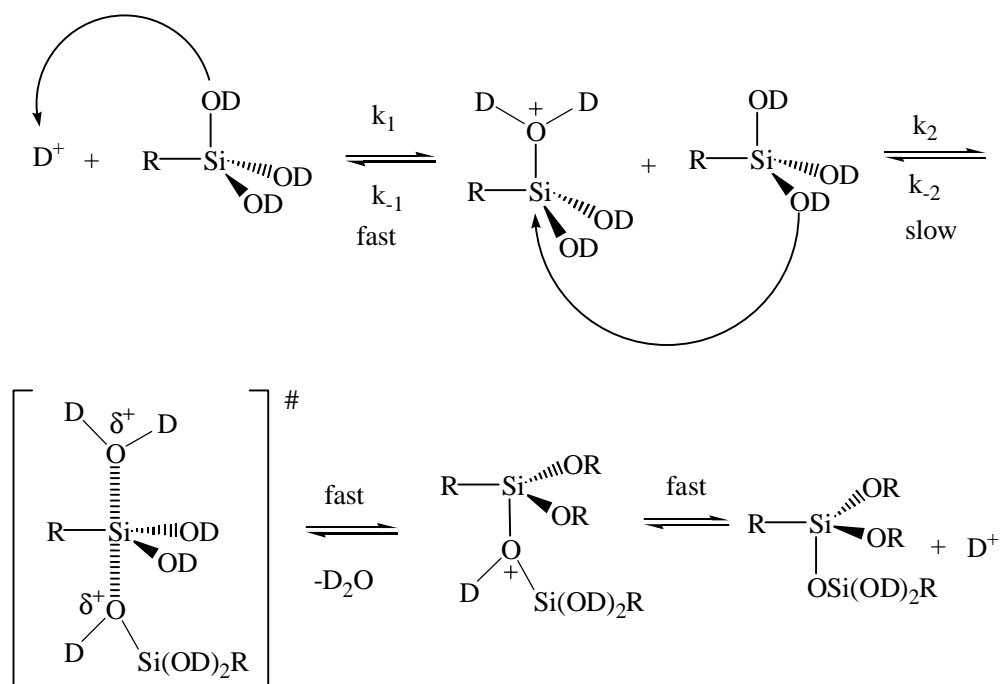


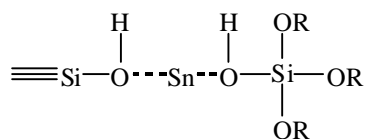
Figure 2.24 The proposed mechanism of acid-catalyzed condensation in a sol-gel reaction.

Modified according to Pohl et al. and Swain et al.^{148, 149}

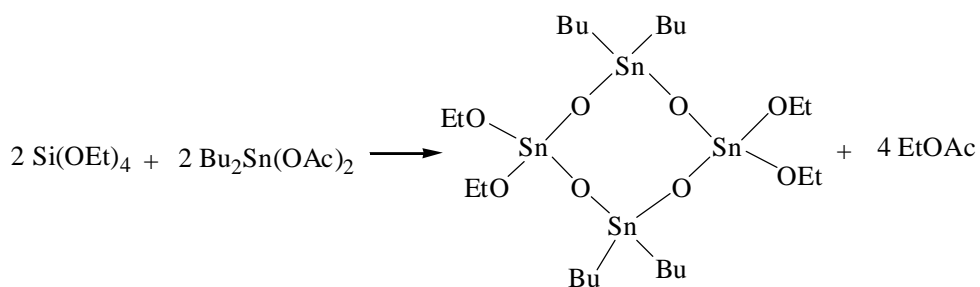
2.3.3 Mechanisms of tin-catalyzed sol-gel reactions

Although acid- or base-catalyzed hydrolyses are commonly used in sol-gel reactions, there is also a need for effective catalysis under neutral, low temperature conditions. Dibutyltin dioctoate^{150, 151} and TAZOR catalysts (DuPont) based on titanium salts³⁹ are effective catalysts for room temperature, moisture vulcanization of silanol/alkoxysilane containing polysiloxanes. Some other metal salts, e.g., dibutyltin dilaurate or dibutyltin diacetate, have also been of great interest, particularly in recent years. The tin-catalyzed sol-gel mechanism will be exclusively discussed in this section because dibutyltin diacetate was utilized as a catalyst in the sol-gel reactions conducted in this research.

The catalyzed mechanism is thought to involve the formation of a complex between tin, alkoxysilane and silanol.¹⁵²



Nagy also proposed formation of an organosilicon stannate as an intermediate.¹⁵³



¹⁵⁰ U.S. Patent 3,161,614 (1964)

¹⁵¹ D. R. Thomas, In *Siloxane Polymers*, S. J. Clarson and J. A. Semlyen (Eds.), PTR Prentice Hall, New Jersey (1993)

¹⁵² A. S. Novikov and Z. N. Nudel'man, *Kauchukbi Rezina*, No.12, 3 (1960)

¹⁵³ J. Nagy, A. Borbely-Kuszmán and J. E. Mark, *Period Polytech Chem. Eng.*, **10**, 139 (1960)

However, it is now believed that small amounts of water from the atmosphere play an important role in tin-catalyzed sol-gel reactions.¹⁵⁴ Jorg and Ernst proposed that hydrolysis of alkoxy silanes is initiated by water to form silanols which subsequently condense to yield a siloxane bond. A series of consecutive hydrolyses and condensations occur to eventually form silica networks. However, the role of the tin catalyst is not fully understood. Van der Weij et al.¹⁵⁵ proposed mechanisms leading to a better understanding of the role of water in these reactions. They postulated that water converts the tin carboxylate into an activated catalytic species. In the first step of this reaction, the tin carboxylate is partially hydrolyzed to yield a tin hydroxide (Figure 2.25). The activated tin hydroxide subsequently reacts with an alkoxy silane to produce an organotin silanolate and alcohol. Lastly, the condensation of the organotin silanolate with silanol produces a siloxane linkage and regenerates an activated tin hydroxide species. This reaction occurs via silanolysis of the Sn-O-Si bond. Severnyi et al. followed a similar line of thought for the tin-catalyzed mechanism except that, in the last step, it was proposed that the reaction occurred via silanolysis of the Si-O-C bond.¹⁵⁶

¹⁵⁴ P. Jorg and W. Ernst, *Chemiker-Ztg.*, **97**, 176 (1973)

¹⁵⁵ F. W. Van der Weij, *Makromol. Chem.*, **181**, 2541 (1980)

¹⁵⁶ V. V. Severnyi, R. M. Minas'yan, I. A. Makarenko and N. M. Bizyuakova, *Vysokomoh Soedin. Ser. A (Eng. trans.)*, **18**, 1464 (1976)

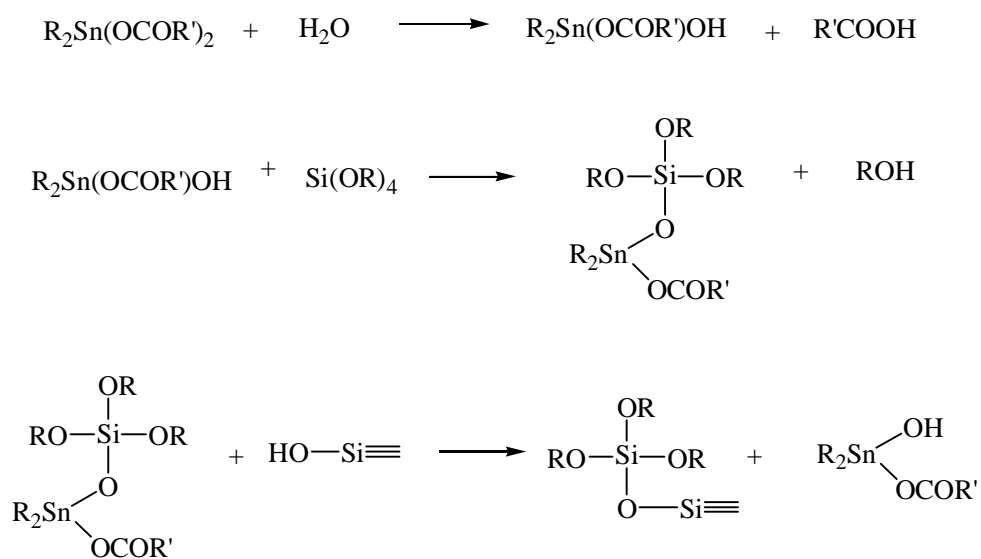


Figure 2.25 The proposed mechanism of a tin-catalyzed sol-gel reaction. Modified according to Reference 151.

2.3.4 Current interests and applications in sol-gel reactions

Due to the exceptional thermal and oxidative stability of silicates^{157, 158} combined with the high optical quality of silica thin films,¹⁵⁹ a wide variety of film coatings have been prepared by sol-gel processes. In addition to simple preparation methods, the mild processing conditions of sol-gel reactions are also attractive. A number of sol-gel film coatings are currently in use.^{141, 160} There are many reasons for coating materials, e.g., to make materials biocompatible,^{134, 161, 162} to improve optical quality,¹⁶³ to increase a material's thermal, mechanical or chemical stability, to increase abrasion resistance, durability or lifetime,¹⁶⁴ and to decrease friction or inhibit corrosion.¹⁶⁵ Most of these properties are particularly important in optical applications, e.g., optical waveguides,¹⁶⁶ UV-shielding films,¹⁶⁷ reflective films,¹⁶⁸ electrooptic and non-linear optical films,^{169, 170} and fluorescent films.¹⁷¹ Other applications for chemical, mechanical and electrical purposes are also important.^{172, 173}

¹⁵⁷ C. R. Helms and B. E. Deal (Eds.), In *The Physics and Chemistry of SiO₂ and the Si-SiO₂ Interface*, Plenum Press, New York (1988)

¹⁵⁸ C. R. Helms and B. E. Deal (Eds.), In *The Physics and Chemistry of SiO₂ and the Si-SiO₂ Interface 2*, Plenum Press, New York (1993)

¹⁵⁹ H. Schmidt and H. Bottner, In *The Colloid Chemistry of Silica*, H. E. Bergna (Ed.), American Chemical Society (1994)

¹⁶⁰ C. H. Winter and D. M. Hoffman (Eds.), In *Inorganic Materials Synthesis: New Directions for Advanced Materials*, American Chemical Society, Washington DC (1999)

¹⁶¹ J. Livage, T. Coradin and C. Roux, *J. Physics: Condense Matter*, **13**, R673-R691 (2001)

¹⁶² D. M. Liu and I. W. Chen, US Patent; The Trustees of the University of Pennsylvania, 6,303,209, October 16, 2001

¹⁶³ E. Barrera, T. Viveros, A. Avila, P. Quintana, M. Morales and N. Batina, *Thin Silica Films*, **346**, 138-144 (1999)

¹⁶⁴ D.D. Erickson, T. E. Wood and W. P. Wood, In *Sol-Gel Synthesis and Processing*, p.73, S. Komarneni, S. Sakka, P. P. Phule and R. M. Laine (Eds.), The American Chemical Society (1998)

¹⁶⁵ B. D. Fabes and W. C. Oliver, *J. Non-Cryst. Solids*, **121**, 348 (1990)

¹⁶⁶ C. L. Luyer, L. Lou, C. Bovier, J. C. Plenet, J. G. Dumas and J. Mugnier, *Optical Materials*, **18**, 211-217 (2001)

¹⁶⁷ H. Dislich and E. Hussmann, *Thin Solid Films*, **77**, 129 (1981)

¹⁶⁸ E. R. La Serra, Y. Charbouillot, P. Baudry and M. A. Aegerter, *J. Non-Cryst. Solids*, **121**, 323 (1990)

¹⁶⁹ Y. Xu, C. J. Chen, J. D. Mackenzie, *Proc. SPIE's 1990 Symp.*, Vol. 1328, p.428, p.441.

¹⁷⁰ I. Lee, M. A. Snipes and J. Covino, In *Sol-Gel Science and Technology*, E. J. A. Pope, S. Sakka and L. C. Klein (Eds.), Ceramic Transaction, v.55, The American Chemical Society, Ohio (1994)

¹⁷¹ R. Reisfeld, M. Eyal, V. Chernyak and R. Zusman, *Solar Energy Materials*, **17**, 439 (1988)

¹⁷² L. L. Hench, In *Ultrastructure Processing of Advanced Structural and Electronic Materials*, Noyes Publications, New Jersey (1984)

Sol-gel film coatings of magnetic nanoparticles are of particular interest in recent years. Magnetic 'nano-coatings' are designed to cover the particles with a nanometer scale layer. Most of the magnetic thin films are utilized in high-density information storage, e.g., recording tapes and disks.¹⁷⁴ Similar coatings have also been attempted for catalytic,¹⁷⁵ and optical filter¹⁷⁶ purposes.

Lee et al. have recently studied the growth of ultra-fine magnetic CoFe_2O_4 particles and thin films introduced by using a sol-gel process.¹⁷⁷ Cobalt ferrites, cubic ferrimagnetic oxides, are candidates for high-density recording devices owing to their high coercivity (5400 Oe) and saturation magnetization (80 emu/g). Silica thin films coated onto these particles can provide excellent chemical stability and mechanical hardness. The CoFe_2O_4 particles were prepared by a pyrolysis method using $\text{Co}(\text{CH}_3\text{CO}_2)_2 \cdot 4\text{H}_2\text{O}$ and $\text{Fe}(\text{NO}_3)_3$ as precursors. They were suspended in a sol-gel medium, and then spin-coated onto a thermally oxidized Si wafer. The magnetic properties of the Co-ferrite powders and films were investigated as a function of annealing temperature. It was found that the saturation magnetization and coercivity of the annealed powders depended strongly on the annealing temperature. The Co-ferrite films annealed at 200 °C and 350 °C exhibited a typical spinel structure whereas those annealed at 650 °C exhibited a single-phase spinel structure without any preferred crystallite orientation. The thin films annealed at 850 °C provided the maximum coercivity at 2550 Oe.

¹⁷³ S. Sakka and T. Yoko, In Structure and Bonding; Chemistry, Spectroscopy and Applications of Sol-Gel Glasses, v. 77, M. J. Clarke, J. B. Goodenough, C. K. Jorgenson, J. B. Neilands, D. Reinen and W. Weiss (Eds.), p.89, Springer-Verlag, Berlin (1992)

¹⁷⁴ R. A. Caruso and M. Antonietti, *Chem. Mater.*, **13**, 3272-3282 (2001)

¹⁷⁵ S. Braun, S. Rappoport, R. Zusmen, D. Avnir and M. Ottolenghi, *Mater. Lett.*, **10**, 1 (1990)

¹⁷⁶ M. R. Bohmer, A. R. Balkenenda, T. N. M. Bernards, M. P. J. Peeters, M. J. van Bommel, E. P. Boonekamp, M. A. Verheijen, L. H. M. Krings and Z. A. E. P. Vroon, In Handbook of Advanced Electronic and Photonic Devices, H. S. Nalwa (Ed), Academic Press, San Diego (2001)

¹⁷⁷ J. G. Lee, H. M. Lee, C. S. Kim and Y. J. Oh, *J. Magn. Magn. Mater.*, **177**, 900 (1998)

Homogeneous incorporation of gold nanoparticle cores within silica gels have been reported by Liz-Marzan et al.¹⁷⁸ To obtain a homogeneous distribution of particle sizes, the surfaces of the gold particles were modified by depositing a thin silica shell before gel formation. Gold particles were prepared by boiling H₂AuCl₄ in the presence of sodium citrate, and then rigorously stirring in sodium silicate solution to deposit silica thin films on the particles. Unlike *in situ* prepared nanoparticle coatings, this process allowed better control of the nanoparticle morphology and properties. Gold nanoparticles were chosen for this system due to the high sensitivity of their optical properties to aggregation and to the environment. Two different sol-gel processes were utilized to prepare silica gels embedded with gold nanoparticles: (1) A sodium silicate method and (2) a tetramethoxysilane (TMOS) method. In both cases, formations of mesopores within the gel structure were observed. The pore sizes were smaller for gels formed by the TMOS method than those formed by the sodium silicate method. This was rationalized with different gelation mechanisms. In the sodium silicate method, gelation originates from the bonding of previously existing polymers, whereas in the TMOS method, gelation arises from silicic acid due to hydrolysis of TMOS. According to transmission electron microscopic (TEM) images combined with UV-visible spectra, the particle size distribution is homogeneous and no aggregation of the particles was observed during the sol-gel reaction in either method. The optical properties of the starting colloid were fully retained in the silica gel since silica thin films are transparent.

¹⁷⁸ Y. Kobayashi, M. A. Correa-Duarte and L. M. Liz-Marzan, *Langmuir*, **17**, 6375-6379 (2001)

2.4 Magnetisms and magnetic materials

2.4.1 Introduction to magnetic materials

Magnetic materials are objects that attract each other and also repel each other depending on their relative orientations.^{179, 180, 181} Magnetite (Fe_3O_4) was the first known magnetic material. A number of magnetic materials are presently utilized for a wide variety of applications.¹⁸² There are several important parameters related to magnetic materials. For example, *magnetic flux density* or *magnetic induction* (B) is the net magnetic response of a medium to an applied field (H).¹⁸³ It is measured in tesla (T) in SI units (International System of Units) and gauss (G) in cgs units (The units based on centimeters, grams and seconds). The relationship is given by the following equation:

$$B = \mu_o (H + M) \quad \text{in SI units}$$

$$B = H + 4\pi M \quad \text{in cgs units}$$

where H is *magnetic field strength* generated by currents and magnetic poles (A/m in SI units and Oersteds in cgs units), M is magnetization and μ_o is the permeability of free space ($4\pi \times 10^{-7}$ H/m). *Magnetization* is defined as the magnetic moment (m) per unit volume (V), thus $M = m/V$. It is measured as A/m in SI units and emu/cm³ in cgs units.

In general, magnetization (M) of a material is dependent on the magnetic field (H) applied on it. Therefore, *magnetic susceptibility* (χ), a magnetic parameter giving an indication of the response of a material to an applied magnetic field, has been used. Magnetic susceptibility is defined as a ratio of magnetization (M) to the applied field (H), $\chi = M/H$. Because M and H

¹⁷⁹ J. P. Jakubovics, In *Magnetism and Magnetic Materials*, 2nd Ed., The Institute of Materials, London (1994)

¹⁸⁰ D. J. Craik and R. S. Tebble, In *Ferromagnetism and Ferromagnetic Domains*, John-Wiley&Sons, New York (1965)

¹⁸¹ R. S. Tebble and D. J. Craik, In *Magnetic Materials*, Willey-Interscience, London (1969)

¹⁸² D. J. Craik, In *Structure and Properties of Magnetic Materials*, Pion Limited, London (1971)

¹⁸³ D. Halliday and R. Resnick, In *Physics*, 3rd Ed., John Wiley&Sons, New York (1978)

have the same dimensions, χ is a dimensionless parameter both in SI and cgs units (multiply the cgs susceptibility by 4π to obtain the SI susceptibility). χ can be expressed in terms of B as follows:

$$B = \mu_o (1 + \chi) H$$

One can define $\mu = 1 + \chi$ and thus

$$B = \mu_o \mu H$$

where μ is *magnetic permeability*.

Both μ and χ are important characteristic parameters of magnetic materials. It is desirable to have materials with large values of μ and χ indicating a significant response to an external magnetic field. χ ranges from values close to zero, both positive and negative, to positive values much greater than one.

Magnetic materials are classified into 5 categories based on their magnetic properties: diamagnetism, paramagnetism, ferromagnetism, antiferromagnetism and ferrimagnetism (Table 2.10).^{179, 184, 185} The atoms of *diamagnetic materials* as a whole have no net magnetic moments since two magnetic moments from two electrons align in opposite directions and cancel each other. Atoms from the other four categories, on the other hand, show net magnetic moments because the cancellation of magnetic moments is only partial. *Paramagnetic materials* are distinguished by the fact that their moments point in random directions at any temperature in an absence of an external magnetic field. Atoms in the other three categories have moments which align in some manner with those of their neighbors. In *ferromagnetic materials*, the magnetic moments become parallel to each other in the same direction. In *antiferromagnetic materials*, the magnetic moments tend to align antiparallel to the neighboring moments. In *ferrimagnetic*

¹⁸⁴ K. J. Standley, In *Oxide Magnetic Materials*, 2nd Ed., Clarendon Press, London (1972)

¹⁸⁵ B. D. Cullity, In *Introduction to Magnetic Materials*, Addison-Wesley Company, Massachusetts (1972)

materials, the tendency is also antiparallel alignment, but either the number or the size of the moments in each direction is unequal. Figure 2.26 depicts the alignment of magnetic moments in each class of materials.¹⁷⁹ The alignment of moments of ferro-, antiferro- and ferrimaterials (Figure 2.26b, c and d) represent materials which are below a “critical temperature”. Above this temperature, the magnetic moments randomize (Figure 2.26a).

Table 2.10 Classification of materials based on magnetic properties.¹⁷⁹

Class	Critical Temperature	Structure on atomic scale	Examples
Diamagnetic	None	Atoms have no permanent dipole moments	Inert gases; many metals, e.g., Cu, Hg, Bi; non-metallic elements, e.g., B, Si, P, S; many ions, e.g., Na ⁺ , Cl ⁻ , and their salts; most diatomic molecules, e.g., H ₂ , N ₂ , water; most organic compounds.
Paramagnetic	None	Atoms have permanent dipole moments. Neighbouring moments do not interact.	Some metals, e.g., Cr, Mn; some diatomic gases, e.g., O ₂ , NO; ions of transition metals and rare earth metals, and their salts; rare earth oxides.
Ferromagnetic	Curie temperature, θ_C	Atoms have permanent dipole moments. Interaction produces $\uparrow\downarrow$ alignment.	Transition metals Fe, Co, Ni; rare earths with $64 \leq Z \leq 69$; alloys of ferromagnetic elements; some alloys of Mn, e.g., MnBi, Cu ₂ MnAl.
Antiferromagnetic	Neel temperature, θ_N	Atoms have permanent dipole moments. Interaction produces $\uparrow\downarrow$ alignment.	Many compounds of transition metals, e.g., MnO, CoO, NiO, Cr ₂ O ₃ , MnS, MnSe, CuCl ₂ .
Ferrimagnetic	Curie temperature, θ_C	Atoms have permanent dipole moments. Interaction produces $\uparrow\downarrow$ alignment, but moments are unequal.	Fe ₃ O ₄ (magnetite), γ -Fe ₂ O ₃ (maghemite); mixed oxides of iron and other elements.

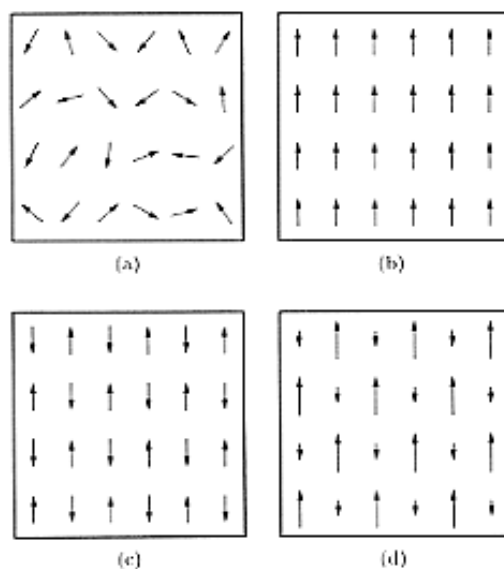


Figure 2.26 Schematic diagram of the alignment of magnetic moments, a) in paramagnetic materials at any temperature, and b) in ferromagnetic materials, c) in antiferromagnetic materials and d) in ferrimagnetic materials.¹⁷⁹

2.4.2 Ferrofluids

Magnetic fluids are colloidal suspensions containing ultrafine ferro- or ferrimagnetic particles.^{186, 187} To date, there are no known “natural” homogeneous fluids which inherently possess ferromagnetic properties.¹⁸⁸ Magnetic fluids, normally called “ferrofluids”, are concentrated, stable suspensions of ultrafine magnetic particles in an appropriate carrier fluid, e.g., esters, hydrocarbons or polysiloxanes. They are typically prepared in the presence of a surfactant to provide colloidal stability. The sizes of colloidal magnetic particles are so small

¹⁸⁶ S. Odenbach, *Adv. Colloid Interface Sci.*, **46**, 263 (1993)

¹⁸⁷ P. C. Scholten, *Int. Magn. Magn. Mater.*, **39**, 99 (1983)

¹⁸⁸ S. W. Charles, In *Magnetic Properties of Fine Particles*, J. L. Dormann and D. Fiorani (Eds.), North-Holland, Amsterdam (1991)

that each particle is a single magnetic domain (~10 nm in diameter), and thus these particles are subject to Brownian motion which hinders sedimentation.

Pioneering research on ferrofluids was begun by Papell¹⁸⁹ in 1965, followed by work by Rosensweig¹⁹⁰ in 1975. Commercial products based on magnetic fluids first became available in the late 1960s.¹⁹¹ Commercial devices containing magnetic fluids are now extensively used, e.g., in rotating shaft seals, magnetic field-promoted separations, printers, hydrostatic bearings, damping devices, measuring devices, sealed motors and acoustic devices.¹⁹¹ Ferrofluids are also now used in coolant systems. In medical applications, ferrofluids have been proposed for use as X-ray and NMR contrast substances,¹⁹² for cell separations,¹⁹³ as drug carriers,¹⁹⁴ and now as internal tamponades for treating retinal detachment.^{195, 196}

In the absence of an external magnetic field, the magnetic moments of each single particle are randomized and the materials are not magnetized. Since the particle sizes are so small, their magnetic moments can rotate essentially instantaneously along an applied magnetic field gradient and this can significantly enhance the strength of the applied field. If the magnetic moments completely randomize once the applied field is removed, the particles are considered “*superparamagnetic*” (Figure 2.27). Superparamagnetic fluids differ from ordinary paramagnetic fluids in that they have high magnetic susceptibility (χ) and are able to be saturated

¹⁸⁹ S. S. Papell, US Patent 3,215,572, assigned to NASA (1965)

¹⁹⁰ R. E. Rosensweig, US Patent, 3,917,538, assigned to Ferrofluidics Corporation (1975)

¹⁹¹ V. E. Fertman, In *Magnetic Fluids Guidebook: Properties and Applications*, Hemisphere Publishing Corporation, New York (1990)

¹⁹² V. G. Bashtovoy, B. M. Berkovsky and A. N. Vislovich, In *Introduction to Thermomechanics of Magnetic Fluids*, Springer-Verlag, New York (1988)

¹⁹³ R. Langer, *Nature*, **392**, 5 (1998)

¹⁹⁴ K. J. Wider, A. E. Senyei and D. G. Scarpelli, *Proc. Soc. Exp. Biol.*, **58**, 141 (1978)

¹⁹⁵ J. P. Dailey, J. P. Phillips and J. R. Riffle, *J. Magn. Magn. Mater.*, **194**, 140 (1999)

¹⁹⁶ J. P. Stevenson, M. Rutnakornpituk, M. Vadala, A. R. Esker, S. W. Charles, S. Wells, J. P. Dailey and J. S. Riffle, *J. Magn. Magn. Mater.*, **225**, 47 (2001)

in moderate fields. In addition, they also differ from typical ferromagnetic materials in that they do not exhibit magnetic hysteresis.

Magnetic hysteresis is a property of magnetic materials in which the magnetic induction (B) for a given magnetic field strength (H) depends upon its previous history. Figure 2.28, plotted as H vs. M , illustrates a typical *hysteresis loop* for magnetic materials having hysteresis.¹⁷⁹ Starting from point O, as magnetic field (H) is applied, magnetization (M) increases, reaches a maximum rate at A, and reaches a constant value at B. At this point, the materials are saturated and M is called “*saturation magnetization*”, abbreviated as M_s . The curve O-A-B is a typical *initial magnetization curve*.

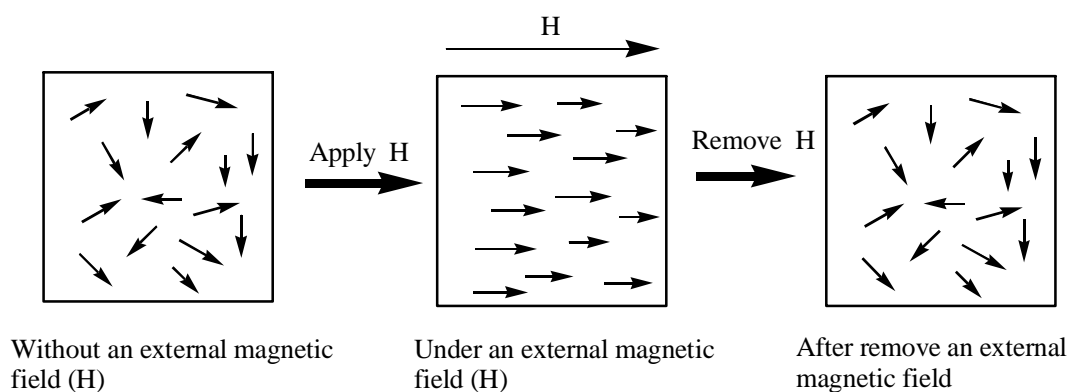


Figure 2.27 A schematic diagram of the properties of superparamagnetic fluids.

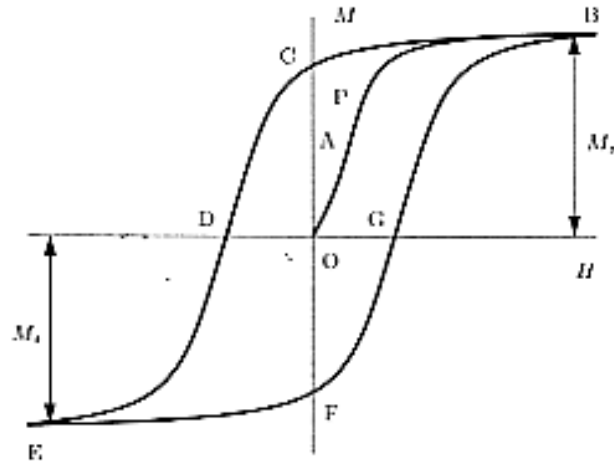


Figure 2.28 A hysteresis loop characteristic of typical magnetic materials.¹⁷⁹

In magnetic materials having hysteresis, M is not superimposed on the curve $B-A-O$ as H is decreased, but decreases more slowly and has a non-zero value when H is zero (point C). H then is applied in the opposite direction to further decrease M until it passes through zero (point D), and then begins to increase in an opposite direction and reaches M_s eventually. At this point, if H is decreased, M follows the curve $E-F-G-B$. Two important parameters are typically used to describe the hysteresis in magnetic materials: remanence and coercivity. The largest magnetization remaining in the magnetic materials in a zero field is called *remanent magnetization* or *remanence* (points C and F). The reversed field (H) required to reduce M to zero from remanence is called the *coercive field* or *coercivity* (points D and G).

A number of magnetic materials have been prepared in recent years. However, only a few can be successfully used to prepare magnetic fluids. Table 2.11 shows currently available magnetic fluids in order of increasing saturation magnetization (M_s).¹⁹⁷ Materials with higher values of M_s , unfortunately, tend to oxidize more rapidly than the lower ones as indicated by the increasingly negative ΔG . Magnetite (Fe_3O_4), ferrites and maghemite ($\gamma\text{-Fe}_2\text{O}_3$) have fairly weak M_s compared to the others, but they are relatively stable in the atmosphere. Although magnetite, the most commonly used ferrofluid, can be oxidized to maghemite ($\gamma\text{-Fe}_2\text{O}_3$), their M_s (fortunately) does not drop significantly. The materials with highest M_s are found in transition and rare-earth metals. However, oxidation of these nanoparticles has been an obstacle and has limited their applications.

Table 2.11 Properties of magnetic fluids.¹⁹⁷

Materials	J (Tesla)	ΔG^* (kJ/mol)
$\gamma\text{-Fe}_2\text{O}_3$	0.52	0
Ferrites	0 to 0.53	N/A
Fe_3O_4	0.60	-97.2
Ni	0.61	-216.3
Co	1.79	-213.4
Fe	2.15	-244.3
FeCo	2.40	N/A

* Gibbs energy of oxidation to the next higher valency

¹⁹⁷ P. C. Scholten, *Chem. Eng. Comm.*, **67**, 331 (1988)

Attempts have been made to protect these particles against oxidation with oxide films. The minimal thickness required to prevent oxygen from contacting nickel¹⁹⁸ or cobalt¹⁹⁹ particles is reported to be 1.5 nm. Since the particle sizes are so small (~10 nm), these thin oxide layers result in only 34% in volume of metal remaining. Therefore, the intrinsic magnetization of the particles is significantly decreased. Utilizing stabilizers as oxygen barriers has also been proposed. However, the stabilized particles still gradually oxidize because oxygen can diffuse through the surfactants at about the same rate as through solvents.

Desired properties for carrier fluids (base fluids) in magnetic fluids include a low evaporation rate, a low melting point and viscosity, chemical inertness, high temperature stability and excellent dispersing capability. However, there are no available candidates which fulfill all of these requirements. Advantages and disadvantages of typical carrier fluids are shown in Table 2.12. Aliphatic hydrocarbons have good chemical stability and excellent dispersant ability, but high viscosities, melting points and/or high vapor pressures tend to limit many applications. Silicone fluids, both linear and cyclic, have many intriguing properties that meet most of the criteria, especially excellent high temperature stability. Nonetheless, stabilizers that are dispersible in silicone fluids are very limited. PDMS-*b*-PCPMS-*b*-PDMS and related pentablock steric stabilizers (PCPMS = poly(3-cyanopropylmethyl)siloxanes)¹⁹⁶ have been prepared in the present work and are extensively discussed in this dissertation.

¹⁹⁸ K. E. Heuslet, In *Passivity of Metals*, R. P. Frankenthal and J. Kruger, p. 771, The Electrochemical Soc., Princeton (1978)

¹⁹⁹ R. Anthore, *J. Physique*, **38** C2, 203 (1977)

Table 2.12 Advantages and disadvantages of typical carrier fluids in magnetic fluids.¹⁹⁷

	Viscosity	Vapor pressure	Chemical stability	High temp. stability	Radiation resistance	Dispersant availability
Aliphatic hydrocarbons	-	-	+	+/-		++
Diesters	+	+	-	-		++
Orthosilicic acid esters	++	+/-	-	-		+
Linear silicones	+	++	+	+		-
Cyclic silicones	+	++	+	++		-
Polyphenylene oxides	+	+	+		++	+
Perfluoro polyethers	++	++	++			-
Polychloro biphenyls	+	+	+*	+		+

++ Excellent, + Good, - Poor

* Dangerous in combination with metallic particles

2.4.3 Stabilization in magnetic fluids

Magnetic fluids are comprised of ultrafine colloidal suspensions of single-domain particles in which the particles, typically $10^{23}/\text{m}^3$, undergo frequent collisions. To obtain stable colloidal magnetic fluids, the attractive forces comprised of magnetic dipole-dipole interactions and van der Waals forces must be overcome by the repulsive forces. The attractive and repulsive interactions operative in magnetic fluids are outlined as follows.

2.4.3.1 Attractive forces

Because each particle in magnetic fluids has a single magnetic dipole, *the magnetic dipole-dipole interactions* between particles are attractive and favor aggregation. Magnetically-induced aggregation as well as sedimentation due to gravitational forces can be overcome by thermal motion (Brownian motion) if the particles are sufficiently small (3-10 nm in diameter).

In addition to magnetic interactions, *London-type van der Waals' forces* also exist in the colloid. These forces are generated from the polarization of one molecule by fluctuations in the charge distribution in the second molecule (dipole-dipole interactions). Van der Waals' forces cannot be overcome by thermal motion because of large negative potential energies when particles are in close contact. Therefore, it is necessary to generate repulsive forces to prevent close contact and obtain stable magnetic dispersions.

2.4.3.2 Repulsive forces

Stabilization in magnetic fluids usually arises from either electrostatic repulsion in which each particle contains the same surface charge, or steric repulsion in which the particles are coated with surfactants. *Electrostatic repulsion* results because particles with surface electric charges prefer to adsorb ions of opposite sign and repel ions of the same sign to neutralize their surfaces (Figure 2.29a).²⁰⁰ This leads to formation of an electric double layer. The inner layer is called the Stern layer and consists of tightly bound ions while the outer layer, the so-called diffusion layer, has scattered ions of opposite charge (Figure 2.30a).²⁰¹ As two particles surrounded by this electric double layer come into close contact, the repulsive potential (ϕ) increases significantly (Figure 2.30b).

Stability of colloidal suspensions can also be achieved by coating each particle with an adsorbed surface layer to provide *steric repulsion* and form a potential barrier preventing particles from approaching each other (Figure 2.29b). In general, surfactants contain anchor groups which adsorb onto the particle surfaces and flexible tails that are soluble in the carrier fluids. When these tails with an appropriate length extend outward into the fluids to avoid particle-to-particle agglomeration, the particles are stabilized by an entropic mechanism. When two particles in the colloidal suspension approach each other, the degree of disorder decreases leading to a decrease in entropy (negative ΔS). Because the enthalpy change is negligible (ΔH), the Gibbs free energy change of particles approaching each other has a positive sign ($\Delta G = \Delta H - T\Delta S$) with the result being steric prevention of particle agglomeration.

²⁰⁰ P. C. Scholten, In *Thermomechanics of Magnetic Fluids*, p.1, B. Berkovsky (Ed.), Hemisphere Publishing Corp., Washington (1977)

²⁰¹ S. Wells, In *Preparation and Properties of Ultrafine Magnetic Particles*, Thesis, The University of Wales, 1989

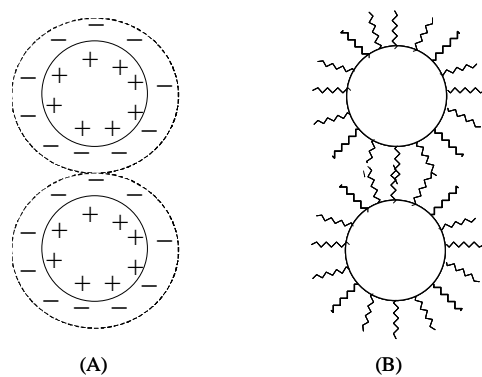


Figure 2.29 A) Electrostatic stabilization, and B) steric stabilization of colloidal suspensions.²⁰⁰

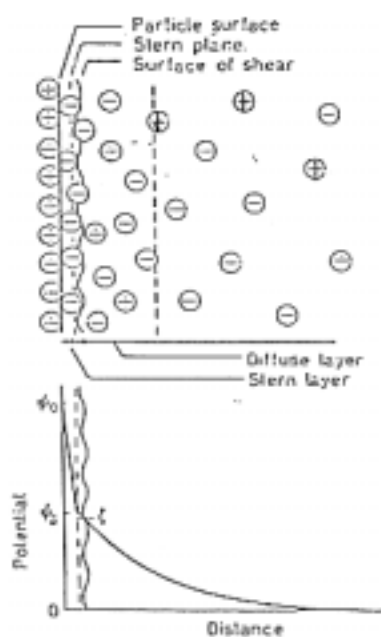


Figure 2.30 A schematic diagram of the electric double layer, and the plot of repulsive potential vs distance between two particles.^{39, 201}

Oleic acid is one of the best known surfactants used to stabilize magnetite particles (Fe_3O_4) in hydrocarbon media. It consists of a C_{17} hydrocarbon chain with a carboxylic acid functional group at one end. It is thought that, under basic conditions, carboxylate anions can adsorb onto the particle surface and the hydrocarbon chain provides steric repulsion. Utilization of block copolymers containing functional groups in one block as surfactants has also been reported for preparing magnetic fluids.^{202, 203}

2.5 Preparation of cobalt magnetic fluids

In recent years, nanoparticle materials have generated a large interest due to their unusual chemical and physical properties. These properties are quantitatively and qualitatively different from those of either the single atoms or bulk materials. Magnetic properties, e.g., superparamagnetism or ferromagnetism, are not inherent in a molecule or an ion but arise from bulk structures. Since interactions between molecules or ions generate such properties, understanding the solid-state structure will allow one to control and manipulate such behavior. Nanomagnetic materials are currently utilized in various applications, e.g., catalysis, high-density data storage devices and sensors.

Cobalt nanoparticles have gained a technologically driven interest owing to their high spin density, and consequently, exceptional magnetic properties. In general, homogeneous colloidal cobalt dispersions can be prepared in the presence of a polymeric stabilizer in a dilute solution of a suitable inert solvent, and a suitable cobalt precursor. Two well-known successful means for preparing such dispersions are the thermal decomposition of organic cobalt precursors

²⁰² Y. Xie, T. Liu, and B. Chu, *Polym. Mater. Sci. Eng.*, **79**, 334 (1998)

²⁰³ T. Hashimoto, M. Harada, and N. Sakamoto, *Macromolecules*, **32**, 6867 (1999)

and the reduction of cobalt salts. It is hypothesized that the reactions can occur in micellar cores formed by amphiphilic block copolymers or block copolymers containing polar and nonpolar sequences in an appropriate selective solvent. Suitable polymeric stabilizers can form micelle structures if their concentration is above the cmc. One block in diblock copolymers or the anchor block in triblock copolymers should consist of functional groups that have an established affinity to adsorb onto, or bond to, the particle surface. The tail block can protrude outward into the solvent or carrier fluid to provide steric stability. In addition, the polymeric stabilizers should be soluble in the selective solvent, preferably at room temperature, and necessarily at the reaction temperature.

Because the micelles exist on a nanoscopic scale, they can be considered nanoscopic reaction vessels. Preparation of stable cobalt dispersions in micelle nanoreactors has been reported as a successful means to obtain extremely narrow size distributions and controlled the particle size by changing the copolymer/cobalt ratio. Krishnan et al. have reported that the size and shape of the resultant cobalt dispersions can be controlled by adjusting the surface tensions of the growing particles.²⁰⁴

2.5.1 Thermal decomposition of $\text{Co}_2(\text{CO})_8$

A number of cobalt carbonyl and cobalt organocarbonyl compounds are suitable cobalt precursors for preparing stable colloidal cobalt dispersions (Table 2.13).²⁰⁵ $\text{Co}_2(\text{CO})_8$ is the most extensively used because of its availability and low cost. The cobalt atoms in the compounds are bound to carbonyl ligands (CO), which can be displaced at the decomposition temperature. The

²⁰⁴ V. F. Puentes and K. M. Krishnan, *IEEE Transactionson Magnetics*, **37**(4), 2210 (2001)

²⁰⁵ T. W. Smith, US Patent 4,252,674, assigned to Xerox Corporation (1981)

decomposition temperature of $\text{Co}_2(\text{CO})_8$ is relatively low compared to those of other carbonyl compounds (Table 2.14) and thus easily decomposes at room temperature.²⁰⁶ Another important feature of $\text{Co}_2(\text{CO})_8$ is that CO gas is volatile and easily removed from the reaction mixture. In addition, the CO gas does not interrupt the decomposition process or the stability of the resultant dispersion. Smith has reported that CO ligands dissociate in the presence of appropriate polymeric stabilizers.²⁰⁶

Table 2.13 Classes of suitable cobalt precursors for preparing cobalt dispersions via thermal decomposition.²⁰⁶

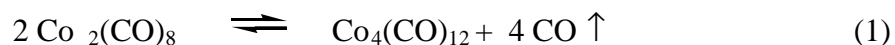
Classes	Example
Cobalt carbonyls	Dicobalt octacarbonyl
Cobalt alkylcarbonyls	Ethylcobalt tetracarbonyl
Cobalt alkenyl carbonyls	Cyclopentadiethyl cobaltdicarbonyl
Cobalt nitrosyls	Nitrosyltriacarbonyl cobalt ($\text{Co}(\text{CO})_3\text{NO}$)
Cobalt acylcarbonyls	Acetylcobalt tetracarbonyl

²⁰⁶ E. Blums, A. Cebers, and M. M. Maiorov, In Magnetic Fluids, Walter de Gruyter, Berlin (1997)

Table 2.14 Physical properties of metal carbonyls.²⁰⁶

Carbonyls	Decomposition Temperature, °C	Density, g/cm ³	Solvent
Fe(CO) ₅	60-250	1.47	Ester, benzene
Fe ₂ (CO) ₉	95-100	2.08	Ditto
Fe ₃ (CO) ₁₂	140	2	Ditto
Co ₂ (CO) ₈	25-52	1.82	Benzene, alcohol
Co ₄ (CO) ₁₂	60	-	Pentane, benzene

The thermal decomposition of Co₂(CO)₈ in hydrocarbon solutions under an inert atmosphere has been well-documented for many years. At temperatures below 90 °C, the decomposition occurs in two consecutive steps. In the first step, the solution decomposition of Co₂(CO)₈ to Co₄(CO)₁₂ accompanied with the release of CO gas takes place. This is instantaneously followed by the irreversible decomposition of Co₄(CO)₁₂ in the second step to produce Co⁰ clusters and release more CO gas.



Research efforts have focused on the first reaction because different results and conclusions have been obtained even though the reactions have been conducted under similar conditions. In heptane, reaction (1) is considered to be either second-order^{207, 208} or a fractional

²⁰⁷ F. Ungvary and L. Marko, *J. Organomet. Chem.*, **71**, 283 (1974)

²⁰⁸ G. Bor and U. K. Dietler, *J. Organomet. Chem.*, **191**, 295 (1980)

order²⁰⁹ whereas, in toluene, it is assigned as either a first-order²¹⁰ or second-order reaction²¹¹. Only a few papers have been published regarding the second step owing to the inhibiting effect of carbon monoxide from the first step.²¹⁰

The decomposition of $\text{Co}_2(\text{CO})_8$ and $\text{Co}_4(\text{CO})_{12}$ in solution can be monitored by IR spectroscopy. Both terminal and bridging carbonyls in the cobalt carbonyl compounds are distinguishable and sharp in the 1800-2200 cm^{-1} regions. Two key absorption regions are of particular interest: 1) the absorption band between 2020 and 2070 cm^{-1} due to terminal CO in both compounds, and 2) 1858 and 1867 cm^{-1} due to bridging CO in both compounds. The molecular structures of $\text{Co}_2(\text{CO})_8$ and $\text{Co}_4(\text{CO})_{12}$ are illustrated in Figure 2.31 showing the bridging and terminal carbonyls. The broadening in the $\text{Co}_2(\text{CO})_8$ IR spectra is generated from two terminal CO bands at approximately 2030 and 2065 cm^{-1} whereas the bridging CO band is very sharp at approximately 1858 cm^{-1} (Figure 2.32).²¹² In the spectrum of $\text{Co}_4(\text{CO})_{12}$, only one terminal band is observed at 2058 cm^{-1} with preservation of the bridging carbonyl band at 1867 cm^{-1} .

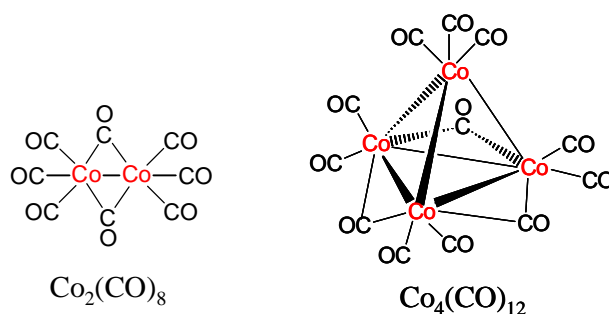


Figure 2.31 Molecular structures of $\text{Co}_2(\text{CO})_8$ and $\text{Co}_4(\text{CO})_{12}$ showing the bridging and terminal carbonyls.

²⁰⁹ M. F. Mirbach, A. Saus, A. M. Krings and K. J. Mirbach, *J. Organomet. Chem.*, **205**, 229 (1981)

²¹⁰ V. M. Gavrilova, V. Yu Gankin, D. M. Rugkovkii and A. G. Trifel, *Gidroformilirovanie*, Kuimya, Leningrad, **114**, (1974)

²¹¹ F. Ungvary and L. Marko, *Inorg. Chim. Acta.*, **4**, 324 (1970)

²¹² R. Tannenbaum, *Inorg. Chim. Acta.*, **227**, 233 (1994)

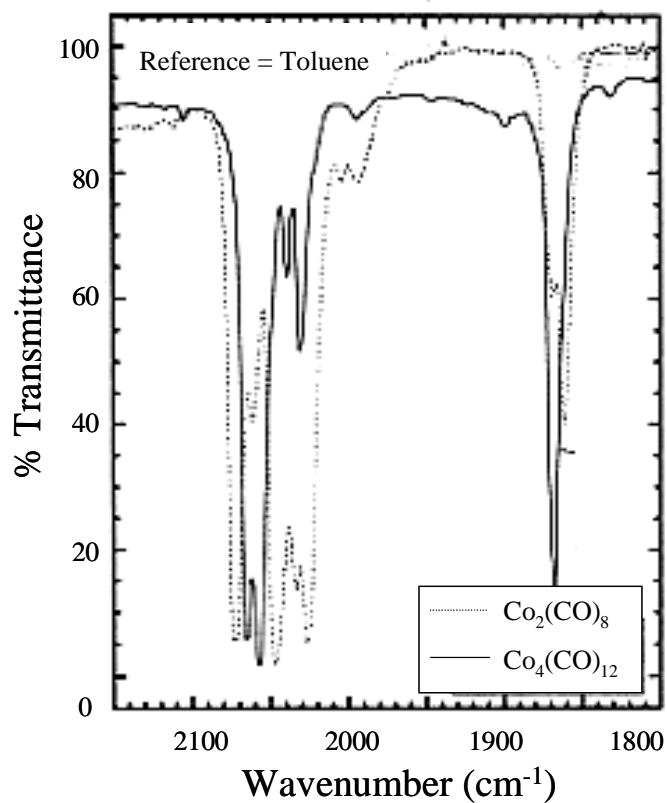


Figure 2.32 IR spectra of Co₂(CO)₈ and Co₄(CO)₁₂ in toluene.²¹²

Effects of polymers and their molecular weights on the sizes of the cobalt particles upon decomposition of Co₂(CO)₈ have been reported (Table 2.15).²⁰⁶ Results suggest the feasibility of controlling particle size in the range of 1 to 100 nm by changing the polymer composition and molecular weight. The resultant cobalt particles are strongly dependent upon the polymer/solvent/metal ratio. In addition, it is also established that the concentration of polar

groups in a polymeric stabilizer can influence the particle size. Specifically, at a very high concentration of polar groups in the polymers, cobalt particles with sizes smaller than 10 nm are obtained.

Table 2.15 Effect of polymer composition on particle size upon decomposition of $\text{Co}_2(\text{CO})_8$ in toluene.²⁰⁶

Polymer Type	Molecular Weight (g/mol)	Size Range (nm)
No Polymer	-	100
Methyl methacrylate-ethyl acrylate-vinylpyrrolidone		
33/66/1	300,000	15-40
0/90/10	100,000	6 - 25*
Polychloropropene	380,000	30-60
Vinyl chloride-acetate-alcohol 9/6/3	-	7-47*
Sulfonamide	21,000	6 - 30
Styrene-acrylonitrile		
100/0	476,000	10 - 30
92/8	100,000	6 - 13
88/12	100,000	6 - 13
Propyleneoxydiol		
	400	6 - 20
	3,000	7 - 30
	440	7 - 40
	6,000	7 - 45
Polyester isocyanate	1,000	5 - 30
Urea-formaldehyde	-	10 - 20
Polyhydroxy polyester	2,500	10 - 20
Alkyd	-	7 - 18
Bisphenol A-polycarbonate	50,000	8 - 45*

* Solvent is chlorobenzene

Commercial surfactants (stabilizers) for preparing stable cobalt particles are currently available. Effects of the surfactant structure on the particle size and colloidal stability upon decomposing $\text{Co}_2(\text{CO})_8$ in toluene are provided in Table 2.16. Sodium bis(2-ethylhexyl)sulfosuccinate (so-called Na(AOT)) ($\text{C}_{20}\text{H}_{37}\text{O}_2\text{SNa}$) has gained particular interest. In all cases, surfactants that can form stable dispersions produce cobalt particles having the diameter equal to or less than 10 nm.

Table 2.16 Influence of commercial surfactants on colloidal stability and particle size upon decomposing $\text{Co}_2(\text{CO})_8$ in toluene.²⁰⁶

Surfactants	Commercial names	Colloidal Stability	Size Range (nm)
Sodium sulfosuccinate	Na(AOT)	+	6.8 ± 0.8
Cesium sulfosuccinate	Cs(AOT)	+	9.2 ± 1.2
4-(1-butyloctyl)-2-ethylbenzoyl-1-sodium sulfonate	Texas-2	+	6.7 ± 0.8
Octyl benzoyl sodium sulfonate	OBS	-	-
Dodecyl benzoyl sodium sulfonate	DDBS	+	7.1 ± 1.6
Dodecyl ammonium propionate	DAP	+	10.1 ± 1.9
Octyl sodium sulfate	-	-	-
Octyl sodium sulfonate	-	-	-
Octyl phenolpolyethoxy ethonal	Triton X-45	-	-

Suitable solvents for preparing colloidal cobalt dispersions should dissolve both $\text{Co}_2(\text{CO})_8$ and the polymeric stabilizers at the reaction temperature. In addition, they must not react with the stabilizers, $\text{Co}_2(\text{CO})_8$, and definitely not with the resultant cobalt dispersions. A wide variety of inert solvents are listed in Table 2.17.²⁰⁵ Blums et al. have reported that aromatic solvents are suitable for preparing stable cobalt particles whereas aliphatic solvents failed to yield stable dispersions.²⁰⁶ It should be noted that this is probably significantly influenced by the nature of the surfactant used.

Table 2.17 Classes of solvents used in preparing cobalt dispersions.²⁰⁵

Classes	Examples
Benzene and alkyl derivatives	Monoalkyl benzene, dialkyl benzene
Halogenated derivatives of benzene	Chlorobenzene, o-dichlorobenzene, p-dichlorobenzene
Straight chains and cyclic hydrocarbons	Decane, octane, pentane, hexadecane, iso-octane, neopentane, cyclohexane, decalin and tetraline
Ethers and alcohols	THF, dialkyl ether, ethyleneglycolmonomethylether, butanol, hexanol, and cyclohexanol
Esters	Alkylacetate, alkylpropionate, and alkylbutylrate
Ketone	Cyclohexanone, mesityl oxide

In general, suitable temperatures for preparing stable cobalt dispersions range from ≈ 100 °C – 170 °C for most systems. The optimum reaction temperature in any given system can be determined by monitoring the rate of CO gas evolution during the reaction. It has been reported that the particle size diminishes as the reaction temperature is increased, but this also may be significantly affected by other concurrent reaction variables.²⁰⁶ Excessive temperatures may lead to undesirable agglomeration.

Preparing self-assembled cobalt nanocrystal arrays via thermal decomposition of $\text{Co}_2(\text{CO})_8$ has been of special interest in recent years.^{213, 214, 215, 216} Wang et al. have reported a successful process for preparing two-dimensional self-assembled cobalt nanocrystals in toluene using Na(AOT) as a stabilizer.^{217, 218} These particles had an average particle size of 9.2 nm and polydispersity of 9%. Electron diffraction patterns indicate that these cobalt particles are crystalline with a face-centered cubic structure (fcc) dominating. In good agreement with these results, Platonova et al. have found that cobalt particles prepared by thermal decomposition of $\text{Co}_2(\text{CO})_8$ in toluene using polystyrene-*b*-(poly-4-vinylpyridine) (PS-*b*-P4VP) as a stabilizer also have the fcc structure²¹⁹. It was hypothesized that these copolymers formed micelle structures in toluene and that micellar cores served as nanoreactors. According to IR spectra, $\text{Co}_2(\text{CO})_8$ forms a cationic-anionic complex with the 4-VP units of the copolymers to form $[\text{Co}(\text{VP})_6]^{2+} [\text{Co}(\text{CO})_4]_2^-$ in the solution. The shape and size of the cobalt particles could be changed by altering the 4-VP/Co ratio. Spherical particles were obtained when limited amounts of cobalt

²¹³ E. Papirer, P. Horny, H. Balard, R. Anthore, C. Petipas, A. Martinet, *J. Colloid Interface Sci.*, **94**(1), 207 (1983)

²¹⁴ E. Papirer, P. Horny, H. Balard, R. Anthore, C. Petipas, A. Martinet, *J. Colloid Interface Sci.*, **94**(1), 220 (1983)

²¹⁵ S. Foster, M. Antonietti, *Adv. Mater.*, **10**, 195 (1998)

²¹⁶ V. F. Puentes, and K. M. Krishnan, *IEEE Transactions on Magnetism*, **37**(4), 2210 (2001)

²¹⁷ J. S. Yin and Z. L. Wang, *NanoStructure Materials*, **11**(7), 845 (1999)

²¹⁸ J. S. Yin and Z. L. Wang, *J. Mater. Res.*, **14**(2), 503 (1999)

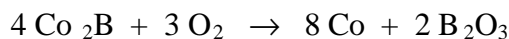
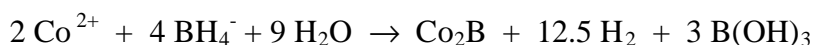
²¹⁹ O. A. Platonova, L. M. Bronstein, S. P. Solodovnikov, I. M. Yanovskaya, E. S. Obolonkoya, P. M. Valetsky, E. Wenz, and M. Antonietti, *Colloid Polym. Sci.*, **275**, 426 (1997)

were used whereas a star-like or cubic morphology was reported for the case of an excess of $\text{Co}_2(\text{CO})_8$.

2.5.2 Reduction of CoCl_2

In addition to thermal decomposition of $\text{Co}_2(\text{CO})_8$, reduction of cobalt chloride (CoCl_2) is a well-known and successful means to produce stable cobalt dispersions with narrow size distributions. The reducing agents used to reduce cobalt salts include borohydride (e.g., superhydride),^{220, 221} alkaline metals,²²² and polyols.²²³ Reducing cobalt salts to cobalt particles via electrochemical reduction has also been reported.²²⁴

The reduction mechanism of cobalt salts by borohydride, the most extensively studied reducing agent, is ambiguous. In addition, borohydride reduction chemistry itself is very complicated. Klabunde et al. found that the structure of the products strongly depends on the reaction conditions, e.g., types of solvents, the presence of oxygen and water.²²⁵ For example, in aqueous solution in the presence of small amounts of oxygen, the following reaction mechanism was proposed:



An excess of oxygen can oxidize the cobalt metal to its oxide derivatives, e.g., CoO and Co_3O_4 .

In nonaqueous solutions, the nonaqueous solvent behaves as a ligand, L, as follows:

²²⁰ G. N. Glavee, K. J. Klabunde, C. M. Sorensen, and G. C. Hadjapanayis, *Langmuir*, **8**, 771 (1992)

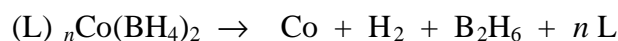
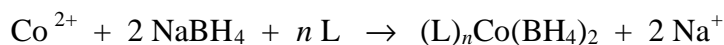
²²¹ H. Bonnemann, W. Brijoux and T. Joussen, *Angew. Chem. Int. Ed. Engl.*, **29**, 273 (1990)

²²² R. D. Rieke, *Acc. Chem. Res.*, **10**, 301 (1977)

²²³ F. Fievet, J. P. Lagier, and M. Figlarz, *MRS Bulletin*, **29** (1989)

²²⁴ D. Hoffmann, W. Schindler, J. Kirschner, *App. Phys. Lett.*, **73**, 3279 (1998)

²²⁵ C. Petit, A. Taleb, and M. P. Pileni, *J. Phys. Chem.*, **103**, 1805 (1999)



Sun et al. have reported the preparation of ϵ -cobalt (cubic structure) particles using superhydride reduction of CoCl_2 in a high temperature solution phase (200 °C) in the presence of a combination of oleic acid and trialkylphosphine as surfactants.²²⁶ Particle size was controlled by selecting an appropriate trialkylphosphine in combination with oleic acid. Specifically, bulky ligands, e.g., $\text{P}(\text{C}_8\text{H}_{17})_3$, produce smaller particles (3-7 nm) whereas small ligands, e.g., $\text{P}(\text{C}_4\text{H}_9)_3$, yielded larger particles (6-11 nm). A size-selection precipitation technique was used to isolate narrow dispersity particles, allowing them to self-organize into 2D and 3D superlattices during slow evaporation of the solvent. Annealing the resultant particles at 300 °C resulted in the transformation of the ϵ -cobalt structure to the hcp (hexagonal close-packed) structure, which is the crystalline structure of the bulk phase of cobalt metal.

Preparations of stable cobalt nanoparticles by reverse micelle techniques have also been widely investigated.^{227, 228, 229} Pileni et al. reported a simple process to produce cobalt nanoparticles with a narrow size distribution via reverse micelles with water-in-oil droplets (isooctane) stabilized by a monolayer of $\text{Na}(\text{AOT})$.²²⁵ The diameters of the droplets were reportedly controlled by the volume of solubilized water in the solution. Reduction reactions of CoCl_2 were carried out in the presence of air using NaBH_4 as a reducing agent. Electron diffraction spectroscopy (EDS) and X-Ray diffraction data (XRD) indicated that cobalt particles produced by these methods were crystalline with the fcc structure.

²²⁶ S. Sun, C. B. Murray, and H. Doyle, *Mat. Res. Soc. Symp. Proc.*, **577**, 385 (1999)

²²⁷ J. Legrand, C. Petit, D. Bazin, and M. P. Pileni, *Appl. Surf. Sci.*, **164**, 186 (2000)

²²⁸ C. Petit, and M. P. Pileni, *Appl. Surf. Sci.*, **162-163**, 519 (2000)

²²⁹ X. M. Lin, and C. M. Sorensen, *Langmuir*, **14**, 7140 (1998)

2.6 Retinal detachment

Recently, polymeric materials have been extensively utilized in surgical treatments of eye diseases and some of those have successfully recovered a degree of vision in many cases. There are two major roles in treating eye diseases using these biomaterials: a) sustained release drug therapy, and b) providing positional support.²³⁰ Sustained release systems are typically employed in the management of infections of the posterior segment whereas the positional support function is widely used in conjunction with scleral buckles in retinal detachment (RD) surgery. This will be the particular focus of this section.

2.6.1 Anatomy of the eye

The eye is a slightly asymmetric sphere with a longitudinal diameter of 2.3-2.5 cm and a transverse diameter of 2.4 cm.²³¹ The volume of the eyeball is approximately 6.5 cm³. Figure 2.33 illustrates a cross-section of the eye. It is comprised of two major parts, an anterior and a posterior segment.²³⁰ The anterior segment is bound by the cornea and lens-iris diaphragm, and contains aqueous humor. The lens is approximately 9-10 mm in diameter. The role of the anterior segment is to focus light onto the retinal photoreceptor cells in the posterior segment. The posterior segment includes, from outside inwards: sclera, choroid, retina and the vitreous cavity. The sclera is comprised mostly of connective tissue. It protects the eye from intra-ocular pressure and maintains the shape of the eyeball as an inflated football. The choroid is a heavily vascularized layer functioning as a blood supplier to support the retinal cells.

²³⁰ M. J. Colthurst, R. L. Williams, P. S. Hiscott and I. Grierson, *Biomaterials*, 21, 649 (2000)

²³¹ I. McDonnell, In *Retina*, v.I, S. Ryan (Ed.), Mosby, Toronto (1989)

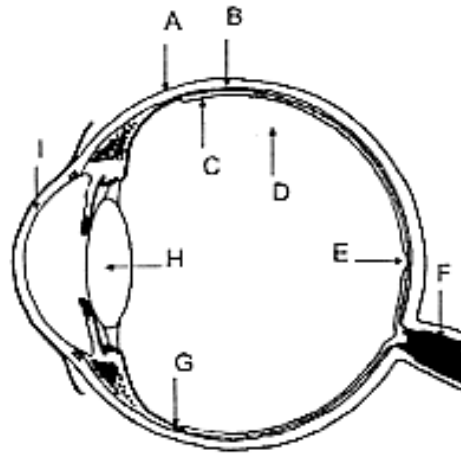


Figure 2.33 Anatomy of the eye: A=sclera, B=choroid, C=retina, D=vitreous cavity, E=fovea, F=optic nerve, G=location of *ora serrata*, H=lens and I=cornea.²³⁰

The retina is comprised of transparent, neurosensory tissue separated from the choroid by Bruch's membrane. The inner surface of the eyeball is coated by the retina except at the blind spot formed by the optic disc (a point where the optic nerve exits the eye). It is 0.1 mm thick at the *ora serrata* (the adhesion site), 0.2 mm thick at the equator and 0.56 mm thick around the optic disc. It contains 10 cell layers of, from the outer layer inwards: retinal pigment epithelium, the photoreceptor layer, the neural or sensory retinal layers and an inner internal limiting membrane. The retinal photoreceptors are supported by the choroid. There are two types of photoreceptors: cones and rods. The cone type receptors, the only type functioning as receptors, are concentrated at the central region of the retina and there are only cone type receptors in the central area of the macula (the fovea). This leads to the central vision of the human eye. For this reason, damage in the macula area can cause serious loss of vision whereas damage to the

surrounding area results in loss of visual field. Since the retina does not have blood vessels to supply oxygen and nutrition directly, it strongly depends on the choroid that contains a number of blood vessels. Therefore, for the retina to be able to use the nutrients, the retina and choroid have to remain in apposition by the suction attraction between these two layers.

The vitreous humor, a transparent gel or fluid, is comprised of water (approximately 99%), collagen, hyaluronan and proteoglycans and functions as a shock absorber, maintaining the shape of the eye and pressing the retina flat against Bruch's membrane. It has an average volume of 4 cm³ in an adult eye.

2.6.2 Retinal detachment

Retinal detachment (RD) is one of the most common diseases in the posterior segment of the eye. It occurs when the neural retina detaches from the choroid, resulting in eventual death of the retina and partial or complete loss of vision. As a normal part of aging, the vitreous gel can undergo liquefaction, shrinkage and separation of the neural retina from the underlying retinal pigment epithelium (Figure 2.34).²³² It may subsequently result in the formation of a tear in the retina at a site of vitreoretinal adhesion (the *orra serrata*). This can provide a pathway for the vitreous fluid to gradually pass through the hole and stay beneath the retina overcoming the suction attraction between the retina and the choroid resulting in detaching the retina from the underlying choroid. As a result, the photoreceptors in the retina fail to receive images with clarity and the corresponding visual field is lost. It appears to the patients as a dark curtain or shadow in vision. If the detached retina is reattached in a short period of time, vision can be restored. However, if the retina remains detached for a long period of time without treatment, it

²³² P. A. Voltairas, D. I. Fotiadis and C. V. Massalas, *J. Magn. Magn. Mat*, **225**, 248-255 (2001)

will slowly die due to lack of oxygen and nutrients supplied from the choroid resulting in complete loss in vision.

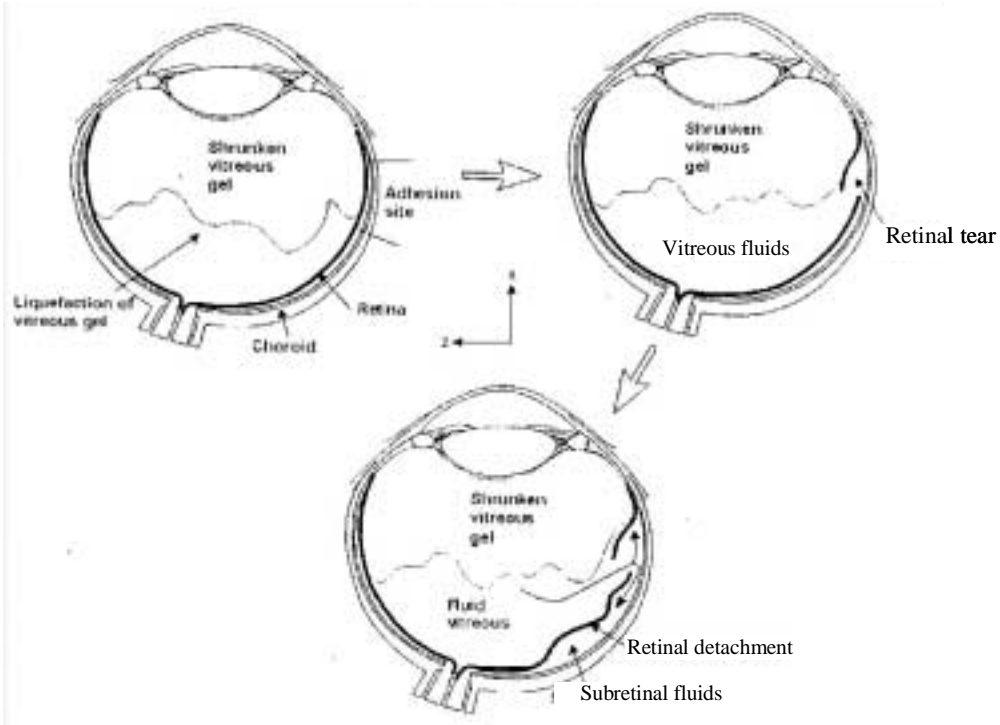


Figure 2.34 Stages of retinal detachment.²³²

The patients who have retinal detachment (RD) can be observed in one of the following forms: rhegmatogenous, nonrhegmatogenous tractional and nonrhegmatogenous exudative.²³³ In rhegmatogenous RD, a retinal tear is observed and the detachment takes place when the vitreous fluids flow through the tear into the subretina. In nonrhegmatogenous tractional RD, traction of the retina from contractile membranes due to shrinkage of vitreous fluids, either intermittent or constant, is observed. In nonrhegmatogenous exudative RD, the vitreous fluids in the subretinal

²³³ J. J. Kanski, In *Retinal Detachment: A Colour Manual of Diagnosis and Treatment*, Butterworths, London (1986)

space is built up leading to the elevation and detachment of the retina from the retinal pigment epithelium. Distinguishing features of retinal detachment are summarized in Table 2.18.^{234, 235}

2.6.3 Current treatment of retinal detachment

Surgery is a frequently successful means for treating retinal detachment. The goal of surgery is to seal the break generated in the retina in order to prevent further fluid flow into the subretinal space leading to reattachment of the detached retina. The current techniques for treating the disease are: a) scleral buckling, and b) using internal tamponades. Scleral buckling involves the use of encircling silicone bands held in place by sutures on or within the sclera to indent and to compress the wall of the eye inward in order to close the holes in the retina (Figure 2.35).²³⁶ A sponge or wedge might be needed as a support between the elastic band and sclera.²³⁷ Treating the rhegmatogenous retinal detachment using this method has a recovery rate around 90%, although a second surgery may be necessary.²³⁸ A major disadvantage associated with using scleral buckling is that it produces an uneven and discontinuous surface to the sclera of the eye leading to excessive and unwanted pressure applied to a non-target area of the sclera.

²³⁴ D. J. Apple and M. F. Robb, In *Ocular Pathology: Clinical Applications and Self-Assessment*, 3rd Ed., The C.V. Mosby Company, St. Louis (1985)

²³⁵ G. O. H. Naumann and D. J. Apple, In *Pathology of the Eye*, Springer-Verlag, New York (1986)

²³⁶ F. W. Newell, In *Ophthalmology: Principles and Concepts*, 6th Ed., The C.V. Mosby Company, St. Louis (1986)

²³⁷ Sr. Batdorf and B. David, US Patent 6,117,170 (2000)

²³⁸ D. M. Marcus, D. J. D'Amico and S. Mukai, *Int. Phthalomol. Clin*, **34**, 97 (1994)

Table 2.18 Distinguished features of retinal detachment.^{234, 235}

Features	Rhegmatogenous	Nonrhegmatogenous Tractional	Nonrhegmatogenous Exudative
Retinal Break	Yes	No	No
Surface	Convex; may be bullous	Dentate or scalloped; rarely if ever reaches ora unless caused by peripheral uveitis	Convex; may not reach ora unless caused by peripheral uveitis
Rarely shifts	No shifting; subretinal fluid appears "sucked" into space under pulled-up retina	Shifting is common; fluid is often dependent	Shifting is common; fluid is often dependent
Height	Bullous from superior hole; shallow from inferior hole; never touches lens	Generally not high	Often high; only type that may touch lens
Treatment	Surgery	Observe; may buckle or band; vitrectomy	Medical-treat underlying cause; for example, apply photocoagulation to leaking vascular channels

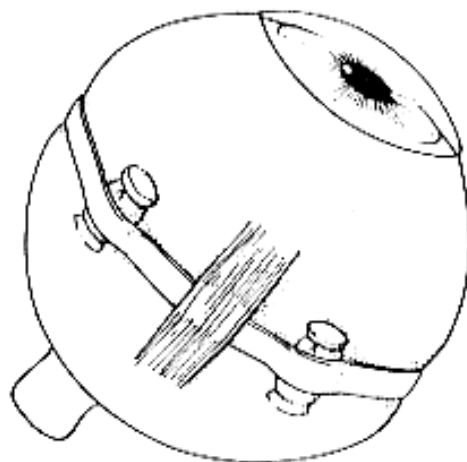


Figure 2.35 Demonstration of the treatment of retinal detachment using scleral buckles.²³⁶

Other less invasive methods than scleral buckling are to inject or infuse gases or liquids as internal tamponades into the vitreous cavity positioning the retinal flap against the retinal pigment epithelium to seal the retinal breaks and block the passage of further vitreous fluids into the subretinal space (Figure 2.36).²³⁹ These materials include halogenated gas (SF_6 , C_3F_8), silicone oils (PDMS), fluorosilicone oils (poly(methyl-3,3,3-trifluoropropyl)siloxane), and perfluorocarbon fluids (perfluorooctane, perfluorodecane, perfluorophenanthrene).²⁴⁰ These materials have to be transparent with a refractive index close to that of the vitreous fluids (a refractive index of water is 1.33), immiscible but not emulsified in the vitreous fluids, having high surface tension and chemically and physiologically inert. The choice of materials used is dependent on the position of the retinal breaks. Namely, silicone oils (a specific gravity of 0.97)

²³⁹ J. P. Dailey, J. P. Phillips, C. Li and J. S. Riffle, *J. Magn. Magn. Mat.*, **194**, 140-148 (1999)

²⁴⁰ M. F. Refojo and F. I. Tolentino, US Patent 5,672,355 (1997)

can float up and seal the holes on the upper retina, leaving the inferior retina unprotected whereas fluorosilicones (a specific gravity of 1.29) can sink down and block the holes on the lower retina, leaving the superior retina unprotected. Moreover, if the retinal breaks are generated on the side of the retina, the patients have to lie down for weeks in order to allow the gases or fluids to completely seal the retinal breaks. This partial support to the retina is a major drawback of this method. Another disadvantage of this method is that the internal tamponades fill up the vitreous cavity, decreasing visual ability, and contact the anterior segment (lens and cornea), causing cataract and glaucoma.

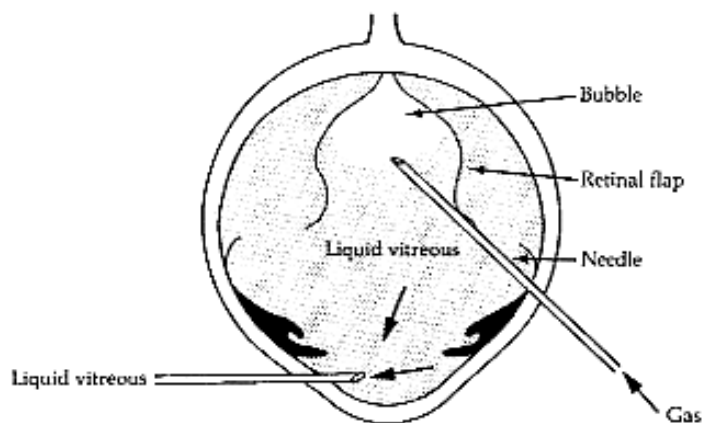


Figure 2.36 Demonstration of the treatment of retinal detachment using internal tamponades.²³⁹

CHAPTER 3 Synthesis and Characterization of Poly(siloxane) Triblock Copolymers

3.1 Synopsis

This chapter discusses the synthesis and characterization of poly(dimethylsiloxane-*b*-(3-cyanopropyl)methylsiloxane-*b*-dimethylsiloxane) triblock copolymers (PDMS-*b*-PCPMS-*b*-PDMS). These copolymers will be used as steric stabilizers for preparing stable cobalt nanoparticle dispersions in toluene or PDMS carrier fluids. D₄CN monomers were first prepared by hydrosilylation of tetramethylcyclotetrasiloxanes (D₄H) and allyl cyanide. Living anionic ring-opening polymerization was employed to open D₄CN monomers and thereby obtain living PCPMS macroinitiators. D₃ monomers were then introduced to the living PCPMS macroinitiators to obtain PDMS-*b*-PCPMS-*b*-PDMS triblock copolymers (Figure 3.1).

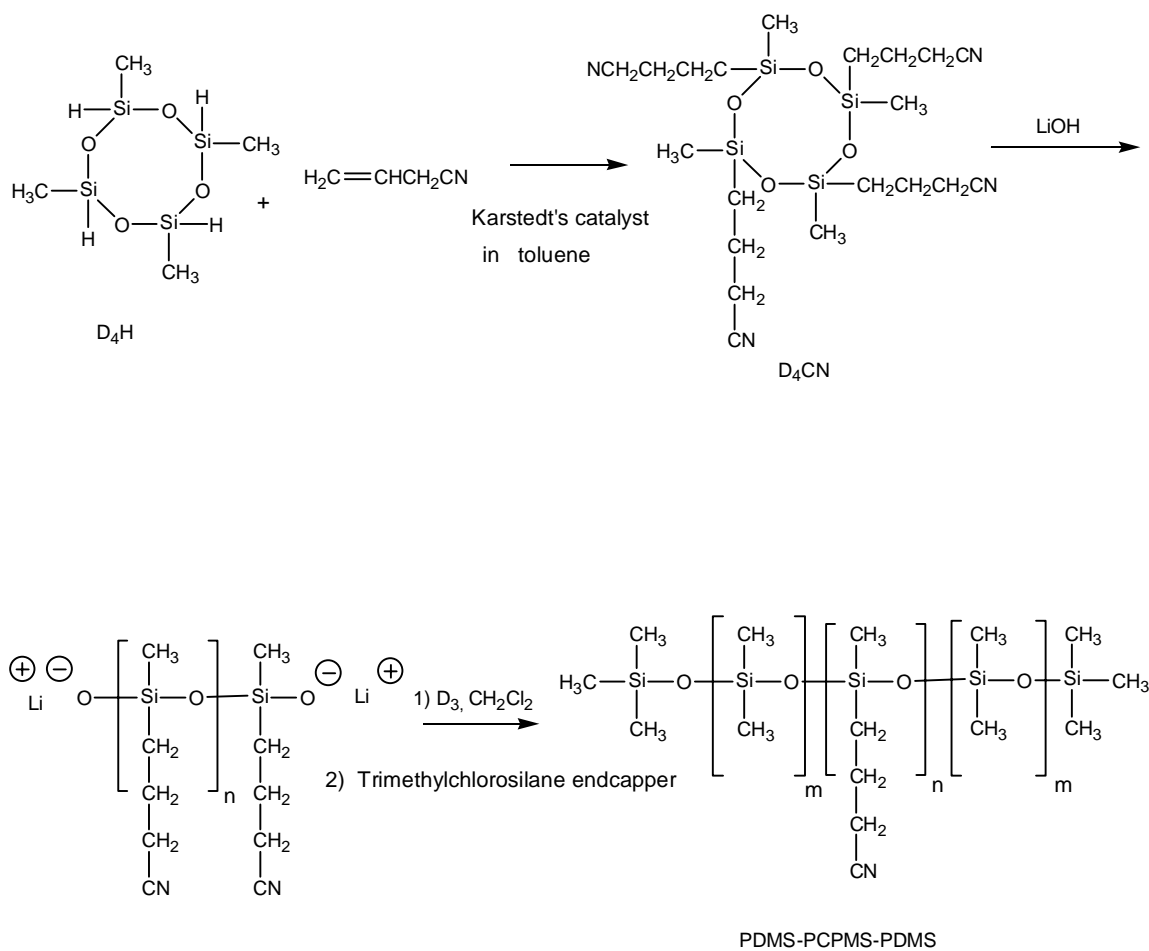


Figure 3.1 Synthetic scheme for preparing PDMS-*b*-PCPMS-*b*-PDMS triblock copolymers.

3.2 Experimental

3.2.1 Purification of solvents and reagents

Dichloromethane (CH_2Cl_2 , FW 84.93, b.p. 40 °C, d. 1.325)

Dichloromethane (Baxter, 99.9%) was washed twice with concentrated sulfuric acid, then with water until neutral. Subsequently, it was pre-dried with anhydrous magnesium sulfate and distilled from phosphorus pentoxide (Fisher, 99.6%) under N_2 .

Tetrahydrofuran (THF, $\text{C}_4\text{H}_8\text{O}$, FW 72.11, b.p. 65-67 °C, d. 0.889) and triethylene glycol dimethylether (TEGDME, $\text{CH}_3\text{O}(\text{CH}_2\text{CH}_2\text{O})_3\text{CH}_3$, FW 178.23, b.p. 216 °C, d. 0.986)

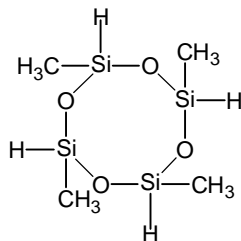
THF (E.M. Sciences, 99.5%) and TEGDME (Aldrich, 99%) were refluxed over sodium (Aldrich, 40% in paraffin) with benzophenone (Aldrich, 99%) under N_2 until the solution was deep purple and fractionally distilled just prior to use. Alternatively, these reagents were dried over lithium aluminum hydride and distilled just prior to use.

Toluene ($\text{C}_6\text{H}_5\text{CH}_3$, FW 92.14, b.p. 110.6 °C, d. 0.865)

Toluene (Fisher) was washed twice with concentrated sulfuric acid and then repeatedly washed with water until neutral. It was then pre-dried with anhydrous magnesium sulfate, stirred over calcium hydride for 24 h and distilled prior to use.

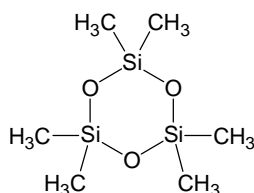
2,4,6,8-Tetramethylcyclotetrasiloxane (D_4H , $\text{C}_4\text{H}_{16}\text{O}_4\text{Si}_4$, FW 240.51, m.p. -69 °C, b.p. 134 °C, d. 0.991)

D_4H was donated by the Dow-Corning Corp. and was dried over calcium hydride and distilled prior to use.



1,1,3,3,5,5-Hexamethylcyclotrisiloxane (D₃, C₆H₁₈O₃Si₃, FW 222.47, m.p. 64-66 °C, b.p. 134 °C, d. 1.02)

D₃ was kindly donated by the General Electric Co. It was purified by stirring over calcium hydride at 80 °C for 12 h, then fractionally distilled at 135 °C under nitrogen into a pre-dried and pre-weighed flask. The D₃ distillate was diluted with dry dichloromethane via cannula (147.4 g dichloromethane and 88.04 g D₃, 37 wt. % D₃) and stored under nitrogen until used.



Allyl cyanide (CH₂=CHCH₂CN, FW 67.09, b.p. 116-121 °C, d. 0.834)

Allyl cyanide (98%, Aldrich) was dried with 4Å molecular sieves (Aldrich) for at least 48 h, then distilled under nitrogen.

Molecular sieves

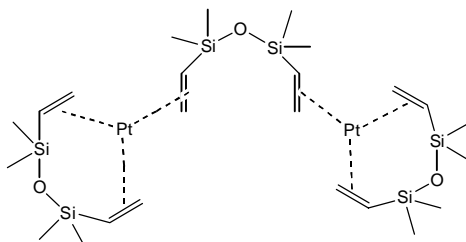
Molecular sieves were activated at 200 °C at 0.5-1 torr for 48 h.

Trimethylchlorosilane ((CH₃)₃SiCl), FW. 108.64, b.p. 57 °C, d. 0.856)

Trimethylchlorosilane (99+%, Aldrich) was distilled under a N₂ atmosphere immediately prior to use.

Pt⁰[1,3-divinyl-1,1,3,3-tetramethyldisiloxane]_{1.5} complex in xylene (2.1-2.4 wt. % Pt) catalyst (Karstedt's Catalyst) (d. 0.90)

Karstedt's Catalyst was purchased from Gelest, Inc., Tullytown, PA and used as received.



Lithium hydroxide monohydrate (LiOH·H₂O, FW 42, d. 1.51)

LiOH·H₂O (99.995%, Aldrich) was ground in a dry nitrogen bag to a fine powder, dried in a vacuum oven for at least 12 hrs. at 80°C to obtain anhydrous LiOH, then stored in a desiccator until used.

3.2.2 Synthesis of 1,3,5,7-tetramethyl-1,3,5,7-tetra(3-cyanopropyl)cyclotetrasiloxane (D₄CN)

A dry 500-mL roundbottom flask, equipped with a condenser topped with a Drierite tube and a magnetic stirbar, was charged with 50 mL (49 g, 0.20 mol) D₄H, 100 mL toluene, 80 mL allyl cyanide (67 g, 1.0 mol, excess) and 0.2 mL Karstedt's catalyst (0.4 mol Pt/mol double bond). The mixture was refluxed and monitored by FTIR and ¹H NMR by noting the disappearance of the Si-H peak at 2170 cm⁻¹ and 4.7 ppm, respectively (≈24 h). Upon completion, the toluene and excess allyl cyanide were removed under reduced pressure, then the

D₄CN was recovered with a short path vacuum distillation at ≈ 500 mtorr and ≈ 235 - 270 °C. The product was a beige, clear, viscous liquid.

*3.2.3 Synthesis of poly[dimethylsiloxane-*b*-(3-cyanopropyl)methylsiloxane-*b*-dimethylsiloxane] triblock copolymers (PDMS-PCPMS-PDMS) with controlled block lengths*

An exemplary procedure for a copolymer with a targeted number average molecular weight comprised of 5000 g/mole PDMS and 5000 g/mole PCPMS blocks is provided. Copolymers with other block lengths were prepared in a similar manner but with different ratios of lithium hydroxide to D₄CN to tailor the molecular weight of the central block, and with different amounts of D₃ relative to the central block to tailor the endblock molecular weights. Table 3.1 shows the formulations used to prepare triblock copolymers with different block lengths. One other variation in these syntheses was that tetrahydrofuran was utilized as the reaction rate promoter in cases of short poly(dimethylsiloxane) endblocks and tetraethylene glycol dimethylether (TEGDME) was often utilized for longer endblocks. TEGDME afforded faster reaction rates which were useful for preparing higher molecular weight blocks, but this promoter was more difficult to remove quantitatively in the copolymer recovery step.

Table 3.1 The formulations used for preparing triblock copolymers with different block lengths.

Copolymer PDMS-PCPMS-PDMS	D ₄ CN (g)	LiOH Initiator		D ₃ (g)	Endcapper (ml)
		g	mol		
5k-2k-5k	10	0.18	7.5×10^{-3}	43.0	1.88
10k-2k-10k	10	0.18	7.5×10^{-3}	85.0	1.88
15k-2k-15k	10	0.18	7.5×10^{-3}	128.0	1.88
5k-5k-5k	10	0.07	2.96×10^{-3}	17.0	0.75
10k-5k-10k	10	0.07	2.96×10^{-3}	34.0	0.75
15k-5k-15k	10	0.07	2.96×10^{-3}	51.0	0.75

The first part of the copolymer synthesis involves preparing controlled molecular weight PCPMS oligomers with terminal lithium siloxanolate. D₄CN (10.0 g) and 0.07 g (0.003 mol) lithium hydroxide were charged to a clean, dry 500-mL roundbottom flask equipped with a mechanical stirrer and nitrogen purge. The mixture was stirred at 140 °C for a minimum of 48 h to reach thermodynamic equilibrium. The approach to equilibrium was monitored by GPC using samples which had been terminated with trimethylchlorosilane. After equilibrium was achieved, 100 mL of dichloromethane were added to the macroinitiator via cannula. A 40-mL aliquot of a D₃-dichloromethane solution (0.43 g D₃ per mL) was added along with 10 mL THF as a reaction rate promotor. Ten mL of promoter (either THF or TEGDME) per 10.0 g D₄CN were added to all block copolymer reactions irrespective of the block molecular weights. Another 60 mL of dichloromethane was added to bring the reaction volume to ≈200 mL and to obtain a clear solution. The disappearance of the D₃ protons at 0.14 ppm from TMS was monitored by ¹H NMR. The reaction was allowed to proceed at room temperature for 7 days (85% monomer

conversion). For other copolymers, the living chains were terminated at approximately 80 to 90% monomer conversion to avoid backbiting reactions due to extremely low concentration of the D_3 monomer. Therefore, 15% excess of D_3 monomer was used in the feed. The triblock copolymers were terminated with an excess of trimethylchlorosilane (0.75 mL, 100% stoichiometric excess of the terminating reagent) via syringe and stirred for approximately 30 minutes. The solution clouds upon termination due to precipitation of LiCl. The excess trimethylchlorosilane and the dichloromethane solvent were removed under reduced pressure. The viscous copolymer was diluted with chloroform and washed repeatedly with water to remove the lithium chloride. The copolymer-chloroform solution was precipitated into methanol to remove nitrile containing siloxane cyclics (from the central block equilibration step) and the THF promoter. The methanol phase was decanted, then the polymer was dried at 80 °C under vacuum overnight. It should be noted that the precipitation procedure into methanol must be repeated several times in cases where TEGDME was used as the reaction promoter. The block molecular weights and the total molecular weights of the triblock copolymers after purification were established using a combination of titration and NMR measurements as described in the Results and Discussion section.

3.3 Characterization

3.3.1 Molecular weight determination

3.3.1.1 Potentiometric titration

Non-aqueous titrations of the macroinitiator central block of the stabilizers were conducted using an MCI automatic Titrator Model GT-05 equipped with a Ag/AgCl double

junction type electrode. The macroinitiators were dissolved in dichloromethane (≈ 1.0 g polymer + cyclics in 20 mL dichloromethane). It was assumed that the concentration of polymer in the polymer-cyclic mixture was 75 wt. % when calculating the amount of polymer to be charged, and to calculate M_n . The samples were titrated with HCl in isopropanol (0.05 N standardized against sodium carbonate). Each sample was titrated in triplicate to obtain an average molecular weight.

3.3.1.2 1H NMR

All 1H NMR spectra were performed on a Varian Unity 400 MHz NMR spectrometer operated at 400 MHz with 4.1 μsec pulse width, and about 100 scans using 5 mm od tubes. The samples were dissolved in CDCl_3 with the sample concentration in the range of 10-20% w/v.

3.3.2 ^{29}Si NMR

All qualitative and quantitative ^{29}Si NMR spectra were acquired on a Varian Unity 400 MHz NMR spectrometer operating at 80 MHz. The samples were prepared with ≈ 0.6 g polymer, 2.4 mL CDCl_3 , and 52 mg tris(acetylacetonato)chromium (III) ($\text{Cr}(\text{acac})_3$). The relaxation reagent was added to all ^{29}Si samples to decrease spin-spin lattice relaxation times (T_1) and obtain quantitative spectra. The ^{29}Si spectra were acquired in 10 mm od tubes using an 11.5 μsec pulse width, a 10 sec. relaxation delay, and about 300 scans.

3.3.3 ^{13}C NMR

All ^{13}C NMR spectra were acquired on a Varian Unity 400 MHz NMR spectrometer operated at 100 MHz with a 12.3 μsec pulse width. CDCl_3 was used as a solvent with the sample

concentration in the range of 20-30% to increase the signal-to-noise ratio. About 1% Cr(acac)₃ was added in some cases to decrease spin-spin lattice relaxation times (T₁).

3.3.4 *Fourier transform infrared spectroscopy (FTIR)*

FTIR spectra were collected on a Nicolet Impact 400 FTIR spectrometer with the samples run neat between potassium bromide salt plates.

3.3.5 *Gel permeation chromatography (GPC)*

Gel permeation chromatograms were acquired in chloroform at 30 °C on a Waters Alliance Model 2690 chromatograph equipped with a Waters HR 0.5 + HR 2 + HR 3 + HR 4 styragel column set and a Viscotek refractive index detector. Polystyrene standard samples were used to establish a universal calibration curve. The sample solution was prepared by dissolving 30-40 mg samples in 10 mL of HPLC grade CHCl₃, and then filtered through a 0.45 µm pore size filter prior to loading into the GPC autosampler.

3.3.6 *Differential scanning calorimetry (DSC)*

DSC was performed using a DuPont 2400 instrument. The samples (about 10 mg) were weighed in aluminum pans before loading into the instrument. After the samples were quickly quenched to about -160 °C using liquid N₂, they were scanned from -150 °C to 0 °C with at 10 °C/minute. Each sample was run twice and there were no significant differences between two scans.

3.4 Results and discussion

3.4.1 Preparation of D_4CN

D_4CN monomers were prepared via hydrosilylation reaction between allyl cyanide and D_4H (Figure 3.1). The reactions were carried out in toluene in the presence of Karstedt's catalyst at reflux temperature for 24 h. Hydrosilylation is a reaction extensively used in the silicone synthesis for preparing monomers containing silicon-carbon bonds and for crosslinking polymers. Because Karstedt's catalyst is soluble and highly reactive in polysiloxane media, it is typically used as a catalyst in these reactions. It is prepared by the reaction of chloroplatinic acid (H_2PtCl_6) with compounds containing vinyl groups on silicon, e.g., divinyltetramethyldisiloxane.²⁴¹

Allyl cyanide was dried with activated molecular sieves to quantitatively remove water and then distilled before use. It was necessary to remove impurities, e.g., sulfur and phosphorus, since they can inhibit the reactivity of the platinum catalyst. An excess of allyl cyanide was used in the reaction to ensure that all Si-H bonds in D_4H were fully reacted. Excess allyl cyanide was easily vacuum stripped from the products at 80 °C under reduced pressure. To remove the catalysts and impurities, D_4CN monomers were recovered by distillation at about 270 °C under reduced pressure.

During the reaction, 1H NMR was used to monitor the reaction progress by observing the disappearance of the Si-H peak ($\delta=4.7$ ppm) (Figure 3.2). Three signals corresponding to the anti-Markownikoff product (peaks b, c, and d) appeared within 30 minutes (Figure 3.3). Approximately ten percent of the Markownikoff product was also observed (peaks e, f, and g). Peak b at $\delta=2.4$ ppm showed a multiplet after 30 min reaction due to the mixture of the allyl

²⁴¹ L. N. Lewix, J. Stein, Y. Gao, R. E. Coborn, and G. Hutchins, *Platinum Metals Rev.*, **41**(2), 66 (1997)

cyanide precursor and 3-cyanopropyl groups in the polymer chains. This signal became a singlet once the excess of allyl cyanide was removed after the reaction was complete. The same is true for the signals in the range of 0 to 0.2 ppm (peak h). The signals at 0.2 ppm corresponding to methyl protons in the D₄H monomer became smaller as the reaction proceeded whereas the peaks at 0.1 ppm corresponding to methyl protons in the polymers became larger. The peak at $\delta=3.05$ ppm corresponding to methyl protons in toluene disappeared once D₄CN was recovered by distillation.

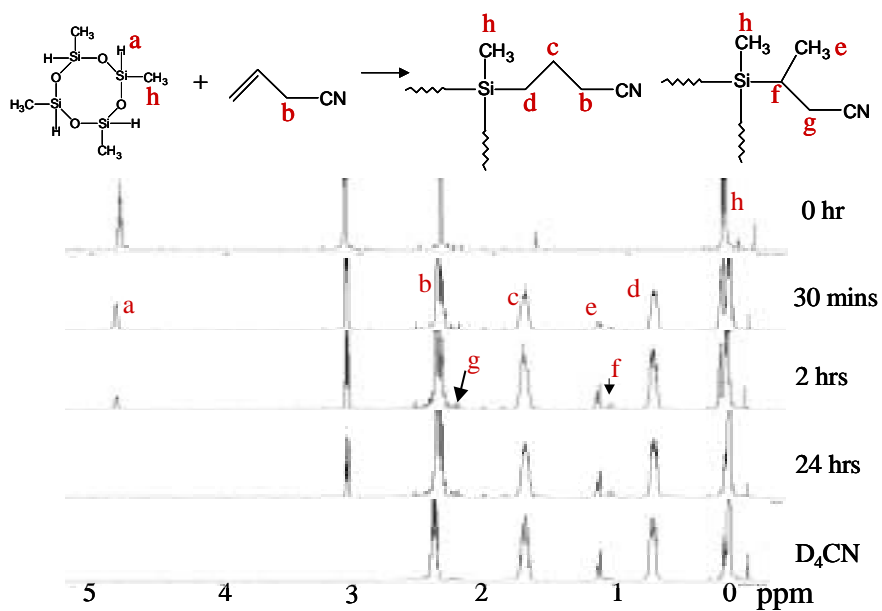


Figure 3.2 ^1H NMR monitoring the progress of D_4CN preparation.

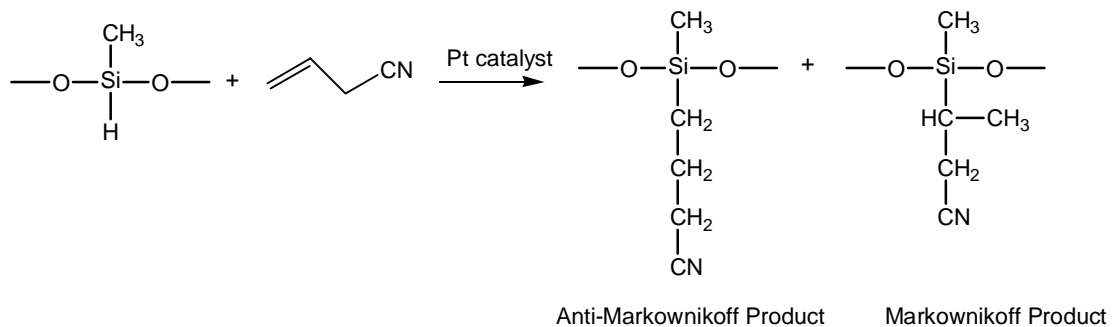


Figure 3.3 Markownikoff and anti-Markownikoff products.

Figure 3.4 shows FTIR spectra of the mixture before the reaction began (spectrum A), after the reaction was complete (spectrum B), and after toluene was removed (spectrum C). The peak at 2350 cm^{-1} corresponding to Si-H stretching disappeared in spectrum B indicating that the D_4H monomer was fully reacted. The peaks corresponding to both toluene overtones and aromatic C-H stretching from toluene at above 3000 cm^{-1} disappeared after it was removed from the mixture.

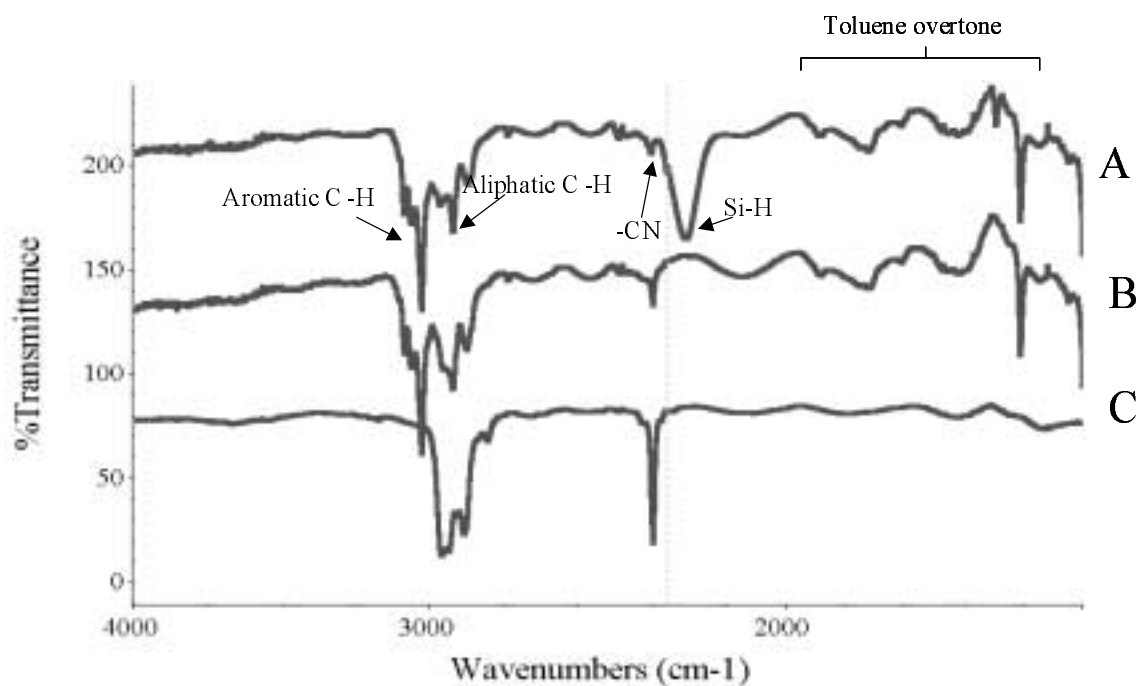


Figure 3.4 FTIR spectra showing the progress of D_4CN preparation.

*3.4.2 Synthesis of poly[dimethylsiloxane-*b*-(3-cyanopropyl)methylsiloxane-*b*-dimethylsiloxane] triblock copolymers (PDMS-PCPMS-PDMS) with controlled block lengths*

The PCPMS central block was first synthesized in the preparation of PDMS-PCPMS-PDMS triblock copolymers. Difunctional PCPMS oligomers were prepared by equilibrating 1,3,5,7-tetra(3-cyanopropyl)-1,3,5,7-tetramethylcyclotetrasiloxane, a cyclic nitrile containing siloxane tetramer (D_4CN), using LiOH as the basic initiator at 140 °C (Figure 3.1). The molar ratio of LiOH to the weight of D_4CN controlled the oligomeric molecular weight. One mole of hydroxide was used for every desired mole of endgroups and one mole of water evolved for every two moles of LiOH (Figure 3.5). The 140 °C reaction temperature combined with an inert gas purge was effective for removing the aqueous by-product. The viscous melt reactions redistributed to yield the equilibrium mixture comprised of 25 wt. % cyclic species and 75 wt. % linear chains (Figure 3.6). It is important that these reactions are conducted in the neat polymer liquid without a solvent to ensure that the minimum 25 wt. % concentration of cyclics results. Small cyclics were formed due to backbiting of the active silanolate species. Therefore, 25% excess of D_4CN was employed in the feed to obtain the targeted molecular weights of PCPMS linear chains.

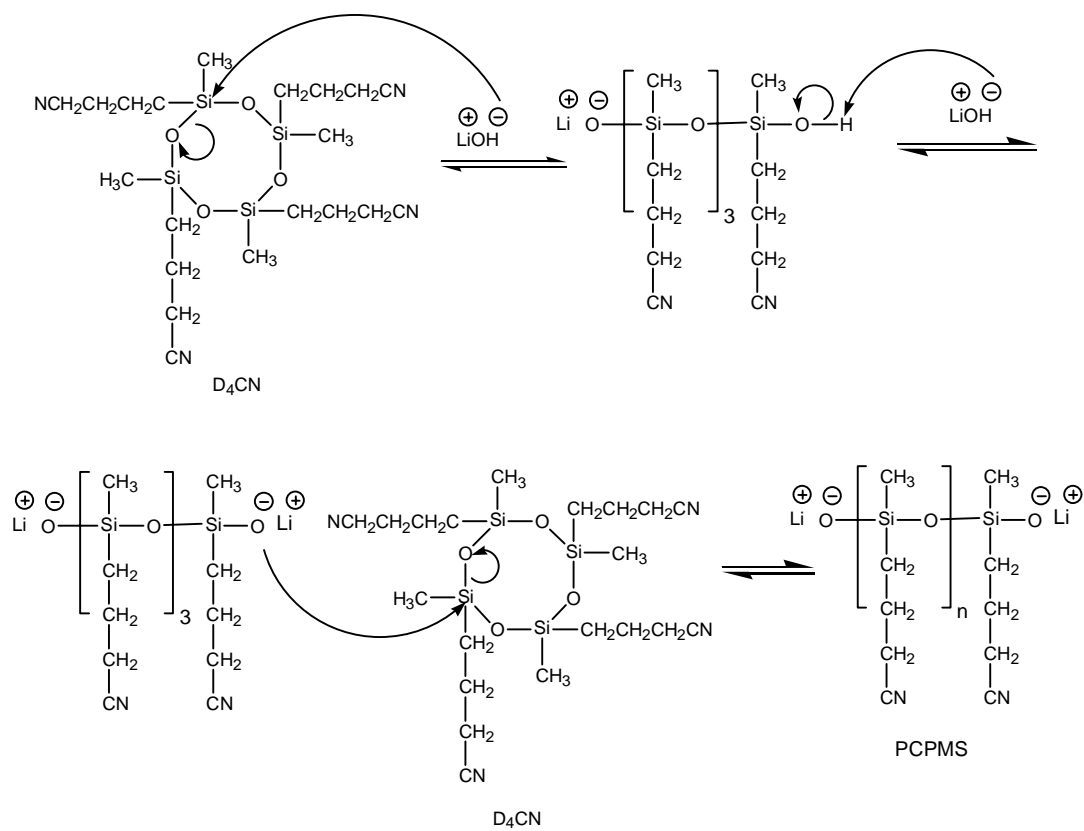


Figure 3.5 Mechanism of D₄CN anionic ring-opening polymerization to obtain difunctional PCPMS oligomers.

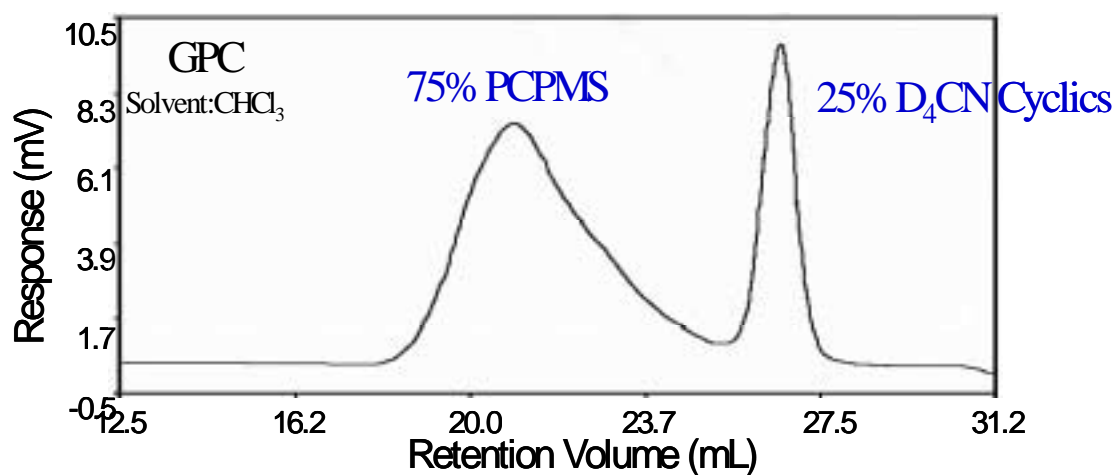


Figure 3.6 Gel permeation chromatograms of D₄CN and PCPMS in CHCl₃.

The use of Li⁺ as the counterion, rather than Na⁺ or K⁺, was important for generating polymers with minimal color. The lithium siloxanolate reactive species is likely more associated relative to sodium or potassium and avoids side reactions. It should also be noted that the Si-O bonds in the (3-cyanopropyl)methylsiloxane species are significantly more reactive toward nucleophiles relative to dimethylsiloxane. Thus, reasonable equilibration rates can be obtained even while using the more associated lithium siloxanolate active species.

Following equilibration of the central PCPMS block, the reaction mixtures were cooled to room temperature and a dichloromethane solution of D₃, along with tetraethylene glycol dimethylether or THF as a reaction rate promoter, were added to polymerize the PDMS endblocks. The chlorinated solvent was necessary to co-dissolve both the polar nitrile containing central PCPMS block and the non-polar D₃ cyclic. Substitution reactions on the chlorinated solvent did not occur due to the weakly nucleophilic nature of the lithium (3-

cyanopropyl)methylsiloxanolate endgroup. D₃ ring-opening was monitored with ¹H NMR by observing the disappearance of the methyl peak from the cyclic monomer at 0.14 ppm and the concurrent growth of the resonance peak corresponding to the methyl protons on the linear poly(dimethylsiloxane) structure at 0.06 ppm (Figure 3.7). The block copolymers were terminated by adding trimethylchlorosilane when the D₃ conversion was 80-90% complete. This early termination was to avoid any backbiting or intermolecular chain-chain substitutions which might occur at extremely low D₃ monomer concentrations. It was recognized that the crossover reaction between (3-cyanopropyl)methylsiloxanolate to dimethylsiloxanolate to initiate the endblocks may not be energetically favorable. Thus, some polydispersity in the endblocks may occur due to a slow crossover reaction.

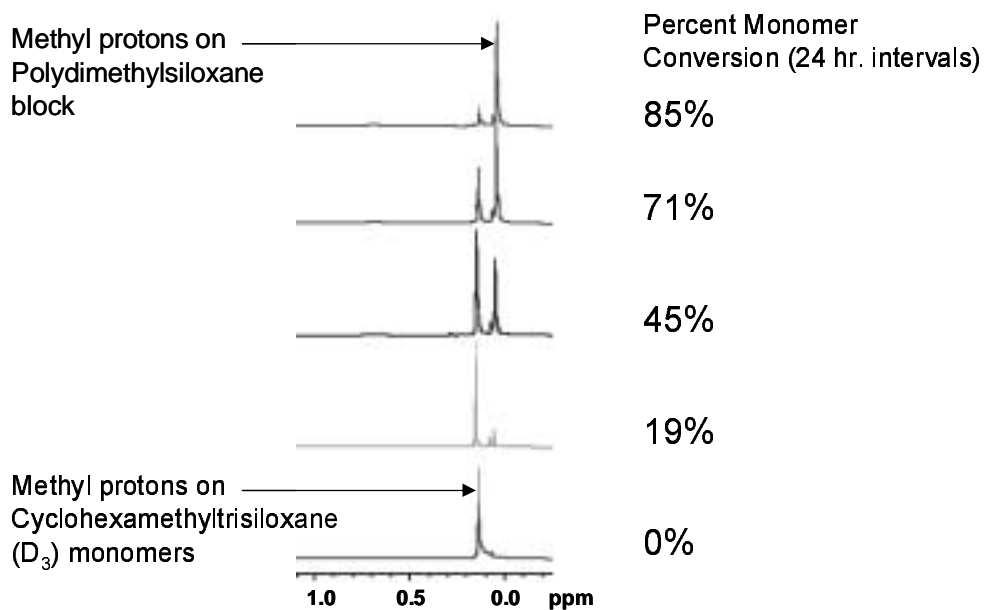


Figure 3.7 Monitoring the living anionic synthesis of the PDMS endblocks on PDMS-PCPMS-PDMS via ¹H NMR.

The concentrations of the PCPMS macroinitiator and D₃ cyclic in the dichloromethane differed for different block molecular weights and compositions, and was dictated by the maximum concentration of reactants which produced the desired transparent solution. When the targeted PDMS endblock lengths were high and the amount of the nonpolar D₃ monomer was correspondingly high, more solvent was required, and in some cases, slight turbidity remained even at low concentrations. For example, a reaction mixture for synthesizing a (15000 g/mole PDMS)-(2000 g/mole PCPMS)-(15000 g/mole PDMS) copolymer containing 6.2 g THF was slightly hazy whereas reaction mixtures for (5000g/mole PDMS)-(5000g/mole PCPMS)-(5000g/mole PDMS) copolymers were transparent at significantly higher concentrations. Reaction rates for the growth of these terminal PDMS blocks were slow, requiring one to even two weeks in some cases. This is a result of the low reactant concentrations and may also be partially attributable to the phase structure of the reaction mixtures.

Block molecular weights and copolymer compositions were calculated based on a combination of titration and proton NMR data. After equilibrating the central PCPMS block, the siloxanolate endgroups were titrated with HCl to obtain the number average molecular weight of that block. The equilibrium 25 wt. % concentration of cyclic species present in these mixtures was taken into consideration in calculating molecular weights from the titration data. An example of the titration plot and a molecular weight calculation is illustrated in Figure 3.8 and Table 3.2, respectively. The calculated molecular weights of the PCPMS central blocks are summarized in Table 3.3.

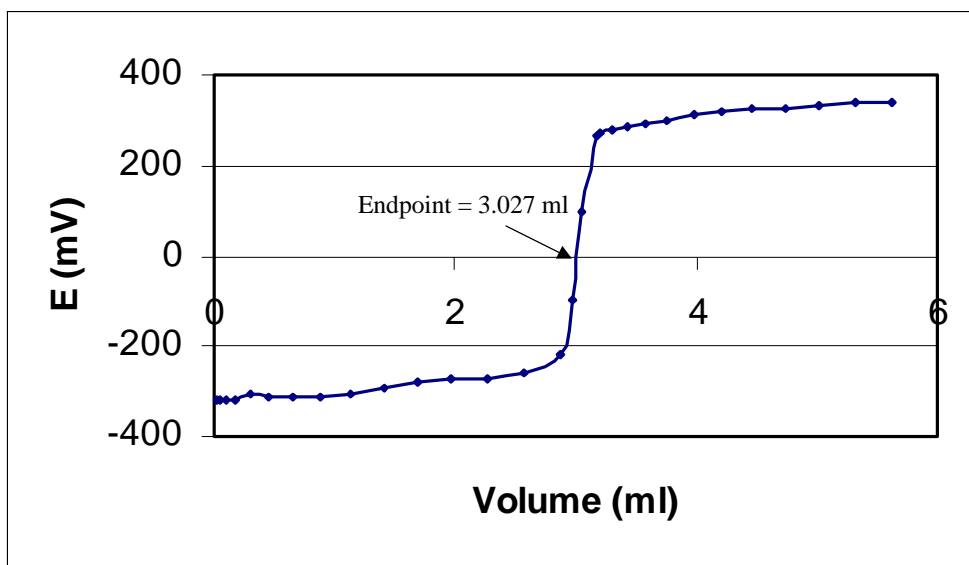


Figure 3.8 A potentiometric titration plot used to determine the molecular weight of the PCPMS central block.

Table 3.2 Number average molecular weight calculations of the PCPMS central block targeted at 2000 g/mol.

Reaction Condition;

HCl titrant was standardized against sodium carbonate; [HCl] = 0.051 M

1.03 g polymers were dissolved in 20.0 ml CH₂Cl₂ to obtain 0.049 g polymer/g solution

The density of CH₂Cl₂ = 1.325 g/ml

Three ml of the polymer solution was used for titration

The endpoint for the titration is 3.027 ml of HCl standard in isopropanol

Adjusting 75% polymers due to the equilibration reaction

$$M_n \text{ of the polymers} = \frac{3 \text{ ml solution} \times 1.325 \text{ g/ml} \times 0.049 \text{ g polymer/g solution} \times 0.75 \times 2}{0.051 \text{ M} \times 3.027 \text{ ml}}$$

$$M_n \text{ of the polymers} = \underline{1900 \text{ g/mol}}$$

Table 3.3 Summary of the calculated M_n of the PCPMS central block determined via potentiometric titration.

Targeted M_n of the Copolymers	Targeted M_n of PCPMS Central Block (g/mol)		Calculated M_n of PCPMS Central Block (g/mol)	Average M_n (g/mol)
5k-2k-5k	2000	Trial 1	1960	1950
		Trial 2	1880	
		Trial 3	2010	
10k-2k-10k	2000	Trial 1	2140	2140
		Trial 2	2130	
		Trial 3	2150	
15k-2k-15k	2000	Trial 1	1950	1990
		Trial 2	1970	
		Trial 3	2050	
5k-5k-5k	5000	Trial 1	4820	4950
		Trial 2	5120	
		Trial 3	4910	
10k-5k-10k	5000	Trial 1	5200	5140
		Trial 2	5120	
		Trial 3	5100	
15k-5k-15k	5,000	Trial 1	4890	4,900
		Trial 2	4820	
		Trial 3	4990	

After copolymerizations of the PDMS endblocks were complete, the polymers were rigorously extracted to remove both unreacted D₃ and the nitrile containing cyclics derived from equilibrating the central block. Their removal was confirmed by the absence of any low molecular weight cyclic species in gel permeation chromatograms of the copolymers. The relative percentages of each block in the copolymer were determined from proton NMR by comparing integrals from the poly(dimethylsiloxane) methyl resonances at 0.06 ppm to the methylene resonances derived from the (3-cyanopropyl)methylsiloxane units ($\delta=0.7, 1.7$ and 2.4 ppm, see Figure 3.9). This relative block composition data, in combination with the central block molecular weights, also enabled calculation of the number average molecular weights of the endblocks. In all cases, the block molecular weights closely paralleled the targeted values (Table 3.4). ²⁹Si and ¹³C NMR spectra of the block copolymers are depicted in Figures 3.10 and 3.11, respectively.

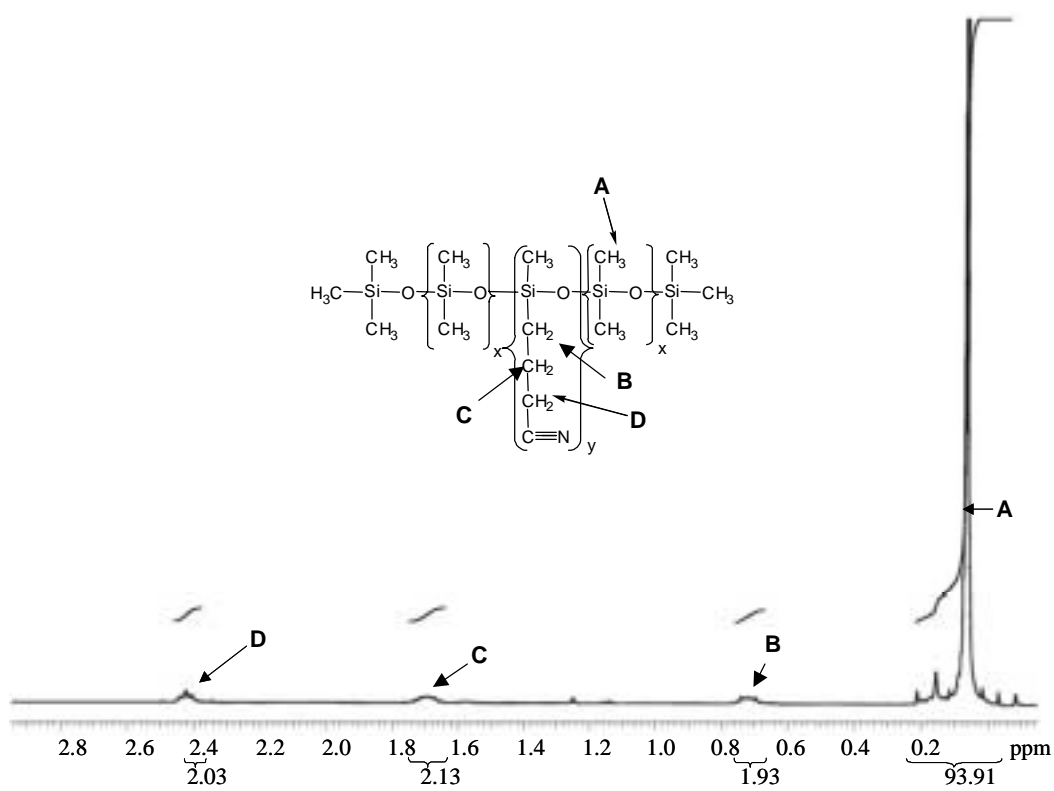


Figure 3.9 ^1H NMR of the PDMS-PCPMS-PDMS triblock copolymers.

Table 3.4 Summary of the calculated M_n of the PDMS-PCPMS-PDMS triblock copolymers determined via combinations of titration and ^1H NMR.

Targeted M_n of PDMS-PCPMS-PDMS	Calculated M_n of PDMS-PCPMS-PDMS
5,000 g/mol-2,000 g/mol-5,000 g/mol	5,200 g/mol-1,950 g/mol-5,200 g/mol
10,000 g/mol-2,000 g/mol-10,000 g/mol	10,800 g/mol-2,140 g/mol-10,800 g/mol
15,000 g/mol-2,000 g/mol-15,000 g/mol	13,600 g/mol-1,990 g/mol-13,600 g/mol
5,000 g/mol-5,000 g/mol-5,000 g/mol	5,300 g/mol-4,950 g/mol-5,300 g/mol
10,000 g/mol-5,000 g/mol-10,000 g/mol	10,800 g/mol-5,140 g/mol-10,800 g/mol
15,000 g/mol-5,000 g/mol-15,000 g/mol	15,200 g/mol-4,900 g/mol-15,200 g/mol

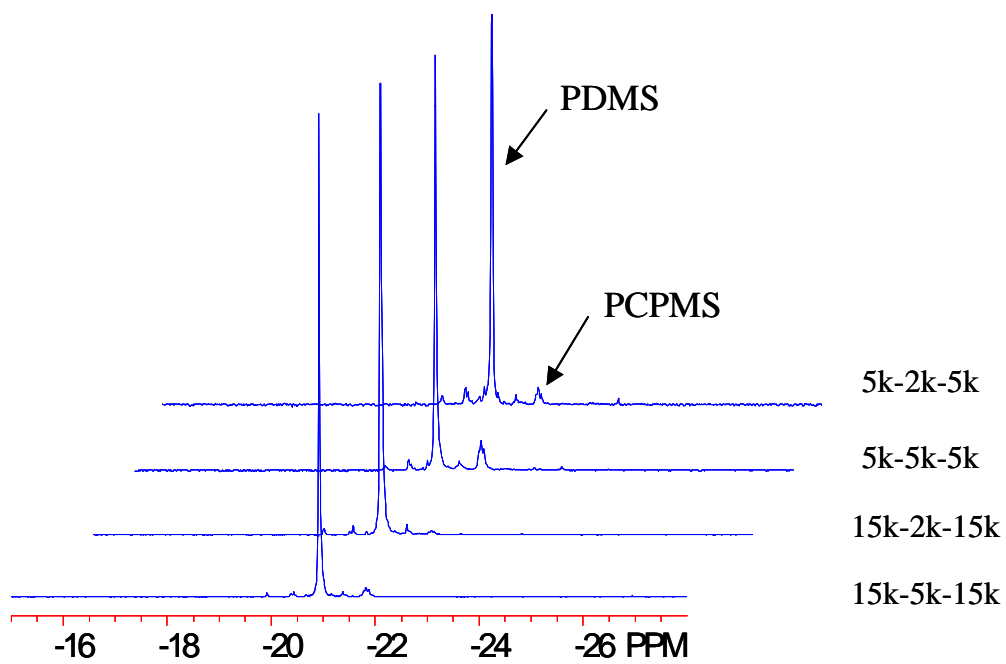


Figure 3.10 ^{29}Si NMR spectra of the polysiloxane triblock copolymers.

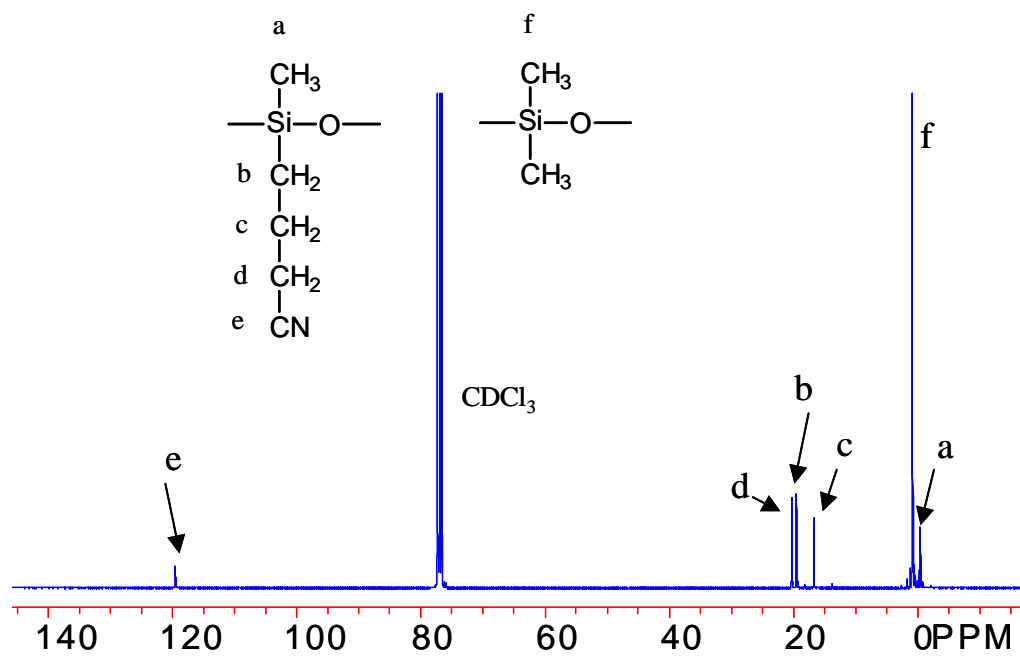


Figure 3.11 ^{13}C NMR analysis of a polysiloxane triblock copolymer.

Bulk thermal properties of these block copolymers indicate that they have “microphase” separated morphologies, even at relatively low block molecular weights (Figure 3.12). Differential scanning calorimetry indicates a T_g for the poly(dimethylsiloxane) block at about -118 °C followed by crystallization at about -90 °C and the characteristic melting peak(s) centered at approximately -50 °C. The fact that the poly(dimethylsiloxane) phase crystallizes further suggests the phase separated nature. The pure poly[(3-cyanopropyl)methylsiloxane] has a T_g at -65 °C and the T_g of the central PCPMS blocks of the copolymers fall in this same region. The two-phase nature of the bulk materials should allow encapsulating the magnetic cobalt particles in the minor PCPMS phase and for the PDMS endblocks to remain as a flexible carrier liquid.

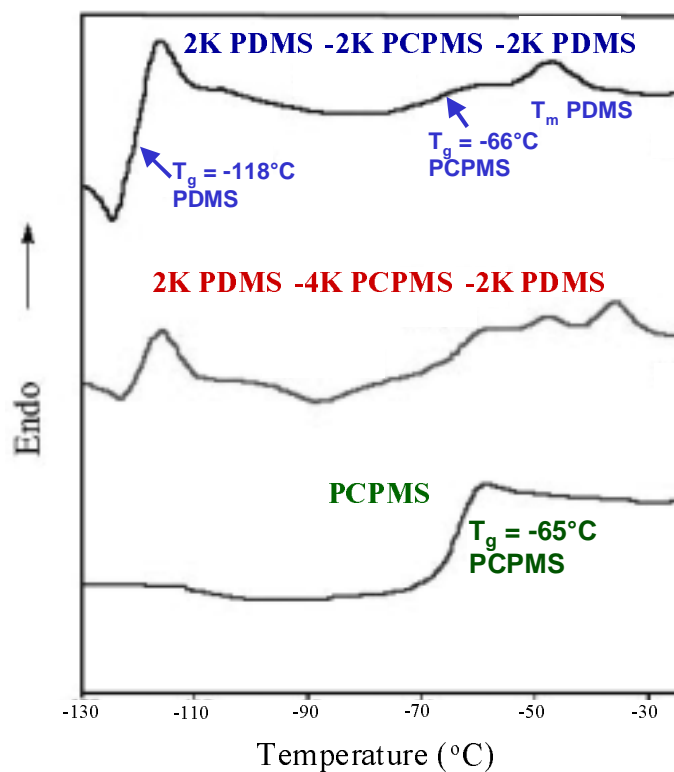


Figure 3.12 DSC thermograms showing microphase separated morphologies of block copolymers (second scan thermograms analyzed at 10 °C/min.).

3.5 Conclusions

D₄CN was successfully prepared by hydrosilylation of D₄H with allyl cyanide in toluene in the presence of Karstedt's catalyst. The PCPMS oligomers were beige, clear liquids. Systematically varied molecular weights of PDMS-PCPMS-PDMS endblocks were then prepared via living anionic polymerization. The calculated molecular weights of the copolymers obtained by the combination of titration and ¹H NMR were in good agreement with the targeted molecular weights. Phase separated morphologies due to the block structures were verified by DSC, with T_gs of the PCPMS central blocks being about -67 °C and T_gs of the PDMS tail blocks around -118 °C.

CHAPTER 4 Synthesis, Characterization and Properties of Stable Cobalt Nanoparticles

4.1 Synopsis

The present section describes cobalt carbonyl ($\text{Co}_2(\text{CO})_8$) thermolysis reactions in the presence of PDMS-PCPMS-PDMS triblock copolymer micelles as reaction sites in either toluene or 2000 g/mol PDMS carrier fluids to obtain stable cobalt dispersions. It is thought that the central nitrile-functional blocks coordinate with the cobalt surface as so-called “anchor” blocks and the poly(dimethylsiloxane) “tail” blocks extend into the carrier fluids to maintain the dispersion. Surface tensiometry in combination with dynamic light scattering measurements indicate that the copolymers form micellar structures in the solution. Relationships among the block lengths in the copolymer stabilizers, the reactant concentrations, dispersion stability, and the resultant cobalt nanoparticle size have been investigated. It is clear that some control over the metal nanoparticle size is possible by adjusting the molar ratio of the dicobalt octacarbonyl precursor to the copolymer.

4.2 Experimental

4.2.1 Purification of solvents and reagents

Toluene ($\text{C}_6\text{H}_5\text{CH}_3$, FW 92.14, b.p. 110.6 °C, d. 0.865)

Toluene (Fisher) was washed twice with concentrated sulfuric acid, and then neutralized with water. It was then dried with anhydrous magnesium sulfate, stirred over calcium hydride for 24 h, and distilled prior to use.

1,1,3,3,5,5,7,7-Octamethylcyclotetrasiloxane (D₄, [(CH₃)₂SiO]₄, FW 296.61, b.p. 175-176 °C, d. 0.956)

D₄ (the Dow-Corning Corp.) was dried over calcium hydride overnight and fractionally distilled prior to use.

Trifluoromethane sulfonic acid (triflic acid, CF₃SO₃H, FW 150.07, b.p. 162 °C, d. 1.327)

Triflic acid (99+%, Aldrich) was used as received.

Hexamethyldisiloxane ([(CH₃)₃Si]₂O, FW 162.38, b.p. 99-100 °C, d. 0.7636)

Hexamethyldisiloxane (99.9%, Gelest, Inc.), used as an endcapping reagent for preparing PDMS carrier fluids, was fractionally distilled prior to use.

Dicobalt octacarbonyl (Co₂(CO)₈, FW 341.95, m.p. 51-52 °C, d. 1.73)

Co₂(CO)₈ (Alfa Easar) stabilized with 1-5% hexane was a dry, dark orange solid. It was stored under argon until used without further purification.

Hexane (CH₃(CH₂)₄CH₃, FW 86.18, b.p. 69 °C, d. 0.659)

Hexane (Burdick and Jackson, HPLC grade) was used as received.

Biphenyl (C₆H₅-C₆H₅, FW 154.21, b.p. 255 °C, m.p. 72 °C, d. 0.992)

Biphenyl (99.5%, Aldrich) was recrystallized in methanol and dried in a vacuum oven.

4.2.2 Synthesis of a 2000 g/mol M_n poly(dimethylsiloxane) carrier fluid (PDMS)

Two hundred mL of octamethylcyclotetrasiloxane (D_4) and 20 mL of the hexamethyldisiloxane endcapping reagent were charged to a 500-mL flame-dried, argon filled, roundbottom flask containing a magnetic stirbar and capped with a septum. The reaction flask was placed in an oil bath at 65 °C. Triflic acid (1.4 mL) was slowly added and the reaction mixture was maintained at the 65 °C temperature for 3 days until thermodynamic equilibrium was achieved. This reaction condition was established by observing the equilibrium composition of peaks via gel permeation chromatography. Following the reaction, 60 mL of ethyl ether was added into the solution and it was then washed with water six times to neutralize the mixture. The equilibrium concentration of D_4 monomer and water were removed under reduced pressure at 120 °C overnight.

4.2.3 Synthesis of a superparamagnetic cobalt fluid stabilized with a (5000 g/mol PDMS)-(5000 g/mol PCPMS)-(5000 g/mol PDMS) block copolymer in toluene

The reaction apparatus consisting of a 500-mL, 3-neck, roundbottom flask equipped with a mechanical stirrer having a vacuum tight adapter, condenser and argon purge was oven dried and assembled under argon. This was placed in a temperature controlled silicone oil heating bath over a hot plate (without magnetic stirrer). Twenty mL toluene and 1.0 g of the copolymer were charged with stirring. After the copolymer dissolved, 1.0 g of bright orange dicobalt octacarbonyl was added and dissolved at room temperature. Immediately upon adding the dicobalt octacarbonyl, a greenish-brown gas fills the flask and refluxes. The oil bath thermocouple was set to 45 °C and the reaction was allowed to slowly warm, then the 45 °C oil

bath temperature was maintained for 45 min. Persistent foaming occurred during this stage which subsided toward the end of the 45 min period. The reaction temperature was raised to 120 °C to yield a greenish-brown solution. Foaming again commences soon after reaching the desired temperature. The reaction was allowed to proceed at 120 °C for 2 h. Upon cooling, a stable dispersion of cobalt nanoparticles in the copolymer-toluene medium resulted.

4.2.4 Preparation of stable cobalt nanoparticle dispersions in 2000 g/mol M_n PDMS carrier fluids

Dispersions with specified cobalt concentrations were prepared in a 2000 g/mole M_n poly(dimethylsiloxane) carrier fluid by first transferring an aliquot of the cobalt dispersion in toluene to a vial, diluting the sample with the appropriate carrier fluid, then removing toluene under reduced pressure. Careful attention was given to exclude oxygen during this process to avoid cobalt particle surface oxidation and preserve the saturation magnetization of these fluids. Quantitative toluene removal was confirmed by the disappearance of the aromatic C-H stretches in the FTIR spectra at $\approx 3000\text{-}3100\text{ cm}^{-1}$.

4.3 Characterization

4.3.1 Surface tension

Surface tension measurements of the copolymer solutions in toluene were conducted at $\approx 26\text{ }^\circ\text{C}$ using a platinum Wilhelmy plate apparatus in combination with a Langmuir-Blodgett trough (KSV 2000, KSV Instruments, Inc., Finland). Surface tensions were calculated using the relationship $\Delta F = \gamma P \cos\theta$ where ΔF is the difference in weight between the wet plate and the wet

plate in contact with the solution, γ is the surface tension, P is the perimeter of the plate and the contact angle θ is assumed to be zero degrees. The copolymer solutions were prepared in toluene at least 24 h before the measurements to allow sufficient time for complete dissolution.

4.3.2 *Dynamic light scattering (DLS)*

Dynamic light scattering measurements on the copolymer solutions in toluene were obtained using a Protein Solutions DynaPro-801TC instrument at 25 °C. The translational diffusion coefficients (D_T) for the molecules in the solutions were calculated from the scattered light intensities. Hydrodynamic radii (R_h) were derived from D_T using the Stokes-Einstein equation. The reported hydrodynamic radii are the average of at least ten measurements. The copolymer solutions were prepared in toluene at least 24 h before the measurements to allow sufficient time for complete dissolution. Copolymer solutions in toluene with concentrations of 0.1 g/L or higher were syringed through 0.1 μm pore filters and those with lower concentrations were syringed through 0.02 μm pore filters prior to surface tension and light scattering measurements.

4.3.3 *Fourier transform infrared spectroscopy (FTIR)*

FTIR spectra were obtained using a Nicolet Impact 400 FTIR spectrometer with the samples run neat between salt plates. At least 32 scans were accumulated for each spectrum.

4.3.4 *Differential scanning calorimetry (DSC)*

DSC was performed using a DuPont 2400 instrument. The samples (about 10 mg) were weighed in aluminum pans before loading into the instrument. After the samples were quickly

quenched to about $-160\text{ }^{\circ}\text{C}$ using liquid N_2 , they were scanned from $-150\text{ }^{\circ}\text{C}$ to $0\text{ }^{\circ}\text{C}$ at $10\text{ }^{\circ}\text{C}/\text{minute}$. Each sample was run twice and transitions taken from the second heating scans were reported.

4.3.5 High performance liquid chromatography (HPLC)

HPLC was used to detect traces of toluene remaining after dialysis of the cobalt dispersions in hexamethyldisiloxane. HPLC was conducted using a Beckman System Gold 128 Solvent Module and 168 NM Detector. Hexamethyldisiloxane (0.1 mL) was withdrawn from the medium outside of the membrane and diluted with 1.0 mL hexane and 0.5 mL of $2.4 \times 10^{-5}\text{ M}$ biphenyl in hexane as an internal standard. The mixture was then injected into a Beckman Ultrasphere silica column with $d_p\ 5\ \mu\text{m}$ and 4.6 mm x 25 cm column size using HPLC grade hexane as a mobile phase.

4.3.6 Transmission electron microscopy (TEM)

TEM photomicrographs were obtained using a Philips 420T TEM run at 100kV. The TEM samples of the cobalt dispersions in toluene or poly(dimethylsiloxane) carrier fluids were prepared by diluting the dispersions with additional toluene to obtain the color of “weak tea.” The solutions were cast onto a carbon-coated grid and the toluene was evaporated. Selected TEM images were analyzed using a fast Fourier transform (FFT) of a 128 pixel square region within the image. The intensities of each pixel of the FFT images were radially averaged. In this process, the pixels of the transformed image were grouped according to their distance from the center of the image (and so their characteristic length scale) and the intensities of each group were summed to provide a total intensity for each length scale.

4.3.7 Electron diffraction spectroscopy (EDS)

Electron diffraction patterns were obtained using a Philips 420T microscope run at 100kV and with a 660 nm camera length in the bright field mode.

4.3.8 X-Ray photoelectron spectroscopy (XPS)

Surface analysis of the cobalt nanoparticles were obtained on a Perkin Elmer X-Ray Photoelectron Spectrometer 5400 Series using a Mg anode operating at 300 watts (14 kV) with the pressure of the system below 5×10^{-6} Pa. Spectra were acquired of a 1mm x 1mm area at a 90° take-off angle. Liquid samples were placed on a copper sample holder and frozen with liquid nitrogen during the measurement.

4.3.9 SQUID magnetometer

Four cobalt nanoparticle dispersions stabilized with a (15000 g/mole PDMS)-(2000 g/mole PCPMS)-(15000 g/mole PDMS) copolymer in a 2000 g/mole M_n PDMS carrier fluid with Co concentrations between 1.6 and 4.1 % were flame-sealed into 4 mm diameter glass tubes under an argon atmosphere. An additional four samples with concentrations between 1.9 and 6.1% were sealed in glass tubes with polycarbonate lids without excluding air from the volume of gas above the liquid. The concentration of each sample is given in Table 4.1.

Magnetic properties of the cobalt dispersions were measured using a SQUID based magnetic susceptometer (Quantum Designs MPMS-7). Magnetic hysteresis loops were measured at 5K after cooling the sample from 220K in a zero or 70 kOe field. The magnetic moment of the sample was measured in fields from -70 kOe to 70 kOe. The time interval between initial and final hysteresis loop measurements of samples 5 – 8 was 180 days, with an

additional measurement taken at an intermediate time point. The time interval between initial and final hysteresis loop measurements of samples 1 – 4 varied from 40-90 days.

Table 4.1 Sample codes and cobalt concentrations of dispersions used for magnetic measurements. Cobalt particles were stabilized with a (15000 g/mole PDMS)-(2000 g/mole PCPMS)-(15000 g/mole PDMS) copolymer and dispersed in a 2000 M_n PDMS carrier fluid.

Air-exposed solutions		Non-air-exposed solutions	
Sample Code	Concentration (% Co)	Sample Code	Concentration (% Co)
1	6.7	5	4.1
2	4.9	6	3.2
3	3.2	7	2.3
4	1.9	8	1.6

4.4 Results and discussion

4.4.1 Analysis of PDMS-PCPMS-PDMS micellar solutions in toluene

One goal has been to investigate cobalt nanoparticle formation in reactions wherein dicobalt octacarbonyl can diffuse into the core of block copolymer micelles, and then thermally eliminate carbon monoxide inside the core. The electron pairs on the nitrile nitrogens of the PCPMS stabilizer central block are believed to interact with the cobalt nanoparticle surfaces to anchor the stabilizer to the particles. It is reasoned that controlling micelle “nanoreactor” size and structure may enable better control over metal particle size, and may also provide improved

copolymer coatings. The stabilizer coating quality is anticipated to be important for minimizing any toxicity issues in-vivo in potential biomedical applications. Thus, understanding the solution structures of the block copolymers in the toluene reaction solvent is a key issue.

Toluene is a good solvent for PDMS but a poor solvent for PCPMS, particularly for higher molecular weight PCPMS oligomers. For example, 3 g/L of an 8000 g/mole M_n PCPMS in toluene is the maximum concentration which is soluble. Only 1 g/L of a 24000 g/mole M_n PCPMS is soluble, whereas 37000 g/mole PCPMS is essentially insoluble in toluene. The PDMS-PCPMS-PDMS block copolymers form micellar solutions in toluene where the PCPMS is concentrated in the micelle cores and PDMS protrudes outward into toluene to form the micellar coronas.

Surface tensions of block copolymer solutions in toluene as well as dynamic light scattering results suggest these solutions contain block copolymer micelles. The surface tension measurements were conducted with a platinum Wilhelmy plate attached with a wire and connected to a balance (Figure 4.1). The plate was first wetted by the solution and the weight of the wet plate was set to zero, then the wet plate in contact with the solution surface was weighed. This weight represents the force pulling the plate down due to contact with the solution surface (ΔF). These ΔF values are proportional to the surface tensions, γ (mN/m), calculated from the relationship $\Delta F = \gamma P \cos\theta$ where P is perimeter of the plate and θ , the contact angle, is assumed to be zero degrees.

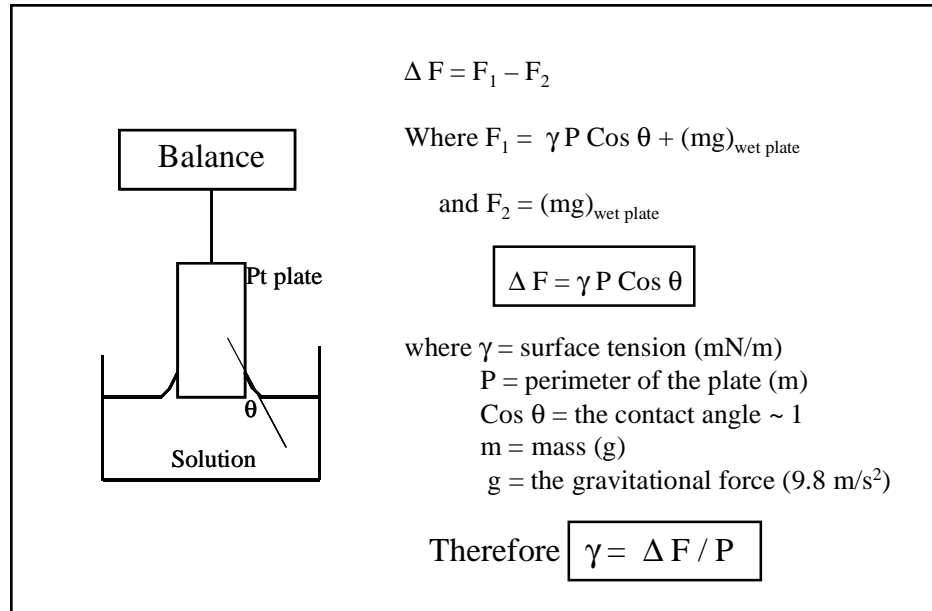


Figure 4.1 Schematic of surface tension measurements: the contact angle θ is assumed to be zero degrees

At sufficiently low copolymer concentrations, surface tensions approached the value for pure toluene (Figure 4.2). The surface tension at the lowest concentration (0.0001 g/L) is close to the reported value of pure toluene at the same temperature ($28.5 \text{ mN}\cdot\text{m}^{-1}$).²⁴² PCPMS center blocks in these materials tend to migrate to the solution surface due to their poor solubility in toluene (Figure 4.3a). Once the copolymer concentrations were increased, surface tensions dropped between ≈ 0.001 and 0.01 g/L , then leveled off for higher concentrations. This result suggests saturation of the solution surfaces by the copolymers (Figure 4.3b) with critical micelle concentrations (cmc) of about $0.01\text{-}0.1 \text{ g/L}$. Further increases in concentration above the cmc lead to micellar solutions (Figure 4.3c). It should be noted that both above and at the cmc, a constant number of single molecules is maintained in the solution. Since micelle formation is a dynamic equilibrium process, these single molecules can constantly diffuse in and out of the micellar structures.

²⁴² R. C. Weast, D. R. Lide, M. J. Astle and W. H. Beyer; CRC Handbook of Chemistry and Physics, CRC Press, Inc., (1989), F-37

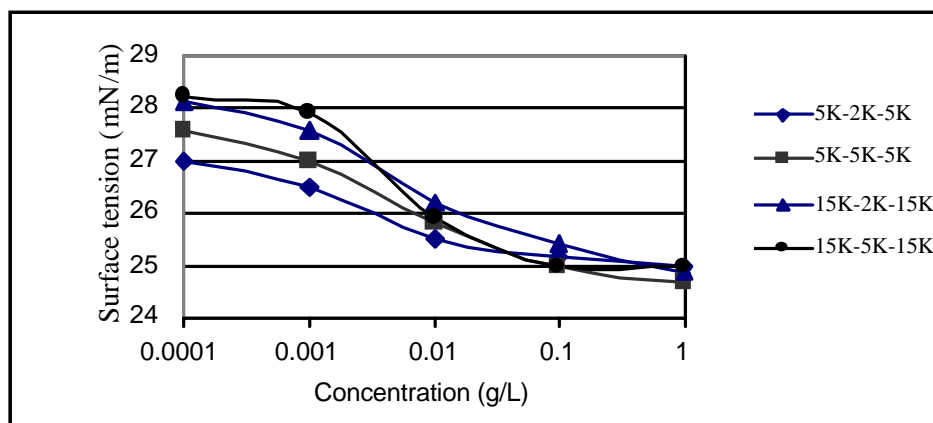


Figure 4.2 Surface tensions of solutions of the PDMS-PCPMS-PDMS triblock copolymers in toluene at 26 °C Showing a cmc of ≈ 0.01 g/L.

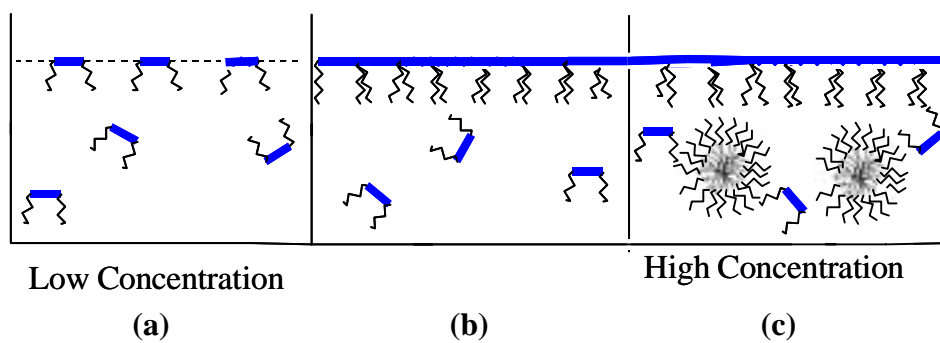


Figure 4.3 Copolymer solutions a) below cmc, b) at the saturation concentration, and c) above cmc.

Surface tension measurements of (15000 g/mole PDMS)-(2000 g/mole PCPMS)-(15000 g/mole PDMS) copolymer solutions in toluene up to 45 °C were also conducted to determine whether the cmc's changed substantially as a function of temperature (Figure 4.4). The 45 °C case was of particular interest because this was the temperature used in the initial stages of the cobalt nanoparticle dispersion syntheses. As expected^{243, 244}, the surface tension values were consistently lower as temperature increased. However, the drops in surface tensions caused by the copolymers occurred over a rather broad concentration region, and no differences in the cmc's could be distinguished (0.01-0.1 g/L from 25-45 °C). This observation suggests that if the cobalt dispersions are prepared at 45 °C or higher with a PDMS-PCPMS-PDMS copolymer concentration higher than the cmc, it is reasonable to assume that micelles are present in the reaction solutions.

²⁴³ S. M. Mahdi and R. O. Skold, *Colloids and Surfaces*, **66**, 203-214, (1992)

²⁴⁴ P. Alexandridis, T. Nivaggioli and T. A. Hatton, *Langmuir*, **11**, 1468-1476, (1995)

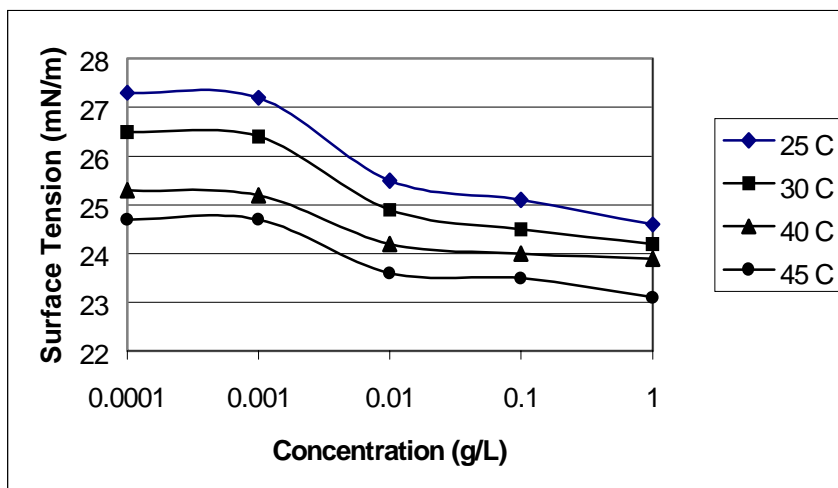


Figure 4.4 Surface tensions of solutions of (15000 g/mole PDMS)-(2000 g/mole PCPMS)-(15000 g/mole PDMS) copolymers in toluene at various temperatures.

Dynamic light scattering measurements further support the micellar solution structures in toluene. When copolymer solutions containing small PDMS blocks (5000 g/mole) were examined, hydrodynamic radii increased from an average of $\approx 3\text{-}4$ nm at 0.001 g/L (indicative of single molecules) to $\approx 11\text{-}12$ nm at 0.01 g/L (indicative of aggregates of molecules) (Table 4.2). This change occurred at somewhat higher concentrations when the PDMS block length was increased to 15000 g/mole. The transitions from molecular to aggregate sizes observed by light scattering occurred in the concentration ranges where cmc's were observed in the surface tension measurements.

Table 4.2 Hydrodynamic radii measured by dynamic light scattering demonstrate large increases in radii at the cmc, consistent with formation of micellar structures.

Concentration (g/l)	Hydrodynamic Radii (R_h) of PDMS-PCPMS-PDMS (nm)	
	5K-2K-5K	5K-5K-5K
5	15.35 ± 0.08	21.35 ± 0.61
1	13.54 ± 0.35	20.43 ± 0.06
0.5	12.80 ± 0.16	18.61 ± 0.09
0.1	12.02 ± 1.11	15.45 ± 2.28
0.01	11.47 ± 0.61	12.19 ± 0.86
0.001	3.38 ± 1.50	4.13 ± 1.03
Concentration (g/l)	Hydrodynamic Radii (R_h) of PDMS-PCPMS-PDMS (nm)	
	15K-2K-15K	15K-5K-15K
5	11.78 ± 0.62	26.70 ± 0.08
1	11.63 ± 0.73	21.77 ± 0.02
0.5	11.86 ± 0.49	21.33 ± 0.15
0.1	11.72 ± 0.65	6.99 ± 0.14
0.01	2.8 ± 0.40	5.25 ± 0.38
0.001	N/A	4.38 ± 0.05

4.4.2 Synthesis of stable cobalt nanoparticles by thermolysis of dicobalt octacarbonyl in the micellar copolymer solutions

The cobalt dispersion reactions were conducted in copolymer-toluene solutions (Figure 4.5) at copolymer concentrations ranging from 10-150 g/L, which is much more concentrated than the solutions investigated by light scattering. Based on our understanding of the structures of the copolymer-toluene solutions, it is reasonable to assume that copolymer micelles as well as micelle aggregates exist under these conditions.

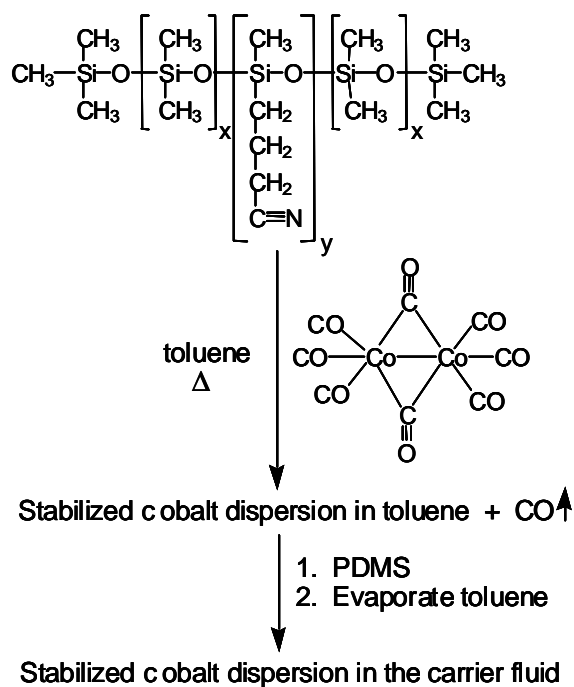


Figure 4.5 Preparation of a cobalt nanoparticle dispersion in toluene.

The progress of a series of reactions was studied by FTIR coupled with TEM microscopy to monitor the transformation of paramagnetic species ($\text{Co}_2(\text{CO})_8$) into superparamagnetic particles (cobalt nanoparticles). These studies were conducted with low (0.2 g), medium (1.0 g) and high (3.2 g) concentrations of $\text{Co}_2(\text{CO})_8$ and 1.0 g of a (15000 g/mole PDMS)-(2000 g/mole PCPMS-(15000 g/mole PDMS) copolymer in 20 mL of toluene (Figure 4.6). It should be noted that one gram of $\text{Co}_2(\text{CO})_8$ theoretically produce 0.34 g of Co metal. The reactions were first heated to 45 °C where the reactions began, and maintained at that temperature for 45 min. Significant foaming initially occurred in this stage due to evolution of carbon monoxide, which subsided toward the end of the 45 min. The carbon monoxide region around 2000 cm^{-1} in the FTIR (Figure 4.7) initially showed three absorbance bands at 2020, 2050 and 2070 cm^{-1} attributed to terminal CO and a peak at 1860 cm^{-1} due to bridging CO in $\text{Co}_2(\text{CO})_8$.²¹² By the end of the 45 min at 45 °C, the absorbances at 2020 and 2050 cm^{-1} had greatly decreased suggesting a large reduction in starting material, and two sharp peaks at 2055 and 2065 cm^{-1} appeared, which were attributed to $\text{Co}_4(\text{CO})_{12}$. The temperature was then raised to 120 °C where the toluene refluxed and foaming caused by additional CO evolution commenced again. After 30 min at this temperature, all CO had disappeared as indicated by the absence CO bands in the FTIR spectra.

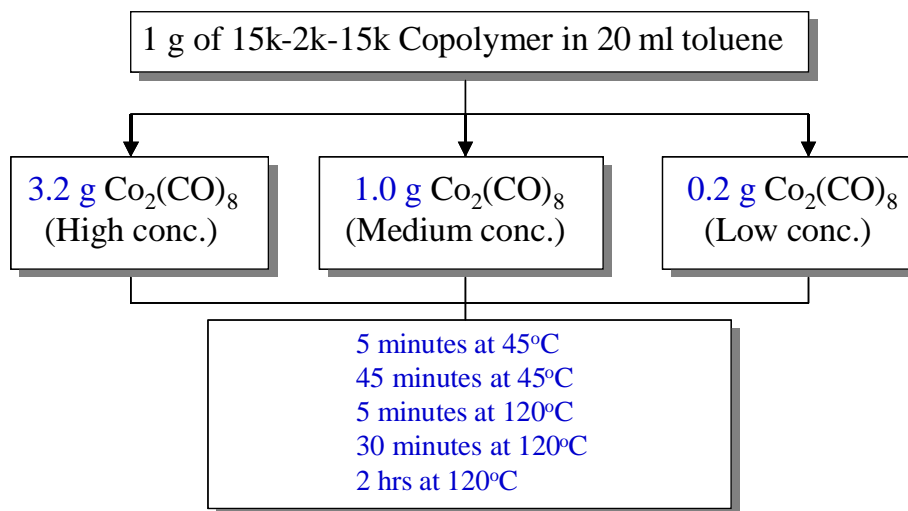


Figure 4.6 Reaction conditions and concentrations used for preparing cobalt nanoparticles.

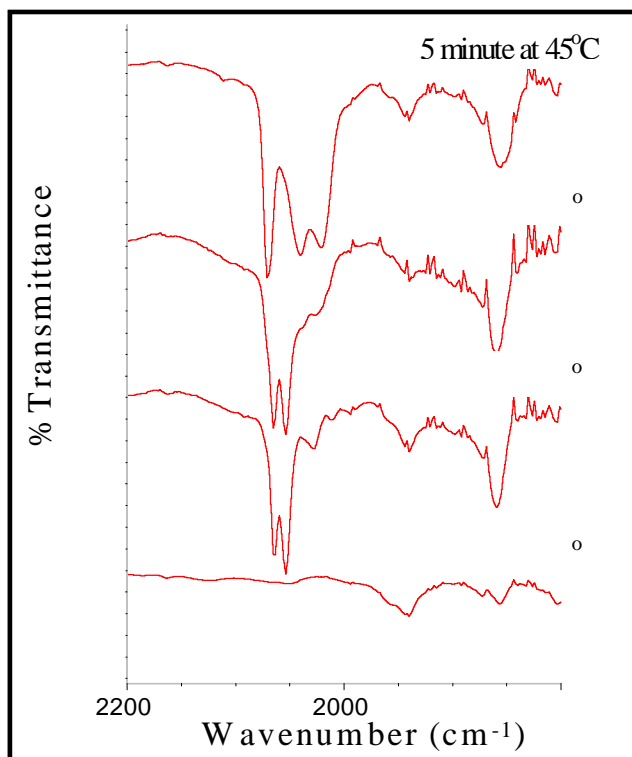


Figure 4.7 FTIR spectra of a cobalt dispersion reaction using 1 g $\text{Co}_2(\text{CO})_8$ and 1 g of a (15000 g/mole PDMS)-(2000 g/mole PCPMS)-(15000 g/mole PDMS) copolymer in 20 mL toluene at different stages.

At all of the cobalt carbonyl to copolymer ratios investigated, TEM photomicrographs from aliquots taken in the early reaction stages (5 min at 45 °C) showed clusters of particles with aggregate sizes 20-50 nm in diameter (Figure 4.8, 4.9, and 4.10). These clusters were thought to

be micelle aggregates essentially stained with $\text{Co}_2(\text{CO})_8$. By contrast, no features were observable in the TEM photomicrographs from analogous copolymer solutions without $\text{Co}_2(\text{CO})_8$. After 45 minutes reaction at 45 °C, the particle aggregates were smaller and appeared denser as evidenced by darkened regions. A significant portion of the $\text{Co}_2(\text{CO})_8$ may have been converted to compounds such as $\text{Co}_4(\text{CO})_{12}$ by this stage. The FTIR showed strong peaks at 2055 and 2065 cm^{-1} attributed to CO groups in $\text{Co}_4(\text{CO})_{12}$, the product from the first step of the solution decomposition of $\text{Co}_2(\text{CO})_8$.²¹² It was reasoned that $\text{Co}_2(\text{CO})_8$ was at least partly decomposed and cobalt paramagnetic species had begun to interact with their counterparts in adjacent molecules/atoms.

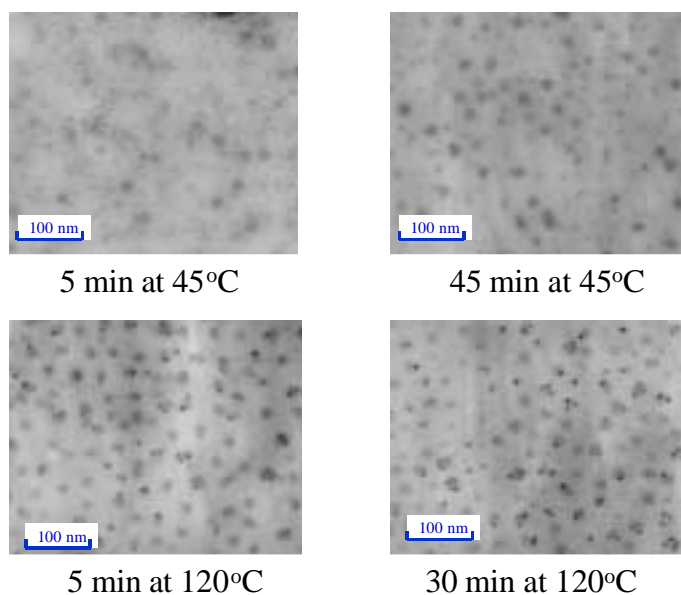


Figure 4.8 TEM micrographs of cobalt dispersions using 0.2 g $\text{Co}_2(\text{CO})_8$ and 1 g of a (15000 g/mole PDMS)-(2000 g/mole PCPMS)-(15000 g/mole PDMS) copolymer in 20 mL toluene at different stages.

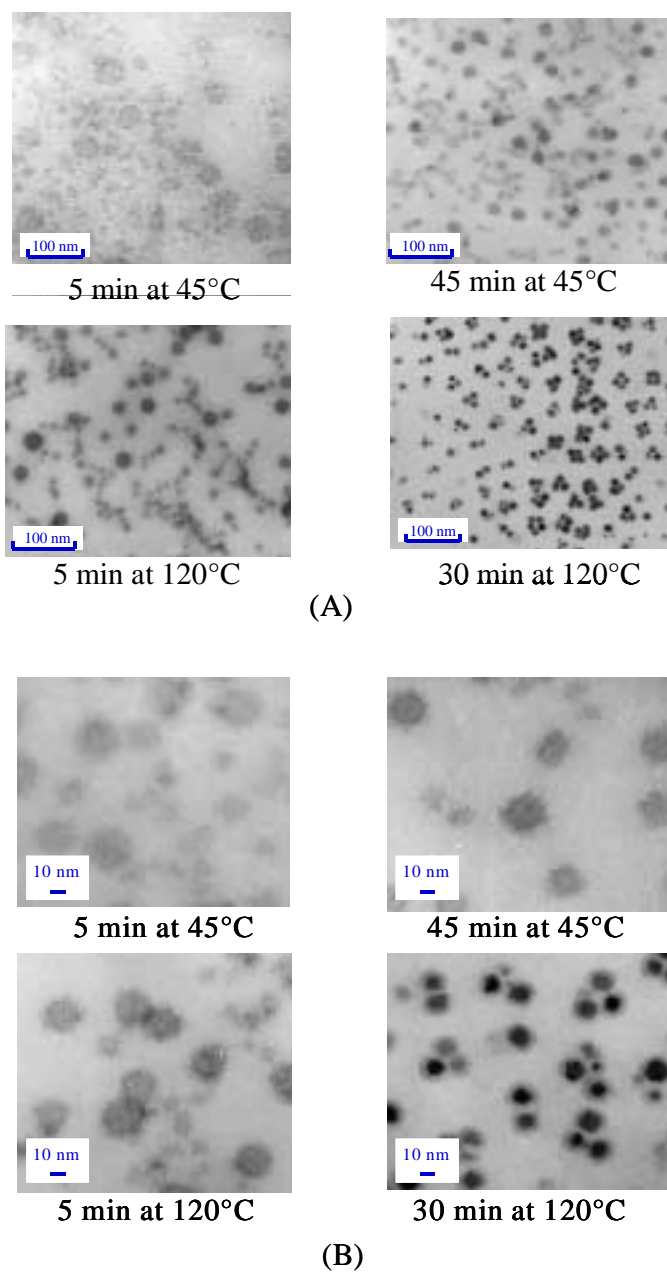


Figure 4.9 TEM micrographs of cobalt dispersions using 1.0 g $\text{Co}_2(\text{CO})_8$ and 1 g of a (15000 g/mole PDMS)-(2000 g/mole PCPMS)-(15000 g/mole PDMS) copolymer in 20 mL toluene at different stages: (A) at low magnification, (B) at high magnification.

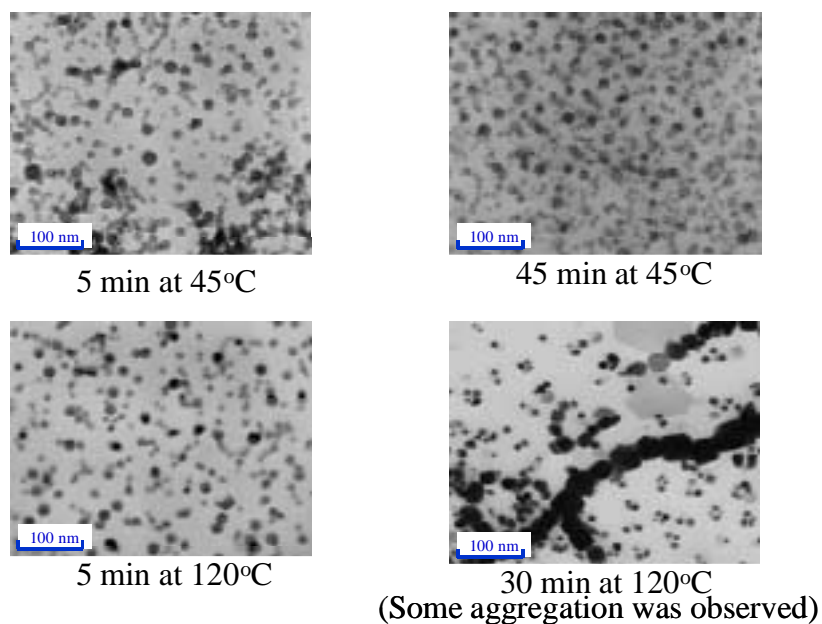


Figure 4.10 TEM micrographs of cobalt dispersions using 3.2 g $\text{Co}_2(\text{CO})_8$ and 1 g of a (15000 g/mole PDMS)-(2000 g/mole PCPMS)-(15000 g/mole PDMS) copolymer in 20 mL toluene at different stages.

The temperature was subsequently raised to 120 °C to further thermolyze the cobalt carbonyl mixtures. After 5 minutes at this temperature, significant foaming again began and the TEM images showed 10-20 nm diameter particles which had further densified significantly over this short period. After 30 minutes at 120 °C, foaming had subsided and all of the CO peaks in the FTIR had disappeared, suggesting that the reactions were complete. In all cases, the average particle sizes after 2 h reaction at 120 °C were equal to those after 30 minutes reaction at the same temperature. However, most of the reactions were maintained at 120 °C for 2 h to ensure that CO was completely removed.

The reaction products prepared with the low and medium cobalt carbonyl to copolymer ratios were transparent, dark, colloidal dispersions without any visible precipitates. The metal particle sizes within each reaction were nearly monodisperse and each particle was surrounded with a well-defined copolymer sheath (Figures 4.8 and 4.9). It is suggested that the apparent homogeneity of the copolymer coatings surrounding each particle may be a result of forming the metal nanoparticles within the copolymer micelles, rather than first forming the particles, then coating them. This issue may be important for the intended biomedical applications of these materials as we strive to develop methodologies which minimize toxicity.

At the higher cobalt carbonyl to copolymer ratio (3.2 g $\text{Co}_2(\text{CO})_8$ to 1 g copolymer), various particle sizes (10, 25 and 45 nm) with some aggregation were observed (Figure 4.10). Thus, the upper limit on the initial molar ratio of $\text{Co}_2(\text{CO})_8$ to copolymer appears to be about 1:1 wt:wt in these reactions to ensure that each particle forms within the micelles and that precipitation is avoided. In addition, undesirably large particles formed in these reactions assembled into oriented chains at this high cobalt carbonyl:copolymer ratio resembling the behavior of “nanoscale magnets” dispersed in the solutions. It was reasoned that dipole-dipole attractions among adjacent magnetically blocked particles had been induced, resulting in particle chain formation.

Interestingly, TEM photomicrographs of the final dispersions formed from the medium concentration cobalt carbonyl:copolymer reactions (1 g cobalt octacarbonyl, 1 g copolymer, 20 mL toluene) showed many particle multiplets consisting of 2-4 small particles, with each particle within the multiplet ≈ 10 nm in diameter, but joined together mostly in triplets and quartets (Figure 4.9). Each of the cobalt particles within the multiplets was individually surrounded with the copolymer sheath. Although this aspect will require further investigation to be well understood, this may be a result of some aggregation of the micelles in the solution during

synthesis. Indeed, the TEM photomicrographs in Figure 4.9 suggest the existence of this multiplet structure throughout the reaction stages. Two to four micelles, grouped together, can be observed in the photomicrograph of the reaction after 5 min at 45 °C, and these become smaller and denser in the later stages (Figure 4.9).

4.4.3 The cobalt dispersion in the presence of an external magnetic field

To determine the stage in the synthesis of the cobalt nanoparticle dispersions where the particles became superparamagnetic, a cobalt dispersion was prepared using 1.0 g of $\text{Co}_2(\text{CO})_8$ and 1.0 g of a (15000 g/mole PDMS)-(2000 g/mole PCPMS)-(15000 g/mole PDMS) copolymer in 20 mL of toluene in the presence of an external magnetic field (provided by a permanent magnet placed under the reaction vessel). Aliquots from the reaction mixture were removed at various stages and investigated with TEM. After the reaction had proceeded for 45 min at 45 °C (after foaming subsided), no differences between this dispersion and that from an analogous reaction conducted under the normal conditions (no external field) were observed, indicating that the particles had not yet become superparamagnetic (Figure 4.11). On the other hand, the dispersion after 5 min at 120 °C (foaming had again commenced) manifested a significant difference from the control reaction (no applied field). Relatively large particles, 20-50 nm in diameter, had formed and were oriented in chains. This suggests that the transition from non-superparamagnetic particles to superparamagnetic particles occurs soon after the 120 °C temperature is employed. It appears that the external magnetic field induced strong magnetic dipole-dipole interactions among the particles which overcame thermal energy, and resulted in oriented chains which were locked in place even after the external magnet was removed.

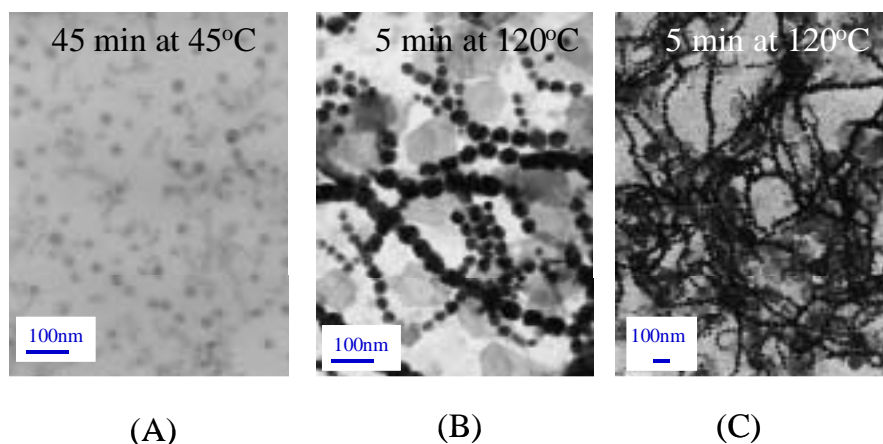


Figure 4.11 TEM micrographs of cobalt dispersions using 1 g $\text{Co}_2(\text{CO})_8$ and 1 g of a (15000 g/mole PDMS)-(2000 g/mole PCPMS)-(15000 g/mole PDMS) copolymer in 20 mL toluene prepared in the presence of an external magnetic field: (A) 45 min. at 45 °C, (B) and (C) 5 min. at 120 °C with different magnifications.

4.4.4 Effects of the $\text{Co}_2(\text{CO})_8$ /copolymer ratio on cobalt nanoparticle size

Controlling particle size in the nanoscale regime to obtain cobalt nanoparticles with a narrow size distribution is of particular interest. Due to their nanoscale size, the particles are single magnetic domains and exhibit superparamagnetic behavior. Formation of larger particles is undesirable because this increases the possibility of aggregation via magnetic attractions between particles.

Results of the controlled particle size studies have been summarized in Tables 4.3a and 4.3b. Reactions with five concentrations of $\text{Co}_2(\text{CO})_8$ with each of four copolymers were conducted in 20 mL of toluene. The block lengths of the copolymers were controlled to investigate any influences of a low (2000 g/mole) molecular weight versus a somewhat higher

molecular weight (5000 g/mole) anchor block length and also a low (5000 g/mole) and higher molecular weight (15000 g/mole) tail block length. In all cases, the anchor block length was significantly shorter than the tail length since previous work has shown this to be the desirable range for providing good steric stabilization.^{196, 239, 245}

The cobalt particle sizes increased from 6 nm in diameter at the low concentration (0.2 g $\text{Co}_2(\text{CO})_8$ (0.07 g Co metal) to 1 g of copolymer) to 10 nm diameter at the medium concentration (1.0 g $\text{Co}_2(\text{CO})_8$ (0.34 g Co metal) to 1 g of copolymer) (Table 4.3A and Figure 4.12). The 6 nm size was attributed to the formation of cobalt nanoparticles in micelle cores where the cores had not been “filled up” with the cobalt carbonyl organometallic precursor. Thus, these early results suggest that some control over particle size in the lower nanoscale regime can be obtained by controlling the cobalt carbonyl to block copolymer ratio. When the cobalt carbonyl to copolymer ratio was increased, the particle diameters were larger up to about 10 nm. Further increases in the ratio resulted in precipitates (3.2 g $\text{Co}_2(\text{CO})_8$ (1.09 g Co metal) to 1 g of copolymer). It seems that once the organometallic precursor concentration was raised high enough to “fill up” the micelle cores, further controlled increases in metal particle size may not be obtainable by this method. No differences in particle sizes were observed as the block lengths of the copolymers were varied in this range (2000 to 5000 g/mol PCPMS, and 5000 to 15000 g/mol PDMS).

Dispersions were also investigated with a constant ratio of $\text{Co}_2(\text{CO})_8$ to copolymers but with systematically varied amounts of toluene (Table 4.3B). As expected, cobalt particle size was independent of the concentrations of $\text{Co}_2(\text{CO})_8$ and copolymers in the toluene. It should be noted that the concentrations of the copolymers in toluene of these reactions are higher than the cmc investigated in surface tension and dynamic light scattering measurements.

²⁴⁵ M. Rutnakornpituk, M.S.Thomson, L. A. Harris, K. E. Farmer, A R. Esker, J. S. Riffle, J. Connolly, and T.G. St. Pierre, *Polymer*, **43**, 2339 (2002)

Table 4.3 Particle size control studies: (A) effects of the ratio of $\text{Co}_2(\text{CO})_8$ to copolymer; (B) effects of the concentration of toluene in the reaction mixtures.

(A)

$\text{Co}_2(\text{CO})_8$ (g)	Copolymer (g)	Toluene (ml)	Particle diameter (nm)		
			15k-2k-15k	5k-5k-5k	15k-5k-15k
0.2	1	20	6	7	7
0.33	1	20	9	10	9
1.0	1	20	10	10	10
1.8	1	20	aggregation	aggregation	aggregation
3.2	1	20	aggregation	aggregation	aggregation

(B)

$\text{Co}_2(\text{CO})_8$ (g)	Copolymer (g)	Toluene (ml)	Particle diameter (nm)		
			15k-2k-15k	5k-5k-5k	15k-5k-15k
1	1	20	10	10	10
1	1	60	12	11	10
1	1	100	12	10	10

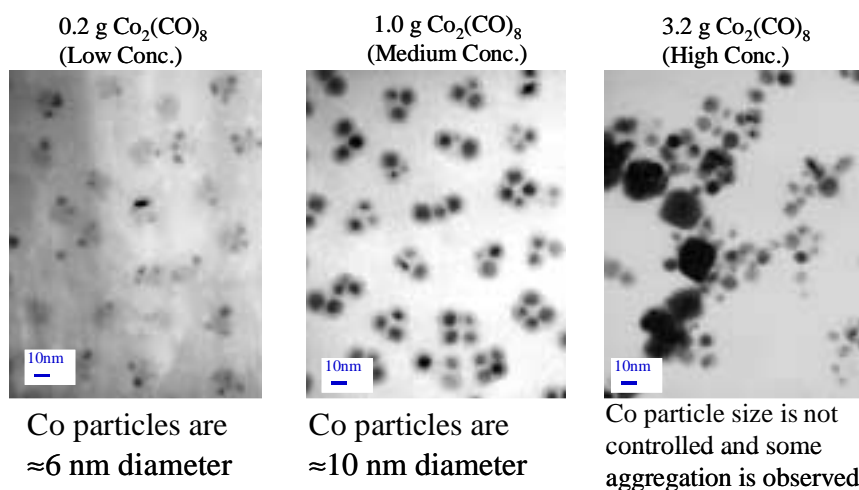


Figure 4.12 TEM micrographs showing the effects of the $\text{Co}_2(\text{CO})_8$ /copolymer ratio on cobalt nanoparticle size.

4.4.5 Formation and characterization of poly(dimethylsiloxane) dispersions

Superparamagnetic cobalt dispersions in low molecular weight PDMS carrier fluids were prepared. A 2000 g/mole PDMS carrier fluid was synthesized via an equilibrium reaction of D_4 using triflic acid as a catalyst. The molecular weight was controlled by using one mole of hexamethyldisiloxane endcapping reagent for every mole of polymer to produce non-functional PDMS. It should be noted that the polysiloxane triblock copolymers with long PCPMS central blocks and short PDMS tail blocks (e.g., (5000 g/mole PDMS)-(5000 g/mole PCPMS)-(5000 g/mole PDMS)) have less solubility in the PDMS homopolymer than those with short PCPMS central blocks and long PDMS tail blocks (e.g., (15000 g/mole PDMS)-(2000 g/mole PCPMS)-(15000 g/mole PDMS)). This corresponds to the fact that high molecular weight PCPMS is insoluble in low molecular weight PDMS. The cobalt dispersions were prepared using 1.0 g of a

(15000 g/mole PDMS)-(2000 g/mole PCPMS)-(15000 g/mole PDMS) copolymer and 1.0 g of $\text{Co}_2(\text{CO})_8$ in 20 mL of toluene and using the reaction conditions previously described. Once the reaction was completed (indicated by the disappearance of CO peaks at 2055 and 2065 cm^{-1} in FTIR), the desired amount of 2000 g/mole PDMS carrier fluid was syringed into the dispersion and the toluene was removed under reduced pressure. The disappearance of the aromatic C-H absorbances above 3000 cm^{-1} in the FTIR suggested that toluene was completely removed. TEM photomicrographs showed that the resultant dispersions had a narrow size distribution comprised of ≈ 10 nm diameter particles with 2-4 particles per multiplet (Figure 4.13).

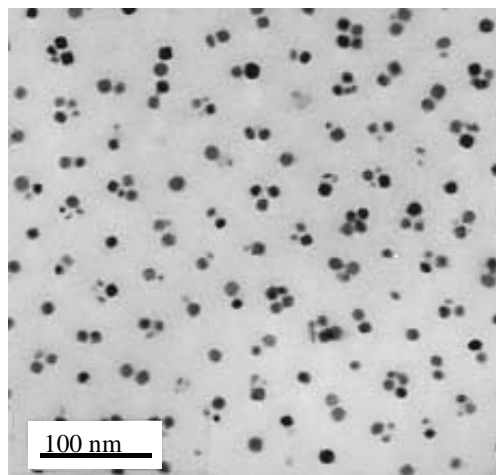


Figure 4.13 TEM micrographs of cobalt dispersions in 2000 g/mol M_n PDMS carrier fluids.

4.4.6 Two-dimensional ordering of superparamagnetic cobalt nanoparticles

A magnetic separation was conducted on a stable cobalt dispersion which had been prepared using 1.0 g of a (15000 g/mole PDMS)-(2000 g/mole PCPMS)-(15000 g/mole PDMS) copolymer, 1.0 g of $\text{Co}_2(\text{CO})_8$, and 20 mL of toluene. The stable dispersion was placed in a weak magnetic field gradient generated by a horseshoe permanent magnet (Figure 4.14). After 24 h, superparamagnetic particles collected in the regions with highest field. Presumably, antiferromagnetic cobalt oxides and small particles remained dispersed in the solution. While the magnetic field was maintained in place, the solution was decanted, then the container with the remaining (strongly superparamagnetic) nanoparticles was rinsed with toluene. The nanoparticles which had been separated by the field gradient of the horseshoe magnet redispersed in the toluene.

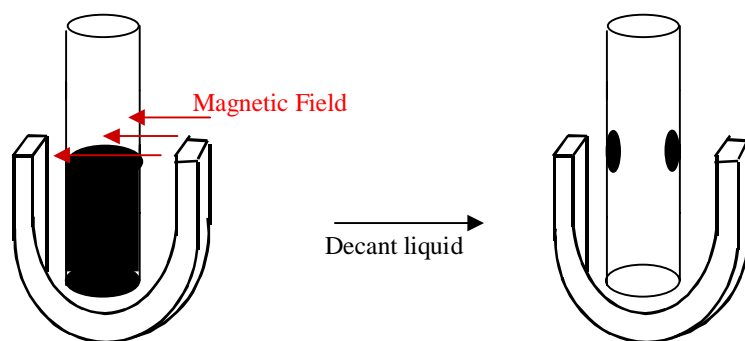


Figure 4.14 Magnetic separation of cobalt dispersions using an externally applied magnetic field gradient.

To prepare samples for transmission electron microscopy, one drop of the solution was cast onto a carbon-coated grid and the toluene was slowly evaporated at room temperature. The resultant dispersion prepared from the particles which were collected in the weak external field gradient formed an ordered, self-assembled cobalt nanoparticle array (Figure 4.15). Although some lesser degree of order appears to be in the original dispersions, the field gradient separation greatly increased the order (Figure 4.16). Radially averaged FFT plots generated from digitized TEM images show clear peaks at approximately 43 nm, 19 nm and 9 nm (Figure 4.17). These 3 length scales can be attributed to intercluster spacing, cluster size, and particle size respectively. The self-assembled array is a result of interparticle interactions. However, it is not possible to determine the source of this interaction from the TEM images. It is also not clear whether the clusters observed are present in the fluid phase, or are formed during evaporation of the fluid.

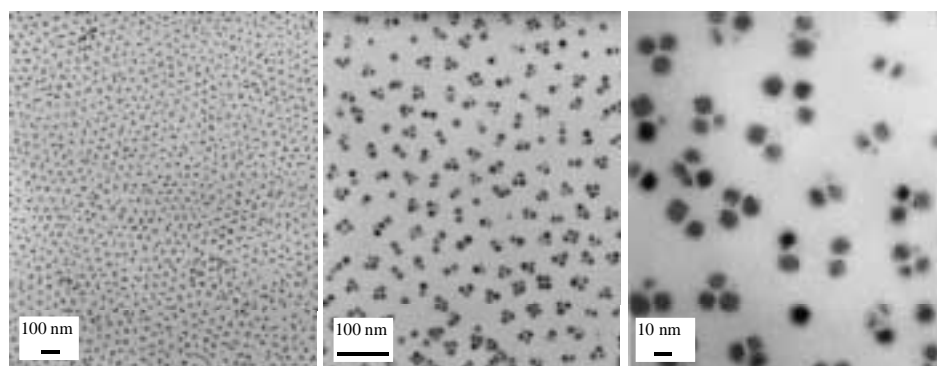


Figure 4.15 Self-assembled two-dimensional ordering of magnetic field separated cobalt nanoparticles on a carbon film from a reaction using 1 g $\text{Co}_2(\text{CO})_8$ and 1 g of a (15000 g/mole PDMS)-(2000 g/mole PCPMS)-(15000 g/mole PDMS) copolymer in 20 mL toluene with different magnifications.

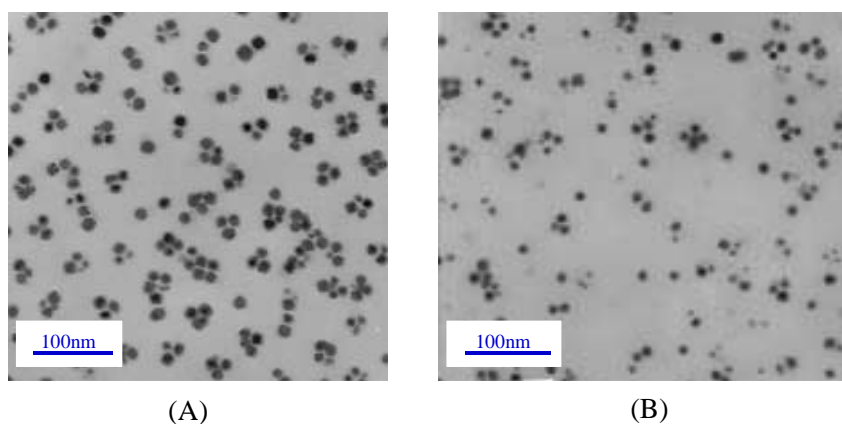


Figure 4.16 TEM micrographs from a reaction using 1 g $\text{Co}_2(\text{CO})_8$ and 1 g of a (15000 g/mole PDMS)-(2000 g/mole PCPMS)-(15000 g/mole PDMS) copolymer in 20 mL toluene showing that the field gradient separation greatly increased the order: (A) in the field with particle sizes of 10 nm, (B) in the decanted liquid with a particle size of 6 nm.

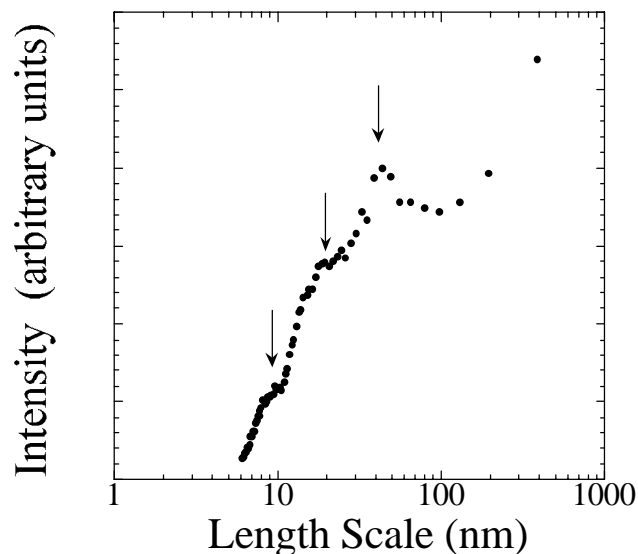


Figure 4.17 Radially averaged FFT data of the central TEM image in Figure 4.14. The arrows indicate the positions of the three characteristic length scales of the image.

4.4.7 Model cobalt nanoparticles coated with PDMS-PCPMS-PDMS copolymers

Estimating the number of cobalt atoms and polymer molecules existing in one particle is also of interest. Model cobalt nanoparticles coated with the copolymers were established, according to the TEM images, to be 10 nm diameter cobalt particles with a 4 nm thick copolymer layer (thickness of the layer was 4 nm) (Figure 4.18). The volume of a 10 nm diameter particle ($\frac{4}{3}\pi r^3$) is $5.24 \times 10^{-19} \text{ cm}^3$. Because the density of bulk cobalt is 8.9 g/cm^3 , the molar atomic weight of cobalt atoms is 58.9 g/mole and Avogadro's number is $6.02 \times 10^{23} \text{ atoms/mol}$, one can estimate that there are 47600 cobalt atoms/particle.

To estimate the number of polymer molecules per particle, the volume of the polymer coating is calculated by subtracting the volume of a 5 nm radius particle (cobalt particle) from the particle with 9 nm radius (cobalt-coated particle) (Figure 4.18). Therefore, the volume of copolymer coating per particle is $2.5 \times 10^{-18} \text{ cm}^3$. Because the density of 15000g/mol-2000g/mol-15000g/mol copolymers (MW = 32,000 g/mol) is 0.975 g/cm^3 and Avogadro's number is 6.02×10^{23} atoms/mol, the estimated number of polymer molecules per particle is 46.

Since the number of nitrile repeating units per molecule in 15000 g/mol-2000 g/mol-15000 g/mol copolymers is 15.7 (the molecular weight of a 3-cyanopropyl(methyl)siloxane repeating unit is 127 g/mol), the estimated number of nitrile groups in the coating per particle is 720. Using the same method of calculation for 15000g/mol-5000g/mol-15000g/mol copolymers, the estimated number of nitrile groups in the coating per particle is 1700 (the number of nitrile repeating units per molecule is 39.4).

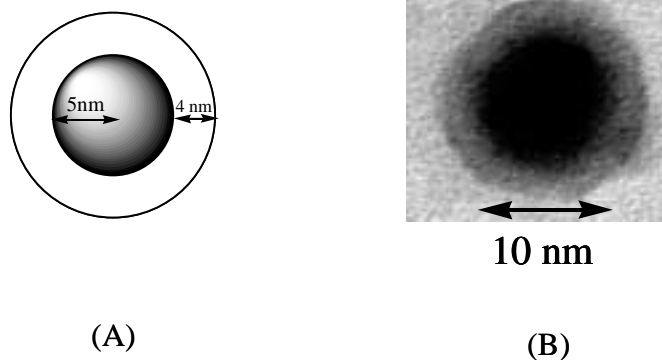


Figure 4.18 Model cobalt nanoparticles coated with PDMS-PCPMS-PDMS copolymers: (A) model, and (B) TEM image of a 10 nm diameter cobalt particle with a 4 nm thick copolymer coating.

Turning now to a consideration of the number of surface sites, the particle surface area required to accommodate an active carboxylic acid group on the head of a surfactant is assumed to be $\approx 0.16 \text{ nm}^2$ (Figure 4.19).²⁴⁶ This area was estimated for the case of magnetite stabilized with oleic acid, and will be assumed to be the area required for accommodating a nitrile unit in this system. Because the surface area of a 10 nm diameter particle ($4\pi r^2$) is 314 nm^2 , the estimated number of nitrile groups required to saturate all the active sites would be 1960 sites per particle ($314/0.16$). It is clear that the estimated number of the surface sites (1960 sites) and the estimated number of nitrile units per particle (720 nitrile groups in 15000 g/mol-2000 g/mol-15000 g/mol copolymers and 1700 nitrile groups in 15000 g/mol-5000 g/mol-15000 g/mol copolymers) are comparable in orders of magnitude.

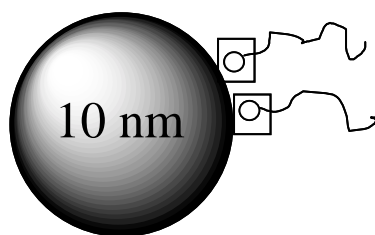


Figure 4.19 Model for estimating the number of surface sites per particle.

²⁴⁶ S. Well, Thesis, "Preparation and Properties of Ultrafine Magnetic Particles", Dept. of Chemistry, The University of Wales, 1989.

4.4.8 Magnetic properties of cobalt dispersions

PDMS dispersions with 1.9 to 6.7 wt% cobalt were prepared as described above. Examples of the magnetic hysteresis curves for samples sealed under an inert, argon atmosphere versus those for samples sealed under an air-containing atmosphere are shown in Figures 4.20 and 4.21. The data appear to be a superposition of a saturated magnetic hysteresis curve owing to a mixture of blocked and superparamagnetic particles and a Brillouin curve owing to the presence of some paramagnetic species. The paramagnetic signal is more apparent in Figure 4.20 than 4.21 and results in a continuing rise in specific magnetization even at 70 kOe. The paramagnetic signal may be due to some cobalt intermediates in the sample which had not been fully reacted. The samples aged in an air-containing atmosphere had specific magnetizations that were not completely saturated at 70 kOe, presumably because of the presence of paramagnetic species. However, specific magnetizations at 70 kOe were approximately 90 to 110 emu/g Co. The samples sealed under an inert atmosphere had specific saturation magnetizations of between approximately 58 and 76 emu/g Co. Saturation specific magnetization for bulk cobalt is approximately 160 emu/g Co (with very little change between liquid helium temperature and room temperature). Saturation specific magnetizations at room temperature for cobalt nanoparticles in PDMS-PCPMS-PDMS copolymers reported previously²³⁹ were in the range 97 to 116 emu/g Co.

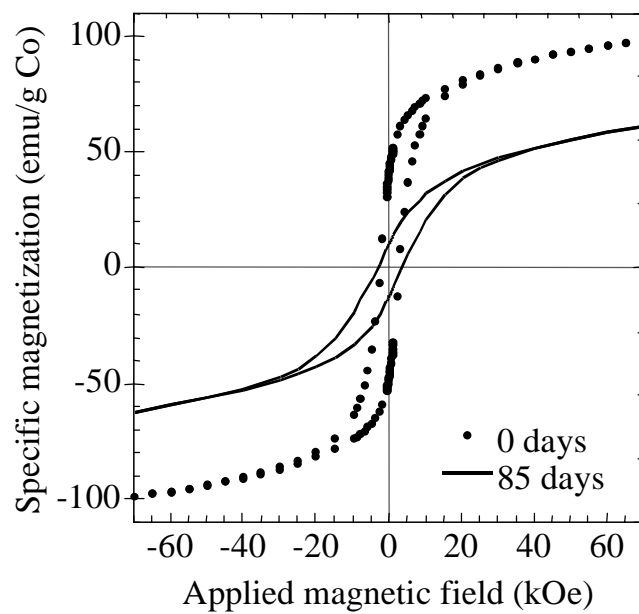


Figure 4.20 Hysteresis loops for an air-exposed cobalt nanoparticle dispersion (sample 3) at 5K after cooling the sample in zero field from room temperature. The loop with the lower specific magnetization values was measured 85 days after the initial loop was recorded.

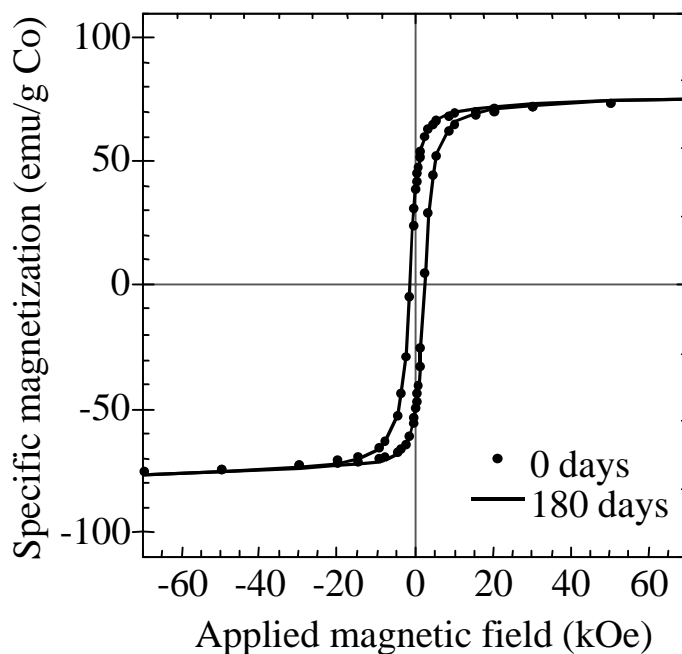


Figure 4.21 Hysteresis loops for a cobalt nanoparticle dispersion sealed under an argon atmosphere (sample 8) at 5K after cooling the sample in a zero field from room temperature. The two loops were recorded 180 days apart.

The specific saturation magnetization was also measured at various time intervals in order to measure the approximate percentage loss of specific saturation magnetization per day. For samples whose magnetization did not fully saturate at 70 kOe, the specific saturation magnetization was taken to be the specific magnetization at 70 kOe. The specific saturation magnetization of the air-exposed samples decreased over the time period of the experiment (Figures 4.20 and 4.22). The rate of specific saturation magnetization loss ranges between 0.3-0.9% per day with the most concentrated samples losing the most magnetization per day. This

possibly is due to a higher rate of oxygen diffusion in the more concentrated samples. The specific saturation magnetization loss most likely is due to oxidation of the cobalt surface to antiferromagnetic oxides.

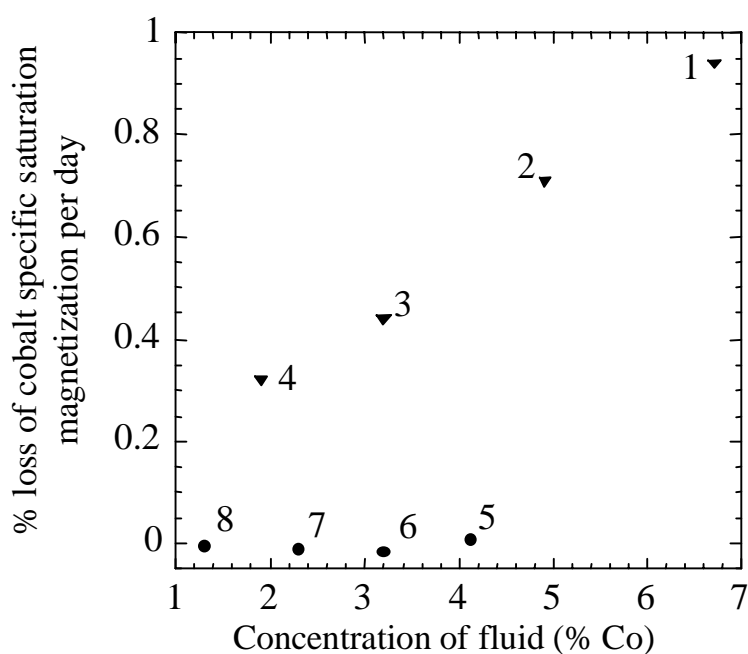


Figure 4.22 Loss of cobalt specific saturation magnetization (or cobalt specific magnetization at 70 kOe) per day as a percentage of the original cobalt specific saturation magnetization (or cobalt specific magnetization at 70 kOe): ● samples sealed under argon, ▼ samples sealed with air. The number beside each point corresponds to the sample code in Table 4.1.

Samples sealed under inert gas had no decrease in specific saturation magnetization during the experimental time period (Figures 4.21 and 4.22). However, there is evidence for the presence of an oxide layer on the surface of the cobalt particles in the non-air-exposed samples. The shift of the center of the hysteresis loop after cooling in an applied field (Figure 4.23) is indicative of exchange anisotropy owing to a layer of antiferromagnetic material, such as cobalt oxide, on the surface of the particle.^{247, 248} The shift of the field-cooled hysteresis loop was stable for the duration of the experiment. Together with the stable specific saturation magnetization of these samples, this implies that no further oxidation occurred over the experimental time period and supports the idea that oxidation occurred before the start of the magnetization measurements (and probably before being sealed under the argon atmosphere). It is possible that an antiferromagnetic cobalt compound other than cobalt oxide has formed on the particle surface but given the possibility of oxidation of particles during removal of toluene from the reaction fluid, it is most likely that a cobalt oxide layer had formed.

The sensitivity of the magnetic properties of the particles to oxidation implies that protection of the cobalt surface against oxidation will be necessary. An approach for accomplishing this will be discussed in chapter 5.

²⁴⁷ C.P. Bean and W.H. Meiklejohn, New Magnetic Anisotropy, *Phys Rev.*, **102**, 1413-1414, (1956)

²⁴⁸ J. Nogués and I.K. Schuller, Exchange Bias, *J. Magn. Magn. Mater.*, **192**, 203 – 232, (1999)

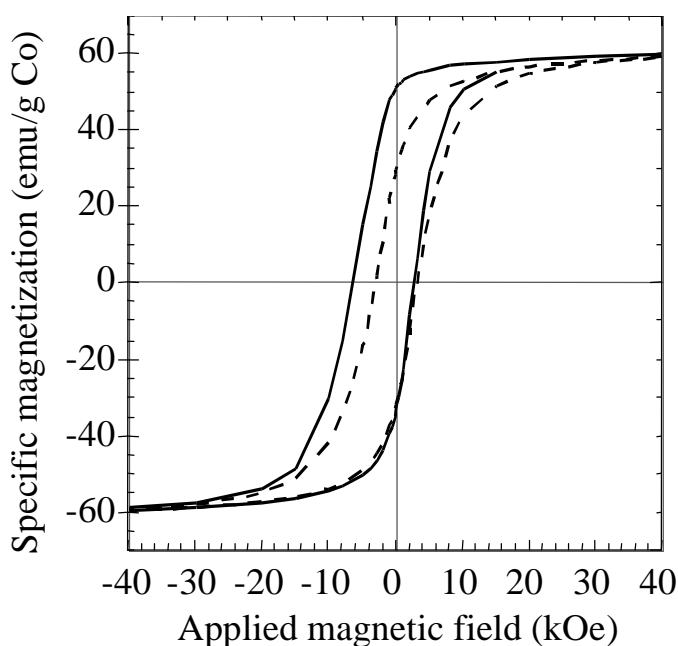


Figure 4.23 Hysteresis loops for sample 5 at 5K after cooling the sample from 220 K in zero field (dashed line) and in a 70 kOe field (solid line).

4.4.9 XPS Surface analysis of the cobalt dispersions

The elemental compositions of the cobalt nanoparticle surfaces coated with the triblock copolymers, but without carrier fluid were investigated. A cobalt nanoparticle dispersion was prepared using 1 g of $\text{Co}_2(\text{CO})_8$ and 1g of a 15000 g/mole PDMS-2000 g/mole PCPMS-15000 g/mole PDMS copolymer in 20 mL toluene, then the toluene was removed at 60 °C under reduced pressure. The cobalt-polymer material was a black, viscous liquid. It was placed on a copper sample holder and frozen with liquid nitrogen for the measurement.

No cobalt peak at ≈ 780 eV was observed (Figure 4.24). This was rationalized by assuming that the triblock polysiloxane copolymer completely covered the cobalt particles. The fact that no bare cobalt is exposed in these materials is promising for the intended biomedical application, since the polysiloxane is nontoxic.

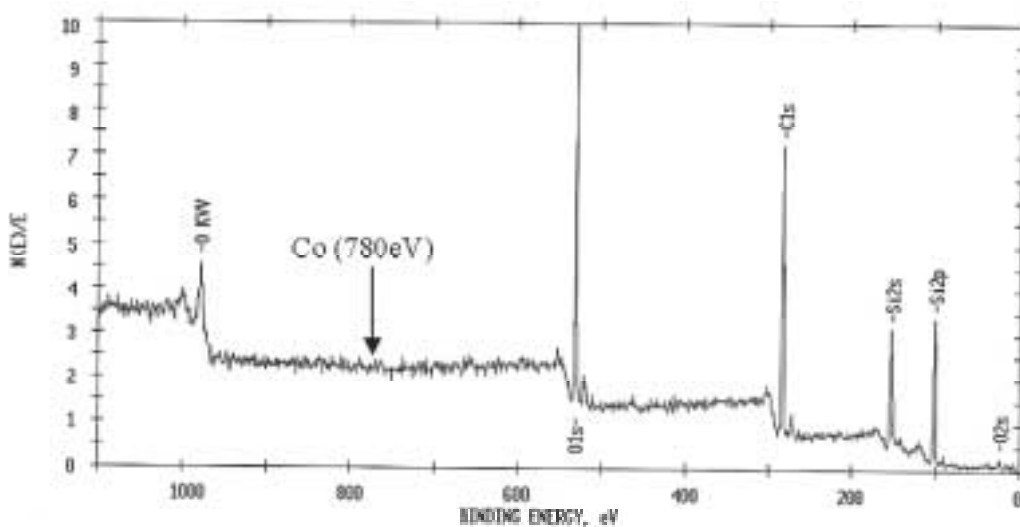


Figure 4.24 XPS spectrum of the cobalt dispersions analyzed at a 90° takeoff angle.

4.4.10 Purification of cobalt dispersions via dialysis

Biocompatibility of the cobalt-polysiloxane materials is an important issue since one objective is to use the materials for treating retinal detachment in human eyes. It is reasoned that coating the cobalt particles with nontoxic polysiloxanes may diminish or eliminate any toxicity of the cobalt. Thus, in addition to coating the cobalt metal with nontoxic polysiloxanes, it was also important to rigorously purify these materials to quantitatively remove toluene.

A cobalt nanoparticle dispersion prepared with 0.5g $\text{Co}_2(\text{CO})_8$ and 0.5g of a 15000 g/mole PDMS-2000 g/mole PCPMS-15000 g/mole PDMS copolymer in 20 mL toluene was transferred to 5 mL of a 2000 g/mol PDMS carrier fluid. The toluene was then vacuum stripped (≈ 0.1 Torr) from the fluid at room temperature overnight. The resultant cobalt dispersion in PDMS with traces of toluene was subsequently transferred to a cellulose acetate dialysis membrane with a 1000 g/mol molecular weight cutoff and submerged in a flask containing 100 mL hexamethyldisiloxane adapted with a mechanical stirrer (Figure 4.25a). The solution was dialyzed at room temperature for two months. Small concentrations of toluene in the original dialysis sample gradually permeated out through the membrane, while hexamethyldisiloxane transferred into the membrane enclosure (Figure 4.25b).

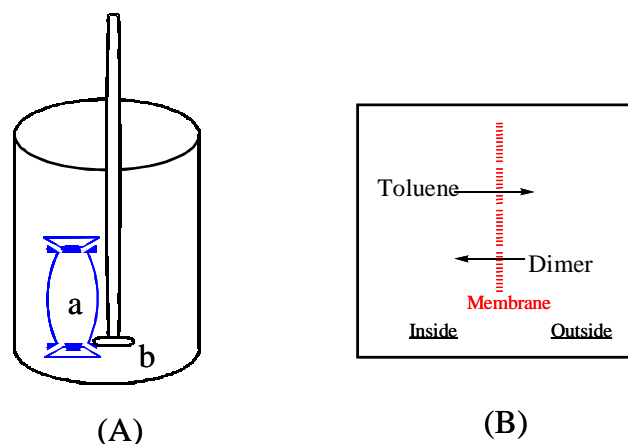


Figure 4.25 (A) Apparatus for dialysis of the cobalt dispersions against hexamethyldisiloxane, and (B) schematic of the ideal diffusion equilibrium between the dimer and toluene through a membrane.

HPLC was utilized to identify traces of toluene in the hexamethyldisiloxane (outside the membrane) every 2-3 days. The ratio of the toluene peak area to the biphenyl peak area (internal standard) was plotted against time (days). The solution was refreshed once the plot started to level off, indicating the equilibrium of the dialysis process (Figure 4.26). At the beginning of this process, most of the toluene was in the membrane enclosure and no toluene was observed in hexamethyldisiloxane (outside the membrane) as indicated in Figure 4.26 at 0 day. Toluene gradually permeated through the membrane during the first 10 days, then reached equilibrium. A standard curve established to determine quantitative amounts of toluene in hexamethyldisiloxane indicates 20 ppm of toluene at the first equilibrium and 2 ppm at the second equilibrium. The

amount of toluene was significantly decreased by this process, which suggests this may be an effective means for removing trace solvent.

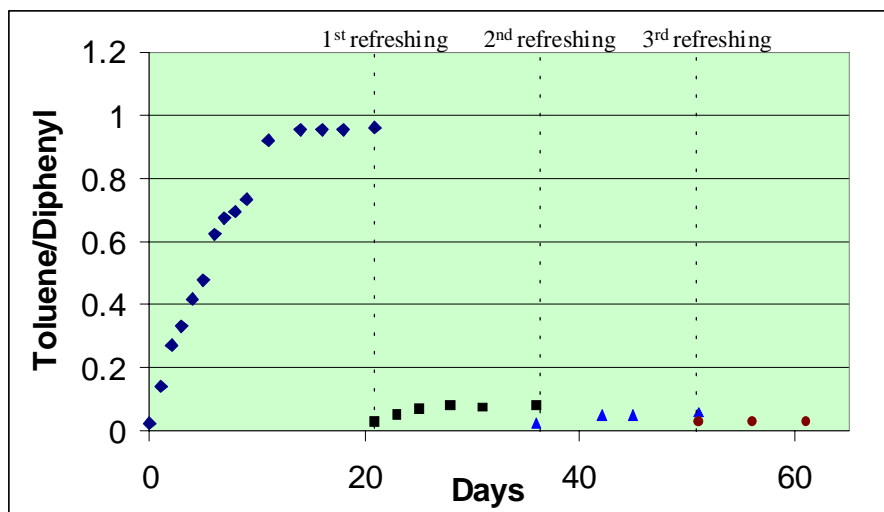


Figure 4.26 Ratio of the toluene/diphenyl peak areas with dialysis time (days) showing a significant decrease of toluene at equilibrium.

4.4.11 Thermal properties of the cobalt dispersions in 2000 g/mol PDMS

Thermal properties of neat triblock copolymers were discussed in chapter 3. In this section, the effect of PDMS carrier fluids and cobalt concentrations on thermal properties of the copolymers will be discussed. The top thermogram in Figure 4.28 shows thermal properties of 50:50 volume% mixtures of the copolymers and a 2000 g/mole PDMS oligomer. The glass transition temperature (T_g) at -127 °C was due to PDMS in both homo- and copolymers. The melting temperature (T_m) at -53 °C was attributed to PDMS homopolymer whereas the T_m at -42 °C was due to the PDMS blocks in the copolymers. The other thermograms displayed thermal

properties of cobalt dispersions with different cobalt contents in the 2000 g/mole PDMS carrier fluid. It should be noted that blends with 2-10 weight percent cobalt in the dispersions were liquid-like materials, whereas cobalt dispersions containing 15-26 weight percent cobalt were gel-like materials.

It is clear that the cobalt concentration in the dispersions did not affect the T_g of PDMS, indicating that the cobalt particles did not interfere with the mobility of PDMS chains in the dispersions. Because an increase in cobalt concentration results in a decrease in PDMS homopolymer content in the dispersions, the peaks due to T_m of PDMS homopolymers ($-53\text{ }^\circ\text{C}$) were smaller whereas the peaks due to the T_m of PDMS in the copolymers ($-41\text{ }^\circ\text{C}$) were larger as cobalt concentrations were raised. Interestingly, the crystallization temperature (T_c) owing to PDMS was consistently decreased from -89 to $-97\text{ }^\circ\text{C}$ as cobalt contents were increased from 2 to 15%. In the dispersions containing 26 weight percent cobalt, the concentration of PDMS homopolymer was so low that only a broad T_m was observable.

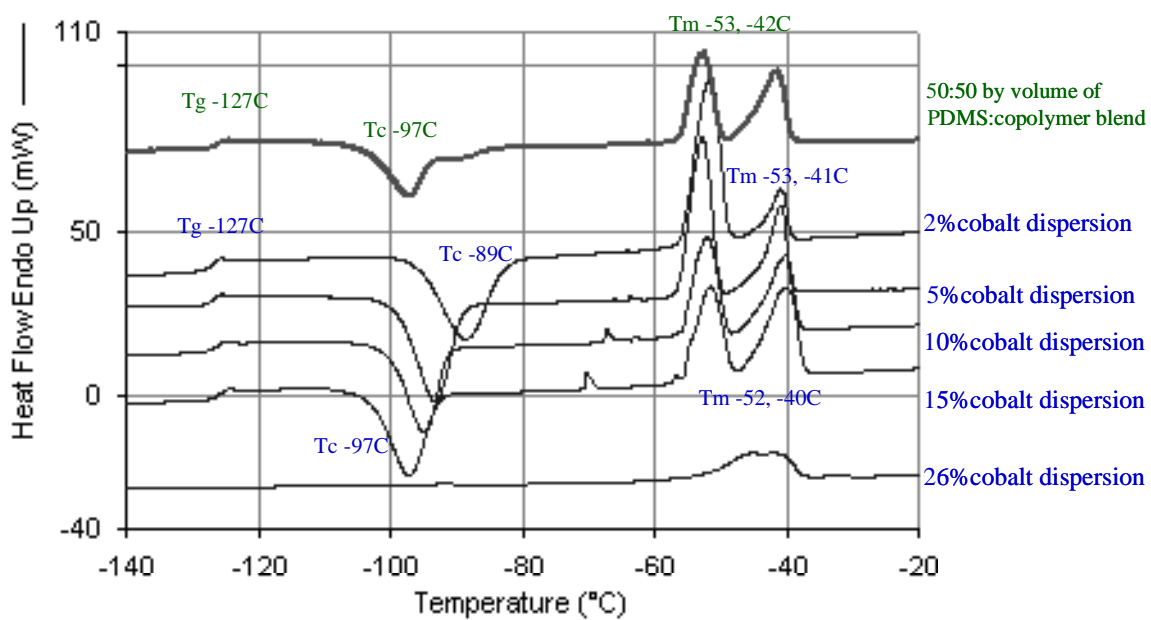


Figure 4.27 Differential scanning calorimetry thermograms of PDMS homopolymer/copolymer blends and cobalt dispersions containing different cobalt concentrations (wt% cobalt).

4.4.12 Determination of crystal structures of cobalt nanoparticles

Electron diffraction spectroscopy is an important technique for determining crystal structures and local orientation of materials^{249, 250}. This technique is usually used to investigate the known crystal system of the specimen. If, indeed, the structure of the specimen is totally unknown, it is necessary to start with symmetry determination to find the point groups and space groups, and then one can deduce its crystal structures. There are two possible crystal structures for cobalt: fcc (face-centered cubic) and hcp (hexagonal close-packed) (Figure 4.28).

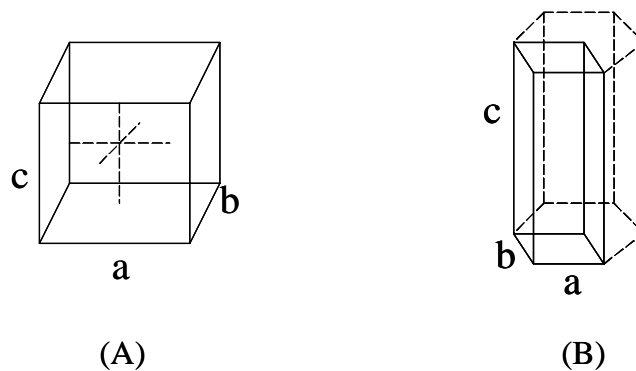


Figure 4.28 Two possible crystal structures of cobalt, (A) fcc, where lattice parameter $a = b = c$, $\alpha = \beta = \gamma = 90^\circ$, and (B) hcp, where lattice parameter $a = b \neq c$, $\alpha = \beta = 90^\circ$, $\gamma = 120^\circ$ ²⁵¹.

²⁴⁹ G. Thomas, and M. J. Goringe, In "Transmission Electron Microscopy of Materials", New York, John Wiley and Sons, 1979.

²⁵⁰ L. C. Sawyer, D. T. Grubb, In "Polymer Microscopy", London, Chapman & Hall, 1987.

²⁵¹ J. F. Nye, In "Physical Properties of Crystals", Oxford, Clarendon Press, 1957.

The size of the rings in the diffraction pattern relates to the d-spacing value of a particular unit cell by the equation:

$$R_i \cdot d_i = \lambda \cdot L = c$$

where R_i is the diameter of the ring i in a diffraction pattern

d_i is the d-spacing value of the ring i of a particular unit cell

λ is the wave length

L is the camera length

c is a constant

This equation can be rearranged to give the following equations:

$$R_i = c / d_i$$

and,

$$R_i / R_{i+1} = d_{i+1} / d_i$$

These indicate that d-spacing values are the reciprocals of the diameter of the ring in the diffraction pattern.

The theoretical d-spacing values of each crystal structure of cobalt can be calculated using the following equations²⁵²:

$$d = a / (h^2 + k^2 + l^2)^{1/2} \quad \text{for fcc crystal structure, and}$$

$$1/d^2 = 4/3 (h^2 + hk + k^2)/a^2 + l^2/c^2 \quad \text{for hcp crystal structure,}$$

where $a = b = c$ for fcc crystal structure,

$a = b \neq c$ for hcp crystal structure,

²⁵² C. Barrett, T. B. Massalski, In "Structure of Metals, Crystallographic methods, principles and data", Oxford, Pergamon Press, 1980.

h , k , and l are the Miller indices which specify the orientation of the planes relative to crystal axes. They are usually reported in the parentheses, e.g., {100}, {210}, which indicate h , k and l values, respectively.

In the fcc cobalt crystal structure, the a , b and c values are 0.35447 nm, whereas, in the hcp crystal structure, the a and b values are 0.25053 nm and c value is 0.40886 nm²⁵³. The theoretical d-spacing values of each crystal structure are calculated as shown in Table 4.4.

Table 4.4 The theoretical d-spacing values of fcc and hcp crystal structures of cobalt.

Ring#	d (fcc)	d (hcp)
1	0.2047 {111}	0.2170 {100}
2	0.1772 {200}	0.2044 {002}
3	0.1253 {220}	0.1917 {101}
4	0.1069 {311}	0.1488 {102}

* The Miller indices of each structure are indicated in parentheses.

²⁵³ A. Taylor, B.J. Kagle, In "Crystallographic Data on Metal and Alloy Structures", New York, Dover Publisher Inc., 1963.

To determine the crystal structure of the cobalt nanoparticles, the ratio of two d-spacing values was calculated (d_i/d_{i+1}) and compared with the reciprocals of the corresponding R values (R_{i+1}/R_i) measured from the electron diffraction pattern. The electron diffraction pattern is illustrated in Figure 4.29. The crystal structure (fcc or hcp) that has the ratio of d-spacing values in agreement with those of the corresponding R values would be deduced as a unit cell of the cobalt nanoparticles.

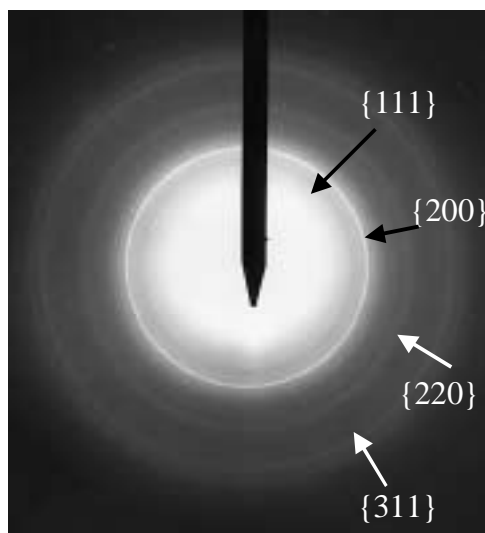


Figure 4.29 Electron diffraction pattern of cobalt nanoparticles.

As shown in Table 4.6, the ratios of the d-spacing values of fcc crystal structure are closely paralleled to those of the corresponding R values, indicating that the crystal structure of cobalt nanoparticles is fcc. In good agreement with this result, it has been previously reported that cobalt dispersions prepared by thermal decomposition of $\text{Co}_2(\text{CO})_8$ in toluene using $\text{Na}(\text{AOT})$ ^{217, 218} or polystyrene-*b*-(poly-4-vinylpyridine)²¹⁹ as a stabilizer also produced the fcc cobalt crystal structure. However, it is apparent that there is an amorphous halo in the diffraction pattern, indicating the existence of amorphous species in the particles as well. This is probably due to the presence of an oxide layer on the surface of the cobalt particles as discussed in section 4.4.8 and Figure 4.23.

Table 4.6 The ratio of d-spacing values of hcp and fcc cobalt crystal structures compared to the inverse ratio of the corresponding R values.

	hcp	fcc		
d_1/d_2	1.0613	1.1546	r_2/r_1	1.1591
d_1/d_3	1.1321	1.6333	r_3/r_1	1.6364
d_1/d_4	1.4582	1.9148	r_4/r_1	1.9182
d_2/d_3	1.0667	1.4145	r_3/r_2	1.4118
d_2/d_4	1.3739	1.6583	r_4/r_2	1.6549
d_3/d_4	1.2881	1.1723	r_4/r_3	1.1722

4.5 Conclusions

Well-defined cobalt nanoparticle dispersions with narrow particle size distributions can be prepared in toluene in the presence of PDMS-PCPMS-PDMS triblock copolymer micelles. Each particle is singly coated with a sheath of the block copolymer which may be important for minimizing toxicity issues in biomedical applications. It is hypothesized that this precision in the size and coating integrity in these dispersions is a result of first making the micellar “nanoreactors”, then forming the particle inside the intended coating material. Some control of particle size in the 6-10 nm diameter range appears possible by controlling the ratio of the organometallic cobalt precursor to the copolymer during synthesis. This size range may also be important for *in vivo* applications since there is substantial evidence suggesting that particles in this size range can be excreted via the renal glomeruli. Ordered self-assemblies of these cobalt particles form spontaneously when the dispersions are cast from toluene. This aspect is not as yet understood, but suggests there must be some interparticle attractions-repulsions which control reasonably long-range order. The electron diffraction pattern indicates that cobalt nanoparticles have the fcc crystal structure.

Magnetic measurements over time clearly show the decrease in magnetic susceptibility over time for dispersions in contact with an air-containing atmosphere, and this has been attributed to surface oxidation. Protection of the particle surfaces against oxidation will be discussed in next chapter. Magnetic measurements also suggest the presence of an oxide layer around each cobalt particle even when sealed under an inert atmosphere.

CHAPTER 5 Preparation of Novel Pentablock Steric Stabilizers and Silica-Coated Cobalt Nanoparticles via a Sol-Gel Process

5.1 Synopsis

The effectiveness of PDMS-PCPMS-PDMS triblock copolymers as steric dispersion stabilizers for colloidal cobalt particles formed via thermolysis of $\text{Co}_2(\text{CO})_8$ in toluene was described in the previous chapter. However, magnetic measurements of these particles show that their magnetic susceptibility decreases over time for dispersions in contact with an air-containing atmosphere, and this has been attributed to surface oxidation. Attempts have been made by others to protect cobalt nanoparticles from environmental oxidation by encapsulating them in graphitic layers using a modified arc-discharge method.^{254, 255} However, the extent of improvement in oxidative stability of the carbon-coated particles over the uncoated ones has not yet been reported. Coating maghemite nanoparticles via a sol-gel process has been reported to be an efficient method to protect them against acid attack.²⁵⁶

This chapter focuses on our work on inhibiting environmental oxidation of magnetic cobalt nanoparticles by coating them with silica shells. Dicobalt octacarbonyl has been thermolyzed in the presence of poly[dimethylsiloxane-*b*-methyltriethoxysilylsiloxane-*b*-(3-cyanopropyl)methylsiloxane-*b*-methyltriethoxysilylsiloxane-*b*-dimethylsiloxane] (PDMS-PMTEOS-PCPMS-PMTEOS-PDMS) pentablock terpolymers (Figure 5.1). The PCPMS central block binds the cobalt and PDMS tail blocks sterically stabilize the cobalt dispersion. The PMTEOS blocks are precursor blocks for the nanoparticle coating process. In addition,

²⁵⁴ X. Sun, A. Gutierrez, M. J. Yacaman, X. Dong, and S. Jin, *Materials Science and Engineering*, **A286**, 157 (2000)

²⁵⁵ H. Huang, S. Yang and G. Gu, *J. Phys. Chem. B.*, **102**, 18, 3420 (1998)

²⁵⁶ Q. Liu, J. A. Finch, Z. Xu, *Chemistry of materials*, **10**, 3936 (1998)

methoxysilane-containing terpolymers has also been prepared as a more reactive alternative to ethoxysilanes.

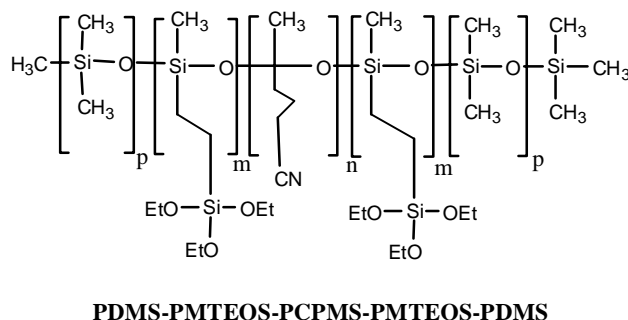


Figure 5.1 A chemical structure of PDMS-PMTEOS-PCPMS-PMTEOS-PDMS pentablock terpolymers

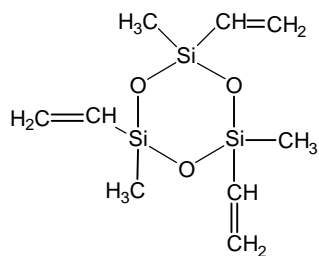
5.2 Experimental

5.2.1 Purification of solvents and reagents

Most of the reagents were purified as described in the experimental section in chapter 3. Otherwise, they were purified as follows:

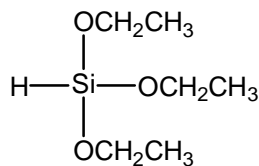
1,3,5-Trimethyl-1,3,5-trivinylcyclotrisiloxane ($D_{3\text{-vinyl}}$, $C_9H_{18}O_3Si_3$, FW 258.5, b.p. 80 °C/20 mm, d. 0.9669)

$D_{3\text{-vinyl}}$ (Gelest, Inc.) was dried over calcium hydride overnight and fractionally distilled prior to use.



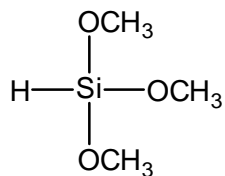
Triethoxysilane ($C_6H_{16}O_3Si$, FW 164.28, b.p. 131-132 °C, d. 0.8753)

Triethoxysilane (Gelest, Inc.) was stored under argon and used as received.



Trimethoxysilane ($C_3H_{10}O_3Si$, FW 122.20, b.p. 86-87 °C. d. 0.860)

Trimethoxysilane (95%, Gelest, Inc.) was stored under argon and used as received.



Dibutyltin diacetate (DBTA, $(\text{CH}_3\text{CO}_2)_2\text{Sn}[(\text{CH}_2)_3\text{CH}_3]_2$, FW 351.01, b.p. 142-145 °C/10mm, d. 1.32)

DBTA (Aldrich) was used as received.

Ammonium hydroxide (NH_4OH , FW 35.05, d. 0.9)

NH_4OH (A.C.S. reagent grade, Aldrich) was used as received.

5.2.2 *Synthesis of poly[dimethylsiloxane-*b*-methylvinylsiloxane-*b*-(3-cyanopropyl)methylsiloxane-*b*-methylvinylsiloxane-*b*-dimethylsiloxane] (PDMS-PMVS-PCPMS-PMVS-PDMS) pentablock terpolymers with controlled block lengths*

A procedure for preparing a terpolymer with a targeted number average molecular weight comprised of 15000 g/mole PDMS, 2000 g/mol PMVS and 2000 g/mole PCPMS blocks is provided. The terpolymers containing 1000 and 4000 g/mol PMVS blocks were prepared in a similar process but with different amounts of $\text{D}_{3\text{-vinyl}}$ relative to the central block to tailor the PMVS block lengths. The first part of the terpolymer synthesis involves preparing controlled molecular weight PCPMS oligomers with terminal lithium siloxanates (Figure 5.2). D_4CN (12.5 g) and 0.24 g (0.01 moles) lithium hydroxide were charged to a clean, dry 500-mL roundbottom flask equipped with a mechanical stirrer and nitrogen purge. The mixture was stirred at 140 °C for at least 48 h to reach thermodynamic equilibrium. The approach to equilibrium was monitored by GPC using samples that had been terminated with trimethylchlorosilane. The ratio of cyclics to linear species at equilibrium was 27 wt% small cyclics and 73 wt% linear chains.

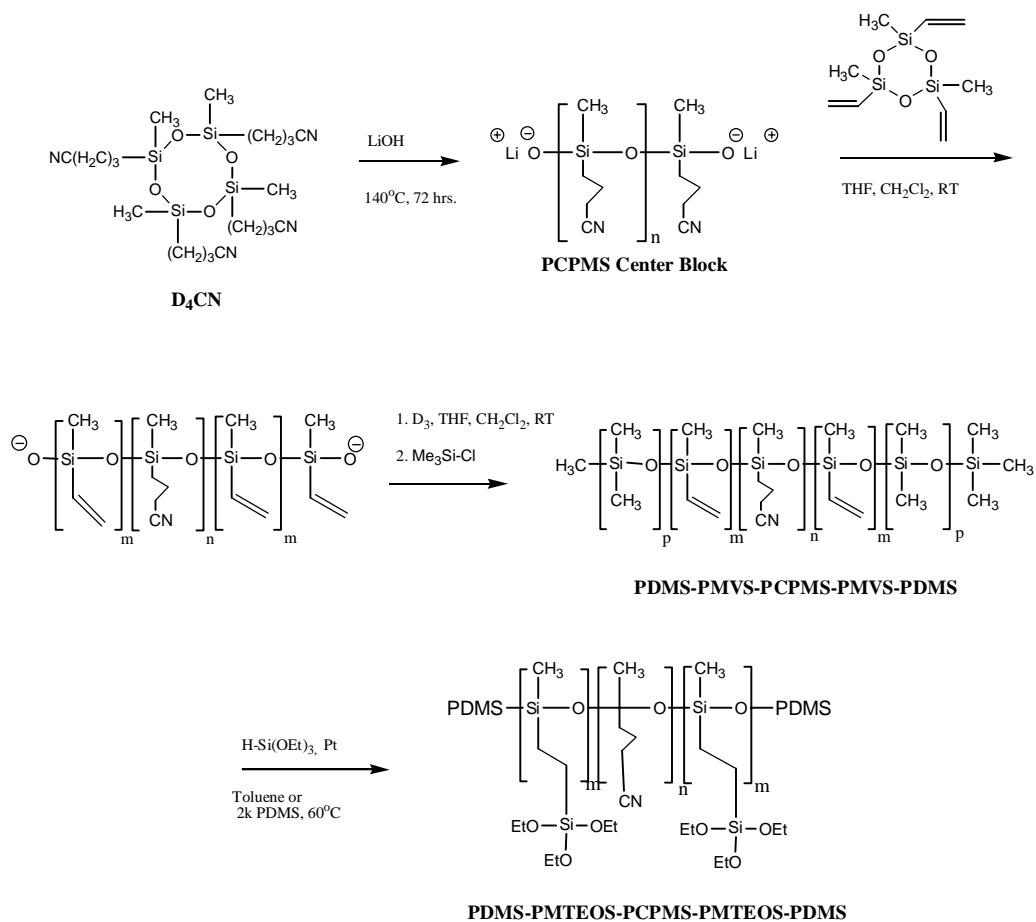


Figure 5.2 Synthesis of PDMS-PMVS-PCPMS-PMVS-PDMS pentablock terpolymers.

After equilibrium was achieved, 250 mL of dichloromethane was added to the macroinitiator via cannula. Twenty-two mL of trimethyltrivinylcyclotrisiloxane (D_3 -vinyl) was added along with 12.5 mL THF as a reaction rate promoter ($\approx 5\%$ of the total volume). Five percent by volume of the promoter was added to all block terpolymer reactions irrespective of the block molecular weights. 1H NMR was used to monitor the progress of the reaction by observing the disappearance of the three signals centered at 0.23 ppm due to methyl protons in the D_3 -vinyl cyclic monomer relative to the set of resonance centered at 0.71 ppm as a reference (corresponds to the methylene protons adjacent to the silicon in PCPMS). After the reaction reached a minimum of 90% conversion, the solution was transferred via cannula to a flame-dried 1000-mL roundbottom flask filled with argon. A 200-mL aliquot of a D_3 -dichloromethane solution (0.85 g D_3 per mL) was added along with an additional 20 mL THF. Another 150 mL of dichloromethane was added to bring the reaction volume to ≈ 600 mL and to obtain a clear solution. The disappearance of the D_3 protons at 0.14 ppm from TMS was divided by a reference integral centered at 0.71 ppm due to methylene protons in PCPMS to monitor the extent of conversion. The reaction proceeded at room temperature for 7 days (85% monomer conversion).

The pentablock terpolymer was terminated with an excess of trimethylchlorosilane (4.4 mL) via syringe and stirred for approximately 30 min. The solution clouds upon termination due to LiCl precipitation. The excess trimethylchlorosilane and the dichloromethane solvent were removed under reduced pressure. The viscous terpolymer was diluted with chloroform and washed repeatedly with water to remove the lithium chloride. The terpolymer-chloroform solution was precipitated into methanol to remove nitrile containing siloxane cyclics (from the

central block equilibration step) and the THF promoter. The methanol phase was decanted, and the polymer was dried at 80 °C under vacuum overnight. The block molecular weights and the total molecular weights of the terpolymers after purification were established using a combination of titration and NMR measurements. The formulations used for preparing the pentablock terpolymers with various block molecular weights are illustrated in Table 5.1.

Table 5.1 Reactant concentrations for preparing pentablock terpolymers with various PMVS block molecular weights. The targeted number average molecular weights are 15000 g/mol for the PDMS and 2000 g/mol for the PCPMS.

Targeted M_n of PMVS block (g/mol)	D ₄ CN (g)	LiOH (g)	D ₃ -vinyl (g)	D ₃ (g)	Trimethylchlorosilane Endcapper (ml)
1,000	12.5	0.24	11	170	4.4
2,000	12.5	0.24	22	170	4.4
4,000	12.5	0.24	44	170	4.4

*5.2.3 Synthesis of poly[dimethylsiloxane-*b*-methyltriethoxysilylsiloxane-*b*-(3-cyanopropyl)methylsiloxane-*b*-methyltriethoxysilylsiloxane-*b*-dimethylsiloxane] (PDMS-PMTEOS-PCPMS-PMTEOS-PDMS) pentablock terpolymers*

An exemplary procedure describes the hydrosilylation reaction of the pentablock terpolymer containing 2000 g/mol PMVS blocks, a 2000 g/mol PCPMS block, and 15000 g/mol PDMS blocks with triethoxysilane in a 2000 g/mol, non-functional PDMS carrier fluid. Hydrosilylations of the pentablock terpolymers with trimethoxysilane were conducted in similar procedures. An alternative variation of this reaction utilizes toluene as a reaction medium. An

advantage of using toluene solvent is that higher cobalt concentrations can be achieved by removing the solvent after the reaction.

The reaction apparatus consisting of a 250-mL, 2-neck, roundbottom flask equipped with a mechanical stirrer having a vacuum tight adapter and capped with a septum and argon purge was flame dried under argon. Twenty mL of the 2000 g/mol PDMS and 1 g of a PDMS-PMVS-PCPMS-PMVS-PDMS pentablock terpolymer (irrespective of the block molecular weights) were charged with stirring. The reaction flask was placed in a temperature controlled, silicone oil-heating bath over a hot plate (without a magnetic stirrer). For hydrosilylation of a terpolymer containing 2000 g/mol PMVS blocks, triethoxysilane (0.25 mL, 0.0013 mol) and Karstedt's catalyst (0.09 mL or 0.5 wt% based on the weight of the polymer, 0.0071 mol Pt per mole vinyl) were charged to the reaction flask. A stoichiometric ratio of triethoxysilyl and vinylsilyl units were used in all hydrosilylation reactions of the terpolymers containing different PMVS block molecular weights. The reactants used for preparing pentablock terpolymers with different PMTEOS or PMTMOS (polymethyltrimethoxysilylsiloxane) block molecular weights are illustrated in Table 5.2. The reaction was allowed to proceed for 2-3 days at 55 °C. ¹H NMR was used to monitor the reaction progress by observing the disappearance of vinyl ($\delta = 5.8$ -6.1 ppm) and Si-H peaks ($\delta = 4.3$ ppm).

A 2000 g/mol PDMS carrier fluid was prepared in an equilibrium ring-opening polymerization of octamethylcyclotetrasiloxane (D₄) in the presence of triflic acid as a catalyst. A detailed discussion of the carrier fluid synthesis has been discussed in chapter 4.

Table 5.2 Reactants used for preparing pentablock terpolymers with various PMTEOS or PMTMOS block molecular weights. The number average molecular weights are 15000 g/mol for the PDMS and 2000 g/mol for the PCPMS. M_n 's of PMVS are as indicated.

Wt of PDMS-PMVS-PCPMS- PMVS-PDMS copolymer (g)	M_n of PMVS block (g/mol)	Solvents (ml) (Toluene or PDMS)	Trialkoxysilane (ml)*		Karstedt's catalyst (ml)
			Triethoxysilane	Trimethoxysilane	
1.0	1,000	20	0.13	0.10	0.09
1.0	2,000	20	0.25	0.18	0.09
1.0	4,000	20	0.46	0.35	0.09

* Either triethoxysilane or trimethoxysilane was used for each reaction.

5.2.4 Preparation of silica-coated cobalt nanoparticles stabilized with a PDMS-PMTEOS-PCPMS-PMTEOS-PDMS pentablock terpolymer in a 2000 g/mol PDMS carrier fluid

Following hydrosilylation of the poly(methylvinylsiloxane) blocks in the terpolymer, the solution was slowly cooled to room temperature. One gram of bright orange dicobalt octacarbonyl was added to all of the cobalt reactions (irrespective of the polymer block lengths) and dissolved at room temperature. The reaction was slowly warmed to 45 °C, and maintained at this temperature for 45 min. The reaction temperature was then raised to 120 °C to yield a greenish-brown solution and maintained at this temperature for 16 h for reactions (for the reaction conducted in 2000 g/mol PDMS) or 2 h (for reactions conducted in toluene). Quantitative CO removal was confirmed by the disappearance of the CO signals from the cobalt carbonyl precursor at ≈ 2020 - 2065 cm^{-1} in the FTIR. When reaction was complete, it was slowly cooled to room temperature under an argon purge.

Once a stable dispersion of cobalt nanoparticles were obtained, 35 μ l of oxygen-free water (for the terpolymers containing PMTEOS derived from the 2000 g/mol PMVS block length) was

added along with 21 μ l of dibutyltin diacetate (DBTA) catalyst (0.1wt%, 1.5×10^{-2} mol of tin per mol of ethoxy group) to condense ethoxysilane and eventually form crosslinked silica shells around the cobalt nanoparticles. The dispersion was stirred at room temperature under argon for a week. The concentrations of water added into these reactions were estimated from the concentrations of ethoxy groups in the terpolymers. One mole of water was used for every two moles of ethoxy groups in all of these reactions. Calculations of the amounts of water needed for preparing the silica-coated nanoparticle dispersions are illustrated in Table 5.3.

Table 5.3 An example calculation of the amounts of water needed for preparing silica-coated cobalt nanoparticle dispersions.

The reaction was performed using 1g of 15k-2k-2k-2k-15k PDMS-PMTEOS-PCPMS-PMTEOS-PDMS in 20ml toluene.

The estimated M_n of the copolymer is 36,000g/mol.

The molecular weight of the vinyl-containing repeating units is 86g/mol.

Amounts of the vinyl-containing repeating units are 4,000g/mol / 86g/mol

$$= 46.5 \text{ repeating units of the vinyl -containing blocks per chain}$$

Numbers of moles of the copolymers are 1.0g/36,000g/mol

$$= 2.76 \times 10^{-5} \text{ mol of polymers}$$

Therefore, numbers of moles of the vinyl-containing repeating units are

$$= 46.5 \times 2.76 \times 10^{-5}$$

$$= 1.28 \times 10^{-3} \text{ mol of the vinyl-containing repeating units}$$

One mole of the vinyl-containing repeating units produces three moles of ethoxysilane.

One mole of water is needed for every two moles of ethoxysilane unit.

Therefore, water content required for this system is

$$= \frac{1.28 \times 10^{-3} \text{ mol vinyl} \times 3 \text{ mol ethoxy} \times 1 \text{ mol water} \times 18 \text{ g/mol water}}{1 \text{ mol vinyl} \times 2 \text{ mol ethoxy}}$$

$$= 0.034 \text{ g} \approx 34 \mu\text{l}$$

Specified cobalt concentrations of the dispersions in 2000 g/mol PDMS as the solvent were achieved by introducing an appropriate amount of carrier fluids at the beginning of the reaction to obtain the targeted cobalt concentration. For reactions conducted in toluene, dispersions with specified cobalt concentrations in the 2000 g/mole PDMS carrier fluid were prepared by first transferring an aliquot of the silica-coated cobalt particles dispersion in toluene to a vial, diluting the sample with the appropriate amount of PDMS carrier fluid, then removing the toluene under reduced pressure. Careful attention was given to exclude oxygen during this process to avoid any cobalt particle surface oxidation and to preserve the saturation magnetization of these fluids. Quantitative toluene removal was confirmed by the disappearance of the aromatic C-H stretches at $\approx 3000\text{-}3100\text{ cm}^{-1}$ in the FTIR.

5.3 Characterization

Most of the characterization techniques were performed on the same instruments described in Chapter 3 and 4. Otherwise, they are described as follows:

5.3.1 Magnetic properties

Magnetization measurements of the cobalt fluids with specified cobalt concentrations were made on a Standard 7300 Series Vibrating Sample Magnetometer (VSM) System (Lake Shore Cryotronics, Inc.). Each measurement was performed using a magnetic power supply with 4-inch electromagnets and a gaussmeter with a ± 30 kG Hall Probe (Figure 5.3). The saturation magnetization of the fluid in emu was read at a magnetic flux density from 8000 gauss to -8000 gauss with 0.1 emu sensitivity. The y-axis intercept of a plot of applied field strength vs.

magnetization provided the value for the saturation magnetization of the fluids in emu. This saturation magnetization value was then normalized with the sample weight and concentration of cobalt in the dispersion to obtain emu/g cobalt.

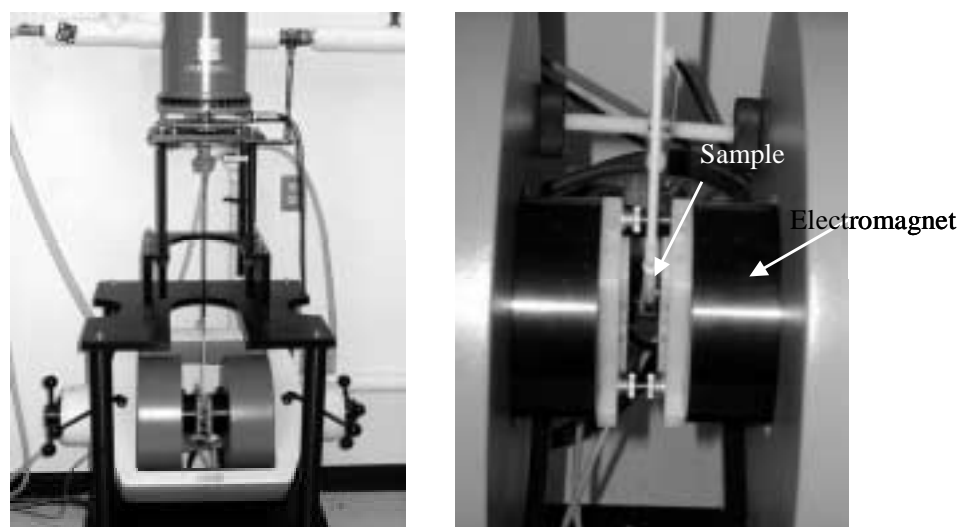


Figure 5.3 Vibrating sample magnetometer (VSM) used for measuring magnetic properties of cobalt dispersions.

5.3.2 *Determination of the cobalt concentrations in the dispersions*

Cobalt content in the dispersions was determined by Desert Analytics, Tucson, AZ, using an Inductively Coupled Plasma (ICP) technique. The measurements were performed by first weighing the sample and treating it with concentrated HNO₃, followed by perchloric acid until the sample was completely dissolved. The sample solution was made up to the specific volume, then ICP was used to determine the cobalt contents. These measurements were carried out along with a standard (a solution with a known cobalt concentration) and a blank solution to calculate quantitative amounts of cobalt in the samples.

5.4 Results and discussion

Silica-protected cobalt nanoparticle dispersions in PDMS fluids were prepared in three stages. First, magnetic cobalt nanoparticles were formed in pentablock terpolymer micelles. Secondly, alkoxy silanes were condensed in solution to form a “pseudo-silica” protective interlayer at the cobalt surface. Finally, the protected cobalt particles were transferred to PDMS carrier fluids with concurrent concentration of the cobalt as the reaction solvent was removed. Each block structure of the polysiloxane pentablock terpolymers fulfilled a separate function. The central “anchor” block containing nitrile groups coordinated to the cobalt nanoparticle surface. The PDMS “tail” blocks stabilized the cobalt nanoparticle dispersions by a steric (entropic) mechanism in PDMS carrier fluids. The trialkoxy silane-containing blocks served as precursors for condensing the silica interlayer surrounding the cobalt particles.

5.4.1 Synthesis of PDMS-PMVS-PCPMS-PMVS-PDMS pentablock terpolymers

The polysiloxane terpolymer stabilizers were synthesized by first conducting a redistribution polymerization of D₄CN to form a difunctional PCPMS macroinitiator (Figure 2). This was then used to initiate (from both ends) sequential living anionic polymerizations of D₃-vinyl, then D₃-Vinyl pendent groups on this terpolymer were then hydrosilylated with trialkoxysilanes to produce the final stabilizers containing the silica precursors. Pentablock terpolymers with 15000 g/mol PDMS, 2000 g/mol PCPMS, and systematically varied M_n's of PMVS blocks (1000, 2000 and 4000 g/mol) were prepared. Previous work discussed in chapter 3 and 4 had demonstrated that the 15000 g/mol PCPMS anchor and 2000 g/mol PDMS tail blocks could effectively stabilize nanocobalt. It is hypothesized that the size of the silica-precursor block should influence the oxygen permeability of the silica interlayer.

Difunctional PCPMS macroinitiators were prepared by equilibrating D₄CN, a cyclic nitrile containing siloxane tetramer, using LiOH as the basic initiator (Figure 5.2). The molecular weight of the polymer was controlled by using one mole of LiOH for every targeted mole of siloxanolate active species (i.e., two moles of LiOH per mole polymer). One mole of hydroxide reacted with the cyclic tetramer to yield an intermediate with one silanol endgroup and one siloxanolate endgroup. The second mole of hydroxide rapidly abstracted the silanol proton to yield the disiloxanolate chain and water. The reaction was carried out at 140 °C under an argon purge to quantitatively remove the H₂O by-product. The mixtures were initially opaque and became transparent within 2 h. Upon equilibration, gel permeation chromatography (GPC) indicated the expected equilibrium composition comprised of 73% linear polymers and 27% cyclic species.

After equilibration of the central PCPMS macroinitiator, D_3 -vinyl, along with THF as a reaction rate promoter, were added to grow the methylvinylsiloxane blocks (PMVS) from the macroinitiator termini in a living anionic polymerization. The D_3 -vinyl ring-opening reaction was monitored with 1H NMR by observing the disappearance of the three methyl resonances from the cyclic monomer centered at 0.23 ppm and the concurrent growth of the resonance peaks corresponding to the methyl protons on the linear methylvinylsiloxane blocks at 0.16 ppm (Figure 5.4). When the D_3 -vinyl conversion was at least 90% complete, a dichloromethane solution of D_3 , along with additional THF, were added to polymerize the PDMS endblocks. The D_3 ring-opening reaction was also monitored with 1H NMR by observing the disappearance of the methyl peak from the cyclic monomer at 0.16 ppm and the simultaneous growth of the methyl proton signal on the linear poly(dimethylsiloxane) structure at 0.06 ppm. The block terpolymers were terminated by adding trimethylchlorosilane when the D_3 monomer reached $\approx 85\%$ conversion. This “early” termination of the PDMS blocks was to avoid any backbiting or intermolecular chain-chain substitutions which might occur at extremely low monomer concentrations.

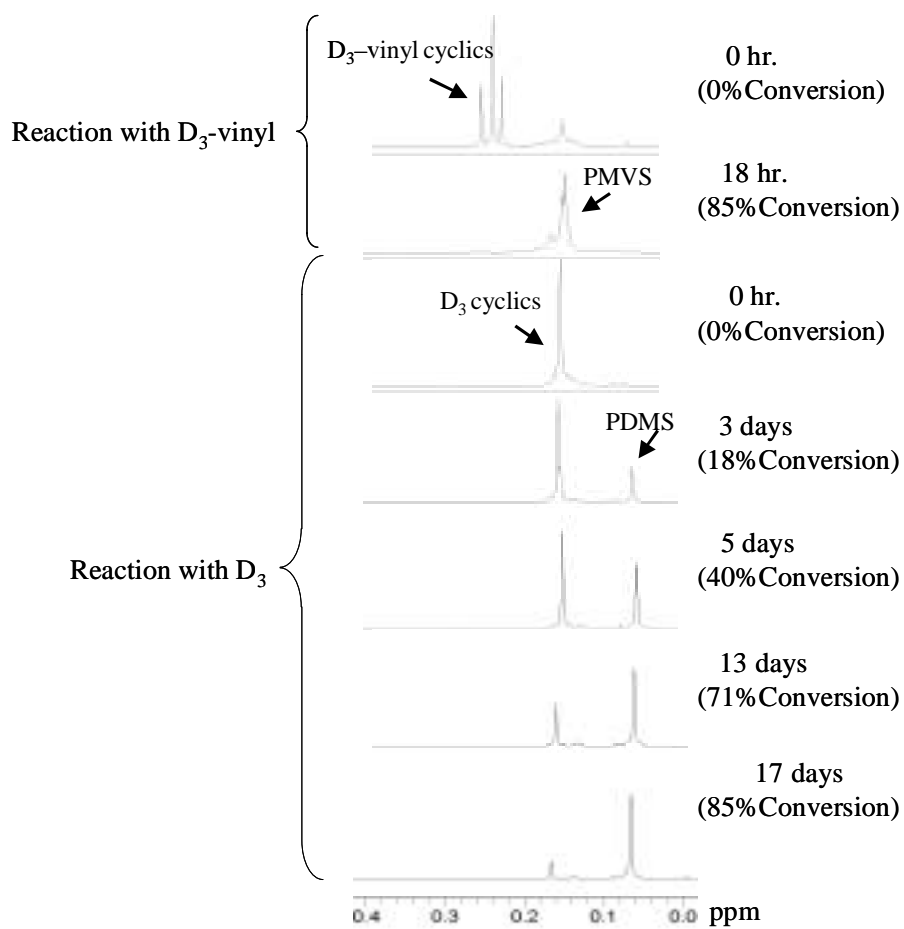


Figure 5.4 ^1H NMR used to monitor the progress of PMVS and PDMS block syntheses.

Block molecular weights and terpolymer compositions were calculated from a combination of titration and ^{29}Si NMR data. After equilibrating the central PCPMS block, the siloxanolate endgroups were titrated with HCl (in isopropanol) to obtain the number average molecular weight of that block. The known 27 wt. % concentration of cyclic species in these mixtures was taken into consideration in calculating molecular weights. The relative percentages of each block in the terpolymer were determined from ^{29}Si NMR by comparing the integrations from the silicon resonance of PDMS at -21.5 ppm and of PMVS at -34.5 ppm to the silicon resonance derived from the PCPMS units at -22.5 ppm (Figure 5.5). The relative block compositions, in combination with the central block molecular weights, enabled calculation of the number average molecular weights of the PMVS and PDMS endblocks. In all cases, the block molecular weights closely paralleled the targeted values.

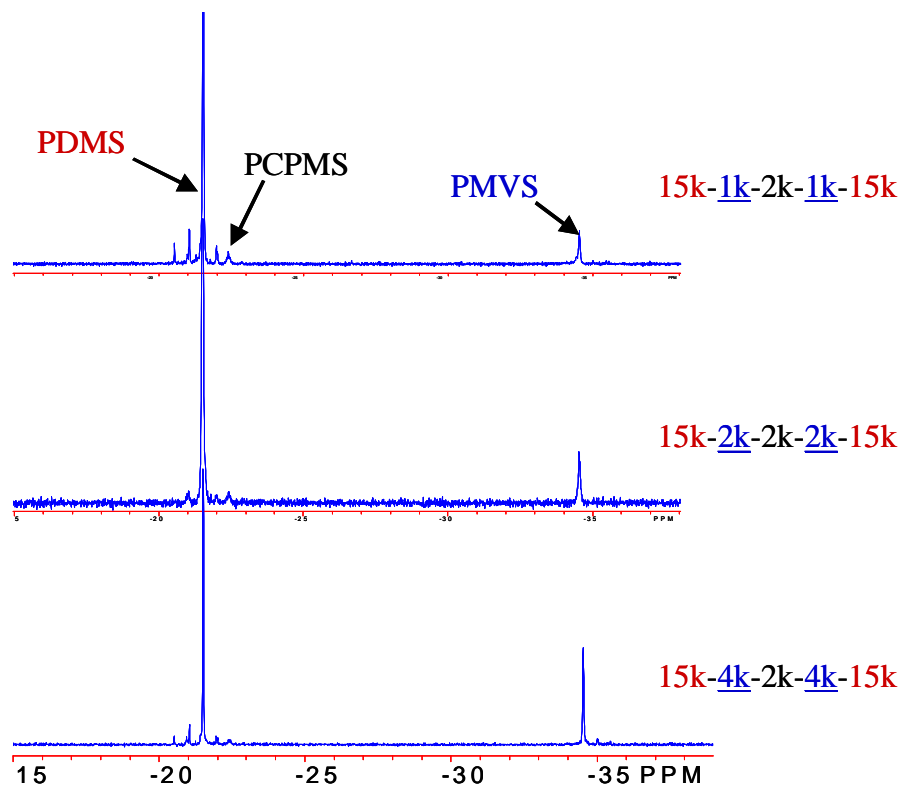


Figure 5.5 Silicon NMR showing the resonances of PDMS, PCPMS and PMVS blocks.

Differential scanning calorimetry (DSC) was used to investigate the microphase-separated morphologies of these block terpolymers. DSC thermograms indicated a T_g for the PDMS homopolymers at about $-127\text{ }^\circ\text{C}$ and a T_g for PMVS homopolymers at about $-133\text{ }^\circ\text{C}$ (Figure 5.6). Glass transition temperatures of PCPMS homopolymers are $\approx -65\text{ }^\circ\text{C}$. PDMS homopolymers, even at relatively low block molecular weights (e.g., 2000 g/mol) crystallize at $\approx -81\text{ }^\circ\text{C}$ (T_c) and have a characteristic melting peak (T_m) centered at $\approx -50\text{ }^\circ\text{C}$. By contrast, PMVS and PCPMS homopolymers are comprised of stereoisomeric mixtures and do not crystallize. The pentablock terpolymers containing 15000 g/mol PDMS tail blocks also crystallize as indicated by a presence of a T_m ($-43\text{ }^\circ\text{C}$) and a T_c ($-73\text{ }^\circ\text{C}$) (the bottom thermogram in Figure 5.5). The fact that the PDMS phase crystallizes also suggests a “microphase” phase separated morphology of the terpolymers. The glass transitions of the PMVS and PCPMS blocks in the terpolymers are ambiguous, probably due to their relatively short block lengths compared to those of PDMS. In addition, the T_g of the PCPMS phase (about $-65\text{ }^\circ\text{C}$) is hidden by the T_m of the PDMS phase ($-73\text{ }^\circ\text{C}$). The microphase separated nature of the bulk materials should allow the magnetic cobalt particles to be encapsulated in the minor PCPMS phase and for the PDMS endblocks to remain as a flexible steric stabilizer. The PMVS blocks serve as precursors for hydrosilylation reactions with trialkoxysilanes to form poly(methyltrialkoxysilane)siloxane blocks which are prepared prior to the cobalt dispersion reactions (Figure 5.2).

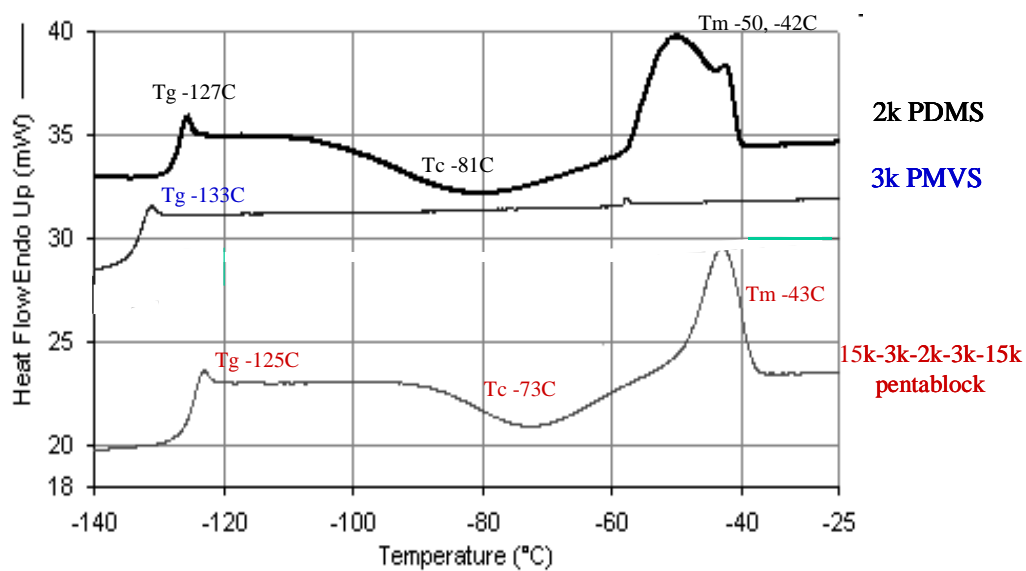


Figure 5.6 Differential scanning calorimetry (DCS) thermograms of PDMS homopolymers, PMVS homopolymers, and PDMS-PMVS-PCPMS-PMVS-PDMS pentablock terpolymers.

5.4.2 Synthesis of alkoxy silane-containing pentablock terpolymers

The final step in preparing the stabilizers was to add the trialkoxysilane functional groups to the vinylsiloxane blocks in a post polymerization reaction. Alkoxysilane-containing pentablock terpolymers were prepared via quantitative hydrosilylation of the pendent vinyl groups with stoichiometric concentrations of either triethoxysilane or trimethoxysilane. It was important that these reactions were conducted in a moisture-free atmosphere so that alkoxysilane functional groups did not condense prior to the cobalt dispersion reactions.

Reactions were investigated in both toluene and 2000 g/mol PDMS solvents in the presence of Karstedt's catalyst. One mole of triethoxysilane was used for every mole of vinylsilane repeat unit in the terpolymers. It is important that the hydrosilylation reaction is conducted in argon and in a moisture-free atmosphere so that the ethoxysilyl functional groups do not condense prior to the cobalt dispersion reactions. Proton NMR was used to monitor the progress of the reaction by observing the disappearance of the vinyl functional groups from the terpolymers and the Si-H groups from triethoxysilane (Figure 5.7). The reaction time required to completely remove vinyl and Si-H groups strongly depends on the molar concentration of the platinum catalyst in relation to the concentration of vinylsilane groups. For example, five days were required to achieve quantitative hydrosilylation in the reaction of 4000 g/mol PMVS where 0.004 moles of Pt per mole of vinyl were present. Only two days were required for completing a reaction with 1000 g/mol PMVS oligomers where the concentration of the platinum catalyst was 0.013 mol Pt per mole vinyl. All of these reactions were quantitative as evidenced by ^{29}Si NMR (Figure 5.8).

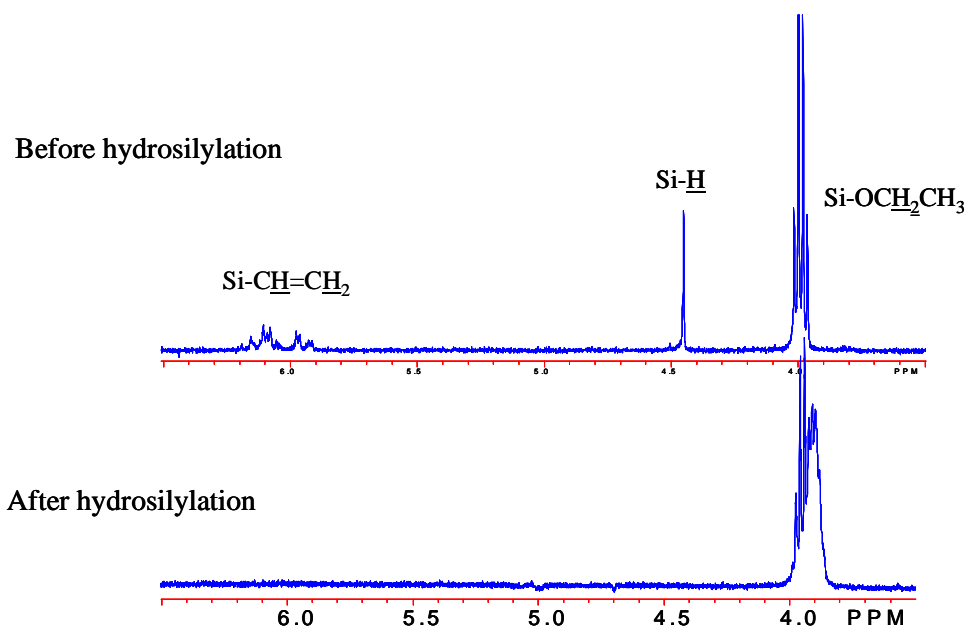


Figure 5.7 ^1H NMR showing the disappearance of vinyl and Si-H groups during hydrosilylation.

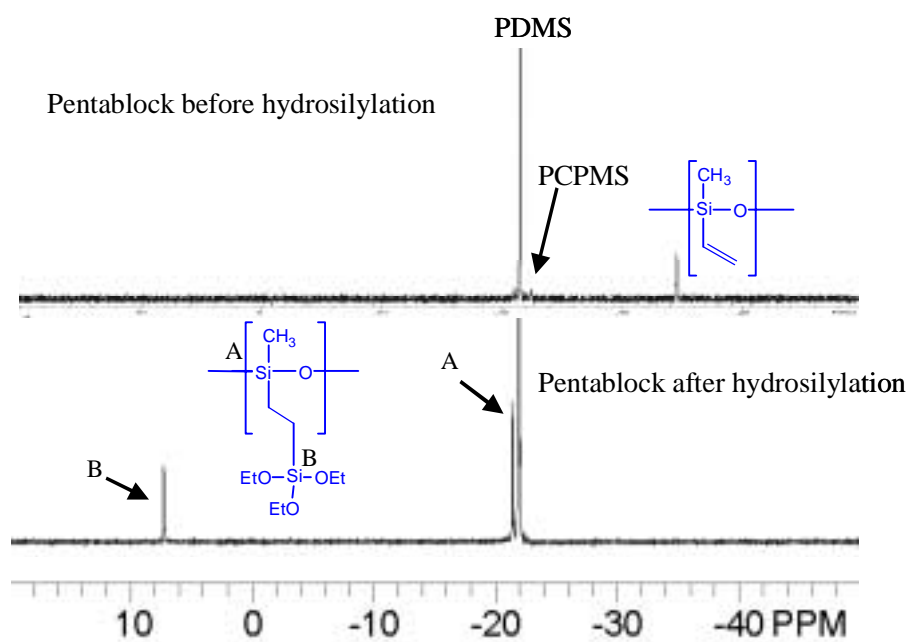


Figure 5.8 ^{29}Si NMR showing the formation of poly(triethoxysilylsiloxane) repeat units.

One alternative to using triethoxysilane to hydrosilylate the vinylsiloxane units in the terpolymers is to employ trimethoxysilane. It is well documented that methoxysilanes are more reactive in sol-gel reactions than ethoxysilanes under similar reaction conditions.²⁵⁷ This yields terpolymers containing alkoxy functional groups with higher reactivities so that they will more readily condense to form silica networks after the cobalt dispersion reactions.

5.4.3 Synthesis of cobalt nanoparticles by thermolysis of dicobalt octacarbonyl in micellar terpolymer solutions of alkoxy silane-containing pentablock terpolymers

One principle in the cobalt formation step was to design reaction conditions whereby the organocobalt precursor diffused into the core of block terpolymer micelles (formed by the stabilizer in solution) and reacted within that core. This yielded well-coated, non-aggregated cobalt nanoparticles. Alkoxy silane groups in the terpolymers were then condensed essentially to form silica shells around the particles and inhibit oxidation (Figure 5.9). It was important to conduct this step in a reaction medium that caused the silica-precursor blocks of the stabilizer to contract, tightly condense, and form a “pseudo-silica” thin film on the particle surface. The nature of the interaction between the blocks comprising the silica layer precursor with the solvent was considered important for achieving “tight” protective layers. It was reasoned that if these blocks extended into the solvent, inter-particle condensation rather than the desired intra-particle condensation might be enhanced.

²⁵⁷ M. Spinu, Dissertation, “Silicon-based organic and inorganic polymers”, Chemistry Department, Virginia Polytechnic Institute and State University, 1990.

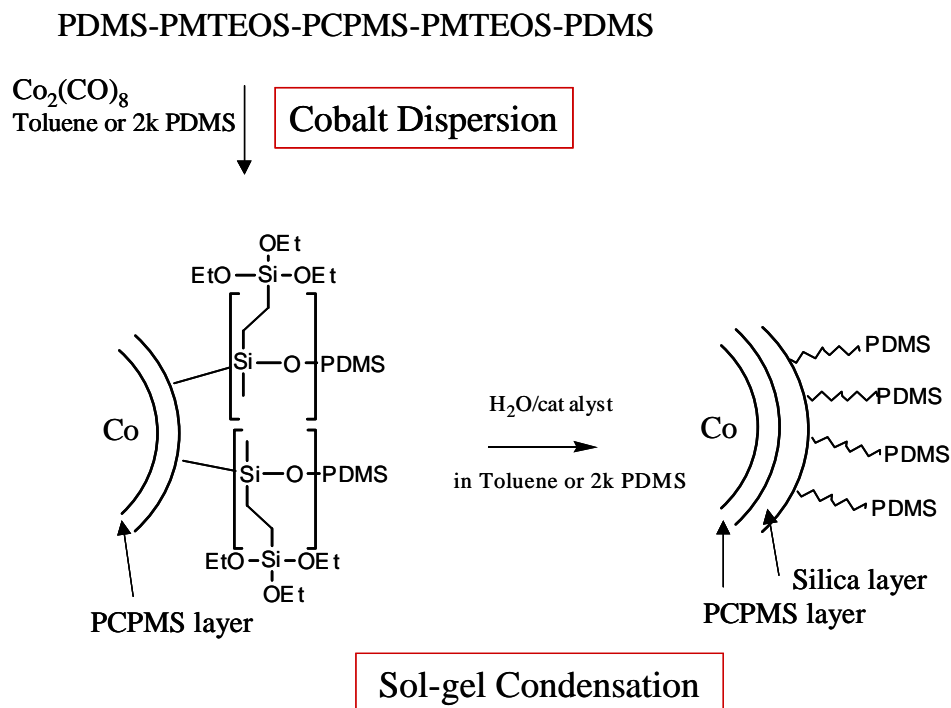


Figure 5.9 Methodologies for preparing silica-coated cobalt nanoparticles.

Toluene is a good solvent for PDMS but a poor solvent for PCPMS, particularly for higher molecular weight PCPMS oligomers. Both surface tension measurements and dynamic light scattering of toluene solutions of PDMS-PCPMS-PDMS triblock copolymers were discussed in chapter 4 and the results suggest the formation of micellar structures. It is thought that the pentablock terpolymers also form micellar solutions in toluene where the PCPMS is concentrated in the micelle cores and long PDMS tail blocks protrude into the medium to form the micelle coronas. Poly(methyltriethoxysilyl)siloxane (PMTEOS) blocks located between PDMS and PCPMS blocks can form silica layer around the particles.

The pentablock terpolymers are thought to form micellar structures in 2000 g/mol PDMS carrier fluids as well. Long PDMS tail blocks (15000 g/mol) form the micelle coronas since their chemical structures are identical to the carrier fluid, whereas PCPMS central blocks are more polar and form micelle cores in the non-polar PDMS.

Dicobalt octacarbonyl was reacted in the pentablock micellar solutions by a procedure similar to that discussed previously with PDMS-PCPMS-PDMS triblock copolymers. The mixtures were heated to evolve the carbon monoxide leaving groups and monitored by FTIR to observe their disappearance. These dispersion reactions in toluene took place more rapidly than in PDMS fluids, which may be caused by the absence of reflux conditions with the polymeric solvent. Both trimethoxysilane and triethoxysilane functional terpolymers were investigated. Stable dispersions formed in reactions using triethoxysilane-containing terpolymer steric stabilizers. Particles in the dispersions had an average particle diameter of ≈ 10 nm with relatively narrow size distribution (Figure 5.10). These cobalt dispersions were transparent, dark red-brown liquids. However, minimal aggregation was observed during the dispersion reactions when the terpolymers containing trimethoxysilanesiloxane units (PMTMOS) were used as steric stabilizers. This is probably due to prematurely reacted methoxysilane groups in the cobalt formation step, and these reactions resulted in unstable dispersions. This was attributed to the labile nature of the less sterically hindered silane.

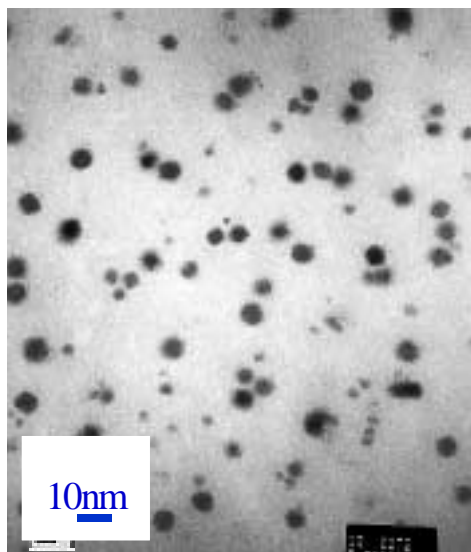


Figure 5.10 TEM image of a dispersion prepared in the presence of a pentablock steric stabilizer with triethoxysilyl-containing silica precursor blocks prepared in PDMS. The dispersion contains 10 nm particles with a relatively narrow size distribution.

5.4.4 Monitoring the sol-gel reaction conversion using reaction models

Oxidation of the cobalt nanoparticles yields antiferromagnetic cobalt oxide layers on their surfaces resulting in decreases in saturation magnetization. Silica networks typically prepared by sol-gel processes are well-known to have extremely low permeabilities to oxygen. Thus, the cobalt nanoparticles were coated with silica shells to protect their surfaces from environmental oxidation.

A wide variety of reaction parameters affect the kinetics and structures of the alkoxide-derived silica networks, e.g., type of alkoxide, type and concentration of solvent and catalyst, water concentration, polymer structure and concentration, and reaction temperature. Both acids and bases have been extensively used as catalysts for the reaction of silicon alkoxides in the sol-gel process. Both hydrolysis and condensation reactions are strongly affected by the presence of a catalyst. McGrath et al. have reported the studies of hydrolysis rate of TEOS in the presence of various concentrations of HCl catalyst ranging from 2.5×10^{-5} to 2.5×10^{-4} mol of HCl/Si-OEt.²⁵⁸ Higher catalyst concentrations produced higher percent conversion of hydrolysis. Yamane et al. found that hydrolysis of tetramethoxysilane (TMOS) occurred rapidly under acidic conditions as compared to the hydrolysis rate under basic conditions.²⁵⁹ This result was in good agreement with Brinker et al. for tetraethoxysilane (TEOS).²⁶⁰ The slower rate of reactions in basic condition allowed one to be able to control the reactions. Keefer showed that silicon alkoxide molecules produced highly crosslinked polymers in base-catalyzed sol-gel reaction, whereas low degrees of crosslinking were obtained when the reactions were conducted in acid-catalyzed solutions.²⁶¹

In addition to acid and base catalysts, the tin-catalyzed sol-gel reaction has also been of particular interest in recent years because of a need for effective catalyst under neutral conditions. Uilk et al. have successfully crosslinked the ethoxysilane oligomer, $(\text{SiO}(\text{OEt})_2)_n$, with $\text{HO}(\text{Me}_2\text{SiO})_n\text{H}$ in the presence of dibutyltin diacetate (DBTA) as a catalyst (6.3×10^{-3} mol

²⁵⁸ J. E. McGrath, J. P. Pullockaren, J. S. Riffle, S. Kilic, and C. S. Elsbernd, In *Ultrastructure processing of advanced ceramics*, J. D. Mackenzie, and D. R. Ulrich (Eds.), John Wiley & Sons, New York (1988)

²⁵⁹ M. Yamane, S. Inoue, A. Yasumari, *J. Non-Cryst. Solids*, **63**, 13 (1984)

²⁶⁰ C. J. Brinker, K. D. Keefer, D. W. Schaefer, T. A. Assink, B. D. Kay, C. S. Ashley, *J. Non-Cryst. Solids*, **63**, 45 (1984)

²⁶¹ K. D. Keefer, In *Better Ceramic Through Chemistry* C. J. Brinker, D. E. Clark, D. R. Ulrich (Eds.), Elsevier, New York, p15 (1984)

of Sn/Si-OEt ²⁶². Therefore, base and tin-catalyzed sol-gel reactions will be focused upon in this dissertation.

Following the dispersion reaction, trace amounts of water and a catalyst were employed in the cobalt dispersions to condense ethoxysilane groups in the terpolymers and essentially form silica networks around the particle surfaces. ¹H NMR spectroscopy was an effective technique to establish reaction parameters for model reactions (sol-gel reactions without cobalt particles). It was assumed that sol-gel reactions conducted in the cobalt dispersions were similar to the model reactions. The sol-gel reaction mechanism is illustrated in Figure 5.11 showing that the condensation requires at least one mole of water for every two moles of alkoxy silane.

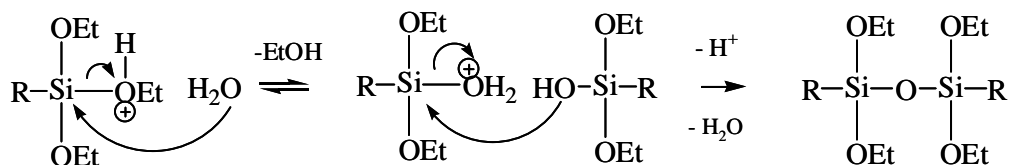


Figure 5.11 Sol-gel reaction mechanism.

To determine the reaction condition for sol-gel reaction, the terpolymers containing 15000 g/mol PDMS, 2000 g/mol PCPMS and 2000 g/mol PMTEOS (ethoxysilanes) or PMTMOS (methoxysilanes) in a solvent were used throughout the studies. Using ethoxysilane-containing terpolymers, the reactions were performed in either 2000 g/mol PDMS carrier fluids

²⁶² J. Uilk, S Bullock, E. Johnston, S. A. Myers, L. Merwin, and K. J. Wynne, *Macromolecules*, **33**, 8791 (2000)

or toluene as solvents. When the reactions were conducted in 2000 g/mol PDMS, 1 g of the terpolymers were dissolved in 20 mL of the carrier fluid. Two sol-gel catalysts, NH_4OH base catalyst and dibutyltin diacetate (DBTA), and a series of water concentrations (water/ethoxysilane molar ratios ranging from 1:2 to 10:1 molar ratio of $\text{H}_2\text{O}:\equiv\text{Si-OEt}$) were investigated. The minimum amounts of catalyst and water that yield highest reaction conversion were desirable. When the reactions were performed in toluene, 1 g of the terpolymers was dissolved in either 80 or 160 mL of the solvent, and the reaction conditions that yielded the highest reaction conversion investigated in 2000 g/mol PDMS (amounts of water and catalyst) were used for the reactions in toluene.

For the reactions using methoxysilane-containing terpolymers in 2000 g/mol PDMS, 1 g of the terpolymers was dissolved in 20 mL of the carrier fluid. Because methoxysilanes are significantly more reactive than ethoxysilanes, the reaction was conducted to investigate the reaction progress without an addition of water and a catalyst. The minimum 1:2 molar ratio of $\text{H}_2\text{O}:\equiv\text{Si-OMe}$ was used in this study. In addition, for the reaction using a catalyst, two alternative catalysts were used to accelerate the reaction rate: NH_4OH (1:1 molar ratio of $\text{NH}_4\text{OH}:\text{H}_2\text{O}$) and dibutyltin diacetate catalysts (0.1 wt% DBTA).

For the reactions using methoxysilane-containing terpolymers in toluene, 1 g of the terpolymers was dissolved in 80 or 160 mL of the solvent. The minimum 1:2 molar ratio of $\text{H}_2\text{O}:\equiv\text{Si-OMe}$ and 0.1 wt% DBTA catalyst was used.

5.4.4.1 Sol-gel reaction models using ethoxysilane-containing pentablock terpolymers

A series of model reactions with systematically varied reaction conditions were conducted in 2000 g/mol PDMS or toluene as the solvent. ^1H NMR was used to monitor the reaction progress by observing the disappearance of methylene protons in ethoxysilane ($\equiv\text{Si}-\text{OCH}_2\text{CH}_3$) at $\delta = 3.90$ ppm along with the corresponding appearance of methylene protons in ethanol ($\text{CH}_3\text{CH}_2\text{OH}$) at $\delta = 3.75$ ppm (Figure 5.12). Aliquots were removed from the reaction at desired time intervals for NMR analyses. An exemplary graph depicting the percentages of $\equiv\text{Si}-\text{OEt}$ remaining in the terpolymers against reaction time (days) is illustrated in Figure 5.13 and 5.15. Decreases in the integrals of the methylene protons in $\equiv\text{Si}-\text{OEt}$ relative to a reference peak (from the DBTA catalyst) were used to determine the percentage of $\equiv\text{Si}-\text{OEt}$ remaining at a certain reaction time. A series of reactions in PDMS were conducted to investigate reaction conditions that yielded high reaction conversions (Figure 5.13). The concentrations of terpolymers (1 g of 15k-2k-2k-2k-15k of PDMS-PMTEOS-PCPMS-PMTEOS-PDMS) and carrier fluids (20 mL of 2000 g/mol PDMS) were held constant while other reaction parameters were varied.

Two sol-gel catalysts, NH_4OH and dibutyltin diacetate (DBTA), and a series of water concentrations were investigated. The DBTA concentrations, which were similar to those reported earlier for silica formation,²⁶² ranged from 7.7×10^{-3} to 0.387 mol of tin per mole of ethoxy group (0.05 to 2.5 weight percent DBTA). All of the reactions conducted with DBTA resulted in >90% conversion of ethoxysilane, whereas even high molar concentrations of ammonium hydroxide (1 OH per 1 ethoxy) resulted in low conversions ($\approx 50\%$). This is probably due to immisibility of the catalyst (NH_4OH) in the solution phase (PDMS). Decreasing in the molar ratio of NH_4OH per ethoxysilane yielded similar results. In contrast, DBTA catalyst was

immediately soluble in the reaction solution once introduced. This can take an advantage over using NH_4OH as a catalyst by increasing the efficiency of the catalyst in the reaction solution. As expected, lower DBTA concentrations required longer times to reach equilibrium. It should be noted that all of these reactions were conducted at low temperatures (25°C) to minimize any cobalt surface oxidation during the sol-gel stage. High ethoxysilane conversions were achieved even with the minimum, stoichiometric concentrations of water (i.e., 1 mole water per 2 moles ethoxy) (Figure 5.13). Thus, all further reactions were conducted with this minimum required water concentration to avoid any aggregation caused by water.

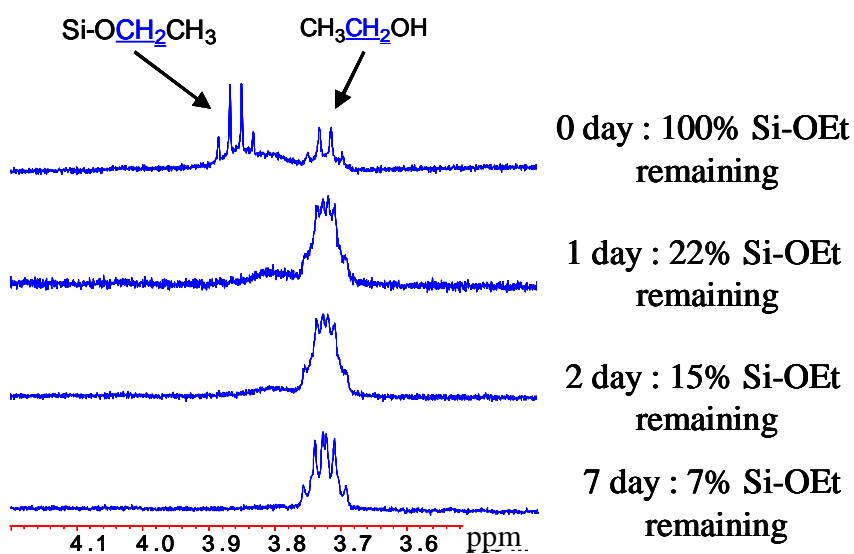


Figure 5.12 Typical ^1H NMR spectra showing the progress of the sol-gel reaction in 2000 g/mol PDMS as the reaction solvent. The reaction was conducted in the presence of a PDMS-PMTEOS-PCPMS-PMTEOS-PDMS pentablock terpolymer which had a 2000 g/mole poly(methylvinylsiloxane) precursor hydrosilylated with triethoxysilyl groups, and with 0.1 wt % DBTA and a stoichiometric, 1:2 molar ratio of $\text{H}_2\text{O}:\equiv\text{Si-OEt}$.

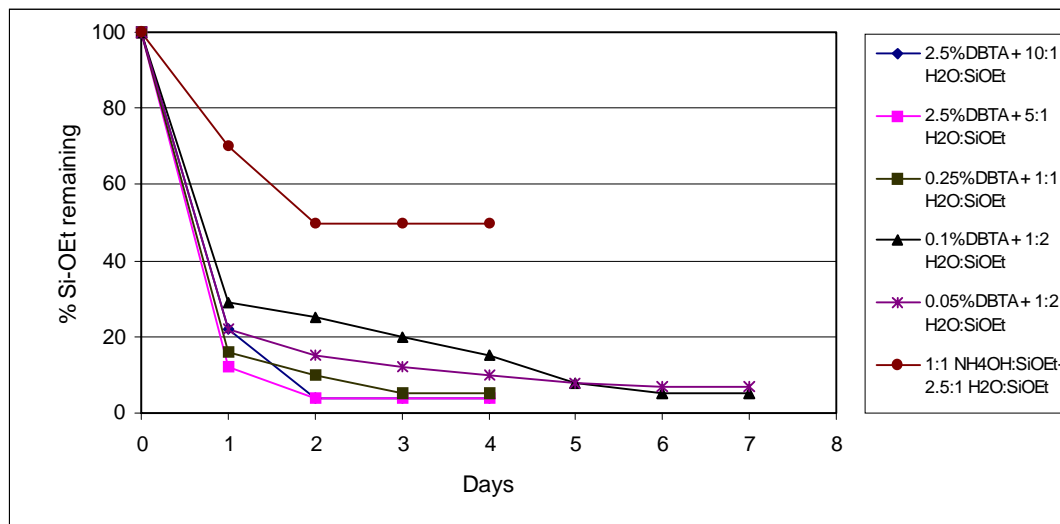


Figure 5.13 Monitoring %≡Si-OEt remaining (100%-%conversion) during sol-gel reaction using 1 g of a 15000 g/mol PDMS-2000 g/mole PMTEOS-2000 g/mol PCPMS-2000 g/mol PMTEOS-15000 g/mol PDMS terpolymer in 20 mL of 2000 g/mol PDMS.

Model cobalt dispersion reactions were conducted in toluene at various terpolymer concentrations. A potential advantage of using toluene as a reaction medium over 2000 g/mol PDMS is that the cobalt dispersions can be conducted in dilute conditions, then toluene can be easily removed and replaced with a desired amount of a carrier fluid. It was reasoned that this might allow dispersions to be obtained with higher concentrations of cobalt, and hence, with higher magnetic responses. Reaction conditions were investigated in dilute (1 g of a 15k-2k-2k-2k-15k PDMS-PMTEOS-PCPMS-PMTEOS-PDMS terpolymer in 160 mL toluene) and concentrated (1 g of a 15k-2k-2k-2k-15k PDMS-PMTEOS-PCPMS-PMTEOS-PDMS terpolymer in 80 mL toluene) solutions. The concentration of DBTA was adjusted to 0.1 wt % of the total solution and the molar ratio of $\text{H}_2\text{O}:\equiv\text{Si-OEt}$ was held constant at 1:2. Typical ^1H NMR spectra of the reactions performed in toluene are illustrated in Figure 5.14. As expected, the reaction conducted at the higher molar amount of DBTA per ethoxysilyl groups (the more dilute condition) reacted faster. Interestingly, it also proceeded to higher conversion (Figure 5.15). It is thought that the ethoxysilane-derived gel might have a better-defined structure (more densely packed) under these more dilute conditions.

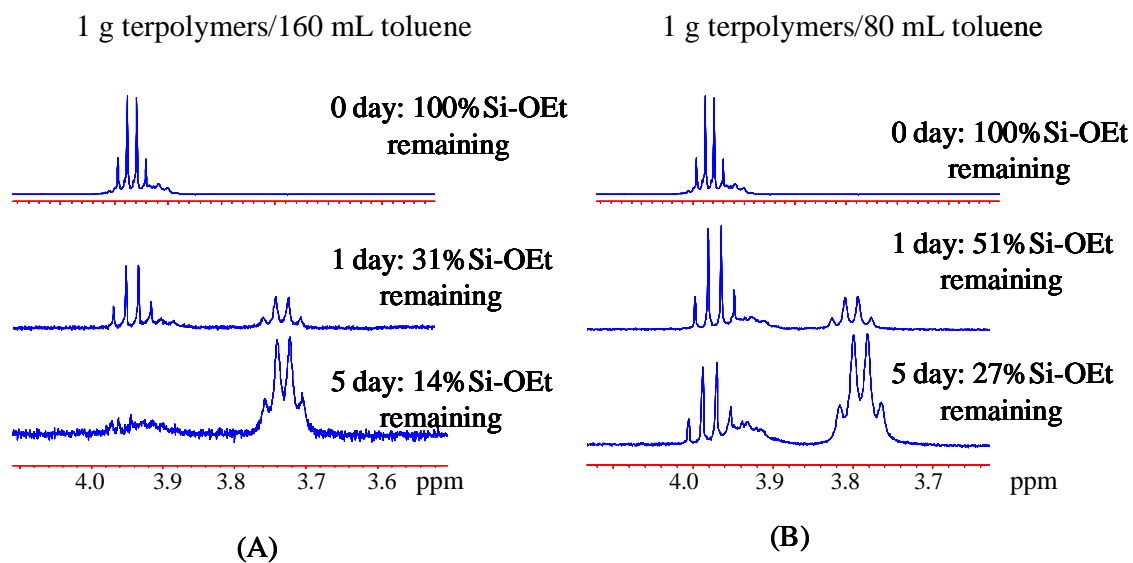


Figure 5.14 Typical ^1H NMR spectra performed in toluene solvent showing the reaction progress of sol-gel reactions. The reaction was performed in the presence of 15k-2k-2k-2k-15k PDMS-PMTEOS-PCPMS-PMTEOS-PDMS pentablock terpolymers with 0.1 wt% DBTA and 1:2 molar ratio of $\text{H}_2\text{O}:\equiv\text{Si-OEt}$ in (A) 160 mL toluene, and (B) 80 mL toluene.

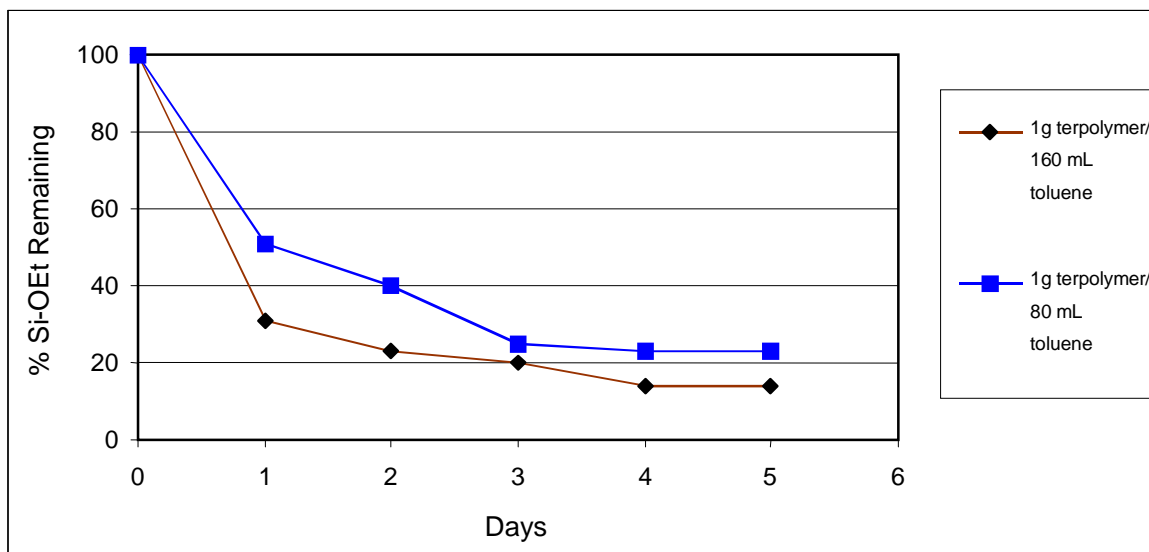


Figure 5.15 Monitoring % \equiv Si-OEt remaining (100%-%conversion) of the sol-gel reaction using 1 g of 15k-2k-2k-15k PDMS-PMTEOS-PCPMS-PMTEOS-PDMS terpolymers in 80 and 160 mL of toluene, 0.1 wt% DBTA and 1:2 molar ratio of $H_2O:\equiv$ Si-OEt.

5.4.4.2 Sol-gel reaction models using methoxysilane-containing pentablock terpolymers

A series of reactions with various reaction conditions were performed in PDMS carrier fluids and toluene as solvents. The disappearance of the methyl protons from methoxysilane ($\equiv\text{Si-OCH}_3$) at $\delta = 3.60$ ppm and the appearance of methyl protons on methanol (CH_3OH) at $\delta = 3.50$ ppm (Figure 5.16 and Figure 5.18) were monitored via ^1H NMR. Plots of % $\equiv\text{Si-OMe}$ remaining in the terpolymers against reaction time (days) are illustrated in Figure 5.17 and 5.19. Similarly to the condensation of $\equiv\text{Si-OEt}$, a decrease of the integral of methyl protons in $\equiv\text{Si-OMe}$ relative to a reference peak (from DBTA catalyst) was used to determine % $\equiv\text{Si-OMe}$ remaining at various reaction times. In the case of no catalyst used in the reaction, the xylene peak (around 2.3 ppm) remaining from Karstedt's catalyst from the hydrosilylation step was used as a reference peak.

It is well known that methoxysilanes are highly reactive species for condensation reactions compared to ethoxysilane species. In addition, it has also been reported that methoxysilanes are able to condense and form silica networks in the presence of trace water without a catalyst (neutral solution).²⁶³ A series of sol-gel reactions with various reaction conditions were performed using 1 g of 15k-2k-2k-2k-15k PDMS-PMTMOS-PCPMS-PMTMOS-PDMS terpolymers in 20 mL of PDMS carrier fluids. The reaction progress was monitored via ^1H NMR (Figure 5.16). These reactions were carried out in the condition with/without water and with/without a catalyst. 1:2 Molar ratio of $\text{H}_2\text{O}:\equiv\text{Si-OMe}$ was used with water and 0.1 wt% DBTA or 2:1 molar ratio of $\text{H}_2\text{O}:\text{NH}_4\text{OH}$ was used in the reaction with a catalyst. As shown in Figure 5.17, one appears to establish various equilibria in various reaction conditions. Apparently, DBTA produced a high degree of sol-gel condensation. In contrast, the

²⁶³ M. Spinu, Dissertation, "Silicon-based organic and inorganic polymers", Chemistry Department, Virginia Tech, 1990.

condensation barely proceeded for the condition without water and a catalyst (94% \equiv Si-OMe remaining after 5 days of the coating process).

The reaction models using toluene as a solvent were also investigated using methoxy-containing terpolymers in various terpolymer concentrations. The reactions were performed in dilute (1 g of 15k-2k-2k-2k-15k PDMS-PMTMOS-PCPMS-PMTMOS-PDMS terpolymers in 160 mL toluene) and concentrated (15k-2k-2k-2k-15k PDMS-PMTMOS-PCPMS-PMTMOS-PDMS terpolymers in 80 mL toluene) conditions using 0.1 wt% DBTA and 1:2 of H₂O: \equiv Si-OMe molar ratio. Typical ¹H NMR spectra of the reactions performed in toluene are illustrated in Figure 5.18. In good agreement with the results obtained in \equiv Si-OEt species, the reaction performed in a dilute condition shows a faster reaction rate and a lower % \equiv Si-OMe remaining (higher %conversion) than those in a concentrated condition (Figure 5.19).

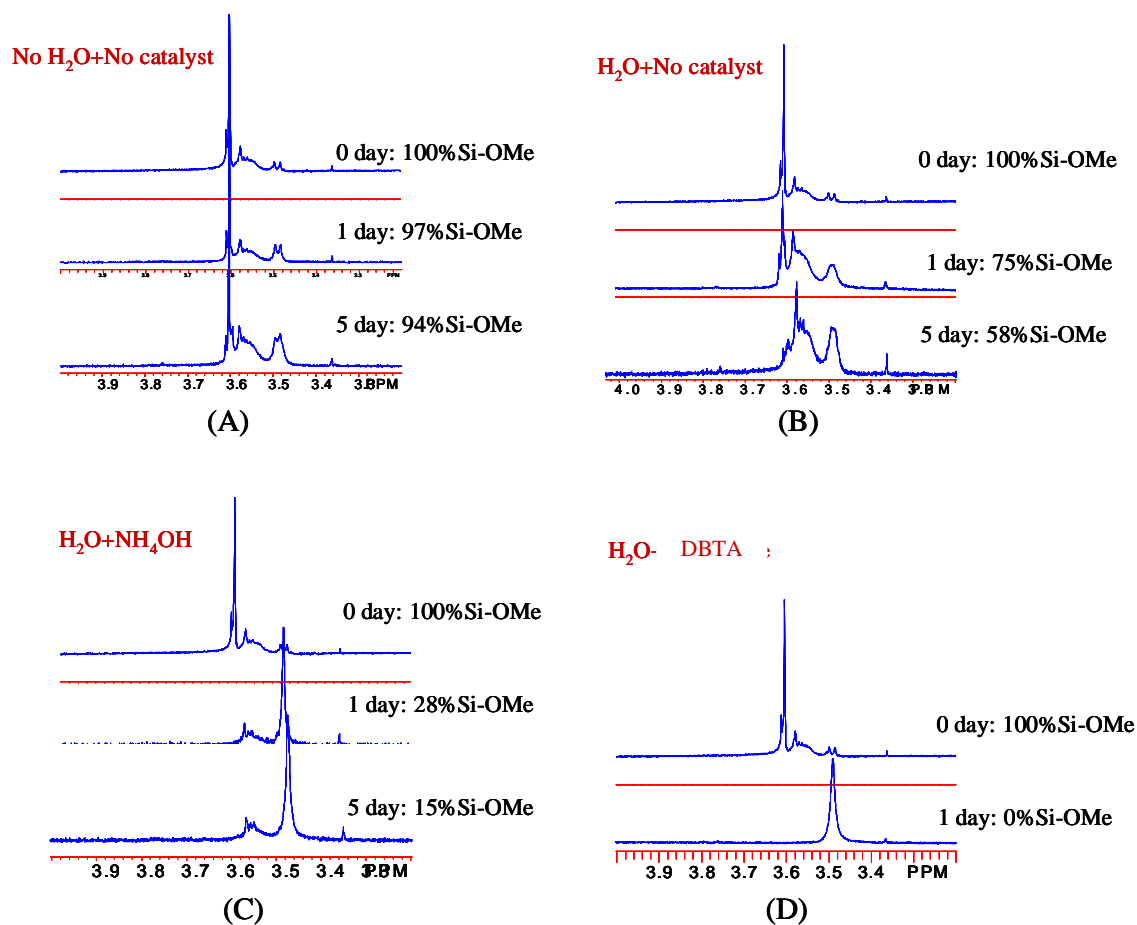


Figure 5.16 Typical ^1H NMR spectra performed in 2000 g/mol PDMS showing the reaction progress of a sol-gel reaction. The reaction was performed in the presence of 15k-2k-2k-15k PDMS-PMTMOS-PCPMS-PMTMOS-PDMS pentablock terpolymers, (A) without H_2O and catalyst, (B) with 1:2 molar ratio of $\text{H}_2\text{O}:\equiv\text{Si-OMe}$ and without catalyst, (C) with 1:2 molar ratio of $\text{H}_2\text{O}:\equiv\text{Si-OMe}$ and 1:1 molar ratio of $\text{NH}_4\text{OH}:\text{H}_2\text{O}$, and (D) with 1:2 molar ratio of $\text{H}_2\text{O}:\equiv\text{Si-OMe}$ and 0.1wt% DBTA catalyst.

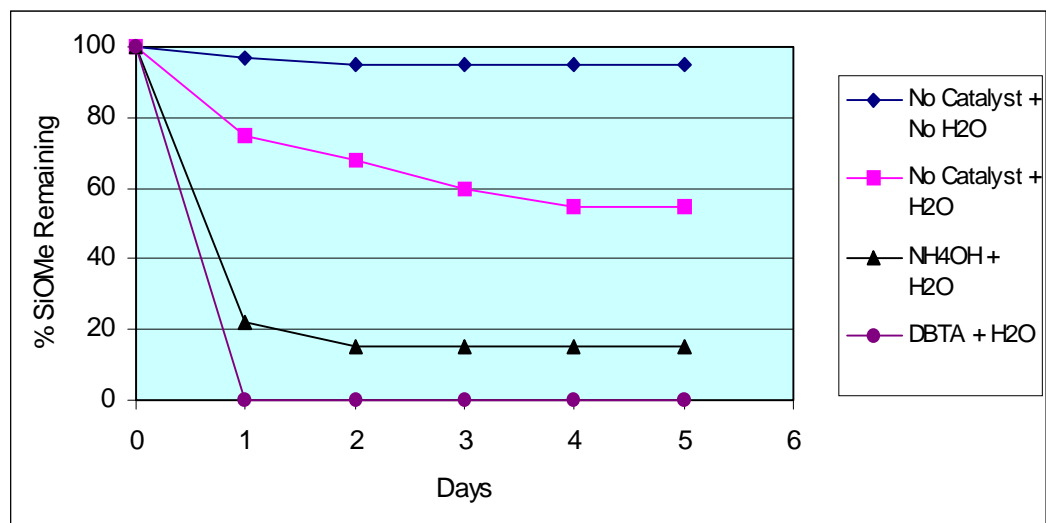


Figure 5.17 Monitoring % \equiv Si-OMe remaining (100%-%conversion) of the sol-gel reaction using 1 g of 15k-2k-2k-2k-15k PDMS-PMTMOS-PCPMS-PMTMOS-PDMS terpolymers in 20 mL of 2000 g/mol PDMS.

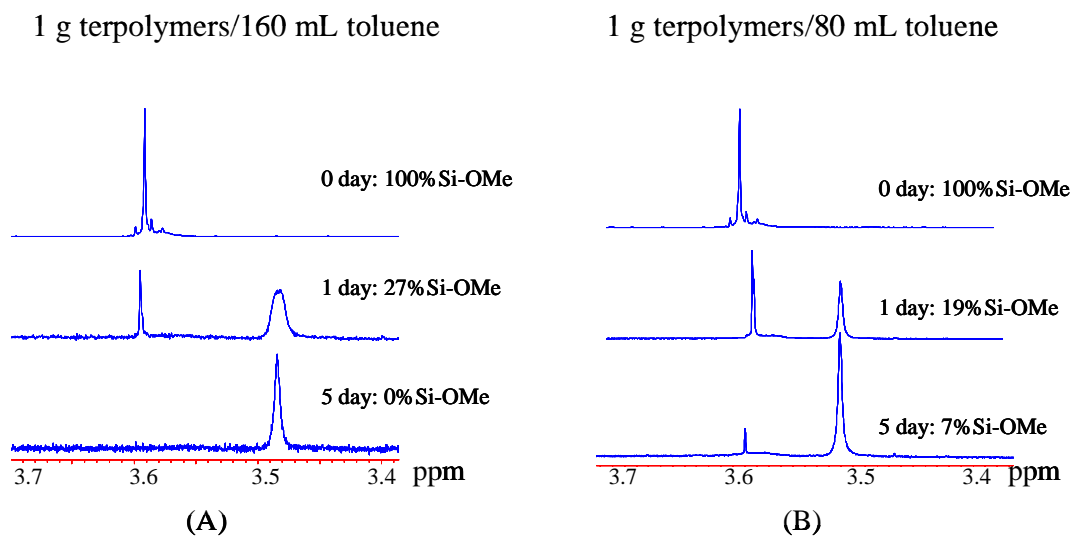


Figure 5.18 Typical ^1H NMR spectra performed in toluene solvent showing the reaction progress of sol-gel reactions. The reaction was performed in the presence of 15k-2k-2k-2k-15k PDMS-PMTMOS-PCPMS-PMTMOS-PDMS pentablock terpolymers with 0.1 wt% DBTA and 1:2 molar ratio of $\text{H}_2\text{O}:\equiv\text{Si-OMe}$ in (A) 160 mL toluene, and (B) 80 mL toluene.

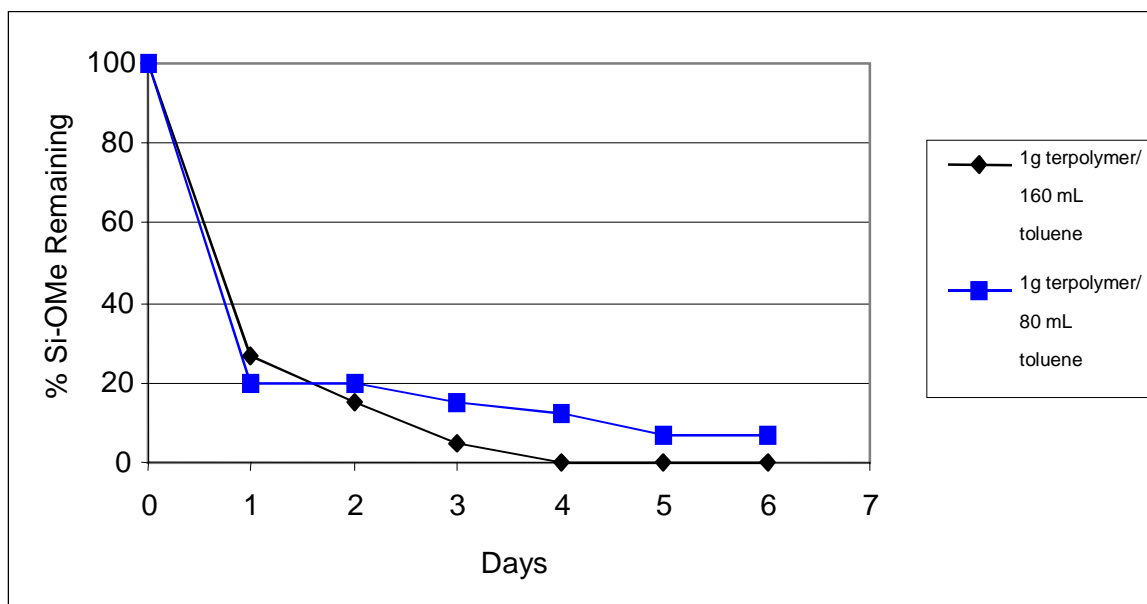


Figure 5.19 Monitoring % \equiv Si-OMe remaining (100%-conversion) of the sol-gel reaction using 1 g of 15k-2k-2k-2k-15k PDMS-PMTMOS-PCPMS-PMTMOS-PDMS terpolymers in 80 and 160 mL of toluene, 0.1 wt% DBTA and 1:2 molar ratio of $\text{H}_2\text{O}:\equiv\text{Si-OMe}$.

Based on results of the model studies, the silica coating reactions around the cobalt particles were investigated with 1 g of terpolymer in 20 mL of PDMS fluid and in 160 mL toluene in the presence of 0.1 wt% DBTA and a 1:2 molar ratio of $\text{H}_2\text{O}:\equiv\text{Si-OEt}$ or $\equiv\text{Si-OMe}$.

5.4.5 Preparation of silica-coated cobalt nanoparticles in 2000 g/mol PDMS carrier fluids

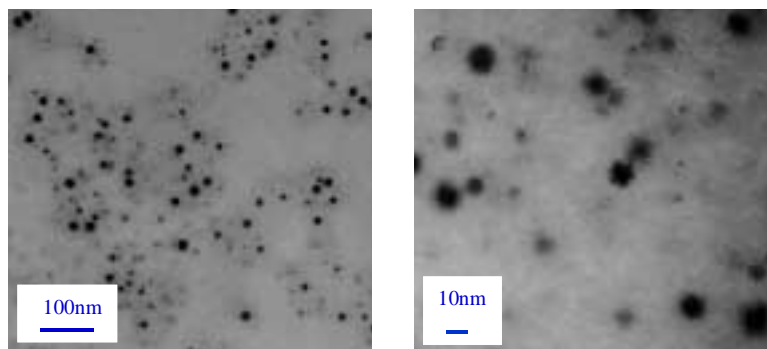
The appropriate conditions determined using the reaction models discussed in the previous section were employed in the cobalt dispersions. Because the cobalt dispersion reaction was conducted using 1 g $\text{Co}_2(\text{CO})_8$ and 1 g terpolymers in 20 mL toluene, another 140 mL of toluene was added to the terpolymer-toluene solution before the sol-gel reaction to bring the reaction volume to 160 mL. When the dispersion reaction was performed in PDMS carrier fluids, no additional PDMS was needed. Once appropriate amounts of water and DBTA were introduced into the cobalt dispersions, they were constantly stirred under argon for one week.

5.4.5.1 Preparation of silica-coated cobalt nanoparticles using ethoxysilane-containing pentablock terpolymers

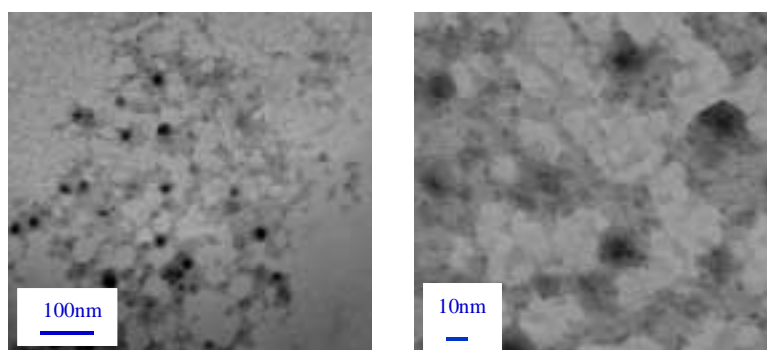
According to TEM images, stable cobalt dispersions after the sol-gel process were obtained when ethoxy-containing terpolymers were used (Figure 5.20A). For the reaction performed in toluene, the reaction solvent was removed and replaced with 2000 g/mol PDMS to obtain cobalt dispersions in biocompatible carrier fluids. The reactions were diluted with 20 mL PDMS and toluene was then removed under reduced pressure. The dispersions yielded approximately 1.6% cobalt concentration in PDMS after removing toluene. However, the dispersions formed gel products after adding PDMS and removing toluene (Figure 5.21A). It is rationalized that ethoxysilanes attached on the surface of one particle might condense with ethoxysilanes on other particles, leading to interparticle crosslinking. Preparation of silica-coated particles in extremely dilute conditions in toluene might diminish or eliminate this problem. In addition, preparation of silica-coated particles in less polar solvents, e.g., cyclohexane, might contract the polar ethoxysilanes to the particle surface and coat each particle

individually. Preparation of the cobalt particles with a well-defined coating will be a subject of further study.

The silica-coated cobalt dispersions prepared in PDMS (1 g $\text{Co}_2(\text{CO})_8$, 1 g terpolymer in 20 mL PDMS) contained approximately 1.6%Co. The dispersions appeared as fluids without any aggregation observed upon coating for one week (Figure 5.21B). Transmission electron microscopy (TEM) showed silica-coated cobalt particles with some interparticle crosslinking (Figure 5.20B). These liquid dispersions were used for further studies of their magnetic properties compared with those of the uncoated samples.



(A)



(B)

Figure 5.20 Transmission electron microscopy (TEM) of cobalt dispersions prepared by using ethoxy-containing terpolymers in 2000 g/mol PDMS: A) before, and B) after silica coatings.



Figure 5.21 A cobalt dispersion prepared by using ethoxy-containing terpolymers in, (A) toluene, and (B) 2000 g/mol PDMS. The image (A) was taken after adding 2000g/mol PDMS and removing toluene.

5.4.5.2 Preparation of silica-coated cobalt nanoparticles using methoxysilane-containing pentablock terpolymers

It should be noted again that when the methoxysilane-containing terpolymers (PMTMOS) were used as steric stabilizers, some aggregation was observed during the cobalt dispersion reaction regardless of the solvents used. More aggregation was observed when this dispersion was subjected to the sol-gel reaction (Figure 5.22). This is probably due to interparticle crosslinking of highly reactive methoxysilanes in fairly concentrated conditions (1 g terpolymer/20 mL PDMS or 1 g terpolymer/160 mL toluene), allowing the particles to agglomerate to each other. Preparing the cobalt dispersion and conducting the sol-gel reaction in a more dilute condition and different solvents are promising areas for considerable future effort.

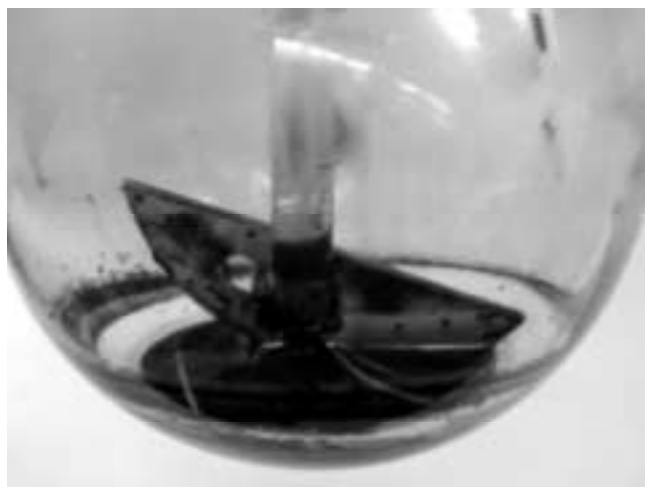


Figure 5.22 Macroscopic aggregation observed when the silica-coated cobalt dispersion reaction was performed in the presence of methoxy-containing pentablock terpolymers.

The conditions and results in sol-gel reactions are summarized in Table 5.4. The cobalt dispersions ($\approx 1.6\%$ Co) containing silica-coated particles prepared in various terpolymer stabilizers in 2000 g/mol PDMS (second entry in Table 5.4) were used for further studies of their magnetic properties compared with those of the uncoated samples.

Table 5.4 Summary of silica-coated cobalt nanoparticles prepared via sol-gel process.

Alkoxy silane group in the Copolymers	Solvent	Co ₂ (CO) ₈	DBTA	H ₂ O:SiOR (molar ratio)	Results
-SiOEt (1g)	160 ml Toluene	1 g	0.1wt%	1:2	Forms stable cobalt dispersions. Gel product after adding PDMS and removing toluene.
-SiOEt (1g)	20 ml PDMS	1 g	0.1wt%	1:2	Forms stable cobalt dispersions. Liquid product.
-SiOMe (1g)	160 ml Toluene	1 g	0.1 wt%	1:2	Minimal aggregation during the cobalt reaction. More aggregation during sol-gel reaction
-SiOMe (1g)	20 ml PDMS	1 g	0.1 wt%	1:2	Minimal aggregation during the cobalt reaction. More aggregation during sol-gel reaction

5.4.6 Magnetic properties of the cobalt nanoparticle dispersions

The dispersions prepared with three different pentablock terpolymers containing 1%Co in 2000 g/mol PDMS were used for studying magnetic properties. The measured magnetic hysteresis curves of the dispersions during sol-gel reaction under argon atmosphere are shown in Figures 5.23, 5.24, and 5.25. The magnetic moments or magnetizations measured via Vibrating Sample Magnetometer (VSM) were normalized with the weight of the samples and %Co in the dispersions to obtain emu/g Co in y-axis. Quantitative %Co determined via the ICP technique is shown in Table 5.5. The average cobalt concentration of each reaction was used to normalize the magnetization values.

Magnetic hysteresis curves showed that the specific saturation magnetization decreased about 10-15% within the first two days of coating (Figure 5.23, 5.24, and 5.25). Saturated magnetic hysteresis curves after 5 and 7 days of coating were superimposed on or insignificantly lower than those after 2 days of coating, indicating that the reduction in saturation magnetization occurs only at the beginning of the coating process. The specific saturation magnetizations

before coating (0 day) of the dispersion prepared in 15k-1k-2k-1k-15k and 15k-4k-2k-4k-15k terpolymers were somewhat lower than those of 15k-2k-2k-2k-15k terpolymers. This is probably due to partial oxidation of the cobalt particles during the dispersion preparation. It should be noted that the hysteresis curve of the dispersion before coating (0 day) of the dispersion in Figure 5.24 (using 15k-2k-2k-2k-15k terpolymers) appeared to be overlaid with those of the dispersion prepared in 15k-2k-15k PDMS-PCPMS-PDMS triblock copolymers. The dispersion prepared in the presence of the triblock copolymers has been discussed in the previous chapter. The magnetic properties over time of the dispersion prepared in triblock copolymers was also investigated overtime to compare the findings with those of the dispersion prepared in pentablock terpolymers.

Table 5.5 Quantitative %cobalt in dispersions prepared in 2000 g/mol PDMS using various pentablock terpolymers. These dispersions were targeted at 1 wt% Co in PDMS.

Copolymers	Days of coating	wt% Cobalt*	Ave.%Cobalt
15k- <u>1k</u> -2k- <u>1k</u> -15k	0	1.00	0.97 ± 0.03
	2	0.99	
	5	0.94	
	7	0.96	
15k- <u>2k</u> -2k- <u>2k</u> -15k	0	0.89	0.82 ± 0.17
	2	1.00	
	5	0.71	
	7	0.62	
15k- <u>4k</u> -2k- <u>4k</u> -15k	0	0.90	0.81 ± 0.10
	2	0.78	
	5	0.88	
	7	0.69	

* Each value contains 1.3% error.

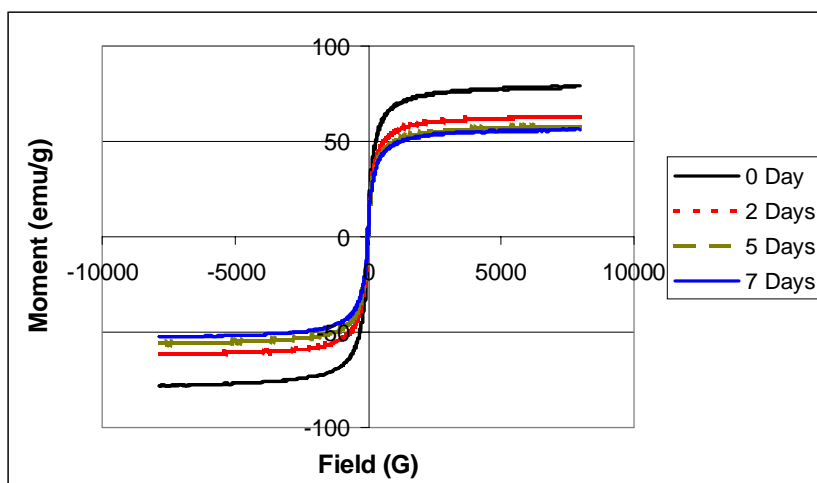


Figure 5.23 The magnetization curves of the dispersion during sol-gel reaction: the dispersion was performed using 1 g of 15k-1k-2k-1k-15k PDMS-PMTEOS-PCPMS-PMTEOS-PDMS terpolymers in 2000 g/mol PDMS carrier fluids.

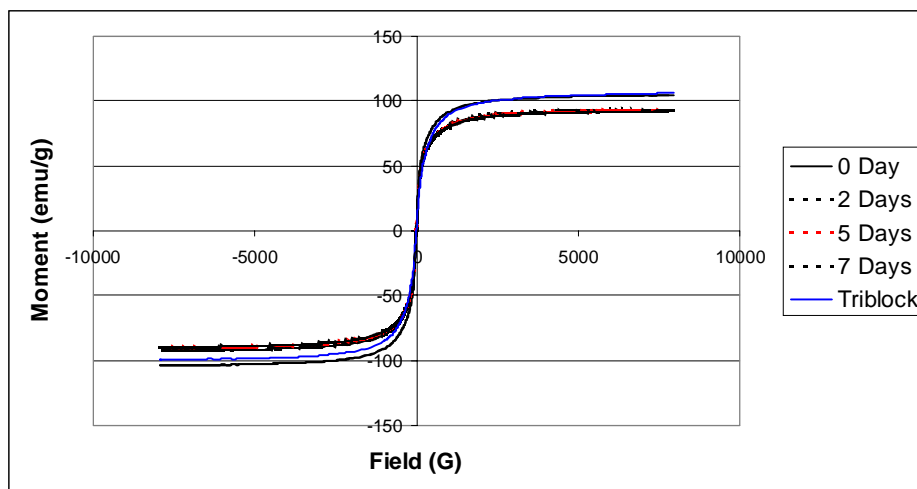


Figure 5.24 The magnetization curves of the dispersion during sol-gel reaction: the dispersion was performed using 1 g of 15k-2k-2k-2k-15k PDMS-PMTEOS-PCPMS-PMTEOS-PDMS terpolymers in 2000 g/mol PDMS carrier fluids.

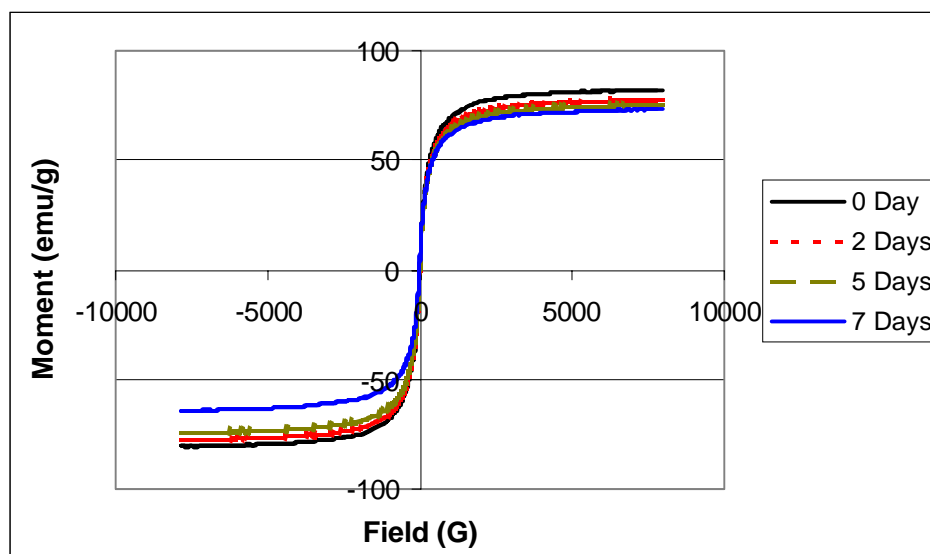


Figure 5.25 The magnetization curves of the dispersion during sol-gel reaction: the dispersion was performed using 1 g of 15k-4k-2k-4k-15k PDMS-PMTEOS-PCPMS-PMTEOS-PDMS terpolymers in 2000 g/mol PDMS carrier fluids.

The specific saturation magnetizations of the dispersions containing silica-coated particles sealed under an inert atmosphere and under an atmosphere containing air were measured at various time intervals (Figures 5.26, 5.27, and 5.28). The specific saturation magnetizations of the dispersions containing particles without silica coating were also investigated as references. The specific saturation magnetizations of the dispersions containing uncoated particles sealed under air-containing atmosphere (▲) drastically decreased over the time period of the experiment. The rate of specific saturation magnetization loss was approximately 0.5% per day (Figure 5.29). This value is closely parallel to the reduction in saturation magnetization of the cobalt dispersions prepared in PDMS-PCPMS-PDMS triblock copolymers (0.6% loss per day). The specific saturation magnetization of the uncoated sample sealed under inert gas (■) had a minimal decrease compared to the one sealed in air. Therefore, the specific saturation magnetization loss was most likely due to oxidation of the cobalt surface to antiferromagnetic oxides.

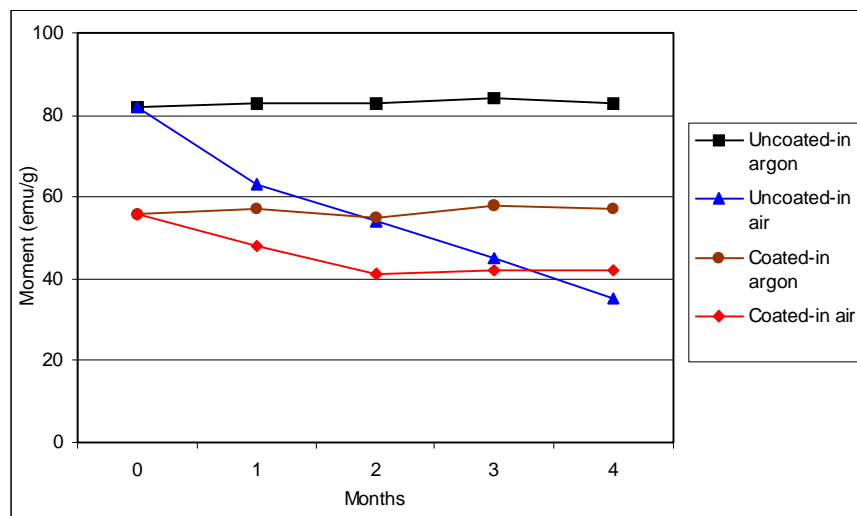


Figure 5.26 The specific saturation magnetization of a dispersion measured at various time intervals. The sample was prepared using 1 g $\text{Co}_2(\text{CO})_8$, and 1 g of 15k-1k-2k-1k-15k PDMS-PMTEOS-PCPMS-PMTEOS-PDMS terpolymers in 20 mL PDMS (approximately 1.6% Co).

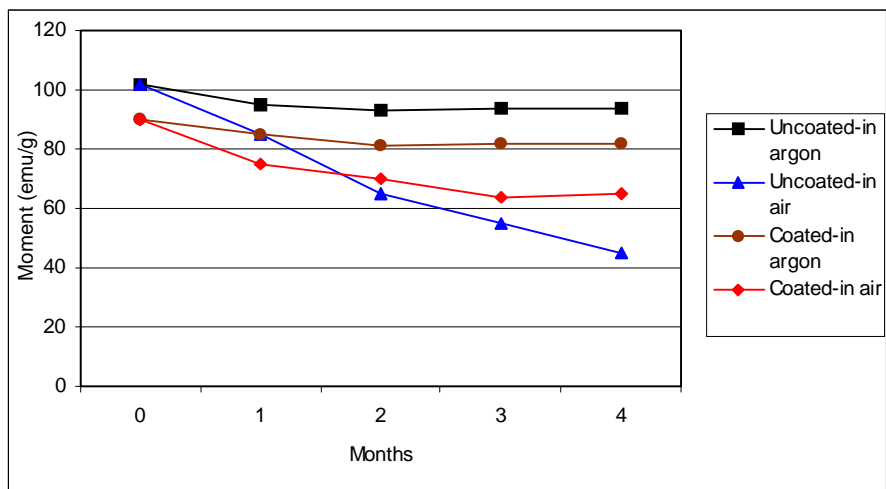


Figure 5.27 The specific saturation magnetization of a dispersion measured at various time intervals. The sample was prepared using 1 g $\text{Co}_2(\text{CO})_8$, and 1 g of 15k-2k-2k-2k-15k PDMS-PMTEOS-PCPMS-PMTEOS-PDMS terpolymers in 20 mL PDMS (approximately 1.6% Co).

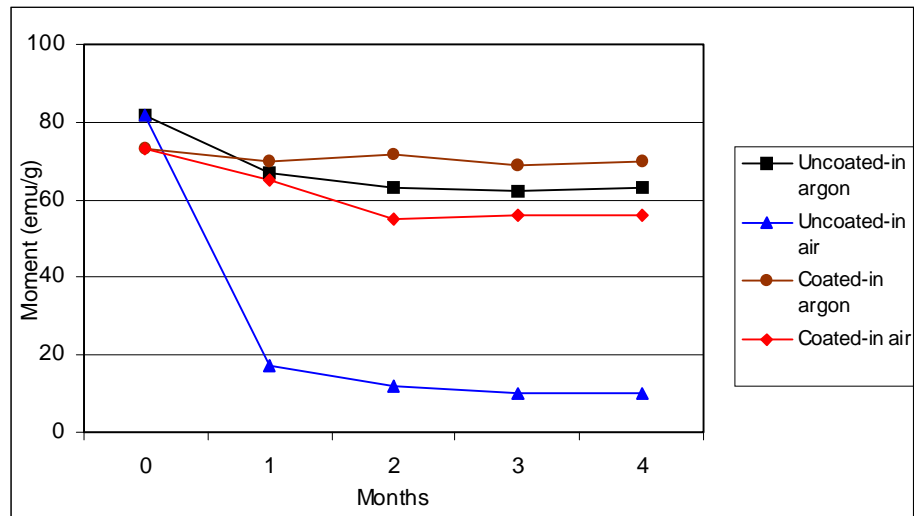


Figure 5.28 The specific saturation magnetization of a dispersion measured at various time intervals. The sample was prepared using 1 g $\text{Co}_2(\text{CO})_8$, and 1 g of 15k-4k-2k-4k-15k PDMS-PMTEOS-PCPMS-PMTEOS-PDMS terpolymers in 20 mL PDMS (approximately 1.6%Co).

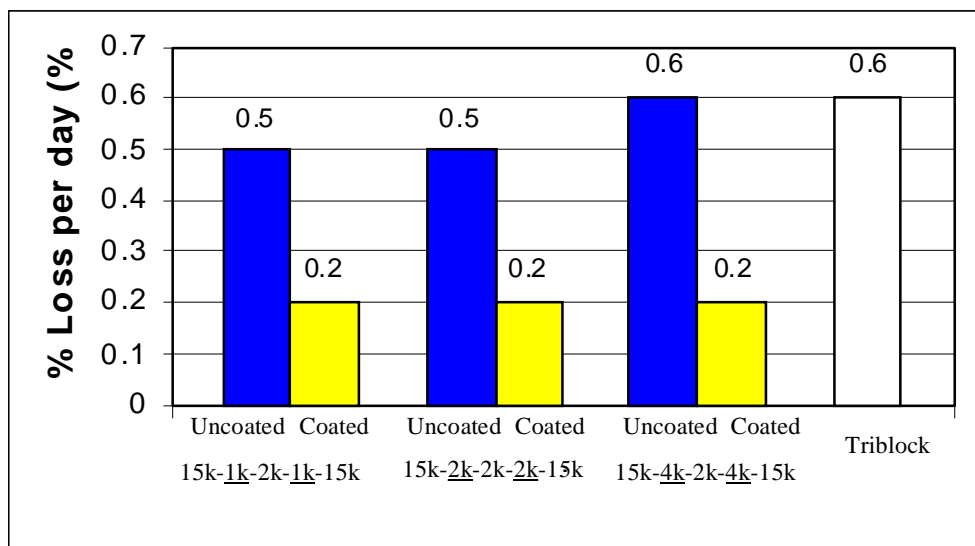


Figure 5.29 Comparison of average percent loss per day within a four-month experimental period between coated and uncoated-nanoparticles in an air-containing atmosphere.

The specific saturation magnetization of the silica-coated samples sealed under inert gas (●) showed insignificant decreases compared to the samples sealed in air (Figures 5.26, 5.27, and 5.28). Interestingly, the dispersions containing silica-coated particles sealed under air-containing atmosphere (◆) showed a minimal reduction in magnetic properties in the first two months, then the materials appeared to stabilize, indicating that coating the particles with silica inhibited the oxidation process. The initial decrease in the specific saturation magnetization in the silica-coated particles was probably due to the porosity in a thin layer of silica films typically found in sol-gel process²⁶⁴. Improvement in coating quality will be a subject of considerable further study.

5.5 Conclusions

Well-defined cobalt nanoparticle dispersions have been successfully prepared in toluene or 2,000g/mol PDMS carrier fluids in the presence of PDMS-PMTEOS-PCPMS-PMTEOS-PDMS pentablock terpolymer micelles. This terpolymer could fill the dual role as both a dispersion stabilizer and a precursor for a nanoparticle coating process. Each particle was individually coated with a sheath of the block terpolymer, which may be important for minimizing toxicity issues in biomedical applications. Nanoscale range particles (on the order of 10 nm) with narrow particle size distribution are necessary for in-vivo applications since they can be excreted from bodies.

The particle surfaces were effectively protected against oxidation by coating with a thin layer of silica film. The aging characteristics of stable dispersions containing higher concentrations of cobalt prepared in low molecular weight solvents, e.g., D₄, and hexamethyldisiloxane, are a subject of further studies.

²⁶⁴ Q. Liu, J. A. Finch, Z. Xu, *Chemistry of materials*, **10**, 3936 (1998)

CHAPTER 6 Conclusions

Cobalt nanoparticle dispersions with narrow particle size distributions can be prepared by thermal decomposition of dicobalt octacarbonyl in either toluene or 2000 g/mol PDMS in the presence of PDMS-PCPMS-PDMS triblock copolymer micelles. These phase-separated block copolymer stabilizers are successfully prepared via living anionic ring-opening polymerization. Each cobalt nanoparticle is singly coated with a sheath of the block copolymers. Coating of the cobalt nanoparticles with non-toxic siloxane stabilizers is thought to minimize or eliminate the toxicity issue in biological applications. Surface analysis of these particles also supports the finding that the particle surface is completely coated with siloxane steric stabilizers. In addition, quantitative removal of toluene solvent from the dispersion via dialysis shows a promising result, which further supports the feasibility for *in vivo* use.

It is hypothesized that the precision in the size and coating integrity in these particles is a result of first preparing the micellar “nanoreactors”, then forming the particles inside the intended coating material. Control of particle size in the range of 6-10 nm diameter is possible by controlling the ratio of dicobalt octacarbonyl precursor to the copolymers. The cobalt particles with nanoscale range and narrow particle size distribution are necessary for *in vivo* applications since they can be excreted from bodies.

Due to their narrow particle size distribution, two-dimensional ordered self-assemblies of these cobalt nanoparticles form spontaneously when the dispersions are cast from toluene. It is hypothesized that there are some interparticle attractions-repulsions which control reasonably long-range order. The number of cobalt atoms and polymer molecules existing in one particle is estimated using model cobalt nanoparticles in combination with the particle size measured from

a representative TEM image. These cobalt nanoparticles with the particle diameter of approximately 10 nm diameter have fcc crystal structure.

Magnetic susceptibility of the cobalt dispersions in contact with an air-containing atmosphere decreases over time. This has been attributed to surface oxidation. Protection of the particle surface by coating with silica thin films has been achieved. PDMS-PMTEOS-PCPMS-PMTEOS-PDMS pentablock terpolymers can fill the dual role as both stabilizers and as precursors for a sol-gel coating process. Specifically, the PCPMS central block binds the cobalt and PDMS tail blocks sterically stabilize the cobalt dispersion whereas the PMTEOS blocks are precursor blocks for the particle silica coating process. Saturation magnetization measurements of the coated-cobalt nanoparticles upon environmental aging suggest that coating them with silica thin films can effectively inhibit the oxidation process.

CHAPTER 7 Recommendations for Future Work

A research effort should be undertaken involving the preparation of the PDMS-PMTEOS-PCPMS-PMTEOS-PDMS pentablock terpolymers containing significant differences in PMTEOS block M_n s, e.g., 1000 g/mol, 5000 g/mol, and 10000 g/mol, and studying the relationship of their lengths to the rate of oxidation. In addition, introducing tetraethoxysilane (TEOS) or tetramethoxysilane (TMOS) during the sol-gel process might provide a better-defined coating to the particles.

When the dispersions were prepared using the ethoxy-containing pentablock terpolymers in toluene, the silica-coated dispersions form gel-like products after adding PDMS and removing toluene as shown in Figure 5.21A (in Chapter 5.4.5.1). It is thought that interparticle crosslinking occurred. In future studies, it would be interesting to perform the sol-gel process in extremely dilute conditions in toluene to prevent interparticle crosslinking. In addition, preparation of silica-coated particles in less polar solvents, e.g., cyclohexane, or hexane, might to contract the polar ethoxysilane blocks to the particle surface and coat each particle individually.

The silica-coated dispersions were successfully prepared in 2000 g/mol PDMS in the presence of ethoxy-containing block terpolymer stabilizers (in Chapter 5.4.5.1). It would be interesting to perform the reaction in other removable solvents that have similar chemical structures to PDMS carrier fluids, e.g., hexamethyldisiloxane, or octamethylcyclotetrasiloxane (D_4). The advantage of using these solvents instead of PDMS is that the reaction can be performed in dilute condition because they can be easily removed from the dispersions by vacuum stripping under reduced pressure. As a result, dispersions with higher cobalt concentration can be produced.

When the dispersions were prepared in the presence of methoxy-containing block terpolymer stabilizers, some aggregation was observed during the cobalt dispersion reaction regardless of the solvents used (in Chapter 5.4.3). More aggregation was observed when these dispersions were subjected to the sol-gel reaction as shown in Figure 5.22 (in Chapter 5.4.5.2). It is hypothesized that some interparticle crosslinking occurred due to the highly reactive methoxysilanes in fairly concentrated conditions, allowing the particles to agglomerate with each other. It would be interesting to perform these reactions under extremely dilute conditions, e.g, 1 g terpolymer/500 mL toluene and 1 g terpolymer/1000 mL toluene, to increase the interparticle distance.

An extension of this research would include verification via XPS of the silica coating on the particle surface. A narrow scan in XPS would provide quantitative determination of the elemental composition on the particle surface. An increase in silicon (Si) and oxygen (O) concentrations due to silica thin films on the silica-coated particles should be observed. This analysis should be done after the cobalt magnetic particles are extracted from the dispersion using an external magnet to remove unreacted species.

Improvement in coating quality of the particles should be a subject of an extension of this research. Annealing the silica-coated cobalt dispersions under argon and holding at a certain temperature for a long period of time might densify the preformed networks and produce densely packed silica thin films around the particles. The specific saturation magnetizations of the annealed samples should then be investigated over time to determine the relationship between time and temperature of the annealing process.

Bibliography

- ¹ F. W. Newell, In *Ophthalmology: Principles and Concepts*, 6th Ed., The C.V. Mosby Company, St. Louis (1986)
- ² J. P. Dailey, J. P. Phillips, C. Li and J. S. Riffle, *J. Magn. Magn. Mat*, **194**, 140-148 (1999)
- ³ Jap. Pat. JP 03011714 to Kanegafuchi Chemical Industry Co., Ltd., 1991.
- ⁴ W. Noll, In *Chemistry and Technology of Silicones*, Academic press Inc., New York (1968)
- ⁵ B. Mazumder, In *Silicon and Its Compounds*, Science Publishers, New Hampshire (2000)
- ⁶ R. B. Sosman, In *The Properties of Silica*, The Chemical Catalog Company, New York (1927)
- ⁷ E. G. Rochow, In *Silicon and Silicones*, Springer-Verlag, Germany (1987)
- ⁸ M. A. Brook, In *Silicon in Organic, Organometallic and Polymer Chemistry*, John Wiley&Sons, Inc., New York (2000)
- ⁹ J. M. Zeigler and F. W. Gordon Fearon (Eds.), In *Silicon-Based Polymer Science: A Comprehensive Resource*, Advances in Chemistry Series 224, American Chemical Society, Washington DC (1990)
- ¹⁰ G. Koerner, M. Schulze and J. Weis, In *Silicones: Chemistry and Technology*, Vulkan-Verlag, Germany (1991)
- ¹¹ F. O. Stark, J. R. Falendar and A. P. Wright, In *Comprehensive Organometallic Chemistry*, v.2, Pergamon Press, New York (1982)
- ¹² F. Liebau, In *Structural Chemistry of Silicates: Structure, Bonding and Classification*, Springer-Verlag, New York (1985)
- ¹³ L. V. Myshlyayeva and V. V. Krasnoshchekov, In *Analytical Chemistry of Silicon*, Translated by J. Schmorak, John Wiley and Sons, New York (1974)
- ¹⁴ C. B. Hurd, *J. Am. Chem. Soc.*, **68**, 364 (1946)
- ¹⁵ X. Chen and J. A. Gardella JR., *Macromolecules*, **27**, 12 (1994)
- ¹⁶ R. J. Roe, *J. Phys. Chem.*, **72**, 2013 (1968)
- ¹⁷ H. F. Mark, N. M. Bikales, C. G. Overberger, G. Menges and J. I. Kroschwitz (Eds.), In *Encyclopedia of Polymer Science and Engineering*, v. 15, Wiley-Interscience Publication, New York (1990), p.204-308.
- ¹⁸ S. Pawlenko, In *Organosilicon Chemistry*, Walter de Gruyter, Berlin (1986)
- ¹⁹ W. Lynch, In *Handbook of Silicone Rubber Fabrication*, Van Nostrand Reinhold Co., New York (1978)
- ²⁰ P. F. Bruins, In *Silicone Technology*, Interscience Publisher, New York (1970)
- ²¹ K. C. Frisch, In *Cyclic Monomers*, Wiley&Sons, New York (1972)
- ²² N. N. Sokolov and S. M. Akimova, *J. Gen. Chem. (USSR)*, **26**, 2276 (1956); 2545 CB trans.
- ²³ D. G. Dobay, U. S. Patent 2,769,829 (1956)
- ²⁴ W. I. Patnode and D. F. Wilcock, *J. Am. Chem. Soc.*, **68**, 362 (1946)
- ²⁵ P. I. Prescott and T. G. Selin, U. S. Paten 3,317,578 assigned to General Electric Company (1967)
- ²⁶ N. Grassie, K. F. Francey and I. G. MacFarlane, *Polym. Degrad. and Stab.*, **2**, 67 (1993)
- ²⁷ T. Takiguchi, M. Sakurai and T. Kishi, *J. Org. Chem.*, **25**, 310 (1960)
- ²⁸ B. Momper, T. Wagner, U. Maschke, M. Ballauff and E. W. Fisher, *Polym. Commun.*, **31**, 186 (1990)
- ²⁹ J. Chajnowski, In *Siloxane Polymers*, S. J. Clarson and J. A. Semlyen (Eds.), PTR Prentice Hall, Englewood Cliffs, New Jersey (1993)
- ³⁰ S. W. Kantor, W. T. Grubb and R. C. Osthoff, *J. Am. Chem. Soc.*, **76**, 5190-5197 (1954)

- ³¹ D. J. Brunelle (Ed.), In Ring-Opening Polymerization; Mechanisms, Catalysis, Structure, Utility, Hanser Publishers, Germany (1993)
- ³² J. B. Carmichael, D. J. Gordon F. J. Isackson, *J. Phys. Chem.*, **71**, 2011 (1967)
- ³³ S. Boileau, In Ring Opening Polymerization, J. E. McGrath (Ed.), ACS Monograph 286, American Chemical Society, Washington, DC, p.23 (1985)
- ³⁴ G. Sauvet, J. J. Lebrun and P. Sigwalt, In Cationic Polymerization and Related Processes, E. J. Goethals, Ed., Academic, New York, p.237 (1984)
- ³⁵ M. Spinu and J. E. McGrath, *J. Polym. Sci., Part A, Polym. Chem.*, **29**, 657-670 (1991)
- ³⁶ P. C. Painter and M. M. Coleman, In Fundamental of Polymer Science; An Introduction Text, 2nd ed., Technomic Publishing, Pennsylvania (1997)
- ³⁷ C. L. Lee and O. K. Johanson, *J. Polym. Sci.*, **A-1**(4), 3013 (1966)
- ³⁸ C. L. Lee and O. K. Johanson, *J. Polym. Sci. Polym. Chem. Ed.*, **14**, 729 (1976)
- ³⁹ C. Li, In Preparation of Nitrile Containing Siloxane Triblock Copolymers and Their Applications As Stabilizers for Siloxane Magnetic Fluids, Master Thesis, Virginia Tech (1996)
- ⁴⁰ J. E. McGrath, In Ring-Opening Polymerization, J. E. McGrath (Ed.), ACS Monograph 286, American Chemical Society, Washington, DC, p.1 (1985)
- ⁴¹ I. Yilgor, J. S. Riffle and J. E. McGrath, In Reactive Oligomers, v.282, Reactive Difunctional Siloxane Oligomers, F. W. Harris and H. J. Spinelli (Eds), p.161, American Chemical Society, Washington DC, (1985)
- ⁴² M. Cazacu, M. Marcu, A. Vlad, D. Caraiman and C. Racles, *Eur. Polym. J.*, **35**(9), 1629-1635 (1999)
- ⁴³ M. T. Btyk, N. N. Baglei and O. D. Kurilenko, *Vysokomol. Soedin., Ser.A*, **17**(5), 1034-9 (1975)
- ⁴⁴ K. D. Belfield and G. Zhang, *Polym. Bull. (Berlin)*, **38**(2), 165-168 (1997)
- ⁴⁵ Q. Wang, G. K. Surya Prakash, G. A. Olah, P. Donal and B. Ketherine, *Recnet Res. Dev. Polym. Sci.*, **2**(pt.2), 555-567 (1998)
- ⁴⁶ Q. Wang, H. Zhang, G. K. Surya Prakash, T. E. Hogen-Esch and G. A. Olah, *Macromolecules*, **29**, 6691-6694 (1996)
- ⁴⁷ G. A. Olah, Q. Wang, G. Golam, G. K. Surya Prakash, H. Zhang, T. E. Hogen-Esch, *Polym. Prepr. (Am. Chem. Soc., Div. Polym. Chem.)*, **37**(1), 805-806 (1996)
- ⁴⁸ G. Toskas, G. Besztercey, M. Moreau, M. Masure and P. Sigwalt, *Macromol. Chem. Phys.*, **196**(9), 2715-35 (1995)
- ⁴⁹ P. Sigwalt, M. Masure, M. Moreau and R. Bischoff, *Makromol. Chem., Macromol. Symp.*, **73**, 146-166 (1993)
- ⁵⁰ M. Rodriguez-Baeza and M. Zapata, *Polym. Bull. (Berlin)*, **36**(2), 173-180 (1996)
- ⁵¹ S. Maisonnier, J. C. Favier, M. Masure and P. Hemery, *Polym. Int.*, **48**(3), 159-164 (1999)
- ⁵² J. V. Crivello and M. Fan, *Macromol. Symp.*, **77**, 413-421 (1994)
- ⁵³ K. D. Belfield and G. Zhang, *Polym. Prep. (Am. Chem. Soc., Div. Polym. Chem.)*, **36**(2), 267-8 (1995)
- ⁵⁴ J. Chojnowski and L. Wilczek, *Makromol. Chem.*, **180**, 117-130 (1979)
- ⁵⁵ P. Sigwalt, *Polym. J.*, **19**, 567 (1987)
- ⁵⁶ L. Wilczek, S. Rubinsztain and J. Chojnowski, *Macromolecule*, **20**, 2345-2355 (1987)
- ⁵⁷ L. Wilczek, S. Rubinsztain and J. Chojnowski, *Makromol. Chem.*, **187**, 39-51 (1986)
- ⁵⁸ M. G. Voronkov, V. P. Mileshekevich and Y. A. Yuzhelevskii, In The Siloxane Bond: Physical Properties and Chemical Transformations, Consultants Bureau, New York (1978)

- ⁵⁹ L. A. Kiefer, In Synthesis and Characterization of Novel Polyester/Polysiloxane and Polyester/Arylphosphine Oxide Copolymers, Ph.D. Dissertation, Virginia Tech (1993)
- ⁶⁰ C. S. Elsbernd, P. M. Sormani, S. Kilic and J. E. McGrath, *Polym. Prep. (Am. Chem. Soc., Div. Polym. Chem.)*, **27**(2), 152-3 (1986)
- ⁶¹ P. M. Sormani and J. E. McGrath, *Polym. Prep. (Am. Chem. Soc., Div. Polym. Chem.)*, **26**(1), 258-9 (1985)
- ⁶² T. C. Kendrick, B. M. Parbhoo and J. W. White, In Comprehensive Polymer Science, G. Allen, J. C. Bevington, G. C. Eastmaond, A. Ledwith, S. Susso and P. Sigwalt (Eds.), v.4, p. 459, Pergamon, Oxford (1989)
- ⁶³ S. W. Kantor and A. R. Gilbert (to Central Electric Co.), U.S. Pat. 2,883,366 (1959)
- ⁶⁴ E. E. Bostick, In Kinetics and Mechanisms of Polymerization, v.2, Ring Opening Polymerization, K. C. Frisch and S. L. Reegan (Eds), p.327, Marcel Dekker, New York (1969)
- ⁶⁵ C. S. Elsbernd, M Spinu, S. Kilic and J. E. McGrath, *Polym. Prep. (Am. Chem. Soc., Div. Polym. Chem.)*, **29**(1), 355-7 (1988)
- ⁶⁶ J. E. McGrath, P. M. Sormani, C. S. Elsbernd and S. Kilic, *Makromol. Chem., Macromol. Symp.*, **6**, 67-80 (1986)
- ⁶⁷ M. Cazacu, M. Marcu, S. Dragon and C. Matricala, *J. Appl. Polym. Sci.*, **60**, 731-734 (1996)
- ⁶⁸ M. Cazacu, M. Marcu, A. Vlad, D. Caraiman and C. Racles, *Eur. Polym. J.*, **35**, 1629-1635 (1999)
- ⁶⁹ M. Szwarc, In Anionic Polymerization: Kinetics, Mechanisms and Synthesis, J. E. McGrath (Ed.), ACS Symposium Series 166, American Chemical Society, Washington DC (1981)
- ⁷⁰ K. Ziegler and K. Bahr, *Chem. Ber.*, **61**, 253 (1928)
- ⁷¹ K. Ziegler, F. Dersch and H. Wolltham, *Ann. Chem.*, **511**, 13 (1934)
- ⁷² H. Dostal and H. Z. Mark, *Phys. Chem. B.*, **29**, 299 (1935)
- ⁷³ P. J. Flory, In Principles of Polymer Chemistry, Cornell Press (1953)
- ⁷⁴ M. Szwarc, M. Levy and R. Milkovich, *J. Am. Chem. Soc.*, **78**, 2656 (1956)
- ⁷⁵ J. March, In Advanced Organic Chemistry; Reaction, Mechanisms and Structure, 4th ed., John-Wiley & Sons, New York (1992)
- ⁷⁶ G. Odian, In Principles of Polymerization, 3rd Ed., p.356, John Wiley & Sons, Inc., New York (1991)
- ⁷⁷ M. Morton, In Anionic Polymerization: Kinetics, Mechanisms and Synthesis, J. E. McGrath (Ed.), ACS Symposium Series 166, American Chemical Society, Washington DC (1981)
- ⁷⁸ U. Maschke and T. Wagner, *Makromol. Chem.*, **193**, 2453-2466 (1992)
- ⁷⁹ C. A. Veith and R. E. Cohen, *J. Polym. Sci. A: Polym. Chem.*, **27**, 1241-1258 (1989)
- ⁸⁰ R. C. Hedden and C. Cohen, *Polymers*, **41**, 6975 (2000)
- ⁸¹ J. M. Yu, D. Teyssie, R. B. Khalifa and S. Boileau, *Polymer Bulletin*, **32**, 35-40 (1994)
- ⁸² C. L. Frye, R. M. Salinger, F. W. G. Fearon, J. M. Klosowski and T. DeYoung, *The Journal of Org. Chem.*, **35**(5), 1308 (1970)
- ⁸³ T. Suzuki, *Polymer*, **30**, 333 (1989)
- ⁸⁴ W. H. Dickstein, *Macromolecules*, **22**, 3882-3885 (1989)
- ⁸⁵ L. Wilczek and J. P. Kennedy, *Polymer Journal*, **19**(5), 531-538 (1987)
- ⁸⁶ T. Zundel, J. M. Yu, L. Lestel, D. Teyssie and S. Boileau, *Macromol. Symp.*, **88**, 177-189 (1994)
- ⁸⁷ A. Kumar and B. E. Eichinger, *Macromolecules*, **23**, 5358 (1990)
- ⁸⁸ S. Boileau, In Anionic Polymerization: Kinetics, Mechanisms and Synthesis, J. E. McGrath (Ed.), ACS Symposium Series 166, American Chemical Society, Washington DC (1981)

- ⁸⁹ M. Morton and E. E. Bostick, *J. Polym. Sci.*, **A3**, 971 (1965)
- ⁹⁰ Y. Gnanou and P. Rempp, *Makromol. Chem.*, **189**, 1997-2005 (1988)
- ⁹¹ J. Chojnowski, K. Rozga, W. Fortuniak and A. Kowalewska, *Makromol. Chem. Macromol. Symp.*, **73**, 183-201 (1993)
- ⁹² E. E. Bostick, In *Block Copolymer*, S. L. Aggarwal (Ed.), Plenum Press, New York (1970)
- ⁹³ H. Kazama, Y. Tezuka and K. Imai, *Polymer Bulletin*, **21**, 31-37 (1989)
- ⁹⁴ R. Milkovich, S. African Pat. No. 280,712 (1963). Assigned to Shell Oil Company.
- ⁹⁵ J. E. McGrath, In *Block Copolymers: Science and Technology*, D. J. Meier (Ed.), MMI Press Symposium Series, v.3, Harwood Academic Publishers, New York (1983)
- ⁹⁶ F. J. B. Calleja and Z. Roslaniec, In *Block Copolymers*, Marcel Dekker, New York (2000)
- ⁹⁷ B. Lindman and P. Alexandridis, In *Amphiphilic Block Copolymers; Self-Assemble and Applications*, P. Alexandridis and B. Lindman (Eds.), Elsevier, New York (2000)
- ⁹⁸ A. Noshay and J. E. McGrath, In *Block Copolymers: Overview and Critical Survey*, Academic Press, New York (1977)
- ⁹⁹ J. B. Plum and J. H. Atherton, In *Block Copolymers*, D. C. Allport and W. H. Janes (Eds.), Applied Science Publishers, London (1973)
- ¹⁰⁰ N. V. Gvodzdic, J. Ibemesi and D. J. Meier, *Proc. IUPAC, Macromol. Symp.*, **69**, 168 (1982)
- ¹⁰¹ S. Andre, F. Guida-Pietrasanta, A. Rousseau and B. Boutevin, *J. Polym. Sci. A: Polym. Chem.*, **39**, 2414 (2001)
- ¹⁰² Y. Yamada and N. Furukawa, *Polymer J.*, **29**(11), 923 (1997)
- ¹⁰³ J. Zhao, S. R. Rojstaczer, J. Chen, M. Xu and J. A. Gardella Jr., *Macromolecules*, **32**, 455 (1999)
- ¹⁰⁴ W. Volksen, J. L. Hedrick, T. P. Russell and S. Swanson, *J. Appl. Polym. Sci.*, **66**, 199 (1997)
- ¹⁰⁵ K. Huan, L. Bes, D. M. Haddleton and E. Khoshdel, *J. Polym. Sci. A: Polym. Chem.*, **39**, 1833 (2001)
- ¹⁰⁶ J. P. Mason, T. Hattori and T. E. Hogen-Esch, *Polym. Prepr. (Am. Chem. Soc., Div. Polym. Chem.)*, **30**(1), 259 (1989)
- ¹⁰⁷ T. C. Chang, H. B. Chen, Y. C. Chen and S. Y. Ho, *J. Polym. Sci. A: Polym. Chem.*, **34**, 2613 (1996)
- ¹⁰⁸ T. C. Chang, H. B. Chen, Y. S. Chiu and S. Y. Ho, *Polym. Degrad. Stab.*, **57**, 7-14 (1997)
- ¹⁰⁹ Y. C. Chun, K. S. Kim and J. S. Shin, *Polym. Int.*, **27**, 177 (1992)
- ¹¹⁰ R. Benrashid, G. L. Nelson, J. H. Linn, K. H. Hanley and W. R. Wade, *J. Appl. Polym. Sci.*, **49**, 523 (1993)
- ¹¹¹ M. Pegoraro, F. Severini, R. Gallo and L. Zanderighi, *J. Appl. Polym. Sci.*, **57**, 421 (1995)
- ¹¹² D. Giurgiu, V. Hamciuc, E. Butuc, V. Cozan, A. Stoleriu, M. Marcu and C. Ionescu, *J. Appl. Polym. Sci.*, **59**, 1507 (1996)
- ¹¹³ Z. Kiraly and B. Vincent, *Polym. Int.*, **28**, 139 (1992)
- ¹¹⁴ E. E. Bostick, In *Block Copolymers*, S. L. Aggarwal (Ed.), Plenum, New York (1970)
- ¹¹⁵ C. Chou and M. H. Tang, *J. Thermal Anal.*, **40**, 657-667 (1993)
- ¹¹⁶ A. Moment, R. Miranda and P. T. Hammond, *Macromol. Rapid Commun.*, **19**, 573-579 (1998)
- ¹¹⁷ J. Selb and Y. Gallot, In *Developments in Block Copolymers-2*, I. Goodman (Ed.), Elsevier Applied Science Publishers, London (1985)
- ¹¹⁸ P. C. Hiemenz, In *Principles of Colloid and Surface Chemistry*, Marcel Dekker, Inc., New York (1977)

- ¹¹⁹ D. J. Shaw, In Introduction to Colloid and Surface Chemistry, 3rd Ed., Butterworths, London (1980)
- ¹²⁰ P. C. Hiemenz and R. Rajagopalan, In Principles of Colloid and Surface Chemistry, 3rd Ed. Revised and Expanded, Marcel Dekker, New York (1997)
- ¹²¹ D. G. Hall, B. A. Pethica, Nonionic Surfactants, Marcel Decker Inc., New York (1967)
- ¹²² D. F. Evans and H. Wennerstrom, In The Colloidal Domain; Where Physics, Chemistry, Biology and Technology Meet, 2nd Ed., Wiley-VCH, New York (1999)
- ¹²³ C. Sandron, *Angrew. Chem.*, **75**, 472 (1963)
- ¹²⁴ Y. Liu, S. H. Chen and J. S. Huang, *Macromolecules*, **31**, 2236 (1998)
- ¹²⁵ P. Alexandridis and L. Yang, *Macromolecules*, **33**, 5574 (2000)
- ¹²⁶ L. Yang and P. Alexandridis, *Langmuir*, **16**, 4819 (2000)
- ¹²⁷ P. Alexandridis and L. Yang, *Macromolecules*, **33**, 3382 (2000)
- ¹²⁸ L. Yang and P. Alexandridis, *Langmuir*, **16**, 8555 (2000)
- ¹²⁹ L. M. Bronstein, D. M. Chernyshov, G. I. Timofeeva, L. V. Dubrovina, P. M. Valetsky and A. R. Khokhov, *J. Colloid and Interface Science*, **230**, 140 (2000)
- ¹³⁰ C. Kim, S. C. Lee, J. H. Shin and J. S. Yoon, *Macromolecules*, **33**, 7448 (2000)
- ¹³¹ A. Kitahara and K. Kon-No, In Colloidal Dispersions and Micellar Behavior, K. L. Mittal (Ed.), ACS Symposium Series 9, American Chemical Society, Washington DC (1975)
- ¹³² K. Iyama and T. Nose, *Polymer*, **39**(3), 651 (1998)
- ¹³³ H. D. Bijsterbosch, M. A. Cohen Stuart and G. J. Flee, *Macromolecules*, **31**, 9281 (1998)
- ¹³⁴ R. C. Mehrotra, In Structure and Bonding; Chemistry, Spectroscopy and Applications of Sol-Gel Glasses, v.77, M. J. Clarke, J. B. Goodenough, C. K. Jorgenson, J. B. Neilands, D. Reinen and W. Weiss (Eds.), p.1, Springer-Verlag, Berlin (1992)
- ¹³⁵ C. Li, Inorganic-Organic Sol-Gel Derived Hybrid Materials as Abrasion Resistant Coatings, Ph.D. Dissertation, Virginia Tech (1999)
- ¹³⁶ J. E. McGrath, J. P. Pullockaren, J. S. Riffle, S. Kilic and C. S. Elsbernd, In Ultrastructure Processing of Advanced Ceramics, J. D. Mackenzie and D. R. Ulrich (Eds.), p.55, A Wiley-Interscience, New York (1988)
- ¹³⁷ Ebelmen, *Ann ales de Chimie et de Physique*, **57**, 319 (1846)
- ¹³⁸ M. Spinu, Silicon-Based Organic and Inorganic Polymers, Ph.D. Dissertation, Virginia Tech (1990)
- ¹³⁹ R. W. Jones, In Fundamental Principles of Sol-Gel Technology, p.1, The Institute of Metal, Great Britain (1989)
- ¹⁴⁰ S. Komarneni, S. Sakka, P. P. Phule and R. M. Laine (Eds.), In Sol-Gel Synthesis and Processing, The American Chemical Society (1998)
- ¹⁴¹ L. L. Hench and D. R. Ulrich (Eds.), In Science of Ceramic Chemical Processing, John Wiley&Sons, New York (1986)
- ¹⁴² K. D. Keefer, In Better Ceramics Through Chemistry, C. J. Brinker, D. E. Clark and D. R. Ulrich (Eds.), North-Holland, New York (1984)
- ¹⁴³ B. K. Coltrain and L. W. Kelts, In The Colloid Chemistry of Silica, H. E. Bergna (Ed.), American Chemical Society (1994)
- ¹⁴⁴ D. R. Urich, *Chemtech*, 242 (1988)
- ¹⁴⁵ Y. Wei, W. Wang, J. M. Yeh, B. Wang, D. Yang, J. K. Murray, Jr. D. Jin and G. Wei, In Hybrid Organic-Inorganic Composites, J. E. Mark, C. Y-C, Lee and P. A. Bianconi (Eds.), ACS Symposium Series 585, American Chemical Society, Washington DC (1995)

- ¹⁴⁶ C. J. Brinker, In *The Colloid Chemistry of Silica*, H. E. Bergna (Ed.), American Chemical Society, Washinton DC (1994)
- ¹⁴⁷ R. K. Iler, In *The Chemistry of Silica: Solubility, Polymerization, Colloid and Surface Properties, and Biochemistry*, Wiley-Interscience, New York (1979)
- ¹⁴⁸ E. R. Pohl and F. D. Osterholtz, In *Molecular Characterization of Composite Interfaces*, Y. Ishida and G. Kumar (Eds.), Plenum Press, New York (1985)
- ¹⁴⁹ C. G. Swain, R. M. Esteve and H. J. Jones, *J. Am. Chem. Soc.*, **11**, 965 (1949)
- ¹⁵⁰ U.S. Patent 3,161,614 (1964)
- ¹⁵¹ D. R. Thomas, In *Siloxane Polymers*, S. J. Clarson and J. A. Semlyen (Eds.), PTR Prentice Hall, New Jersey (1993)
- ¹⁵² A. S. Novikov and Z. N. Nudel'man, *Kauchukbi Rezina*, No.12, 3 (1960)
- ¹⁵³ J. Nagy, A. Borbely-Kuszmán and J. E. Mark, *Period Polytech Chem. Eng.*, **10**, 139 (1960)
- ¹⁵⁴ P. Jorg and W. Ernst, *Chemiker-Ztg.*, **97**, 176 (1973)
- ¹⁵⁵ F. W. Van der Weij, *Makromol. Chem.*, **181**, 2541 (1980)
- ¹⁵⁶ V. V. Severnyi, R. M. Minas'yan, I. A. Makarenko and N. M. Bizyuakova, *Vysokomoh Soedin. Ser. A (Eng. trans.)*, **18**, 1464 (1976)
- ¹⁵⁷ C. R. Helms and B. E. Deal (Eds.), In *The Physics and Chemistry of SiO₂ and the Si-SiO₂ Interface*, Plenum Press, New York (1988)
- ¹⁵⁸ C. R. Helms and B. E. Deal (Eds.), In *The Physics and Chemistry of SiO₂ and the Si-SiO₂ Interface 2*, Plenum Press, New York (1993)
- ¹⁵⁹ H. Schmidt and H. Bottner, In *The Colloid Chemistry of Silica*, H. E. Bergna (Ed.), American Chemical Societ (1994)
- ¹⁶⁰ C. H. Winter and D. M. Hoffman (Eds.), In *Inorganic Materials Synthesis: New Directions for Advanced Materials*, American Chemical Society, Washington DC (1999)
- ¹⁶¹ J. Livage, T. Coradin and C. Roux, *J. Physics: Condense Matter*, **13**, R673-R691 (2001)
- ¹⁶² D. M. Liu and I. W. Chen, US Patent; The Trustees of the University of Pennsylvania, 6,303,209, october16, 2001
- ¹⁶³ E. Barrera, T. Viveros, A. Avila, P. Quintana, M. Morales and N. Batina, *Thin Silica Films*, **346**, 138-144 (1999)
- ¹⁶⁴ D.D. Erickson, T. E. Wood and W. P. Wood, In *Sol-Gel Synthesis and Processing*, p.73,S. Komarneni, S. Sakka, P. P. Phule and R. M. Laine (Eds.), The American Chemical Society (1998)
- ¹⁶⁵ B. D. Fabes and W. C. Oliver, *J. Non-Cryst. Solids*, **121**, 348 (1990)
- ¹⁶⁶ C. L. Luyer, L. Lou, C. Bovier, J. C. Plenet, J. G. Dumas and J. Mugnier, *Optical Materials*, **18**, 211-217 (2001)
- ¹⁶⁷ H. Dislich and E. Hussmann, *Thin Solid Films*, **77**, 129 (1981)
- ¹⁶⁸ E. R. La Serra, Y. Charbouillot, P. Baudry and M. A. Aegerter, *J. Non-Cryst. Solids*, **121**, 323 (1990)
- ¹⁶⁹ Y. Xu, C. J. Chen, J. D. Mackenzie, *Proc. SPIE's 1990 Symp.*, Vol. 1328, p.428, p.441.
- ¹⁷⁰ I. Lee, M. A. Snipes and J. Covino, In *Sol-Gel Science and Technology*, E. J. A. Pope, S. Sakka and L. C. Klein (Eds.), Ceramic Transaction, v.55, The American Chemical Society, Ohio (1994)
- ¹⁷¹ R. Reisfeld, M. Eyal, V. Chernyak and R. Zusman, *Solar Energy Materials*, **17**, 439 (1988)
- ¹⁷² L. L. Hench, In *Ultrastructure Processing of Advanced Structural and Electronic Materials*, Noyes Publications, New Jersey (1984)

- ¹⁷³ S. Sakka and T. Yoko, In *Structure and Bonding: Chemistry, Spectroscopy and Applications of Sol-Gel Glasses*, v. 77, M. J. Clarke, J. B. Goodenough, C. K. Jorgenson, J. B. Neilands, D. Reinen and W. Weiss (Eds.), p.89, Springer-Verlag, Berlin (1992)
- ¹⁷⁴ R. A. Caruso and M. Antonietti, *Chem. Mater.*, **13**, 3272-3282 (2001)
- ¹⁷⁵ S. Braun, S. Rappoport, R. Zusmen, D. Avnir and M. Ottolenghi, *Mater. Lett.*, **10**, 1 (1990)
- ¹⁷⁶ M. R. Bohmer, A. R. Balkenenda, T. N. M. Bernards, M. P. J. Peeters, M. J. van Bommel, E. P. Boonekamp, M. A. Verheijen, L. H. M. Krings and Z. A. E. P. Vroon, In *Handbook of Advanced Electronic and Photonic Devices*, H. S. Nalwa (Ed), Academic Press, San Diego (2001)
- ¹⁷⁷ J. G. Lee, H. M. Lee, C. S. Kim and Y. J. Oh, *J. Magn. Magn. Mater.*, **177**, 900 (1998)
- ¹⁷⁸ Y. Kobayashi, M. A. Correa-Duarte and L. M. Liz-Marzan, *Langmuir*, **17**, 6375-6379 (2001)
- ¹⁷⁹ J. P. Jakubovics, In *Magnetism and Magnetic Materials*, 2nd Ed., The Institute of Materials, London (1994)
- ¹⁸⁰ D. J. Craik and R. S. Tebble, In *Ferromagnetism and Ferromagnetic Domains*, John-Wiley&Sons, New York (1965)
- ¹⁸¹ R. S. Tebble and D. J. Craik, In *Magnetic Materials*, Willey-Interscience, London (1969)
- ¹⁸² D. J. Craik, In *Structure and Properties of Magnetic Materials*, Pion Limited, London (1971)
- ¹⁸³ D. Halliday and R. Resnick, In *Physics*, 3rd Ed., John Wiley&Sons, New York (1978)
- ¹⁸⁴ K. J. Standley, In *Oxide Magnetic Materials*, 2nd Ed., Clarendon Press, London (1972)
- ¹⁸⁵ B. D. Cullity, In *Introduction to Magnetic Materials*, Addison-Wesley Company, Massachusetts (1972)
- ¹⁸⁶ S. Odenbach, *Adv. Colloid Interface Sci.*, **46**, 263 (1993)
- ¹⁸⁷ P. C. Scholten, *Int. Magn. Magn. Mater.*, **39**, 99 (1983)
- ¹⁸⁸ S. W. Charles, In *Magnetic Properties of Fine Particles*, J. L. Dormann and D. Fiorani (Eds.), North-Holland, Amsterdam (1991)
- ¹⁸⁹ S. S. Papell, US Patent 3,215,572, assigned to NASA (1965)
- ¹⁹⁰ R. E. Rosensweig, US Patent, 3,917,538, assigned to Ferrofluidics Corporation (1975)
- ¹⁹¹ V. E. Fertman, In *Magnetic Fluids Guidebook: Properties and Applications*, Hemisphere Publishing Corporation, New York (1990)
- ¹⁹² V. G. Bashtovoy, B. M. Berkovsky and A. N. Vislovich, In *Introduction to Thermomechanics of Magnetic Fluids*, Springer-Verlag, New York (1988)
- ¹⁹³ R. Langer, *Nature*, **392**, 5 (1998)
- ¹⁹⁴ K. J. Wider, A. E. Senyei and D. G. Scarpelli, *Proc. Soc. Exp. Biol.*, **58**, 141 (1978)
- ¹⁹⁵ J. P. Dailey, J. P. Phillips and J. R. Riffle, *J. Magn. Magn. Mater.*, **194**, 140 (1999)
- ¹⁹⁶ J. P. Stevenson, M. Rutnakornpituk, M. Vadala, A. R. Esker, S. W. Charles, S. Wells, J. P. Dailey and J. S. Riffle, *J. Magn. Magn. Mater.*, **225**, 47 (2001)
- ¹⁹⁷ P. C. Scholten, *Chem. Eng. Comm.*, **67**, 331 (1988)
- ¹⁹⁸ K. E. Heuslet, In *Passivity of Metals*, R. P. Frankenthal and J. Kruger, p. 771, The Electrochemical Soc., Princeton (1978)
- ¹⁹⁹ R. Anthore, *J. Physique*, **38** C2, 203 (1977)
- ²⁰⁰ P. C. Scholten, In *Thermomechanics of Magnetic Fluids*, p.1, B. Berkovsky (Ed.), Hemisphere Publishing Corp., Washington (1977)
- ²⁰¹ S. Wells, In *Preparation and Properties of Ultrafine Magnetic Particles*, Thesis, The University of Wales, 1989
- ²⁰² Y. Xie, T. Liu, and B. Chu, *Polym. Mater. Sci. Eng.*, **79**, 334 (1998)
- ²⁰³ T. Hashimoto, M. Harada, and N. Sakamoto, *Macromolecules*, **32**, 6867 (1999)

- ²⁰⁴ V. F. Puentes and K. M. Krishnan, *IEEE Transactions on Magnetics*, **37**(4), 2210 (2001)
- ²⁰⁵ T. W. Smith, US Patent 4,252,674, assigned to Xerox Corporation (1981)
- ²⁰⁶ E. Blums, A. Cebers, and M. M. Maiorov, In *Magnetic Fluids*, Walter de Gruyter, Berlin (1997)
- ²⁰⁷ F. Ungvary and L. Marko, *J. Organomet. Chem.*, **71**, 283 (1974)
- ²⁰⁸ G. Bor and U. K. Dietler, *J. Organomet. Chem.*, **191**, 295 (1980)
- ²⁰⁹ M. F. Mirbach, A. Saus, A. M. Krings and K. J. Mirbach, *J. Organomet. Chem.*, **205**, 229 (1981)
- ²¹⁰ V. M. Gavrilova, V. Yu Gankin, D. M. Rugkovkii and A. G. Trifel, *Gidroformilirovanie, Kuimya, Leningrad*, **114**, (1974)
- ²¹¹ F. Ungvary and L. Marko, *Inorg. Chim. Acta.*, **4**, 324 (1970)
- ²¹² R. Tannenbaum, *Inorg. Chim. Acta.*, **227**, 233 (1994)
- ²¹³ E. Papirer, P. Horny, H. Balard, R. Anthore, C. Petipas, A. Martinet, *J. Colloid Interface Sci.*, **94**(1), 207 (1983)
- ²¹⁴ E. Papirer, P. Horny, H. Balard, R. Anthore, C. Petipas, A. Martinet, *J. Colloid Interface Sci.*, **94**(1), 220 (1983)
- ²¹⁵ S. Foster, M. Antonietti, *Adv. Mater.*, **10**, 195 (1998)
- ²¹⁶ V. F. Puentes, and K. M. Krishnan, *IEEE Transactions on Magnetics*, **37**(4), 2210 (2001)
- ²¹⁷ J. S. Yin and Z. L. Wang, *NanoStructure Materials*, **11**(7), 845 (1999)
- ²¹⁸ J. S. Yin and Z. L. Wang, *J. Mater. Res.*, **14**(2), 503 (1999)
- ²¹⁹ O. A. Platonova, L. M. Bronstein, S. P. Solodovnikov, I. M. Yanovskaya, E. S. Obolonkoya, P. M. Valetsky, E. Wenz, and M. Antonietti, *Colloid Polym. Sci.*, **275**, 426 (1997)
- ²²⁰ G. N. Glavee, K. J. Klabunde, C. M. Sorensen, and G. C. Hadjapanayis, *Langmuir*, **8**, 771 (1992)
- ²²¹ H. Bonnemann, W. Brijoux and T. Jousen, *Angrew. Chem. Int. Ed. Engl.*, **29**, 273 (1990)
- ²²² R. D. Rieke, *Acc. Chem. Res.*, **10**, 301 (1977)
- ²²³ F. Fievet, J. P. Lagier, and M. Figlarz, *MRS Bulletin*, **29** (1989)
- ²²⁴ D. Hoffmann, W. Schindler, J. Kirschner, *App. Phys. Lett.*, **73**, 3279 (1998)
- ²²⁵ C. Petit, A. Taleb, and M. P. Pileni, *J. Phys. Chem.*, **103**, 1805 (1999)
- ²²⁶ S. Sun, C. B. Murray, and H. Doyle, *Mat. Res. Soc. Symp. Proc.*, **577**, 385 (1999)
- ²²⁷ J. Legrand, C. Petit, D. Bazin, and M. P. Pileni, *Appl. Surf. Sci.*, **164**, 186 (2000)
- ²²⁸ C. Petit, and M. P. Pileni, *Appl. Surf. Sci.*, **162-163**, 519 (2000)
- ²²⁹ X. M. Lin, and C. M. Sorensen, *Langmuir*, **14**, 7140 (1998)
- ²³⁰ M. J. Colthurst, R. L. Williams, P. S. Hiscott and I. Grierson, *Biomaterials*, **21**, 649 (2000)
- ²³¹ I. McDonnel, In *Retina*, v.I, S. Ryan (Ed.), Mosby, Toronto (1989)
- ²³² P. A. Voltairas, D. I. Fotiadis and C. V. Massalas, *J. Magn. Magn. Mat*, **225**, 248-255 (2001)
- ²³³ J. J. Kanski, In *Retinal Detachment: A Colour Manual of Diagnosis and Treatment*, Butterworths, London (1986)
- ²³⁴ D. J. Apple and M. F. Robb, In *Ocular Pathology: Clinical Applications and Self -Assessment*, 3rd Ed., The C.V. Mosby Company, St. Louis (1985)
- ²³⁵ G. O. H. Naumann and D. J. Apple, In *Pathology of the Eye*, Springer-Verlag, New York (1986)
- ²³⁶ F. W. Newell, In *Ophthalmology: Principles and Concepts*, 6th Ed., The C.V. Mosby Company, St. Louis (1986)
- ²³⁷ Sr. Batdorf and B. David, US Patent 6,117,170 (2000)
- ²³⁸ D. M. Marcus, D. J. D'Amico and S. Mukai, *Int. Phthalamol. Clin*, **34**, 97 (1994)

- ²³⁹ J. P. Dailey, J. P. Phillips, C. Li and J. S. Riffle, *J. Magn. Magn. Mat.*, **194**, 140-148 (1999)
- ²⁴⁰ M. F. Refojo and F. I. Tolentino, US Patent 5,672,355 (1997)
- ²⁴¹ L. N. Lewix, J. Stein, Y. Gao, R. E. Coborn, and G. Hutchins, *Platinum Metals Rev.*, **41**(2), 66 (1997)
- ²⁴² R. C. Weast, D. R. Lide, M. J. Astle and W. H. Beyer; CRC Handbook of Chemistry and Physics, CRC Press, Inc., (1989), F-37
- ²⁴³ S. M. Mahdi and R. O. Skold, *Colloids and Surfaces*, **66**, 203-214, (1992)
- ²⁴⁴ P. Alexandridis, T. Nivaggioli and T. A. Hatton, *Langmuir*, **11**, 1468-1476, (1995)
- ²⁴⁵ M. Rutnakornpituk, M.S.Thomson, L. A. Harris, K. E. Farmer, A. R. Esker, J. S. Riffle, J. Connolly, and T.G. St. Pierre, *Polymer*, **43**, 2339 (2002)
- ²⁴⁶ S. Well, Thesis, "Preparation and Properties of Ultrafine Magnetic Particles", Dept. of Chemistry, The University of Wales, 1989.
- ²⁴⁷ C.P. Bean and W.H. Meiklejohn, New Magnetic Anisotropy, *Phys Rev.*, **102**, 1413-1414, (1956)
- ²⁴⁸ J. Nogués and I.K. Schuller, Exchange Bias, *J. Magn. Magn. Mater.*, **192**, 203 – 232, (1999)
- ²⁴⁹ G. Thomas, and M. J. Goringe, In "Transmission Electron Microscopy of Materials", New York, John Wiley and Sons, 1979.
- ²⁵⁰ L. C. Sawyer, D. T. Grubb, In "Polymer Microscopy", London, Chapman & Hall, 1987.
- ²⁵¹ J. F. Nye, In "Physical Properties of Crystals", Oxford, Clarendon Press, 1957.
- ²⁵² C. Barrett, T. B. Massalski, In "Structure of Metals, Crystallographic methods, principles and data", Oxford, Pergamon Press, 1980.
- ²⁵³ A. Taylor, B.J. Kagle, In "Crystallographic Data on Metal and Alloy Structures", New York, Dover Publisher Inc., 1963.
- ²⁵⁴ X. Sun, A. Gutierrez, M. J. Yacaman, X. Dong, and S. Jin, *Materials Science and Engineering*, **A286**, 157 (2000)
- ²⁵⁵ H. Huang, S. Yang and G. Gu, *J. Phys. Chem. B.*, **102**, 18, 3420 (1998)
- ²⁵⁶ Q. Liu, J. A. Finch, Z. Xu, *Chemistry of materials*, **10**, 3936 (1998)
- ²⁵⁷ M. Spinu, Dissertation, "Silicon-based organic and inorganic polymers", Chemistry Department, Virginia Polytechnic Institute and State University, 1990.
- ²⁵⁸ J. E. McGrath, J. P. Pullockaren, J. S. Riffle, S. Kilic, and C. S. Elsbernd, In Untrastructure processing of advanced ceramics, J. D. Mackenzie, and D. R. Ulrich (Eds.), John Wiley & Sons, New York (1988)
- ²⁵⁹ M. Yamane, S. Inoue, A. Yasumari, *J. Non-Cryst. Solids*, **63**, 13 (1984)
- ²⁶⁰ C. J. Brinker, K. D. Keefer, D. W. Schaefer, T. A. Assink, B. D. Kay, C. S. Ashley, *J. Non-Cryst. Solids*, **63**, 45 (1984)
- ²⁶¹ K. D. Keefer, In Better Ceramic Through Chemistry C. J. Brinker, D. E. Clark, D. R. Ulrich (Eds.), Elsevier, New York, p15 (1984)
- ²⁶² J. Ulk, S Bullock, E. Johnston, S. A. Myers, L. Merwin, and K. J. Wynne, *Macromolecules*, **33**, 8791 (2000)
- ²⁶³ M. Spinu, Dissertation, "Silicon-based organic and inorganic polymers", Chemistry Department, Virginia Tech, 1990.
- ²⁶⁴ Q. Liu, J. A. Finch, Z. Xu, *Chemistry of materials*, **10**, 3936 (1998)

Vita

Metha Rutnakornpituk, the second of four children to Ponchai and Rassamee Rutnakornpituk, was born in Khon Kaen, Thailand on January 23, 1973. After graduating from Chumpae Suksa junior high school, he accepted the scholarship for students in the Development and Promotion for Science and Technology Talents Project of Thailand (DPST) and continued his education in Kaennakorn Wittayalai high school, Khon Kaen. He was supported by the DPST scholarship until he graduated from Khon Kaen University with a Bachelor of Science degree in Chemistry in 1996. Following his graduation, he accepted a teaching position at Naresuan University, Pitsanulok, Thailand. In 1997, he entered the graduate school at Virginia Polytechnic Institute and State University (Virginia Tech) to pursue his doctoral degree in organic polymer chemistry under the advisement of Professor Judy S. Riffle. Upon completion of his Ph.D., he will continue his work at Naresuan University as a professor in organic polymer chemistry.